Bulk Lifetime Limiting Defects in Czochralski Silicon and Graphene Oxide as a Surface Passivation Material

A THESIS SUBMITTED TO THE UNIVERSITY OF MANCHESTER IN FULFILLMENT OF THE REQUIREMENTS FOR THE DEGREE OF DOCTOR OF PHILOSOPHY IN THE FACULTY OF SCIENCE AND ENGINEERING

2018

By

Michelle Vaqueiro Contreras

School of Electrical and Electronic Engineering

Contents

List of Figures

Abstract

Crystalline silicon continues to be the backbone of solar cell technologies. Enormous efforts towards process optimisation, cell architecture and defect identification, amongst others, thus continue to be made in order to push the limits of achievable efficiencies. Consequently, this thesis aims to provide an improved understanding of a variety of defects related to light element impurities commonly found in silicon materials used for cell fabrication, and their effect on the minority carrier lifetime.

This thesis begins with a chapter which includes the motivation and outline of the present document. There, a summary of the most important aspects of the presented investigations and the relevance of the carried out work is described. In the subsequent chapter, a review on diverse silicon materials used for solar cell fabrication and the characterization techniques applied by the author for the shown studies is conferred. The most important chapters then are those which follow Chapter 2, where all the contributions from this thesis are presented in the form of published, submitted or submission-pending papers. Lastly, a concluding chapter is presented with final remarks from the contributions from the thesis and further work.

Amongst the most important contributions from this work stand out the following:

1. The identification of a lifetime-limiting complex which includes atomic H on its composition in phosphorous-doped Cz-Si crystals containing high levels of O and C. These findings thus include the rather controversial remark of having the ubiquitous H as a detrimental impurity for solar cell fabrication.

2. The identification of two previously unreported spectroscopic signals related to two thermal-donor species present in P-doped Cz-Si which have recently been suggested to limit the minority carrier of the material in literature. By means of various junction capacitance techniques evidence disproving the validity of such suggestion is provided.

3. The demonstration of a previously undetected spectroscopic signal attributed to

a BO-complex in B-doped Cz-Si. Complex that appears to be related to the responsible defect of the decades-long problem of light-induced degradation occurring in solar cells made from this type of materials during the first few days of their operation.

4. The demonstration of graphene oxide as a potential cheap alternative for silicon surface passivation, and the identification of its primary passivation mechanism as a field-effect coming from the GO's negative surface charge.

Declaration

No portion of the work referred to in this report has been submitted in support of an application for another degree or qualification of this or any other university or other institute of learning.

Copyright

Acknowledgements

An arrow can only be shot by pulling it backward. When life is dragging you back with difficulties, it means that you are about to be launched into something great.
So, just focus and keep aiming.
Unknown

There are no words which can even begin to express how happy and grateful I am to have been able to reach this new landmark in my life. I am proud to say that the time I have spent in this country (UK) and this university has given me so many tools to tackle with courage those challenges that are awaiting ahead for me. However, any of these could have been possible without the support given to me from God and all the magnificent people he has surrounded me with.

To begin with I need to thank **ALL** my family, yes I am talking about you: mom, dad, grandma, sisters, cousins, aunties and uncles... so many that I need more fingers than I have to count them all! I consider myself to be extremely blessed for having you by my side.

Thanks must also go to all my friends who have turned into my second family and have made this journey much more pleasant than I have expected, and sometimes at least bearable. Thank you very much to Michelle D., Iñaki, Gonzalo, Omar, Adriana R., Bart, Salvador, Paco, Rakesh, Jack, Chris, Daniel M., David,Freddy and the rest of my dearest friends, for their advice, help, support, encouragements and influence.

I would also like to thank my supervisors and mentors Tony Peaker, Vladimir Markevich, Matthew Halsall and Aravind Vijayaraghavan for having the patience and dedication to listen and support (at least some) of my ideas. What is more, to have had so many enlightening discussions with me and demonstrate me what it takes to be a remarkable scientist. I am also thankful to all the members of the university's staff who helped me with getting things done even when adverse circumstances in the labs presented themselves. Thank you to Mal Mcgowan, Maddy Coke, Chloe Holroyd and James Fitzsimons. Finally, I would like to thank CONACyT for sponsoring my studies.

List of publications

Recombination Centers Resulting from Reactions of Hydrogen and Oxygen in n-type Czochralski Silicon (Publication No. 1)			
V. P. Markevich, M. Vaqueiro-Contreras, J. Mullins, M. Halsall, B. Hamilton, L. I. Murin, R. Falster, J. Binns, E. Good, J. Coutinho, J. Medford, C.L. Reynolds Jr., and A. R. Peaker			
Status: Published	**Citation**: V. P. Markevich *et al.,* Recombination centers resulting from reactions of hydrogen and oxygen in n-type Czochralski silicon, in: 2016 IEEE 43rd PV Spec. Conf., 2016, pp. 688 – 693.		
Authors contributions			
Experimental work	Theoretical work	Writing	Editing & discussion
V. P. Markevich and M. Vaqueiro-Contreras	J. Coutinho	V. P. Markevich, M. Vaqueiro-Contreras and A. R. Peaker	J. Mullins, M. Halsall, B. Hamilton, L. I. Murin, R. Falster, J. Binns, E. Good, J. Coutinho, J. Medford, C.L. Reynolds Jr.

Powerful recombination centers resulting from reactions of hydrogen with carbon–oxygen defects in n-type Czochralski-grown silicon (Publication No. 2)			
M. Vaqueiro-Contreras, V. P. Markevich, M. P. Halsall, A. R. Peaker, P. Santos, J. Coutinho, S. Öberg , L. I. Murin, R. Falster, J. Binns, E. V. Monakhov, and B. G. Svensson			
Status: Published	**Citation**: M. Vaqueiro-Contreras *et al.,* Phys. Status Solidi RRL 11, 1700133 (2017).		
Authors contributions			
Experimental work	Theoretical work	Writing	Editing & discussion
M. Vaqueiro-Contreras and V. P. Markevich	P. Santos and J. Coutinho	M. Vaqueiro-Contreras	V. P. Markevich, A. R. Peaker, M. P. Halsall, Santos, J. Coutinho, S. Öberg , L. I. Murin, R. Falster, J. Binns, E. V. Monakhov and B. G. Svensson

Lifetime degradation of n-type Czochralski silicon after hydrogenation (Publication No. 3)			
M. Vaqueiro-Contreras, V. P. Markevich, J. Mullins, M. P. Halsall, L. I. Murin, R. Falster, J. Binns, J. Coutinho, and A. R. Peaker			
Status: Published	**Citation**: M. Vaqueiro-Contreras *et al.*, Journal of Applied Physics 123, 161415 (2018).		
Authors contributions			
Experimental work	Theoretical work	Writing	Editing & discussion
M. Vaqueiro-Contreras and V. P. Markevich	J. Coutinho	M. Vaqueiro-Contreras	V. P. Markevich, A. R. Peaker, J. Mullins, M. P. Halsall, L. I. Murin, R. Falster, J. Binns and J. Coutinho

Theory of a carbon-oxygen-hydrogen recombination center in n-type Si (Publication No. 4)			
P. Santos, J. Coutinho, S. Öberg, M. Vaqueiro-Contreras, V. P. Markevich, M. P. Halsall and A. R. Peaker			
Status: Published	**Citation**: P. Santos *et al.*, Phys. Status Solidi A, 1700309 (2017).		
Authors contributions			
Experimental work	Theoretical work	Writing	Editing & discussion
M. Vaqueiro-Contreras and V. P. Markevich	P. Santos and J. Coutinho	P. Santos, J. Coutinho and M. Vaqueiro-Contreras	S. Öberg, V. P. Markevich, A. R. Peaker and M. P. Halsall

Electron emission and capture by oxygen-related bistable thermal double donors in silicon studied with junction capacitance techniques (Publication No. 5)			
V. P. Markevich, M. Vaqueiro-Contreras, S.B. Lastovskii, L.I. Murin, M. P. Halsall and A. R. Peaker			
Status: Submitted	**Citation**: Under editorial revision - Journal of Applied Physics (2018).		
Authors contributions			
Experimental work	Theoretical work	Writing	Editing & discussion
V. P. Markevich and M. Vaqueiro-Contreras	-	V. P. Markevich and A. R. Peaker	M. Vaqueiro-Contreras, M. P. Halsall, S.B. Lastovskii and L.I. Murin

Direct Observation of the Boron-Oxygen Complex Precursor Responsible for Light Induced Degradation in Silicon Photovoltaic Cells (Draft No. 1)			
M. Vaqueiro-Contreras, V. P. Markevich, M. P. Halsall, J. Coutinho and A. R. Peaker			
Status: In progress for submission	**Citation**: -		
Authors contributions			
Experimental work	Theoretical work	Writing	Editing & discussion
M. Vaqueiro-Contreras and V. P. Markevich	J. Coutinho	M. Vaqueiro-Contreras and V. P. Markevich	A. R. Peaker, M. P. Halsall and J. Coutinho

Graphene oxide films for field effect surface passivation of silicon for solar cells (Publication No. 6)			
M. Vaqueiro-Contreras, C. Bartlam, R.S. Bonilla, V. P. Markevich, M. P. Halsall, A. Vijayaraghavan and A. R. Peaker			
Status: Published	**Citation**: M. Vaqueiro-Contreras *et al.*, Sol. Energy Mater Sol. Cells, p. 189–193, 187 (2018).		
Authors contributions			
Experimental work	Theoretical work	Writing	Editing & discussion
M. Vaqueiro-Contreras and C. Bartlam	-	M. Vaqueiro-Contreras	C. Bartlam, R.S. Bonilla, V. P. Markevich, M. P. Halsall, A. Vijayaraghavan and A. R. Peaker

CHAPTER 1

INTRODUCTION

It has been the aim of the author to convey throughout the pages of this thesis the work she has dedicated herself to do in the past three years. Work that has had the goal of pushing the limits of our understanding in the area of silicon photovoltaics. It is her belief that technological advances in areas such as the one of photovoltaics are on the way of making a huge difference in the world we are living in. She is convinced, however, that for truly making a difference it is of paramount importance not to loose sight on the pursuit of an increased collective knowledge and deep understanding of both, scientific matters, and the planets needs; where the human and environmental needs are equally weighted. Therefore, a significant component of the authors motivation is to be an active contributor to the transition of our society from the currently non-renewable-energy dependent standpoint to a more environmentally-friendly and sustainable one.

1.1 Motivation

Solar cell technology is one of the most appealing green technologies for the energy industry at the present day. However an energy hungry society such as the one we live in, requires any given technology to push to the very limits of development to improve the conversion efficiencies. This is now even more essential due to the world's commitment to keep the global temperature rise below 2 degrees Celsius after the establishment of the Paris agreement on the 4th of November of 2016.

Many efforts have been made towards the achievement of such a goal which have now led solar energy generation to be one of the cheapest way of power generation, undercutting coal and nuclear in several countries [11].

Despite all the improvements already achieved however, the fundamental Shockley–Queisser 30% conversion efficiency limit with silicon technologies has not been

reached. This is partly caused by the non–radiative recombination losses in the used materials due to crystal impurity presence. Therefore, understanding and mitigation of the effects caused by these impurities is still of paramount importance for the achievement of improved efficiencies.

With this in mind the objective of this research is to find and understand electrically active defects in crystalline silicon, and the study of some surface passivation materials for silicon. The materials we will be focusing here include both: phosphorous– and boron–doped mono–crystalline silicon. Materials that combined currently take 32.2% of the global annual solar cell production, with boron–doped silicon as the leading sharer [2].

Hence, two thirds of the results chapters will be dedicated to study the effects of impurities that are largely present in these materials, such as carbon, oxygen, hydrogen and boron. While the last third will be devoted to new studies on graphene oxide, which in recent years has gained a lot of attention, thanks to the graphene revolution, as a cheap alternative to current surface passivation materials.

1.2 Outline

In this research project we aim to understand the interaction of some commonly occurring impurities in crystalline silicon and how they affect its effective minority carrier lifetime. Broadly speaking this thesis is divided in four parts, including: **i)** literature review of relevant background topics (Chapter 2), **ii)** defects in phosphorous–doped silicon [1] (Chapter 3), **iii)** defects in boron–doped silicon [2] (Chapter 4), with the inclusion of a chapter on graphene oxide (GO) as passivation material for *p*–type silicon (Chapter 5), and **iv)** a conclusions chapter with this research highlights, contributions and the discussion of further work (Chapter 6). Each results chapter (i.e Chapters 3 - 5) include extended information on its relevance, related previous work and it is presented in the form of published or submitted peer reviewed articles.

Firstly, an overview on silicon photovoltaics principles, solar and electronic grade silicon production methods and their characteristics is presented. This is followed by an explanation of lifetime limiting recombination mechanisms in silicon, and a collection of characterization techniques which were used throughout this work.

Secondly, a chapter on the investigations of a recently found powerful recombination centre in phosphorous-doped silicon is presented. This, somewhat controversial,

[1] Henceforth referred interchangeably to *n*–type silicon
[2] Henceforth referred interchangeably to *p*–type silicon

study shows how carbon, oxygen and hydrogen impurities interact in silicon to severely reduce the bulk lifetime of the material and form a family of at least four defect levels in the Si gap. The controversy residing in the fact that hydrogen is an impurity deliberately incorporated into silicon during processing due to its proven passivation capabilities. Nevertheless, the case of its interaction with carbon and oxygen in *n*-type material has been overlooked, and so here we show that a significant detrimental effect is likely to arise from its presence in high carbon material. Details of this effect is presented in form of already published material which is shown within the chapter. In addition, on the last section of the chapter results related to a previously undetected DLTS signal which we assign to the bistable thermal double donors (BTDDs) in *n*-type silicon is given. Oxygen-related thermal donors which have been largely investigated since the early 80's have recently regained significant attention within the silicon research community. This because of their unavoidable presence in Si, which lately have been argued to be responsible for reductions in carrier lifetime. Through a series of electrical measurements and characterisation we conclude that these defects act as effective carrier traps but not as powerful recombination centers and thus do not limit the minority carrier lifetime.

Thirdly, a chapter focusing on a long studied problem affecting the solar industry and commonly identified as the "LID problem", for its acronym *light–induced degradation*, is presented. LID constitutes a major commercial problem in B-doped cells resulting in up to 10_{rel} % degradation occurring during the first days of operation, which even though has been reported to be mitigated by hydrogen passivation is still not fully understood. Here we show for the first time the observation of a DLTS signal related to the complex responsible for the degradation of boron–doped silicon after carrier injection. This peak is related to a deep level defect, which appears not to be a recombination centre but rather a carrier trap and precursor of the LID responsible centre. Furthermore, our results strongly suggest the involvement of a shallow level in the recombination process. This is in contrary to the existing literature which attributes the carrier recombination to a pair of deep levels within the band–gap. These proposed traps however have never been detected by any other technique besides lifetime spectroscopy and thus making their chemical and physical identification very speculative. Accordingly, detailed information of our careful observations and hypothesis is presented in the form of an article which is in the process of completion and submission for publication.

Fourthly, an investigation of graphene oxide as a passivation agent on p-type silicon to reduce surface recombination is presented in Chapter 5. This chapter introduces an extended review of GO's structure and properties which have not been included on the literature chapter (Chapter 2), which sets the foundation for its proposed potential application as a passivation material. This is then followed by the demonstration through a series of experimental studies that low surface recombination velocities can be achieved by the deposition of GO on some silicon materials. Furthermore, detailed studies on the mechanisms responsible for this passivation have been carried out and reported. It is demonstrated that the so-called field-effect passivation is the dominant process taking place on the surface after deposition, in opposition to the existent speculation of a chemical passivation given in literature. These results are presented in the form of a published article.

Lastly, a conclusions chapter will summarise the key results of this thesis, their relevance to the photovoltaics community and the discussion of some of the required further work.

CHAPTER 2

SILICON PHOTOVOLTAICS

The increasing global population and the energy requirement that comes with it, has provoked a massive interest towards green energy generation which carries with it several social and environmental benefits. To mention a few there are: economic growth, job creation, carbon emission reduction, increased energy access, improved energy security and air pollution reduction.

Many technologies have thus been applied all around the world to take part in this green-energy transformation endeavour. On the top of the applied technologies there are hydropower, wind and photovoltaic (PV) generation (see Fig. 2.1). Even though hydropower generation is still the green technology with the highest installed generation capacity in the world, it has not been growing as much in the last decade [1]. On the other hand, wind and solar PV generation have been steadily growing in the past decade. Last year PV energy generation grew by 32% followed by wind with 10% growth [1]. Such an impressive growth in PV has largely been achieved thanks to the drop in fabrication cost and improved module efficiencies. There has been a decrease of 73% in the global weighted average levelised cost of electricity of utility-scale solar PV since 2010 [11] and an increase in efficiencies from about 12% to 22.8% [12]. The latter being the averaged commercial efficiency of silicon-based modules for residential applications [2, 12].

All this growth thus indicates that the international market is strongly betting in favour of PV technologies. This however, also includes the development of PV technologies based on distinct materials and not just in silicon wafers. Substantial investment and work for example has been applied to develop and improve technologies based on: Copper indium gallium selenide (CIGS), Cadmium telluride (CdTe), and perovskites amongst others. Even though tremendous advances in efficiency by the use of these materials have been achieved, as shown in Figure 2.2, the highest efficiencies of commercial devices have been achieved with silicon-based cells. It has

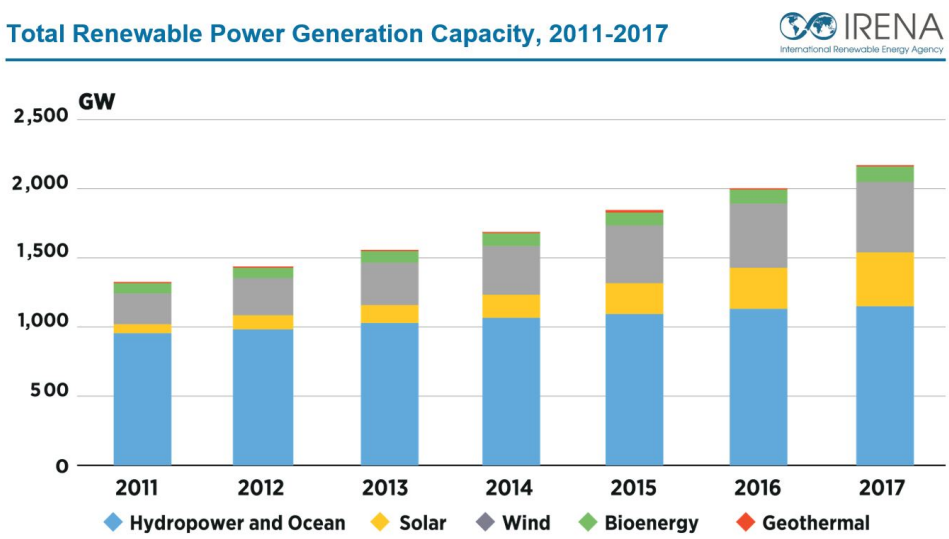

Figure 2.1: Global power generation capacity (2011-2017), taken from [1].

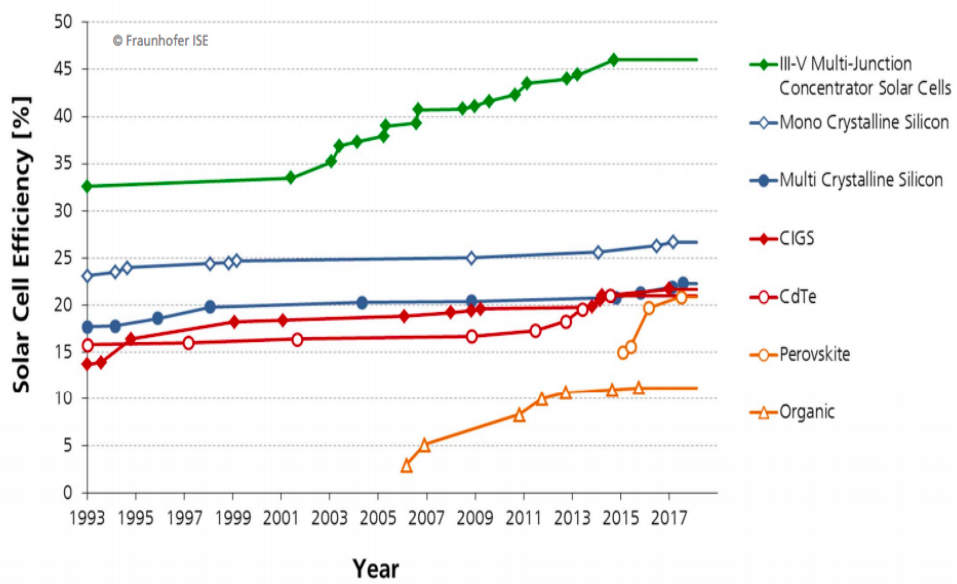

Figure 2.2: Development of laboratory solar cell efficiencies, taken from [2].

therefore been the interest of the author during the course of her doctoral studies to investigate those characteristics of silicon materials which have been known to limit the achievable efficiencies in the solar cells made from them.

In this particular chapter we aim to convey a general picture of the relevant materials used for this technology, the details of a PV cell operation, the lifetime limiting recombination mechanisms that reduce these cell efficiencies, and the characterization techniques used throughout this project for the identification of defects in silicon.

2.1 Silicon for solar: growth and characteristics

The PV technologies currently available in the market are usually divided on three categories: thin film (Cd-Te, a-Si and CIGS), multicrystalline silicon (mc-Si), and mono-crystalline silicon (mono-Si), solar cells. The data show that from these technologies only 4.5 % of the global PV production was dedicated to thin films last year, a percentage that has actually been decreasing in the last five years [2]. On the other hand and despite some initial fluctuation in past years, mono-Si-based production increased approximately 9% last year to reach a 32.3% of the total PV production [2]. This, while mc-Si PV production is still ahead of the rest, has been slowly but steadily increasing since 2008, accounting last year for 60.8% of the total production.

These numbers thus add up to a remarkable value of 93% of the world's PV production in 2017 dedicated solely to silicon materials. It is then important to introduce some of the most used silicon growth methods applied for wafer production. Noting that during crystal growth large quantities of impurities can be introduced/formed due to various process conditions. And as we will show in later chapters, some of these impurities can severely limit the efficiency of the cell made from the given material if care is not taken during its growth.

2.1.1 Cast silicon

As it has been mentioned before, the PV market is largely focused on solar cells from multicrystalline silicon, which is produced by the so-called directional solidification processes. Such processes have been used for decades and consist in pouring melted polysilicon or upgraded-metallurgical silicon (UMG-Si) feedstock into a crucible and allowing it to solidify by controlling temperature gradients [15]. An schematic of this method is shown in Figure 2.3(a).

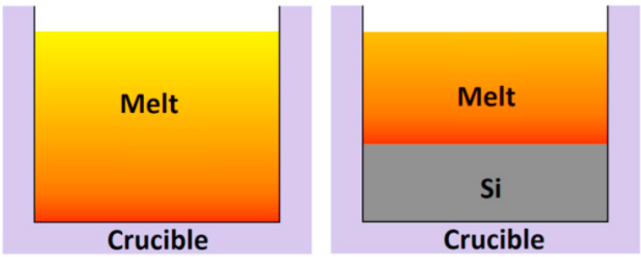

(a) Standard unseeded cast process. Reproduced from [13].

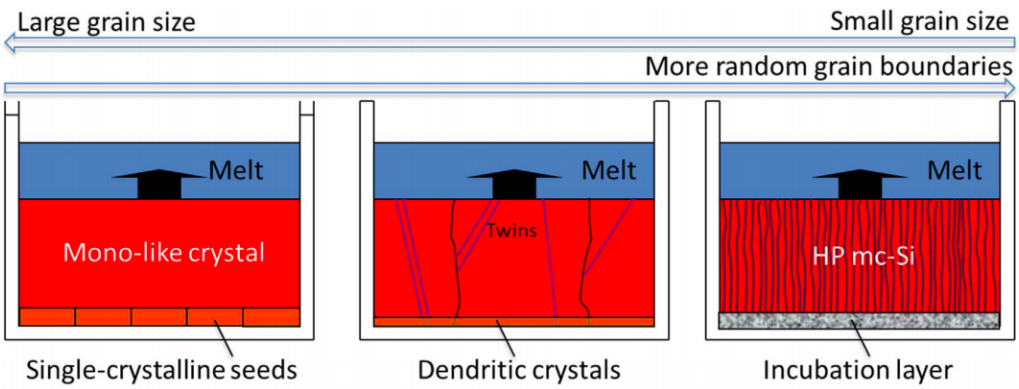

(b) Seeded directional solification processes. From left to right, mono-like Si growth, Dentritic growth and HPMS growth. Reproduced from [14].

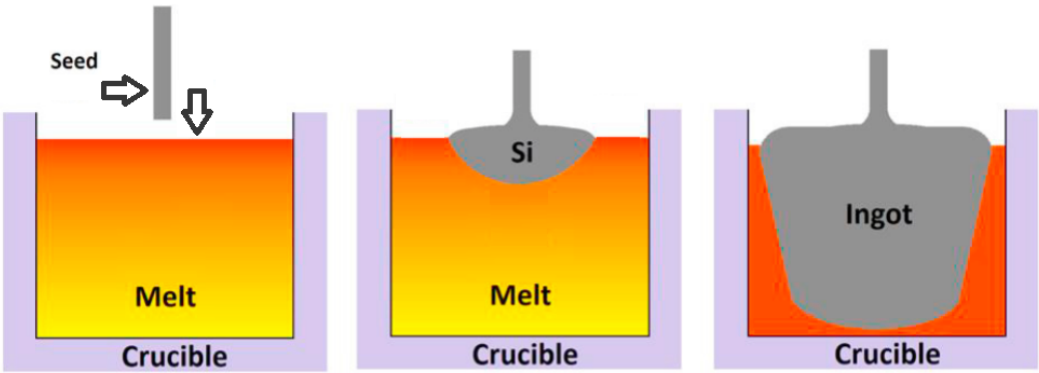

(c) Noncontact-crucible silicon process. Reproduced from [13].

Figure 2.3: Crucible-cast silicon methods.

Due to the maturity of this technology it has been possible to mass produce mc-Si wafers for relatively low costs. Nevertheless, this cheap cost has been achieved at the expense of material quality. On the one hand there is the incoming contamination from the feedstock used for silicon crystallization. The feedstock quality depends on the applied method for metallurgical silicon (MG-Si) purification which is obtained by the reduction process of raw quartz in the presence of carbon. This purification can generally be attained by various processes which can broadly speaking be divided in two categories identified as: the chemical route and the metallurgical route of purification. The chemical route involves the purification of the MG-Si by its transformation to trichlorosilane via hydrochlorination and subsequent distillation, such as the so-called Siemens process. This process has been largely developed and can lead to extremely pure polysilicon rods, however its application require the use of very high-temperature reactors which are not environmentally friendly nor energetically efficient and thus very costly. Alternatively, the metallurgical route involves the purification by metallurgical methods such as controlled fusion, re-fusion and solidification which is many times more energetically efficient that the chemical route. However, the resulting material from this process suffers from rather high levels of metallic and light impurity contamination such as Fe, Cu, Ni, B, P, Ca and Cl. Several studies have been conducted to determine the maximum allowable concentration of these impurities for acceptable solar cell efficiencies, nevertheless the purity of the UMG-Si still under the one given by the chemical route.

On the other hand however, even when the quality of the used feedstock in the casting process is high, presence of extended defects i.e grain boundaries and dislocations still exist. These unwanted characteristics are largely related to the direct contact the crystal has with the crucible during growth, or to the crystallographic defects generated by the seeds. Nevertheless, even when seeds are not used during growth, the crucible contact to the silicon promotes an abundance of grain nucleation sites and confinement of the crystal to its walls at high temperatures. In addition, there is the introduction of species during growth such as C, O, P, B, Cu, Al, Ni, Fe, Mn, Cr, Ti and Mo which can be very significant. Many efforts in the field of defect engineering have and continue to be made towards the reduction of these defects. For instance by the application of gettering processes, or crucible-coating materials such as Si_3N_4, SiO_2 or Si for the impurity shielding [15, 16]. These procurements have in turn yielded to material with acceptable efficiency levels for commercialization.

However, there is still a lot of scientific work dedicated to improving casting methods and so new methodologies keep emerging. A few reviews such as the ones provided by Kivambe *et al.* and Lan *et al.* in Ref. [13] and [16], respectively, give a good insight into these technologies. The most relevant amongst those are the so-called high-performance mc-Si (HPMS) growth, the mono-like silicon growth and the noncontact-crucible silicon process (NOC-Si). The mono-like silicon process as described by Stoddard in Ref. [17], and depicted in Figure 2.3(b), emerged as a potential low-cost high-quality PV silicon material, which was once predicted to take over the market [13]. Nevertheless, this technology presented some drawbacks that did not have the time to be resolved before a new technology arose, the HPMS method [13, 14, 18]. The HPMS was introduced in 2011 by Lan's group during the 5th International Workshop on Crystal Growth Technology (2011) [19], and consists in the utilisation of small randomly placed Si-crystal seeds as depicted in Figure 2.3(b). In fact, as described by the author, this method originated serendipitously while pursuing to improve the dendritic method also depicted in Figure 2.3(b). Since then this technology has been adopted by several companies and reaching a remarkable 21.63% efficiency in some of the cells fabricated with it [19].

Even though the aforementioned methods have allowed more affordable prices for commercialisation, significant cost related to the still present impurities in the crystals that reduce the efficiencies need to be reduced. With this problem in mind, other technologies have been actively explored to reach the goal. For instance the NOC-Si method, also known as the Kyropoulos method [15] and shown in Figure 2.3(c), have recently regained attention [13]. The idea behind this method is to avoid in-diffusion of impurities from the crucible, and reducing stress and grain nucleation from the crucible walls. In the process there is no contact to the walls since nucleation of the crystal begins by seeding at the top of the crucible and allowing solidification by either pulling and/or controlling the temperature distribution of the furnace. Cells made from these materials have been proved to achieve 19.6% efficiencies and milliseconds lifetime [13].

2.1.2 Czochralski and Continuous-Czochralski

This method was named after J. Czochralski, a Polish chemist who established a technique for the measurement of the metal crystallization velocities in 1918. Nevertheless,

it was the work of Teal and his team [20] that proposed a modified version of Czochralski's basic principle to grow mono-crystalline ingots that has incrementally been used in solar industry [2, 21]. The Czochralski (Cz) method is by far the most widely used process to produce high quality mono-crystalline silicon in the solar industry. Its purity has allowed the fabrication of remarkably high efficiency cells of record breaking values [11]. The Cz method is capable of reducing the impurity concentrations in the grown crystal by careful pulling and rotation control in the process due to segregation. The segregation coefficient in the Cz process is so high that most of the metallic impurities during growth remain in the melted silicon and thus separated from the grown solid crystal. Therefore and different from, the silicon crystals produced by the cast process described in the previous section, Cz is not very susceptible to those high impurity levels coming from low quality feedstock [22]. This property gives the Cz process a huge advantage in cost from the initial material required for growth over the cast silicon. A typical Cz silicon crystal system is depicted in Figure 2.4(a), and the growth process can be summarised in four steps as follows:

1. Polysilicon chunks are melted at temperatures above 1420°C in a quartz crucible under inert atmosphere.

2. The melted silicon is kept at high temperatures while all traces of solid disappear and all tiny bubbles are expelled, this is to avoid voids in the crystal.

3. A small piece of crystal with the desired orientation called a seed is then placed on top of the melt until it starts to melt. Afterwards the seed is pulled out with a specific withdrawal speed and rotation velocity. Optimisation of these velocities and the temperature of the melt yield to the silicon ingot desired characteristics such as the diameter. During this process inert gas (usually argon) is injected from top to bottom inside the chamber to flush the produced silicon monoxide (SiO) and carbon monoxide (CO) produced by the process.

4. Finally, when the desired diameter is achieved the process of controlling the pulling rate and temperature continues almost until the end of the melted silicon. Towards the end of the growth the pulling rate is reduced, mainly due to heat radiation from the crucible which increases the temperature of the exposed ingot. In addition, it is necessary to gradually decrease the diameter of the growing crystal near the end of the growth to avoid or minimize thermal shock which can cause slip dislocations at the tail. When the diameter is small enough it can be separated from the melt without dislocations.

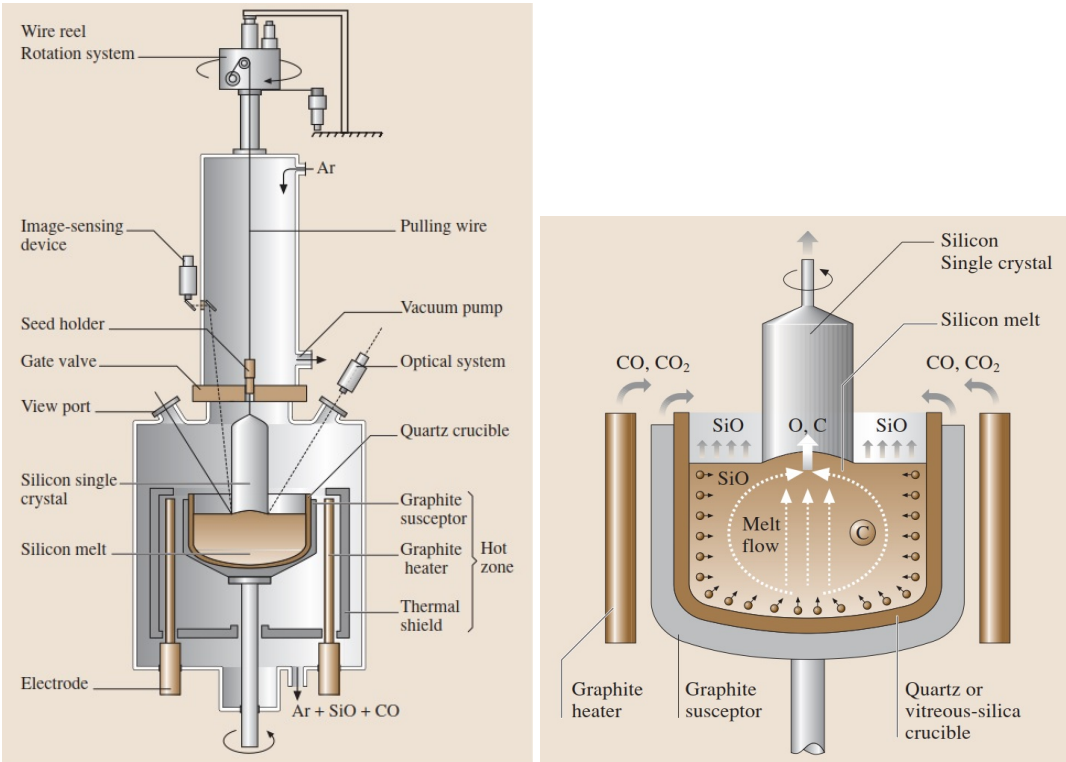

(a) Schematic of a typical Czochralski crystal growth system

(b) Schematic of carbon and oxygen introduction during crystal growth

Figure 2.4: Czochralski single-crystal growth method schematics taken from [3].

Even though this method has increasingly being used for PV production due to the low chemical defect concentration typically obtained, and its almost non-existent structural defect concentration, it is still not perfect. This because there are some impurities that are inevitably introduced to the ingot during growth and can greatly affect the properties of the material.For instance there exist the light element impurities such as C and O which are unavoidably encountered in Cz-Si. The main sources of these defects are depicted in Figure 2.4(b), for instance from the quartz crucible and the graphite heaters. The reaction that occurs due to the interaction of the crucible and the melted silicon produce SiO. Most of this SiO is evaporated and expelled with argon, nevertheless, the rest of it is incorporated to the silicon crystal yielding to average O concentrations of $\sim 3-5\text{x}10^{17}\text{cm}^{-3}$. In the case of C we know that its incorporation ($< 2\text{x}10^{17}\text{cm}^{-3}$) is mainly coming from the polycrystalline chunk material and the generated CO on the graphite components [23].

Several techniques have actively been applied to reduce the level of contaminants

by process optimisation and set up modifications, which have in turn made Cz material purer and in some cases cheaper to produce. This is why despite the still present contaminants the Cz method is the most widely used process in solar industry for monocrystalline silicon growth. As a matter of fact, Cz market share is predicted to keep growing for at least five years before reaching a plateau [21], therefore its electrical property characterization remains a hot topic in the literature.

◇ **Continuous Czochralski**

Crystal growth by Czochralski method gives many advantages to the silicon industry, however its production cost is not optimum. This is because it is largely dependent on the cost of the quartz crucible. Furthermore, in the conventional CZ process only one crystal is grown per crucible charge. Meaning that the crucible is just used once and then discarded. The reason being that the small leftover of melted silicon cracks the crucible as it cools down from the very high temperature process. One approach to tackle this problem is the so-called *Continuous Czochralski* (CCZ) method, which was first demonstrated by Fiegl [24] in 1983 based on a two-container system. In the CCZ method the quartz crucible is constantly feed with polysilicon in order to maintain a constant volume of melt and hence avoid the cracking.

In addition to cost reduction by crucible recycle in CCZ silicon, the growing conditions can be considered steady [3]. This is a great advantage over the conventional CZ method which due to its unsteady kinetics arising from the change in melt conditions, provokes many inhomogeneities in the grown crystal. For instance, the significant oxygen introduction in conventional CZ can be largely reduced by the volume and aspect ratio of the melt manipulation in the CCZ method [24, 25]. It should be mentioned however that the different thermal histories of each part of the grown crystal do play an important roll on its uniformity. Therefore it is a common practice to apply some post-growth treatments such as high temperature annealing that are required to achieve better quality crystals.

2.1.3 Float Zone

The float zone method (FZ) was firstly used to refine binary alloys and was invented by Theurer in 1962 [26]. This method, similar to the Cz method, has enabled the growth of high purity silicon crystals, and have arrived to be known as “electronic-grade” silicon (EG-Si)[15]. However, due to cost limitations this is a method not commonly

used in the solar cell industry. In fact, according to the 2017's International technology roadmap for photovoltaics (ITRPV) report, this material will cease to be used for PV mass production in the following years. Nevertheless, it is still largely used in PV literature since it can serve as a control sample for many defect identification studies because of its low impurity content [27, 28].

Unlike Czochralski growth, the FZ method does not require the contact of the growing ingot to a crucible material or heaters, and during growth the crystal seed with desired orientation is placed at the bottom and not on top of the melt. Moreover, different from the CZ method the FZ process consists in the conversion of a polysilicon rod to a single-crystal ingot by passing the melted rod through a heated coil which does not exist in the CZ set-up. We outline the process in three key steps which are also depicted in Figure 2.5:

1. The crystal seed of desired orientation is contacted and fused with the tip of the polysilicon rod, which is called the *seeding*.

2. After seeding, a thin neck of 2-3 mm in diameter and 10-20 mm in length is formed, the so-called *necking* process. This is a key process since it is used to eliminate dislocations in the crystal caused by thermal shock.

3. Finally, the polysilicon rod is passed all along the coil with a predetermined power and travel rate. Parameters that are used to control the shape of the molten zone and the ingot final diameter.

Overall FZ crystal growth is well known for its remarkable purity, which is the result of the low level of interaction with external materials that the ingot is subjected to during growth and the high segregation coefficient. This low level interaction give rise to the almost negligible ($1x10^{16}cm^{-3}$) concentration of oxygen in FZ silicon. These high quality crystals allow to achieve high resistivity wafers of between 10 and $>$ 10,000 Ω cm whereas with CZ grown ingots this it not possible and resistivities of 50 Ω cm or below can only be achieved.

It must be pointed out however that there are some defects in FZ silicon which are also unavoidable and can lead to cell efficiency losses. For instance, depending on growth rate and thermal gradient ratio during the FZ growing process, there always exists the incorporation of intrinsic defects (i.e self-interstitials and vacancies). Recently Grant *et al.* [28] have shown that heat-treatments of FZ samples in the range 450 - 700 °C results in a severe reduction in minority carrier lifetime in both, *n*- and

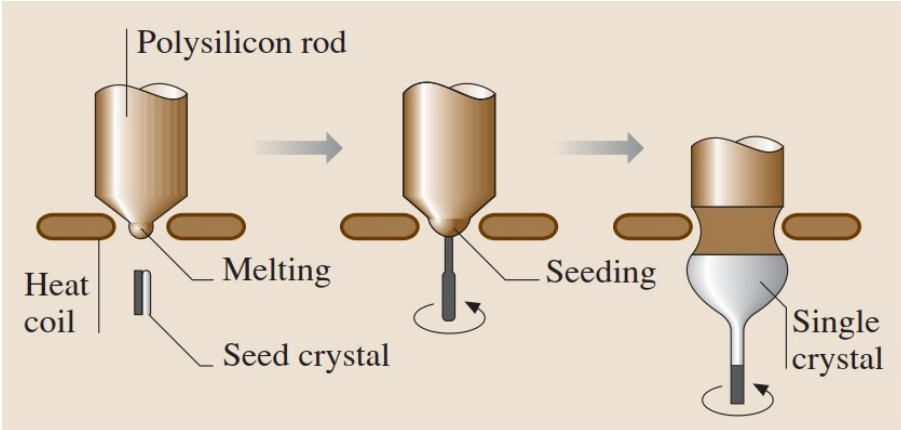

Figure 2.5: Float zone single-crystal growth method schematics reproduced from [3].

p-type silicon. Their studies suggest that this degradation is related to vacancies in the material, but also determines that high temperature annealing processes ($>$ 1000 °C) can permanently annihilate the responsible defects. However, this is not the only case of degradation of FZ material that has been recently reported. Another important observation was made in 2015 by Grant *et al.*[29] in a set of *p*-type samples that were phosphorous gettered at 880 °C or illuminated with 0.2 suns intensity for 24 h and resulted in the degradation of *p*-type FZ material. They proposed that the defect behind the degradation could not be related to the boron-oxygen (BO) complex responsible for light-induced-degradation (LID) in Cz silicon, but that it is instead related to a lattice-impurity or an impurity-impurity metastable defect. Further studies have also discarded the possibility of BO to be responsible for the degradation [30, 31] and suggested the involvement of hydrogen in the complex [30]. Many more studies are however still required to fully identify the lifetime limiting defects in FZ material and the idea of it being prone to degradation established.

2.2 Recombination in crystalline silicon

So far we have reviewed the significance of PV in relation to today's power generation demand, and introduced the top silicon growth methods used by the solar industry which will allow for competitive prices to fulfil such demand. In this section we summarise key aspects of a solar cell operation and describe the mechanisms by which recombination of carriers in semiconductors occur. We then finalise the section by discussing some existing surface passivation materials used for the reduction of the unavoidable active recombination centres at the silicon surface.

The generation of energy by a photovoltaic cell consists primarily of four steps. Firstly, sunlight generates a pair of carriers (electron-hole pair) through the excitation of an electron from the valence band to the conduction band. Secondly, the carriers are separated by the junction and a current flow is generated. Thirdly, an agglomeration of the generated negative/positive charges (electrons/holes) is created in the n-doped/p-doped material. Fourthly, the agglomeration promote the formation of an electric field between the charges in opposite direction of the intrinsic electric field in the junction with a strong enough net force that limit the diffusion of the carriers through the junction. So that, when the emitter and back contact are in a short-circuit configuration a current flows through the emitter until it closes the circuit at the rear contact. This whole process is known as the *generation* mechanism and is what PV researchers strive to optimise.

However in reality there are several other processes occurring within the applied semiconductor materials that hinder the achievement of optimal generation rates. These antagonistic processes are the so-called *recombination* mechanisms which prevent the entire generated carrier collection at the contacts of the devices and they exists because of the presence of electrically active defects in silicon. Defects that are introduced during silicon growth or solar cell production processing. So, henceforth we will define the most important recombination mechanisms and their mathematical representations. This will then build the foundation for the understanding of the lifetime limiting defects studied in Chapters 3 and 4.

The four recombination mechanisms which we will discuss in the following sections are present in every silicon crystal in different proportions and are directly related to the lifetime of the minority carriers, τ. Nevertheless, experimentally it is the so-called effective lifetime,τ_{eff}, what we most often use to characterise the materials. τ_{eff} is composed by the sum of the reciprocals of each recombination lifetime, namely: Shockley-Read-Hall lifetime, τ_{SRH}, Auger lifetime, τ_{Aug}, radiative lifetime, τ_{rad}, and surface lifetime, τ_{surf}, and expressed as:

$$\frac{1}{\tau_{eff}} = \left(\frac{1}{\tau_{SRH}} + \frac{1}{\tau_{Aug}} + \frac{1}{\tau_{rad}}\right) + \frac{1}{\tau_{surf}} = \frac{1}{\tau_{bulk}} + \frac{1}{\tau_{surf}} \tag{2.1}$$

Equation 2.1 allows to understand the relevance of the recombination mechanisms on the overall minority carrier lifetime, which we know directly affect the efficiency of the terminated solar cell.

Now, generally speaking, we can classify the recombination mechanisms as *intrinsic* or *extrinsic* recombination mechanisms. Within the intrinsic mechanisms we have

the *radiative recombination* and the *Auger recombination*, mechanisms that are always present in the crystal to some extent, no matter what growth technique is used. The most common occurrences of these two mechanisms involve band to band transitions, however sometimes discretely formed levels within the band gap can also take part in the recombination process. On the other hand, the extrinsic mechanisms requires the presence of these intermediate levels as stepping stones for the electrons to encounter with the holes and recombine. The most usual defects that introduce transition levels in silicon are: a) vacancies or voids, b) interstitial/self-interstitial atoms, c) dislocations, d) precipitates, e) substitutional atoms, and f) dangling bonds. This type of recombination process is commonly termed *Shockley-Read-Hall (SRH) recombination*.

In order to gain a better understanding on each of these processes in the following sections we will describe their principles.

2.2.0.1 Radiative recombination

Just as it is designed to occur in light-emitting diodes (LED), the radiative recombination consists in the direct annihilation of an electron-hole pair while releasing the excess energy in the form of a photon of equal energy as the band gap. This is actually the inverse process of optically-excited generation. Now, because this event requires an electron to fall from the conduction band to the valence band and encounter with a hole to recombine, the radiative recombination rate directly depends on the available free electrons and holes in the conduction and valence bands respectively. Thus, we can express the net recombination rate U_{rad} in the form:

$$U_{rad} = B(np - n_i^2) \tag{2.2}$$

where the coefficient B reflects the probability of a radiative transition and is particular of each semiconductor. In the case of crystalline silicon, the coefficient in the literature is found to be $B = 1$ x 10^{-14} cm^{-3}s^{-1} [32]. Similarly, n and p represent the electron and hole densities respectively. Finally, n_i stands for intrinsic carrier concentration.

If now we consider non-equilibrium concentrations of electrons and holes such that

$$n = n_0 + \Delta n \text{ and } p = p_0 + \Delta p$$

where n_0/p_0 and $\Delta n/\Delta p$ represent electron/hole equilibrium concentrations and electron/hole excess carrier densities respectively and assume charge neutrality ($\Delta n = \Delta p$).

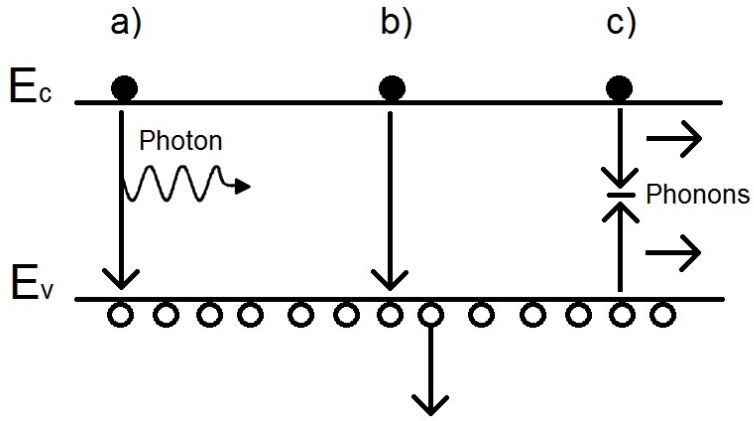

Figure 2.6: Recombination mechanisms: a) **Radiative** recombination, b) **Band to band Auger** recombination and c) **Multiphonon** or **SRH** recombination.

Then, we can express the radiative recombination lifetime τ_{rad} as

$$U_{rad} = B(n_0 + p_0)\Delta n + B\Delta n^2 \quad \Rightarrow \quad \tau_{rad} = \frac{1}{B(n_0 + p_0) + B\Delta n} \tag{2.3}$$

This expression can be further simplified when the conditions of low-level injection ($\Delta n \ll n_0 + p_0$) and high-level injection ($\Delta n \gg n_0 + p_0$) are met, giving rise to the relationships[1]:

$$\tau_{rad_{LLI}} = \frac{1}{BN_{dop}} \quad \text{and} \quad \tau_{rad_{HLI}} = \frac{1}{B\Delta n} \tag{2.4}$$

with N_{dop} standing for doping concentration (usually in the range $10^{13} - 10^{20}$ atoms per cm^3 [32]). It is possible to see from Eq. 2.4 that in the low-level injection regime τ_{rad} remains constant and proportional to the inverse of doping concentration. While under high-level injection conditions τ_{rad} decreases as the injection increases, this independently of doping concentration. An schematic diagram of the radiative recombination is included in Figure 2.6 (a).

2.2.0.2 Band to band Auger recombination

Auger recombination is traditionally considered to be a three-particle interaction process. This is due to the fact that when an electron-hole pair recombine the released energy is absorbed by another free carrier which in turn releases its energy mainly by lattice vibrations. This process is shown in Figure 2.6 (b). If we assume that the charge

[1]Henceforth subscripts *HLI* and *LLI* represent high-level injection and low-level injection, respectively.

carriers are non-interacting quasi-free particles [33], then, depending on the charge of the third carrier we can define the Auger recombination rate U_{Aug} to be either proportional to n^2p (*eeh*-process) or p^2n (*ehh*-process) and calculate the net recombination with

$$U_{Aug} = C_n(n^2p - n_0^2p_0) + C_p(np^2 - n_0p_0^2) \tag{2.5}$$

where C_n and C_p represent the Auger coefficients of the *eeh*- and the *eeh*-process, respectively. Correspondingly, for Auger recombination we can relate the lifetime τ_{Aug} to the injection level as follows:

for n-type silicon

$$\tau_{Aug_{LLI}} = \frac{1}{C_nN_D^2} \quad \text{and} \quad \tau_{Aug_{HLI}} = \frac{1}{(C_n + C_p)\Delta p^2}, \tag{2.6}$$

and for p-type silicon

$$\tau_{Aug_{LLI}} = \frac{1}{C_pN_A^2} \quad \text{and} \quad \tau_{Aug_{HLI}} = \frac{1}{(C_n + C_p)\Delta n^2} \tag{2.7}$$

As can be seen from Eq. 2.6 and 2.7, the Auger lifetime is generally dependent on the inverse square of the carrier density ($\tau_{Aug} \propto 1/n^2$). This shows a stronger dependence on injection level than τ_{rad}, resulting in the Auger process being the dominant mode recombination for high injection levels in silicon. Moreover for low-level injection conditions, τ_{Aug} will remain constant and dependent on the inverse square of doping concentration.

2.2.0.3 Shockley-Read-Hall (SRH) recombination

The presence of lattice imperfections (e.g vacancies, interstitials, etc.) in silicon introduce discrete energy levels within the band gap as depicted in Figure 2.6 (c). Such energy levels effectively help the free carriers to encounter and recombine.

In this work we will focus in two specific classes of interactions through intermediate levels. The first interaction occurs when the generated transition level acts as a *recombination center*. In this case a free electron from the conduction band (CB) and a free hole from the valence band (VB) are successively captured by the defect level and annihilate each other. Or, when an electron relaxes from the CB to the defect level and then relaxes again to reach the VB and recombine with a hole. This last process can also appear in opposite direction, so that the hole from the VB is captured by the defect

level and then attracted to the CB where it recombines with an electron.The second interaction happens when the defect level act as a *trap*. This process can be identified when a free carrier is captured by the defect level and subsequently injected back to its previous energy state either in the valence or conduction band. Meaning that the defect level interacts with only one of the two bands and no recombination occurs.

The dynamics of the recombination through mid-gap discrete levels were first analysed by Shockley and Read [34] and Hall [35] in 1952, deriving the equation for the recombination rate U_{SRH} for a single defect as:

$$U_{SRH} = \frac{np - n_i^2}{\tau_{p0}(n+n_1) + \tau_{n0}(p+p_1)} \tag{2.8}$$

with

$$\tau_{p0} \equiv [\sigma_p \nu_{th} N_T]^{-1} \quad , \quad \tau_{n0} \equiv [\sigma_n \nu_{th} N_T]^{-1} \tag{2.9}$$

and

$$n_1 \equiv n_i \exp\left(-\frac{E_c - E_T}{kT}\right) \quad , \quad p_1 \equiv n_i \exp\left(-\frac{E_T - E_v}{kT}\right) \tag{2.10}$$

with Eq.2.9 expressing the fundamental hole and electron lifetimes in relation with thermal velocity of charge carriers ν_{th}, trap concentration N_T, and capture cross-sections of holes and electrons, σ_p and σ_n, respectively. While Eq.2.10 defines statistical factors in terms of the intrinsic carrier concentration, n_i, the position of the conduction and valence band edges, E_c and E_v, respectively, and the energy of the trap , E_T.

As it follows from the derivation of the radiative and Auger lifetime expressions, the SRH lifetime τ_{SRH} is given by:

$$\tau_{SRH} = \frac{\tau_{n_0}(p_0 + p_1 + \Delta n) + \tau_{p_0}(n_0 + n_1 + \Delta n)}{n_0 + p_0 + \Delta n} \tag{2.11}$$

From Eq. 2.11 it can be seen that the SRH lifetime depends on carrier injection level and the dopant density (through n_0 and p_0), this in addition to the trap specific properties such as trap concentration, trap energy level and capture cross-section. This is the type of defects referred to as *deep level defects*. Furthermore, for such deep levels, the SRH lifetime can be simplified for the cases of low- and high- injection conditions such that we can express it as follows:

$$\tau_{SRH_{LLI}} = \tau_{p0} \quad \text{and} \quad \tau_{SRH_{HLI}} = \tau_{n0} + \tau_{p0}, \quad \text{for n-type silicon} \tag{2.12}$$

and

$$\tau_{SRH_{LLI}} = \tau_{n0} \quad \text{and} \quad \tau_{SRH_{HLI}} = \tau_{n0} + \tau_{p0}, \quad \text{for p-type silicon} \tag{2.13}$$

As can be seen from Eq. 2.12 and 2.13 the SRH lifetime increases with injection density and the greater difference between τ_{n0} and τ_{p0} the greater the increase in SRH lifetime will be.

2.2.0.4 Surface recombination

We have discussed that it is extremely difficult to attain perfect silicon crystals due to process contamination and stress in Section 2.1. Nevertheless, it is even harder to avoid the abrupt discontinuity created at the surface/interface of the crystal during wafer cut, which results in a large quantity of incomplete silicon bonds. Such dangling bonds give rise to a great density of electrically-active defects and therefore a very effective recombination centers. It is obvious that this recombination mechanism at the surface is then a special case of SRH recombination. And what makes it a special case is the fact that unlike SRH bulk centres these defects do not usually occupy a single energy level. Meaning that they are very often continuously distributed throughout the bad gap [32]. Therefore, the interface trap density $D_{it}(E_t)$ and the capture cross-sections $\sigma_n(E_t)$ and $\sigma_p(E_t)$ are dependent of the trap energy E_t. This is an extended formalism and is used to calculate the numerous defect levels existent in reality, while Eq. 2.8 still valid for individual interface traps. Thus, the overall surface recombination U_s is given by [36]:

$$U_s = (n_s p_s - n_i^2) \int_{E_v}^{E_c} \frac{\nu_{th}\, D_{it}(E_t)}{\frac{n_s + n_1}{\sigma_p(E_t)} + \frac{p_s + p_1}{\sigma_n(E_t)}}\, dE_t \tag{2.14}$$

Here, n_s and p_s stand for the electron and hole density at the surface and n_1 and p_1 are given in Eq. 2.10.

In contrast to the bulk recombination given by Eq.2.8, the surface recombination rate U_s is a rate per unit area instead of per unit of volume. This difference makes it necessary to define a new quantity for the characterization of surface recombination,

the so-called *surface recombination velocity S* and expressed by the following equation:

$$S \equiv \frac{U_s}{\Delta n} \tag{2.15}$$

Even though the S value is very often used in literature for surface recombination quantification, for a symmetrically passivated wafer with $S < 250$ cm/s [32, 37], Eq. 2.1 can be also related expressed as

$$\frac{1}{\tau_{eff}} = \frac{1}{\tau_{bulk}} + \frac{2S_{eff}}{W} \tag{2.16}$$

where following from Eqs. 2.14 - 2.16 can be written as

$$S_{eff} = \frac{1}{\Delta n} \frac{n_s p_s - n_i^2}{(n_s + n_1)/(\nu_{th}\, D_{it} \sigma_p(E_t)) + (p_s + p_1)/(\nu_{th}\, D_{it} \sigma_n(E_t))} \tag{2.17}$$

where S_{eff} is an effective recombination velocity that is also widely used for surface recombination characterization [4].

2.2.0.4.1 Surface passivation materials

The efficiency of solar cells is severely affected by recombination losses at the surface of the wafer [4]. In fact, record-breaking efficiencies in silicon cells have been partially the result of outstanding surface passivation levels achievements [4]. The application of certain techniques to reduce surface recombination is called *surface passivation* and it is a topic of extensive research up to this day [38]. There are primarily two types of passivation, the so-called *chemical passivation* and *field-effect passivation*. On the one hand, chemical passivation follows from the expression (2.14), where it is shown that the surface recombination rate, U_s, is proportional to the interface trap density, D_{it}. Accordingly, one way to decrease U_s is by the reduction of existing unsaturated atoms at the surface, for instance by means of atomic hydrogen introduction, thin dielectric or semiconductor films. On the other hand, the field-effect passivation also follows from Eq.2.14 which shows that the highest recombination rate is achieved when the ratio p_s/n_s is approximately equal to σ_n/σ_p [39]. Therefore, one can also reduce the surface recombination by decreasing the density of one carrier type at the surface, which can be achieved by two methods. One approach is the formation of an electric field penetrating the semiconductor surface modifying the surface carrier concentration. The second

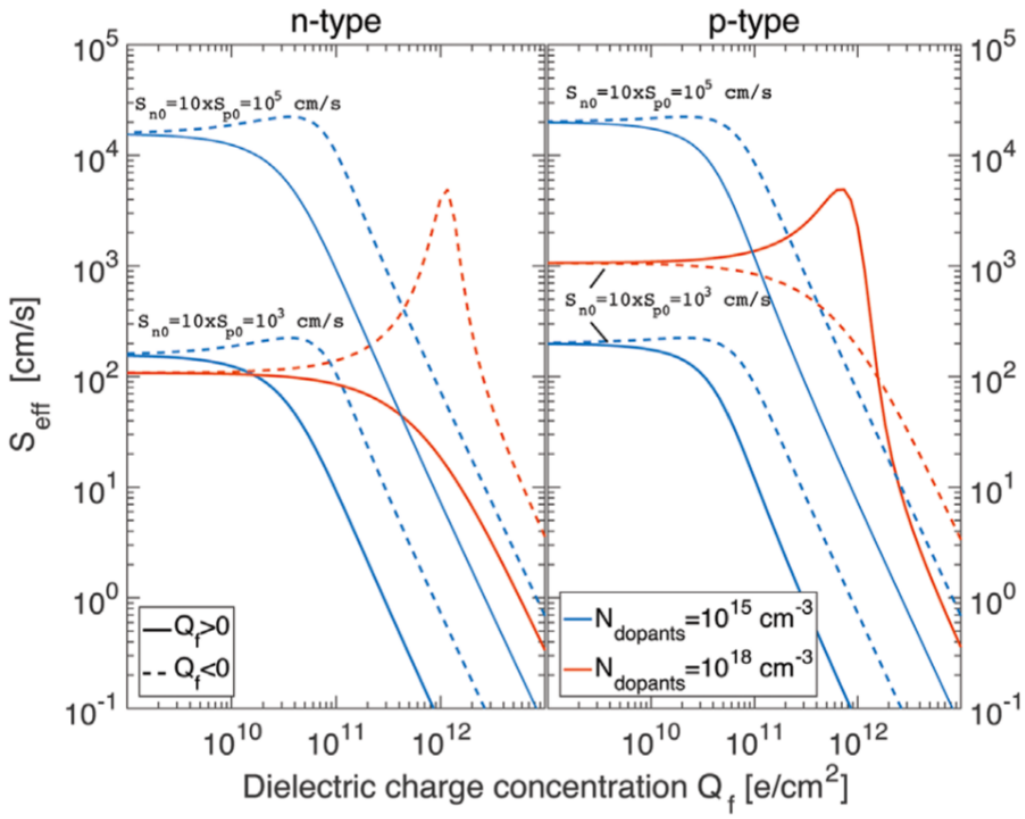

Figure 2.7: S_{eff} of n- and p-type Si with $\nu_{th}D_{it}\sigma_n(E_t) = 10 \times \nu_{th}D_{it}\sigma_p(E_t)$, $\Delta_n = 10^{15}cm^{-3}$ calculated from Eq.2.17 as a function of positive and negative Q_f, dopant concentration $N_{dopants}$, and uniform interface charge $Q_{it} = 10^{11}e/cm^{-2}$ reproduced from [4].

approach is the introduction of dopants in high concentrations of either carrier type near the surface, which will form a gradient of charge carriers near the surface. In this review however, we will only pay attention to that case where the field-effect is achieved by the formation of an electric field by dielectric material fixed charge, Q_f.

An insightful simulation on the effect of the dielectric-material fixed charge in the effective recombination velocity, S_{eff}, firstly presented by Dingemans *et al.* in [37] and extended by Bonilla *et al.* in [4] is shown in Figure 2.7. From these results we can conclude that the effect of Q_f in the field-effect passivation is specially prominent for values of $Q_f > 10^{11}$ cm^{-2}. Furthermore, it is evident from the same figure that when $Q_f > 0$ the passivation is expected to be better than when $Q_f < 0$. The reason of the latter being that capture velocity of electrons is higher compared to that of holes which is commonly observed at dielectric/silicon interfaces [4].

However, speaking in general terms the effectiveness and suitability of a passivation material depend on three key characteristics:

1. **Characteristics of the wafer to be passivated:** Doping type and silicon resistivity.
2. **Physical properties of the passivation material:** Thermal/UV/long-term stability, parasitic absorption, refractive index, fixed charge and lattice constant, among others.
3. **Processing requirements:** Surface cleaning and synthesis methods.

In this section the most applied surface passivation dielectric-materials in industry are reviewed, and the overall advantages and disadvantages of each method are described. It should be noted however that this review is intended to give the reader a broad but concise idea of the characteristics of these materials and that for more detailed information dedicated literature related to these topics should be reviewed, such as Refs. [4, 37, 40] and references therein.

◇ **SiO_2**

SiO_2-Si interfaces are well known for their extreme intrinsic quality. In fact, since the early stages of the metal-oxide-semiconductor (MOS) technology development this quality has been taken advantage of and studied extensively [41]. One of the benefits of SiO_2 on Si amongst others is its passivation capability, which have been heavily exploited in the context of silicon solar cell [4, 42, 43, 44, 45, 46]. In recent years many literature articles have shown a regained attention in SiO_2-based passivation techniques. Extraordinary levels of passivation have been demonstrated with these techniques primarily by the application of external charges to the dielectric or by deliberate introduction of H species [47, 48, 49, 50]. However, there are some limitations to this material so a list of the summarised of advantages and disadvantages of SiO_2 is presented in the following:

Advantages -High level of chemical passivation on both *p*-type (S_{eff} = 7.01 cm s^{-1} [51]) and *n*-type (S_{eff} = 0.17 cm s^{-1} [49, 50]) silicon over a large range of doping levels.
-The passivation level can be increased by the application of capping layers of SiN_x or Al_2O_3 [48].

-It has been synthesised using low temperatures by means of atomic layer deposition [52]

Disadvantages -Low level of intrinsic field-effect passivation (low fixed charge (Q_f) usually in the range of $10^{10} - 10^{11}$ cm^{-2} [37]).
- The passivation achieved by low-temperature synthesis is significantly lower than the one obtained by thermal oxidation processes.
-Thermally grown SiO_2 is not very suitable for *p*-type Si rear passivation. This is due to cost, complexity and possible detrimental effect under high temperature conditions on the bulk quality. Nevertheless, SiO_2/SiN_x stacks had been considered [37].

◇ ***a*-SiN$_x$:H**

Amorphous-silicon nitride (*a*-SiN$_x$:H or SiN$_x$ for brevity), by plasma-enhanced chemical vapour deposition (PECVD) is by far the most widely used front passivation technique in crystalline silicon (*c*-Si) photovoltaics [4]. Extensive research has been carried out on SiN$_x$ properties for PV since early 90's when the advancements in the plasma deposition were made. From there on SiN$_x$ has been climbing up to become the number one technology in the market, nevertheless there are also some issues related this material which need to be kept in mind. Within its advantages and disadvantages we can find the following:

Advantages -Extraordinary passivation can be achieved in both *p*-type and *n*-type Si, as low as 0.67 cm s^{-1} [53] and 0.17 cm s^{-1} [54] S_{eff} values have been achieved, respectively.
-Tunable optical properties are reflected in high quality AR coatings from SiN$_x$ [37].
-The relatively high hydrogen content in SiN$_x$ films introduce H atoms to the bulk material during firings, which in turn passivate bulk defects.
-N-rich SiN$_x$ are highly thermally stable as needed for cell processing. In addition they can be useful as capping layers on Al_2O_3 and other materials.

Disadvantages -Poor etchability, limiting the chemical-etching usual procedures for local openings in solar cell fabrication.

-High absorption in the UV range of the sun spectrum, which reduces the short-circuit current of the cell.
-Si-rich SiN_x films are needed for optimal surface passivation, however N-rich SiN_x exhibit higher thermal and chemical stability.
-N-rich SiN_x films are necessary to acquire the benefits of a field-effect passivation ($\sim 10^{12}$ cm^{-2}).
-The passivation quality is severely diminished during long-term annealing treatments.
-It requires careful optimization of the plasma deposition parameters to obtain the best possible quality passivation.
-Not suitable for *p*-type Si rear passivation due to inversion layer shunting.

♢ *a*-Si:H

Hydrogenated amorphous silicon (*a*-Si:H) is, in contrast to the previous dielectric materials, a semiconductor. Because of this, its successful application as passivation material in solar (i.e be able to provide AR and insulating properties) *a*-Si:H requires to be used in conjunction with other materials. Even though this material has not been as popular as the previously reviewed materials it has some remarkable properties that can and have been recently exploited in literature [4, 37, 47, 55, 56] and will be summarised together with its limitations in the following:

Advantages -High quality interfacing with Si.
-Low temperature processing.
-High-level level passivation can be achieved in both *p*-type (S_{eff} = 3.1 cm s^{-1} [57]) and *n*-type (S_{eff} = 0.06 cm s^{-1} [47]) Si.

Disadvantages -Parasitic absorption effect.
-Very low thermal stability during high-temperature processes. This limits its use of *a*-Si:H in screen-printed solar cells.
-Non-significant field-effect passivation is achieved by intrinsic *a*-Si:H ($Q_f \sim +3\text{x}10^{12}$ cm^{-2}).
-Requires the adoption of stacking techniques to make it feasible for high efficiency solar cell applications.

♢ Al_2O_x

Even though aluminium oxide (Al_2O_x) passivation properties were reported a couple of decades ago in 1989 by Hezel and Jaeger [58]. It just started to gain real interest after 2004 [59] by the introduction of Al_2O_x synthesized by atomic layer deposition (ALD) and PECVD. Since then a huge number of publications have emerged exploring its properties [37, 40, 60, 61, 62]. One remarkable property of Al_2O_x films is its negative charge, which is very advantageous to *p*-type silicon-surface cells compared to the widely used SiN_x and SiO_2 which display positive charges that lead to shunting losses [63]. This property together with all the advances in the optimisation of Al_2O_x deposition methods have led to the adoption of this technology in almost 100 % of the market share, leaving less than 5% share to other technologies [21]. The most relevant characteristics of these films are listed below:

Advantages -Very low recombination velocities have been achieved (S_{eff} = 0.95 cm s^{-1} [64] and S_{eff} = 0.45 cm s^{-1} [65], for *p*- and *n*-type Si, respectively).
-High field-effect passivation is achieved because of its intrinsic fixed charges ($Q_f \sim -5x10^{12}$ cm^{-2}).
- Al_2O_x and Al_2O_x/SiN_x can be used to replace Al-backsurface field (Al-BSF) leading to:
1. Lower surface recombination
2. Improved internal reflection
3. Reduced wafer bow in thin wafers
- For *n*-type Si cells Al_2O_x negative Q_f has served as an excellent p^+ emitter passivation material.
-The application of ALD Al_2O_x allows precise thickness control and uniformity over large deposition areas. In addition it requires relatively low substrate temperatures ($\sim$ 100- 350 °C) and can produce multilayer structures.
-No significant parasitic absorption occur since only light with wavelengths less than 200 nm is absorbed by Al_2O_x.

Disadvantages -Low growth rate which is closely related to the substrate temperature.

-Deposition parameters need to be controlled rather carefully to achieve optimal passivation effect.
-In order to activate the passivation, annealing treatments are required (optimal values were found to be 350 - 450 °C [40]).
-The passivation level decreases with injection levels $> 10^{15}$ cm^{-3} reflecting Auger recombination.
- Passivation dependence on injection level is significantly higher in n-type Si than in p-type. This has been explained to be due to the negative Q_f which enhances recombination in the inversion layer.
-The passivation decreases after firing (∼800 °C for few seconds) however is generally stable for screen printed solar cells or simply solved by the application of capping layers in industrial processes [21].

2.3 Characterization techniques

In this section it is the author's intention to supply information about the principles of operation of several experimental techniques that were applied to characterise the materials of interest. On the one hand a collection of junction spectroscopy and/or junction-based techniques are reviewed. These include some of the most sensitive and widely used approaches for deep-level defect characterization such as the deep level transient spectroscopy and some other more basic but equally important methods such as capacitance-voltage and admittance spectroscopy. On the other hand, an explanation about one of the most extensively used non-destructive methods for minority carrier lifetime measurements, the microwave photo-conductance decay method, is described.

2.3.1 Junction-based characterization

Since the 1970's a wave of material characterization techniques utilising semiconductor junction devices arose [66]. The test devices for the characterization include Schottky barrier diodes and p-n structures. These structures allows us to take advantage of the carrier depleted region in their junctions to more accurately control the occupancy of defects producing energy levels within the band-gap and to detect small changes produced by the scarce carriers in there present for characterization [67].

Throughout this work the most commonly used structure for electrical characterisation was the Schottky barrier diode whereby a metal comes into contact with a semiconductor to form the junction. So, for our measurements, the Schottky diode was prepared under clean-room conditions by firstly evaporating 1 mm diameter circles of Au (diodes) on top of *n*-type silicon samples though a shadow mask. Then, Al ohmic contact was evaporated onto the backside of the silicon samples. Lastly, we used ceramic substrates with gold strips on top to hold the samples by gluing with silver ink the ohmic contact side of the sample to a few Au strips and then bonding a gold wire from the diode to another Au strip. A schematic of the finished diode is presented in Figure 2.8. A very similar structure was used for the *p*-type silicon cases, but with the substitution of Au for Ti to form the Schottky barrier. In addition, when the minority carrier transient spectroscopy (MCTS) technique was used a small un-evaporated area was left open on the backside of the sample to allow optical excitation.

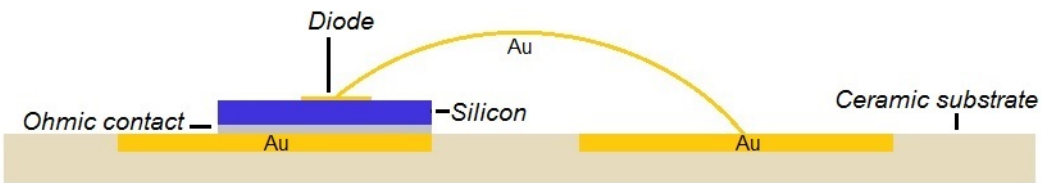

Figure 2.8: Schematic of the prepared Schottky diodes.

2.3.1.1 Capacitance-voltage techniques

Capacitance-voltage (CV) characterization is one of the most commonly applied techniques in the semiconductor industry. This technique allow us to measure various characteristics [67, 68, 69]:

1) Ionized dopant concentrations, which in the shallow-dopant case equals the carrier concentration.

2) The depletion region width.

3) The electric-field distribution.

4) The built-in voltage .

The principle used in the CV technique is based on the dependence of the depletion region with respect to the applied voltage. The capacitance (C) is measured under a small ac signal, of high frequency, usually in the range of 10mV to 100mV and 1 MHz, respectively. Then it is possible to calculate the capacitance given by the following

relation:

$$C = -\frac{dQ}{dV} \tag{2.18}$$

where Q is the semiconductor charge and V is the junction voltage. An impedance analyser measures the resulting ac current and from the complex impedance extracts the capacitance value. Now, when the diode is under reverse bias i.e. a positive voltage is applied to the n-type silicon the total voltage across the structure is

$$V = V_{bi} + V_{bias} \tag{2.19}$$

where V_{bias} is the applied voltage and V_{bi} is the built-in voltage. Furthermore, we can relate the measured capacitance with dielectric permittivity (ε) and depletion depth (W) by the equation

$$C = \frac{\varepsilon_0 \varepsilon_s A}{W} = qAN(W)\frac{dW}{dV_{bias}} \tag{2.20}$$

where ε_0 and ε_s represent the vacuum and semiconductor permittivity, respectively. A represents the area of the diode and N the doping concentration. From Eq.2.20 it is evident that the only way that Q can vary with applied voltage is by expansion or contraction of the depletion region. Moreover, from Eq. 2.20 we can solve for acceptor or donor concentrations ($N_A^- \mid N_D^+$) in the following manner

$$N(W) = -\frac{C^3}{q\varepsilon_0 \varepsilon_s A^2 (dC/dV)} = \frac{2}{q\varepsilon_0 \varepsilon_s A^2 (d(1/C^2)/dV)} \tag{2.21}$$

Furthermore, providing that the doping is uniform, it is possible to plot $1/C^2$ against V_{bias} to generate a straight line whose slope relates to $N_A^- \mid N_D^+$ an intercepts with V_{bi} on the voltage axis. However, it needs to be kept in mind that Eqs. 2.19 - 2.21 only hold when absolutely depleted regions are assumed and since this is not the real-life case, the so called *Debye tail* should be taken into consideration for an adequate deep-level characterization [67].

2.3.1.2 Deep level transient spectroscopy

Deep Level Transient Spectroscopy (DLTS) is a powerful and efficient technique used for characterizing deep level impurities in semiconductors i.e impurities such as the ones described in Section 2.2. Even though publications on transient measurements of deep states started earlier, the first clear experimental introduction of the measurement

principles was published by Sah *et al.* [70] in 1970. Afterwards, D. V. Lang [71] in 1974 introduced what is now the widely used DLTS method, which is an analogue signal processing technique of what was published before. It uses the capacitance of a p-n junction or a Schottky barrier as a probe to measure the changes in charge state of a deep-level. This technique is very effective at analysing deep states in a quick and complete form. It can be used to characterize majority and minority carrier traps. Furthermore, information about the trap's concentration, energy and capture cross-sections can be obtained with this technique [67, 69].
The full spectroscopic analysis is in general the result of three simple steps:
1. Free carriers are introduced by either electrical or optical methods to fill the deep traps.
2. Subsequent thermal emission processes give rise to a transient response in capacitance.
3. The transient is analysed by signal processing algorithms while the temperature is changed at a constant rate.

Usually in DLTS measurements the introduction of free carriers is achieved by applying a zero voltage bias pulse during a short period (typically 1 ms) to the normally reverse biased depletion region. This results in a shift in Fermi level and the filling of deep states by majority carriers. The diode is then restored to its basal reverse bias and by maintaining a high enough temperature the carriers are thermally re-emitted from the trap. This emission is monitored by small ($\sim$ pico-Farads) change in capacitance (ΔC). In DLTS the exponential change of capacitance is sampled at two times t_1 and t_2, typically in the range of 0.1 ms to 1s, time that is referred to as the *rate window*. The principle of the a capacitance transient measurement is presented in Figure 2.9.

According to the SRH model [34], the fraction of electron occupancy or occupation factor, f_T, in terms of: capture cross-sections $\sigma_n \mid \sigma_p$, capture coefficients $c_n \mid c_p$, thermal velocity ν_{th}, emission rates $e_n \mid e_p$, number of occupied traps by electrons n_T and number of empty traps $N_T - n_T$, is equal to

$$f_T = \frac{c_n n + e_p}{e_n + c_p p + c_n n + e_p} \tag{2.22}$$

with

$$c_n = \sigma_n \nu_{th} \qquad \text{and} \qquad (c_n + e_p)(N_T - n_T) = (e_n + c_p n) n_T \tag{2.23}$$

Thus, for the emission of majority carriers i.e. electrons in n-type material or holes

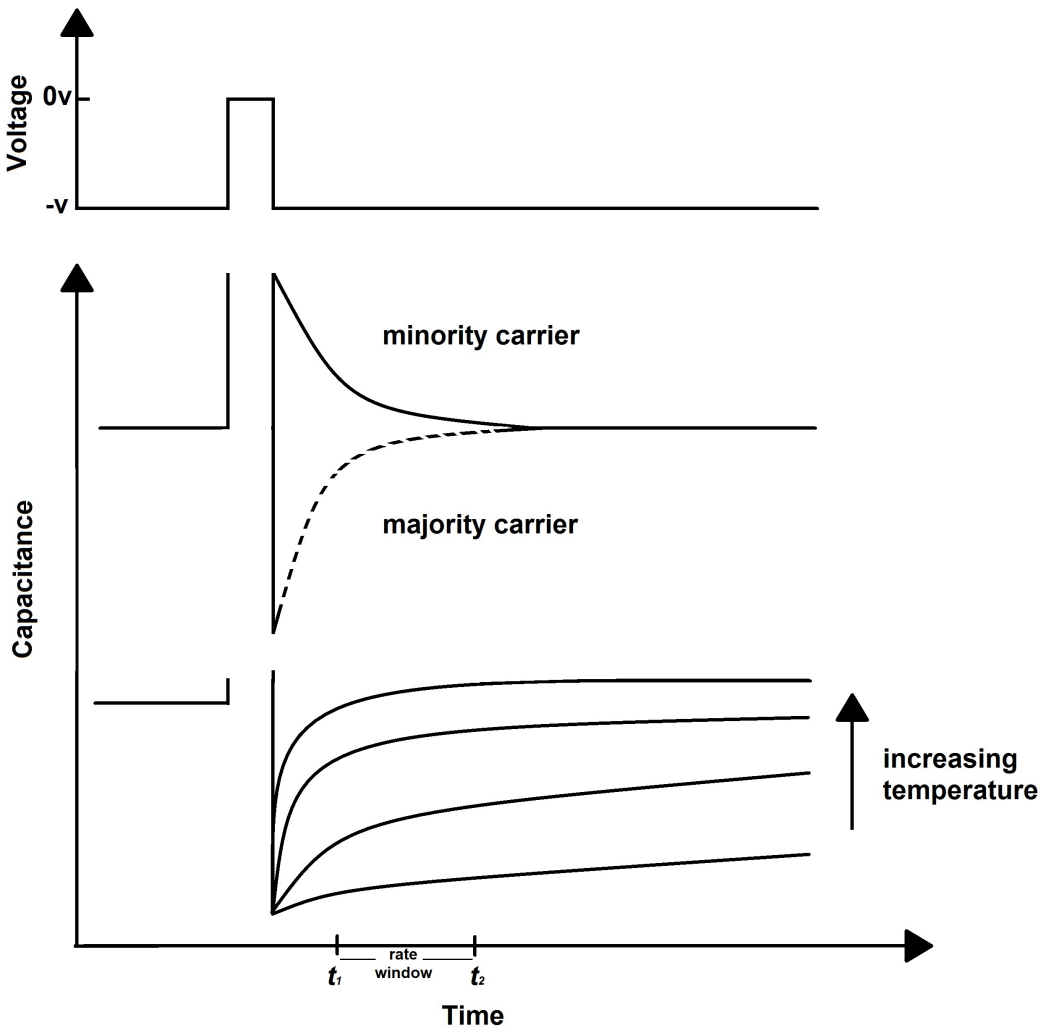

Figure 2.9: Principle capacitance transient measurements.

in p-type we have

$$\Delta C(t) = \Delta C_{tot}(1 - e^{-t/\tau}) \tag{2.24}$$

while for minority carrier emission (opposite than majority carriers in p- and n-type materials)

$$\Delta C(t) = \Delta C_{tot}(e^{-t/\tau}) \tag{2.25}$$

In order to calculate the emission rates of the carriers using thermal energy the most common relationship is given by

$$e_n(T) = \sigma_n \nu_{th} N_c e^{-\Delta_G/kT} \tag{2.26}$$

where k is the Boltzmann coefficient, Δ_G is the Gibbs free energy change for ionization of the state per electron-hole pair. Since the time constant changes rapidly with temperature because of the k term, it is possible to plot the emission rate spectra (ΔC *vs* T) by varying the temperature. This occurs because a peak appears when the emission rate matches the system time constant i.e. when

$$\frac{1}{e_n} = \tau = \frac{(t_1 - t_2)}{\ln(t_1/t_2)} \tag{2.27}$$

giving as a result the DLTS spectrum. In addition, if the $\log(e_n/T^2)$ is plotted against $1/T$, a plot that is referred to as an *Arrhenius plot*, it is possible to obtain the activation energy E_a from the gradient of the line and A_n from the intercept with the vertical axis at $T = \infty$, and it is used to calculate the apparent capture cross-section. It most be clear however that the activation energy extracted from the Arrhenius plot is effectively the average of the defect's enthalpy (Δ_H) over the measured temperature range when the last is weakly temperature dependant. This enthalpy can differ rather significantly from the Gibbs free energy depending on temperature and the defect's entropy (Δ_S) according to $\Delta_G = \Delta_H - T\Delta_S$. Therefore, for an adequate defect characterisation it is precise to directly measure both $e_n(T)$ and σ_n at the desired temperature and use eq. 2.26. A realization of the idea of the DLTS technique is depicted in Figure 2.10. The DLTS method is a very useful tool for trap characterization, however its detectivity depends on the carrier concentration. Usually it is possible to observe and analyse results from samples with trap concentrations $> 10^{-4}n$. In optimal conditions of the system a detectivity $> 10^{-6}n$ is achievable. Noting that detectivity is linearly

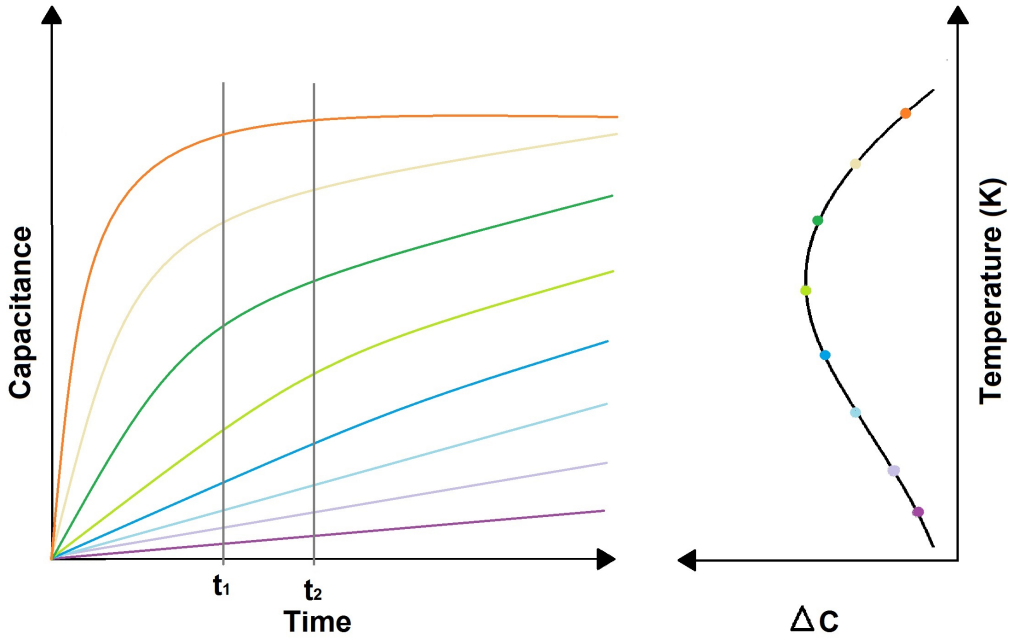

Figure 2.10: Realization of the DLTS idea.

proportional to carrier concentration. So, if we take a sample with 20 Ω· cm resistivity as an example, it would be possible to attain a detectivity of 10^{10} cm^{-3} defects with a conventional DLTS system [69].

2.3.1.2.1 Laplace deep level transient spectroscopy

Even though conventional DLTS has largely served to identify a plethora of defects throughout the years, a major limitation still exists on its application. This is its inability to distinguish between two levels whose emission rates are of similar values, where the core problem lays on the noise presence. Noting that high noise levels hinder the possibility of finding a unique solution to the de-convolution problem for superimposed transient separation [67, 69].

There is however a proven and elegant technique which was developed in the early 90's that has allowed high emission rate resolution in DLTS measurements [72, 73]. It is based on the application of the inverse Laplace transform to effectively translate the data from the time domain to the frequency domain to find an approximate singular solution. This method was firstly applied in Manchester in the year 1991. It was realised by the use of the widely known Tikhonov [74] regularization method together with the publicly available numerical algorithm CONTIN [75]. The first to discriminate as

much as possible the existence of multiple exponential components which arise not always from the defects but from the high measurement noise levels and the second to numerically perform the Laplace transformation. In consequence this method has become to be known as Laplace DLTS (LDTS).

It is important to note however that LDTS, different from conventional DLTS, analyses the samples at fixed temperatures and over a range of emission rates. Thus, multiple scans at different temperatures are required for completion of an Arrhenius plot.

Significant resolution improvements compared to conventional DLTS have been attained with this technique and has allowed for the characterization of defects in semiconductors which otherwise would have passed undetected. Such a case is clearly exemplified in publication No. 1 presented in Chapter 3 of this thesis.

2.3.1.3 Minority carrier transient spectroscopy

In accordance to the background theory of DLTS given in Ref. [71] it is also possible to measure minority as well as majority carriers emissions of the traps under investigation with this technique. And knowing that minority carrier capture in the low injection regime is the rate limiting process in recombination, its characterization becomes highly important.

In Ref. [71] the application of a forward pulse is shown to be used to populate the traps within the gap with minority carriers and the measurement of their spectra. For this forward biasing approach it is a common practice to study the materials using n^+p or p^+n structures instead of using p-n junctions or Schottky barriers. This is because the predominately extended depletion region to a single side of the junction given by the n^+p or p^+n structures allows for the assumption of being predominately injecting minority carriers during the forward pulse [67]. However, the interpretation of results from the latter technique can be ambiguous, and so, non-definitive [67, 76]. Therefore a much more relevant technique for minority carrier trap characterization also arose, and it is now referred to as Minority Carrier Transient Spectroscopy (MCTS). In this technique the minority carrier occupancy is promoted by optical means, where the utilised wavelengths are slightly above band-gap values. This technique's application was firstly described and applied by Hamilton *et al.* [77] in 1979 and further developed to what we now know to be the MCTS technique by Brunwin *et al.* [76].

The excitation light used during MCTS measurements can be applied either from the front of a Schottky semi-transparent diode or from the backside. Nevertheless, backside illumination should be prioritised whenever possible since it ensures almost

pure minority carrier occupancy of the trap states compared to the front light injection. This is because the latter would certainly create majority carriers within the depletion region that would then take part in the capture kinetics of the defect. Such situation can be almost completely avoided by the backside approach. Here given the appropriate conditions, the electron-hole pairs can be generated at a minority carrier diffusion length from the junction so that the depletion field would repel majority carriers, and only minority carrier would populate the states in the gap with big enough minority capture cross sections.

The MCTS technique has thus being largely exploited during the present work and the most relevant results will be shown in Chapters 3 and 4.

2.3.1.4 Admittance spectroscopy

Thermal admittance spectroscopy, also simply known as admittance spectroscopy (AS) is an uncomplicated but powerful junction-based technique that was first described more than 50 years ago on the basis of Schottky-Read-Hall theory [78]. Moreover, just as the DLTS technique, the AS technique detects the thermal emission of trapped carriers from a particular defect levels in the gap but with a few distinctions in methodology which will be discussed in this section. Nevertheless, prior to the explanation of its theoretical implications it is important to point out some advantages and disadvantages that AS poses over the widely used DLTS method.

On the one hand, AS advantages include 1) the possibility of probing much shallower states than DLTS [6, 79], 2) Since steady dc bias voltages are not necessary for AS as they are for DLTS, leaky diodes can still be characterised [6], 3) in samples where the temperature of interest falls in the freeze-out range (i.e where emission rates are very fast) and DLTS cannot probe them, AS oscillatory biasing can still modulate the trap occupancy to some extent and so the observation of the traps would be possible [6], and 4) given the simplicity of the technique it is very easy to set-up and carry out measurements [6, 67]. On the other hand however, DLTS has proven to be a very reliable tool for a more complete characterization of defects, which includes direct capture cross section and minority carrier occupancy measurements which are not possible with AS [6, 67]. However one more thing is worth noting, this is that for a long time the detectivity of DLTS has been known to surpass that of AS, nevertheless just this year claims about achievable similarities in this respect have been published by Bollman *et al.* in Ref. [5]. These results look quite promising, however it is now a matter of time to prove their validity.

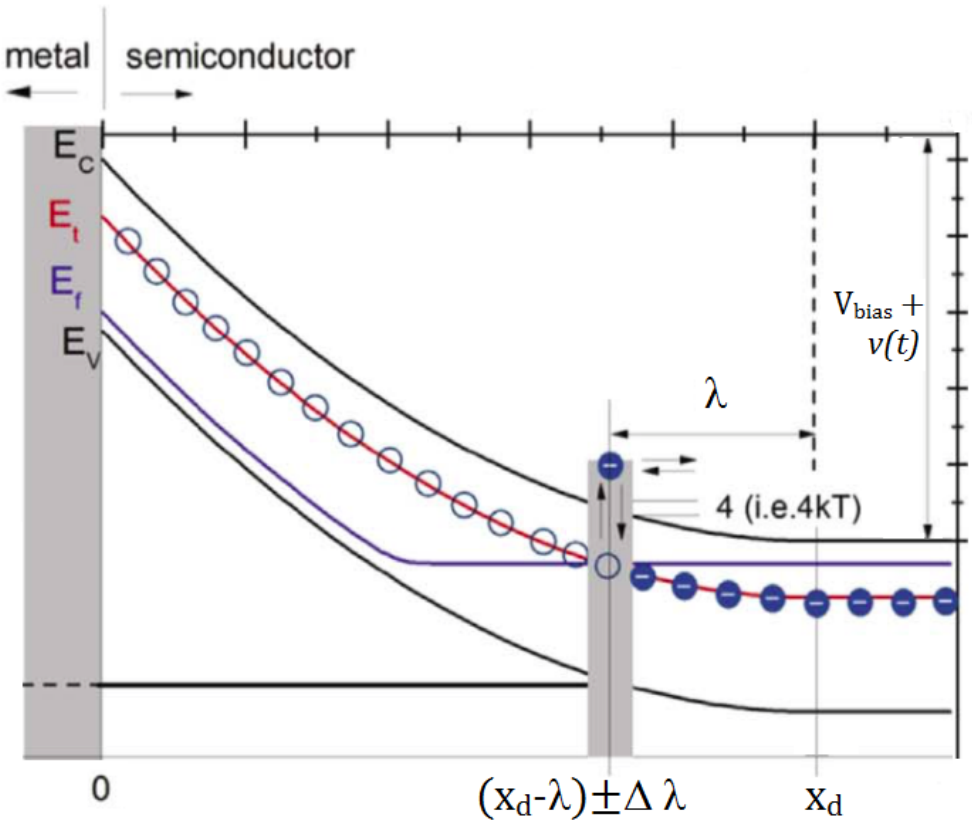

Figure 2.11: Band bending schematic representing the capture and emission of carriers from the trap, t, of energy, E_t, during oscillatory biasing, $v(t)$, mounted on a fixed dc reverse bias, V_{bias}. Adapted from [5].

We will now describe the AS method and introduce those key equations that lay its foundation for an adequate defect characterization, further details can be found in Refs. [6, 78]. Firstly, for this method sample preparation resembles that which is required for DLTS, i.e either Schottky barrier diode (SBD) or p-n junction fabrication. Then, an impedance analyser and a cryostat are required for admittance monitoring of the sample at various temperatures. Noting that well designed circuitry for low noise data acquisition and accurate temperature control are required for precise measurements.

In the AS method a sample is subjected to a small amplitude ac signal, $v(t)$, of distinct frequencies, f_t, which modulates the Fermi level and so the free-carrier trap occupancy in the gap as schematically represented in our given example of a SBD on n-type material [2] in Figure 2.11. Such modulation is reflected in changes in admittance, $Y(\omega)$, whenever there exists a trap level disturbing the angular frequency of the test

[2]Note that similar arguments apply for SBD on p-type materials and p-n junctions.

signal $v(t)$. The AS technique can be applied either on a frequency- or temperature-scan basis [6], similar to LDLTS and conventional DLTS, respectively.

So, we began defining the admittance as

$$Y(\omega) = G(\omega) + jS(\omega) \tag{2.28}$$

and the susceptance as

$$S(\omega) = \omega\, C(\omega) \tag{2.29}$$

where ω equals the angular frequency ($2\pi f$), $C(\omega)$ is the capacitance per unit area, and $G(\omega)$ stands for conductance, as per convention. Then we relate these, as derived in Ref. [6], to the mean trap depth, $\bar{x}_t$, where the trap's energy E_t crosses the Fermi level E_F, the depletion region edge depth, x_d, as well as with the trap and dopant concentrations N_t and N_d, respectively, and thus having

$$Y(\omega) = \left(1 - \frac{\bar{x}_t}{x_d}\right) \frac{\omega^2 g_t}{f_t^2 + \omega^2} + j\,\omega \left[\frac{\varepsilon_s \varepsilon_0}{x_d} + \left(1 - \frac{\bar{x}_t}{x_d}\right) \frac{f_t g_t}{f_t^2 + \omega^2}\right] \tag{2.30}$$

where

$$f_t = f_0 \left(1 + \frac{\bar{x}_t}{x_d} \cdot \frac{N_t}{N_d}\right), \tag{2.31}$$

and

$$g_t = f_0 \frac{\varepsilon_s \varepsilon_0}{x_d} \cdot \frac{N_t}{N_d} \tag{2.32}$$

with the relaxation rate constant for majority carriers on a n-type sample defined as $f_0 = c_n + e_n = \tau^{-1}$. A couple of important observations with respect to the latter value must however be mentioned. These are: firstly that the value $\bar{x}_t$ considered here is assumed constant, hence $\bar{x}_t = x_d - \lambda$, where λ is defined as $\lambda = \sqrt{(2\varepsilon_s\varepsilon_0/q^2 N_d)/(E_F - E_t)})$ and depicted in Figure 2.11, and secondly, that here we also assume a uniform free carrier distribution in the depletion region making possible to write $c_n(\bar{x}_t) = e_n$ and hence $f_0 = 2e_n$. However, this latter definition of f_0 has many times been overlooked in literature where authors directly assume $f_0 = f_t$ which strictly speaking only holds for those cases when $\bar{x}_t/x_d \approx 0$ according to Eq. 2.31.

It then follows from Eqs. 2.28 - 2.30 that the capacitance per unit area, is given by the imaginary part of $Y(\omega)$ as

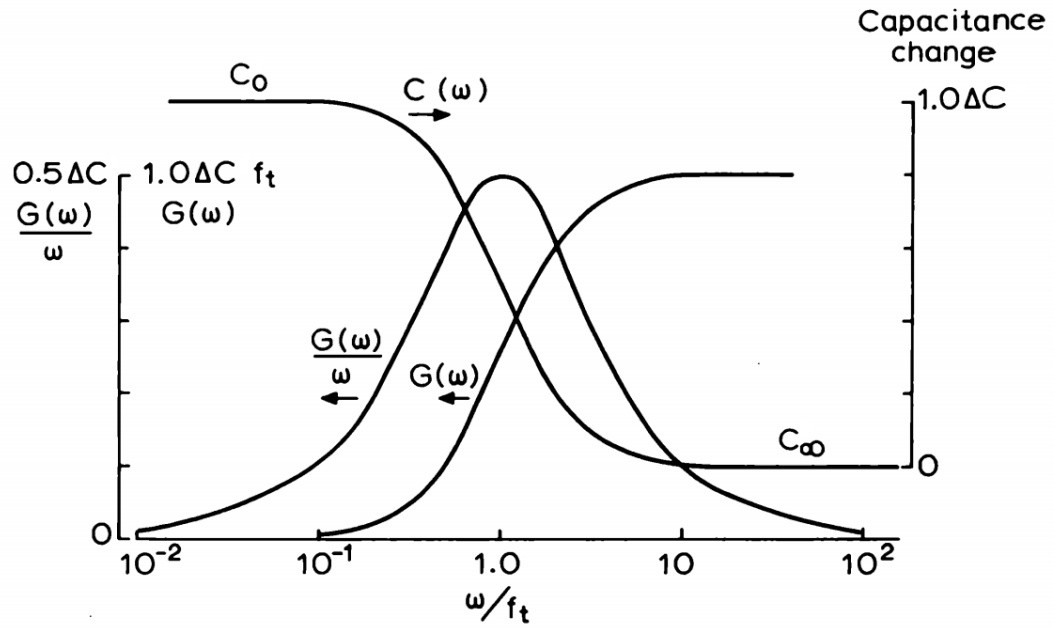

Figure 2.12: $C(\omega)$, $G(\omega)$ and $G(\omega)/\omega$ curves calculated from Eqs.2.33 and 2.36 plotted as a function of the normalized angular frequency ω/f_t. Adapted from [6].

$$C(\omega) = \frac{\varepsilon_s \varepsilon_0}{x_d} + \left(1 - \frac{\bar{x}_t}{x_d}\right) \frac{f_t g_t}{f_t^2 + \omega^2} \tag{2.33}$$

with its limits on the high frequency ($\omega \gg f_t$), C_∞, and low frequency ($\omega \ll f_t$), C_o, regimes as

$$C_\infty = \frac{\varepsilon_s \varepsilon_0}{x_d} \quad \text{and} \quad C_o = C_\infty + \Delta C, \tag{2.34}$$

respectively, where

$$\Delta C = \frac{g_t}{f_t}\left(1 - \frac{\bar{x}_t}{x_d}\right). \tag{2.35}$$

On the other hand, also as defined in Eq. 2.28, the conductance is given by the real part of $Y(\omega)$ as

$$G(\omega) = \frac{\omega^2 g_t}{f_t^2 + \omega^2}\left(1 - \frac{\bar{x}_t}{x_d}\right) = \Delta C \cdot f_t \left(1 + \frac{f_t^2}{\omega^2}\right).^{-1} \tag{2.36}$$

So, given the simplified Eqs. 2.33 and 2.36 we are now able to calculate values for $C(\omega)$ and $G(\omega)$ and relate them to experimental observations. Exemplary curves are

shown in Figure 2.12. From a physical process perspective then we can relate the observed behaviour of $C(\omega)$ and $G(\omega)$ at low frequencies ($\omega \gg f_t$) behaving as expected from an ideal RC circuit, i.e having the voltage dependent current ($i(t) = Y(\omega)v(\omega)$) leading the applied voltage $v_t(t)$ by $\pi/2$, since the deep levels are responding in-phase with $v_t(t)$. However, as the frequency increases to reach $\omega \approx f_t$ the traps cannot respond instantaneously any more to $v_t(t)$ and so the flow of charge to and from the traps now lags behind it reducing the initial $\pi/2$ lead from $i(t)$ and advancing it to match the phase of $v_t(t)$. This effect translate into a reduction of the imaginary component of $i(t)$ which we term capacitance but increases the the real component that we call conductance, effects that are appreciable in 2.12. Furthermore, from the same figure it is possible to observe that at a half-height of each step ($C(\omega)$ and $G(\omega)$) and according to calculations the value of ω equals that of f_t. This in addition to the calculation of $G(\omega)/\omega$ on the same figure where it is shown that for this curve a peak with maxima, $G(\omega)/\omega|_{max}$, at $\omega = f_t$ of height $\Delta C/2$ occurs. This peak maxima then corresponds to the emission rate of the trap whose logarithm can be plotted against the reciprocal of the measured temperature to obtain the activation energy, E_a, and the apparent capture cross-section. Furthermore, by measuring $G(\omega)/\omega|_{max}$ we are able to determine N_d from the combination of Eqs. 2.31 , 2.32 and 2.35 such that

$$\frac{\Delta C}{C_\infty} = \frac{N_t}{N_d}\left[\frac{1-(\bar{x}_t/x_d)}{1+(\bar{x}_t \cdot N_t/x_d \cdot N_d)}\right] \tag{2.37}$$

and moreover, given the conditions $N_t \ll N_d$ and $\bar{x}_t/x_d \approx 0$ Eq. 2.37 can be further simplified to give

$$\frac{\Delta C}{C_\infty} = \frac{N_t}{N_d}. \tag{2.38}$$

Consequently provided adequate set-up experimental conditions we are left with enough information to take advantage of the AS method to characterise the shallow or deep trap under investigation through Eqs. 2.33, 2.36 and 2.37. Results taken from careful measurements using this technique will be introduced in Chapter 4.

2.3.1.5 Reverse recovery method

One of the very first methods for recombination rate quantification is the pulsed recovery diode current method which is now know as the Reverse Recovery method (RR) [68, 78, 80, 81]. First described by Pell in 1953 [80] and subsequently expanded by Kingston [81] and Lax *et al.* [82] in 1954, the method was devised to capitalise on the

leakage current commonly present in p-n junction devices. In these devices the current cannot respond instantaneously to abrupt changes in polarization, thus making some carriers to get "stuck" or stored during a period of time until either the electric field sweep them out, or they recombine. Thus by simply studying the current response of a p-n junction during an abrupt change from forward to reverse polarisation we are able to determine the carrier's recombination rate of the device [83]. Furthermore, this technique does not restrict sample geometry which largely increases its field applicability [80, 83].

Once more the experimental set-up for this technique is rather simple. It can be realised with the use of any modern signal generator and oscilloscope equipment to generate the pulsed biasing on the diode and then record the current response through a series resistance (See Figure 2.13 inset). In fact, by the use of similar equipment as early as in 1971 Dean *et al.* [83] demonstrated its applicability for lifetime measurements of $\approx$1 ns, whereas Mauch *et al.* [84] just last year claimed that some modifications to the technique allow the achievement of $\approx$ 100 ps resolution. Even though this technique is much more applied for power device characterization which strive for the achievement of faster switching conditions we can still take advantage of it for our characterisation purposes in this work. Typical current-time and voltage-time responses are shown in Figure 2.13. There, a forward current, I_f, flows through the device up to time $t = 0$ during a forward voltage pulse producing V_f. At time $t = 0$ the forward current is switched to reverse current, I_r, with $I_r \approx (V_r - V_f)/R$. At this point the carrier density at the junction begins to drop, and continues to do so until time t_s which is defined as the storage time. After time t_s is reached a reverse-biased depletion region begins to form at an exponential rate until it reaches its steady-state value. This last process is retarded by the time it takes to extract the remaining carriers injected during the forward biasing and the time needed to charge up the depletion capacitance [83].

From the current response then it is easy to distinguish two key phases, the storage phase, $0 \leq t \leq t_s$, and the recovery phase, $t > t_s$, which can be represented by an exponential of time constant, T_r. The storage time which is often well defined can then be related to the effective minority carrier lifetime, τ_{eff} [68], by the expression [85]

$$t_s = \tau_{eff}\left[\ln\left(1+\frac{I_f}{I_r}\right) - \ln\left(1+\frac{Q_s}{I_r\tau_{eff}}\right)\right] \tag{2.39}$$

So, if we assume that the semiconductor charge, Q_s, does not depend on I_r or I_f,

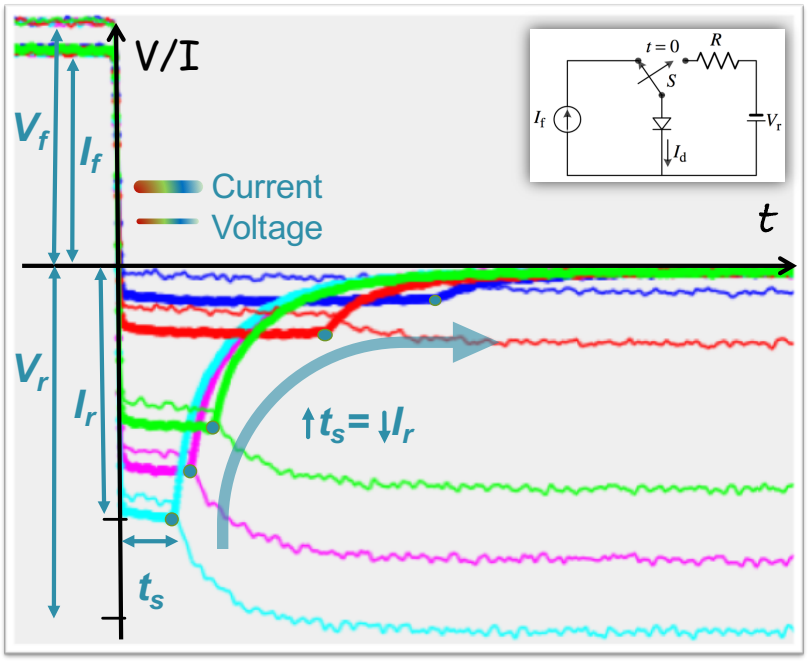

Figure 2.13: Current and voltage curves measured from a n^+p sample with decreasing I_r (i.e. decreasing V_r) from bottom to top, demonstrating the reverse recovery effect. (Inset) Reverse recovery circuit schematic.

which is often the case provided $I_r \ll I_f$ [68, 85], then the term $Q_s/I_r\tau_{eff}$ can be considered constant. Furthermore, the effect of heavily doped emitter and surface recombination can be virtually eliminated by maintaining the condition $I_r \ll I_f$. Therefore plotting t_s against $\ln(1+I_f/I_r)$ as shown in Figure 2.14 will have a slope value equal to the τ_{eff} and an intercept equal to $1+Q_s/I_r\tau_{eff}$.

Even though the RR method is not the most accurate method for lifetime characterisation, specially in the high injection and low lifetime regime, it still being used because acceptable accuracy is attainable under normal experimental conditions [68].

2.3.2 Microwave photo-conductance decay

Within the well-established methods for effective lifetime testing of silicon material there is the Microwave photo-conductance decay (μPCD) method. This method, as its

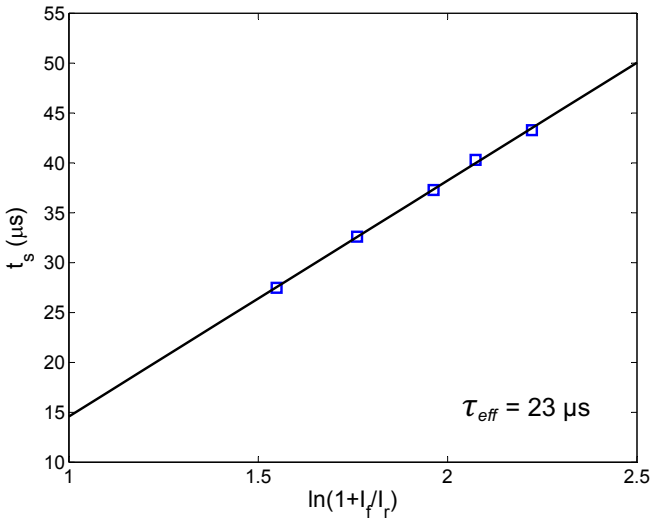

Figure 2.14: Storage time as a function of $\ln(1+I_f/I_r)$ measured from a n^+p sample.

name implies, is based in the photo-conductance decay technique developed in 1955 by Stevenson and Keyes [86], whereby electron-hole pairs are optically generated and their post-excitation decay is monitored as a function of time. Initially this monitoring was done through contacted samples and current monitoring, nevertheless the method has now evolved to a non-contacting method for convenience [68], which is the case of the μPCD technique. This is a very well known and accepted method for the reliability, simplicity and quickness of its measurements, which include high resolution over large mapping areas. For its application the sample preparation is also very simple, since any given silicon sample in the form of a slice of dimensions preferably bigger than 1.5 cm $\times$ 0.25 cm $\times$ 0.25 cm [68] and passivated with the material of choice [87] can easily be placed on the system's plate for measurements. It is still based on the optical excitation of a semiconductor, e.g. a LASER source, and the subsequent measurement of its change in conductivity, $\Delta\sigma$, with time.

So, by considering that the conductivity can be related to the electron and hole carrier mobilities, μ_n and μ_p, and excess carrier density, Δ_n and Δ_p, respectively, as well as to the effective lifetime [34, 86] as

$$\Delta\sigma = q(\Delta_n\mu_n + \Delta_p\mu_p) \approx \exp\left(-\frac{t}{\tau_{eff}}\right) \tag{2.40}$$

we can experimentally increase the conductivity of the sample by optically generating electron-hole pairs ($\Delta n + \Delta p$) with a light pulse and then measure the decay of the photo-conductivity in order to determine the recombination lifetime.

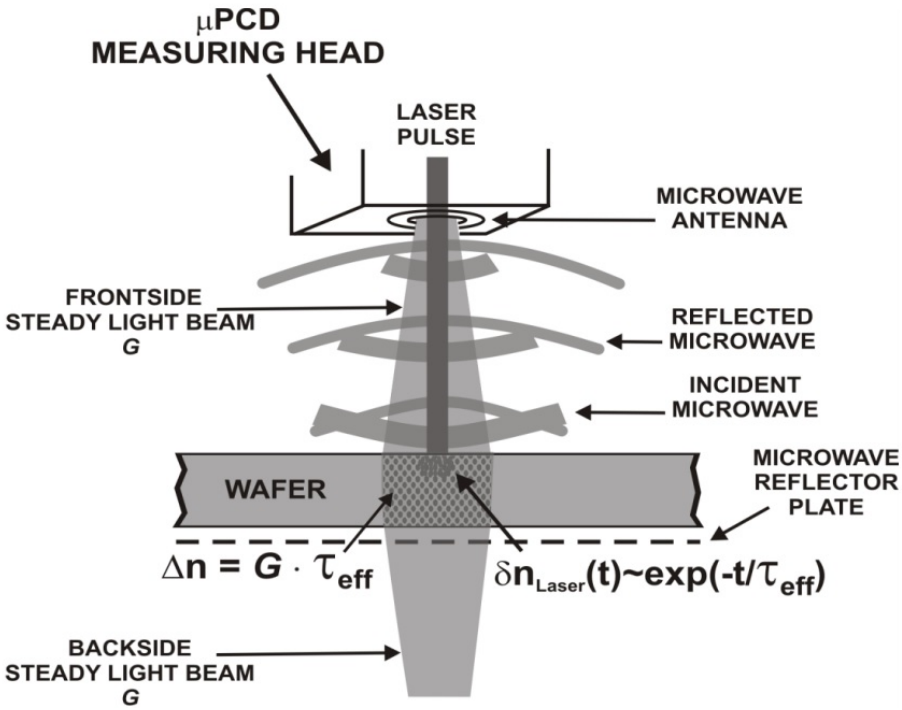

Figure 2.15: Schematic of a Quasi-steady-state microwave photoconductance decay system. Reproduced from [7].

For the studies reported in this thesis the system schematic depicted in Figure 2.15 was used. The pulsed LASER at the top is used to generate excess carriers which will modify the conductivity of the sample as per shown in Eq. 2.40. The conductivity changes are then detected by microwave reflection (see Fig. 2.15), whose reflected, $P(\sigma)$, and incident, P_{in}, power ratio is proportional to the conductivity. So, perturbing the conductivity from its steady-state, σ, to $\sigma + \Delta\sigma(t)$ leads to a change in power, ΔP of the reflected power, which can be reduced to the form $\Delta P/P = C\Delta\sigma$, when $\Delta\sigma$ is considered small [88]. Nevertheless, it is important to remember that $\Delta\sigma$ is proportional to the sample resistivity and the excess carrier concentration, as well as those being related to the microwave propagation and skin depth [68, 88]. Thus making it of paramount importance for accurate lifetime measurements to consider the resistivity an excess carrier parameters of each sample. For instance during the use of high injection levels, the skin depth of the microwaves used for the photo-conductivity detection decreases with in creased carrier concentration which will not allow the microwave reflector to be reached causing measurement errors. Furthermore, at the low injection level regime deviations occur in the presence of a significant amount of trap levels. In such case the photoconductivity will exhibit a much longer decay time constant due to

trapping an will no longer be proportional to the recombination lifetime [88, 89]. So, even though the μPCD method has proved to be highly reliable some precautions still need to be taken when applying it [89].

CHAPTER 3

LIFETIME LIMITING DEFECTS IN PHOSPHOROUS-DOPED SILICON

Crystalline silicon since the early 50's has been, and will continue to be, for the close foreseeable future, the backbone of solar cell technologies [90]. These include *p*-type and *n*-type, mono- and multi- crystalline based cells. Tremendous efforts have been made by many research groups to push the limits of achievable efficiencies by process optimisation, cell architectures development and optimisation, passivation material developments and defect identification and deactivation, amongst others. Such efforts have opened the possibility to reach in some cases the so desired competitive prices demanded by consumers [11]. However, technology improvements continue to be one of the three a main cost reduction drivers, together with competitive procurement and an increase in project developers [11]. Technological improvements must however include high efficiency and high durability cells. One of the latest approaches to such improvements in the market has been to change their production lines from *p*-type based cells to *n*-type based cells.

Historically, as has happened to many other technologies, solar cell fabrication had its strongest development when it was mostly funded by and dedicated to space exploration. This particular scenario was then favourable for the application of *p*-type cells due to its higher resistance to radiation. However at present *p*-type silicon remains as the most widely used material for solar cells for terrestrial applications. This at the beginning worked reasonably well because of p-type silicon high electron mobilities and cheaper processing prices. Nevertheless some issues related to the properties of the material have become of greater importance in the past few decades when more research has been focused in the aforementioned technological improvements. Such issues include the light-induced degradation (LID) effect [30], the light and elevated temperature induced degradation (LeTID) [91] and higher relative susceptibility

to transition metals, amongst others [92]. These has given rise to an increased interest in the use of *n*-type based cells which do not suffer from such degradation effects or they are not as severe as the ones encountered in *p*-type based cells [92, 93].

In this chapter results from the author's investigations of some interactions between the light element impurities: carbon, oxygen and hydrogen in *n*-type silicon will be presented. In addition recent investigations on the trapping behaviour of oxygen-related bistable thermal double donors (BTDDs) in *n*-type material will also be given. All these results are presented in the form of published, or submitted for publication, articles. Such articles will be preceded by an overview of the publications and a literature review on carbon (Section 3.1.1), oxygen (Section 3.1.2) and hydrogen (Section 3.1.3) impurities in silicon. Recalling that since the earliest period of Si growth, oxygen was one of the first impurities to be recognised as technologically relevant, followed by multiple studies on carbon which were found to form a variety of electrically active complexes in Si and finishing with the current wave of extremely popular atomic hydrogen in what Newman referred to as the "hydrogen period" [94].

Accordingly, in Section 3.2 a careful and detailed study on the carbon, oxygen and hydrogen interactions in silicon is presented in the form of four published articles. Firstly, a conference paper presented at the 2016 IEEE 43rd Photovoltaic Specialists Conference (PVSC) is given as Publication No.1. Its contents include preliminary results and hypothesis firstly devised from a set of Cz, C-Cz and Fz samples of known high-[O_i] and injected with atomic hydrogen. It was observed by means of DLTS, LDTLS and MCTS analysis, the formation of a set of electron (E_1-E_4) and hole (H_1-H_4) traps. So, their thermal behaviour, identified relationship to hydrogen and oxygen, proposed potential complex structure, and demonstrated effect on the minority carrier lifetime after wet etching is then presented in the paper. However, in this initial argument it was proposed that the complex responsible for the degradation was formed by a single hydrogen atom and two oxygen atoms (oxygen dimer). Such argument was later to be corrected by further investigations presented in publication No.2. In this publication it is demonstrated that not only hydrogen and oxygen were involved in the formation of the complex but also substitutional carbon, and that a single oxygen atom was present in the process. Strong evidence provided by infrared-absorption spectra was obtained to link the formation of CO complexes prior to COH-related traps (H_1 and H_2) formation after hydrogen injection. In addition, density functional calculations provided by our collaborators at the University of Aveiro in relation to our experimental results were presented to propose a COH minimum energy atomistic

structure, which give rise to the introduction of an acceptor level at an energy similar to the experimentally determined one. Further in this paper we attribute the source of the demonstrated lifetime degradation after hydrogen injection to the H_1 and H_2 traps, supported by throughout studies of their electrical properties characterisation.

In publication No.3 strong evidence of a detrimental impact on minority carrier lifetime on the *n*-type Si:O+C samples caused by the COH complex formation after silicon nitride deposition is presented. In this article our previous hypothesis of the widely used SiN_x:H passivation/antireflection coating being harmful for the material was confirmed. It is shown that even though low temperature treatments were able to momentarily dissociate the COH complexes, these would reform upon cooling when enough H^- was present. Furthermore, careful studies on the electrical properties of the not so harmful electron traps (E_1-E_4) is presented. It is argued, however, that there is a close relationship between the E_1-H_1 and E_2-H_2 traps, and thus the assignment of E_1 and E_2 to the second acceptor levels of the two COH complexes responsible for H_1 and H_2 was made. Even though the E_1 and E_2 have been observed and studied previously in literature and had been suggested to be either of donor or single acceptor character, our results indicate these traps to have more of a second acceptor level characteristics.

Publication No.4 given at the end of the first section of this chapter was aimed to present a deeper insight on the theoretical implications and characteristics of the experimentally observed COH complexes in *n*-type Cz silicon. Collaboration with theoretical physicists P. Santos, J. Coutinho and S. Öberg allowed us to obtain a more complete picture of the possible structure of the COH complexes which resulted in the degradation of the lifetime. It is argued that it is likely that the C, O and H atoms are bound to a common Si atom, where C sits on a substitutional site, O is bond-centered between two Si atoms and H occupies a tetrahedral interstitial site. Such a structure, which is in its negative state, gives rise to a distinctly stable configuration whose introduced energy level agrees well to the experimental data.

Later in Section 3.3 another set of results which are presented in the form of an article that has been submitted to the Journal of Applied Physics is given (publication No.5). There, a previously unseen spectroscopic signal obtained by DLTS measurements related the so-called oxygen-related bistable thermal double donors (BTDDs) on their BTTD-0 and BTDD-1 deep-donor states is shown. For these studies a range of Schottky barrier diodes and p^+-n junctions fabricated on n-type Czochralski-grown Si materials were subjected to various junction capacitance techniques for these defects electrical characterisation. The values of activation energy for electron emission from

the BTTD-0 and BTDD-1 levels have been determined to be rather high and unusual for defects in Si which were previously preventing an easy detection through DLTS. From our observations we argue that these BTTDs are effective trapping centers but do not act as recombination centers, this in contrary to recent speculations made by Tomassini *et al.* in Ref. [95]. These results are technologically relevant since there has been a renewed interest in oxygen-related TD studies. This is specially the case in *n*-type silicon which is projected to be the material of choose in forthcoming years in solar and which has been observed to degrade allegedly by TD presence [96].

3.1 Light impurities in silicon

3.1.1 Oxygen

As discussed in Sections 2.1.1 and 2.1.2 the amount of interstitial oxygen inevitably encountered in crystalline silicon tends to exceed the 10^{17} cm^{-1} mark. Therefore extensive research on the topic has been carried out as early as the mid 1950's [97] when first significant oxygen-related effects were observed on resistivity increments in silicon after 430-450 °C heat treatments. These effects were found to be reversible after $>$ 500 °C annealing treatments [98], results that sparked a wave of increased interest in oxygen-related defects in silicon that has led to the now very solid understanding of a variety of these defects [94]. To begin with, it is now widely accepted and justified that oxygen is present in the silicon lattice preferentially occupying a bond-centred interstitial site, where it is electrically inactive [94, 99]. Furthermore, O_i atoms at room temperature are very stable and immobile. It is only when relatively-high temperature processes are applied when O_i diffuse and begin to form oxygen complexes and SiO_2 precipitates.

Two key advantages of oxygen presence in Si have been recognised since over half century ago, and these are: 1) the appreciable enhancement of mechanical strength and stability in the existence of crystal dislocations, noting that dislocation-free Si does not show significant enhancement [97], and 2) gettering of various impurities [97, 100, 101]. Nevertheless, there is also the not very advantageous aspects from the oxygen presence in the crystalline Si lattice. On this side we can perhaps emphasise two cases: a) the so-called thermal double donor (TDD) formation [98, 102, 103], and b) the oxygen-containing defects which act as recombination centres [94, 97, 104].

With respect to the TDD formation which has been extensively studied through many different characterization technique applications we know that they are formed upon heat-treatment of oxygen-rich silicon at temperatures in the range of to 350 - 550 °C [105, 106, 107, 108, 109, 110, 111]. Very early isothermal annealing experiments showed that the formation rate and the maximum concentration of TDDs were dependent on the 3rd and 4th powers of the oxygen concentration [112], setting the TDD structure to contain oxygen clusters or precipitates which act as donors [113]. Multiple subsequent investigations concluded that there exits at least 17 different species of these donors (TDD-0 to TDD-16) which distinguish between one another by their incorporated number of oxygen atoms [94, 109]. Within these species some of highest interest are the TDD-0, TDD-1 and TDD-2 which have been identified to be bistable and with negative-U characteristics [106, 107] nevertheless there are still some questions to answer with respect to their structure and bistability [94, 114]. Moreover, various recent claims of TDD being responsible for lifetime degradation in silicon have been reported in literature [95, 96, 115] which has raised the interest of a deeper understanding of these defects and the quantification of their harmful potential in cell efficiencies.

On the other hand, however, there is the case of the recombination active oxygen-containing defects in Si which include an older, but still very significant, problem related to the light induced degradation i.e the B-O degradation [30, 116, 117]. The B-O complex has been held responsible for up to $10\%_{rel}$ reduction of conversion efficiencies of solar cells made from *p*-type Cz Si [30] which signify an unacceptable reduction and a huge problem for industry. However, despite over 40 years of dedicated efforts to understand the composition and recombination mechanisms behind these complexes, no unified answer has been given in literature. In this thesis results from investigations on the B-O complex will be presented together with the latest literature review on the topic in Chapter 4). In addition to the B-O complex however there exist other oxygen-containing impurities that have been observed to decrease the minority carrier lifetime of various materials. Amongst them there exist the following cases: oxygen precipitates [118, 119, 120, 121, 122], vacancy-oxygen complexes which include divacancies- and trivacancies- oxygen centers [123, 124, 125, 126], SiO_2 precipitates [127], and recently found also a family of complexes suggested to be related to Al and O impurities [128, 129]. In general, oxygen related impurities in Si are largely studied in the literature because of oxygen unavoidable presence in most relevant materials and thus making its related effects understanding of paramount importance.

3.1.2 Carbon

Similar to oxygen, carbon is a light element impurity largely encountered in Si. It mainly originates from graphitic components, contaminant gases and/or the feedstock during growth (see Chapter 2.1). Carbon is known to preferably occupy substitutional sites in the crystal, where it is electrically inactive, nevertheless it produces local strain due to its smaller size as compared to Si [130]. Furthermore carbon is a highly electronegative and chemically reactive making it prone to several interactions including those with Si, O and H. In general carbon related defects are technologically important since for example in the form of C_i-C_s complexes, it is utilised to improve the performance of Si optical emitters [131], in the form of C_s it can trap self-interstitials (I_{Si}) which reduces boron transient enhanced diffusion (TED) for homogeneous doping profiles [132], it can also be used for Au and Cu gettering [133, 134] and for thermal donor deactivation [110]. However, not much attention has been paid into the detrimental effect studies of carbon in literature until recent years. This is partially because of the previous general opinion of carbon being mostly present on its electrically neutral state in Si, and also because no very good sensitivity techniques for the measurement of its concentration were available, leading to rather low detectability of a few times 10^{15} cm^{-3} by means of Fourier-transform infrared spectroscopy (FTIR) [135]. Consequently, as the technology progressed to lower detection limits in the early 2000's more studies related to carbon effects in Si device performance arouse. This has in turn led to further techniques development for the [C] measurements such as photo-luminescence (PL) and/or improvements in FTIR data analysis which have been reported to achieve detections between 1×10^{12} and 1×10^{15} cm^{-3} in the past half decade [135, 136, 137]. Amongst the carbon-related defects that have driven such an interest in their study we can point out the following. On the one hand those defects that act as precursors to self-interstitial nucleation and formation of complexes such as I_{Si}-C_i, I_{Si}-C_i-C_s, I_{Si}-C_i and C_i-C_i [132, 138]. Remembering that C_i created during irradiation or non-ideal temperature crystal growth and is highly reactive and hence promotes the aforementioned defect formation [139, 140]. On the other hand however there are those complexes formed due to interaction of C and other impurities, which include: $C_i - O_i$ [138], I_{Si}-C_i-O_i [138], C_s-H [141] and C-V-O complexes [142]. The particular case of carbon and oxygen complexes however has always been of interest, since very early studies showed a strong interaction between the two impurities [143]. For instance oxygen precipitation which causes minority carrier recombination has been largely studied and found to be of paramount importance for high efficiency

cell fabrication [144, 145]. Moreover, it has been suggested in literature that the known C interactions with oxygen dimers can lead to a decrease in the B-O defect related to the LID effect in Si [146], however very recent investigations have added to previous speculations that C would somehow participate in the B-O formation process instead of eliminating it [147]. Most of the literature however has been overlooking the detrimental effect of carbon in silicon and further studies are required, since as it will be shown in this chapter, carbon-oxygen complexes are the precursors to the formation of a very powerful recombination center in *n*-type silicon in the presence of hydrogen and so making these materials prone to conversion efficiency degradation during processing (see Section 3.2).

3.1.3 Hydrogen

Hydrogen is one of the most ubiquitous impurities in silicon materials since it is readily incorporated from chemicals and gases utilised during crystal growth and/or device processing [148]. This incorporation is not always desired or even detected. Nevertheless, since the 1970's it has been acknowledged that multiple advantageous effects emerge from its presence within the Si crystals [149, 150], this has led to a path of increased intentional incorporation of H in several semiconductor based technologies. There is however a rather significant issue with respect to this practice in industry, and this is that many of the key physical mechanisms underlying the hydrogen positive effects continue to be poorly understood leading to contradictory theories and variations [151, 152, 153]. Such contradictions are known to arise from the difficulty of isolating experimental observations related to hydrogen-related impurities, since H is highly reactive and thus interacts with a plethora of other impurities, and because of the poor sensitivity achieved by the available direct-measurement techniques for hydrogen quantification [148, 151, 154]. For these reasons hydrogenation of silicon, in particular for solar applications, is a very active research field and new discoveries and theories continue to appear in literature with the intention of getting a better understanding of its properties.

The passivation mechanisms of hydrogen in silicon are as mentioned before not fully understood, however its incorporation to silicon crystals is largely accepted to be advantageous and it is thus well established. Moreover hydrogenation processes together with gettering procedures are strongly argued to be key for high-efficiency next-generation Si solar cells [155, 156]. One remarkable example is the deliberate

H introduction to multi-crystalline silicon materials from the PECVD SiN_x:H anti-reflection coatings in solar cell fabrication which has been reported essential for enhanced bulk and surface passivation [157, 158]. Mainly due to hydrogen's ability to interact with many impurities and passivate them such as metallic impurities (Fe, Ni, Cu, Cr, Au and Ag) [159, 160], oxygen-related thermal donors [161] and crystalline defects [150, 162] amongst others. Furthermore, in recent investigations atomic H has been suggested to passivate the defect responsible of the severe light induced degradation in *p*-type silicon [30, 49, 163, 164] and an increased number of publications addressing the importance of H charge state manipulation have emerged [165, 166].

There is however a down side of hydrogen which tends to be left aside in literature, and it is associated to the hydrogen-related defects in silicon. Some of the cases where H has been proven to play a detrimental role include: 1) extended structural defects formation, such as the so-called platelets [167], 2) silicon embrittlement [168], 3) oxygen diffusivity enhancement [153, 169, 170], and 4) electrically active impurity and complex formation [171, 172] (See also Section 3.2). Moreover, a very recent paper has attributed hydrogen presence to the observation of the so-called light and elevated temperature induced degradation (LeTID) in *p*- and *n*-type Cz materials [173]. Nevertheless investigations on this last degradation process are fairly new and presents yet another case of the lack of fundamental understanding and abundant speculation in the literature. In addition to the hydrogen-related degradation in silicon, there is the problem of weak bonding of hydrogen to the passivated defects (i.e low thermal stability) which tend to lead to a reactivation of the defects after rather low temperature treatments which can cause instability problems within the material and make the hydrogen passivation ineffective [164].

In the following two sections, investigations on defects related to the reviewed light element impurities are presented. Investigations aim to pursue a better understanding of defects encountered in currently used materials in the solar industry.

3.2 The C-O-H defect

Publication No.1

Recombination Centers Resulting from Reactions of Hydrogen and Oxygen in n-type Czochralski Silicon

Recombination Centers Resulting from Reactions of Hydrogen and Oxygen in n-type Czochralski Silicon

V. P. Markevich[1], M. Vaqueiro Contreras[1], J. Mullins[1], M. Halsall[1], B. Hamilton[1], L. I. Murin[2], R. Falster[3], J. Binns[4], E. Good[4], J. Coutinho[5], J. Medford[6], C.L. Reynolds Jr.[6], and A. R. Peaker[1]

[1]Photon Science Institute, University of Manchester, M13 9PL, UK, [2]Materials Research Center NAS, Minsk 220072, Belarus, [3]SunEdison Semiconductor Ltd, viale Gherzi 31, 28100 Novara, Italy, [4]SunEdison Inc., 7832 N. Leadbetter Rd., Portland, Oregon 97203, USA, [5]Department of Physics and I3N, University of Aveiro, 3810-193, Portugal, [6]Dept of Materials Science & Engineering, NCSU, Raleigh 27695, NC, USA

***Abstract* — Hydrogen is often present in silicon solar cell fabrication introduced, for example, from silicon nitride anti-reflection layers. In general this has an important beneficial effect in reducing surface recombination. In this paper we show that in n-type Czochralski material the hydrogen reacts with interstitial oxygen related defects to form powerful recombination centers which reduce the minority carrier lifetime in the silicon region into which the hydrogen has diffused. We have studied electronic grade silicon and solar silicon grown by continuous Czochralski techniques. Hydrogen has been introduced into the silicon by wet etching, remote hydrogen plasma and from silicon nitride films. DLTS, MCTS and Laplace DLTS have been used to characterize and quantify parameters of the recombination centers and microwave photoconductivity decay to measure the minority carrier lifetime. The dominant recombination center has an acceptor level at 0.36 eV from the valence band. This center anneals out in the range 150 to 200°C but reforms on cooling.**

***Index Terms* — Czochralski silicon, hydrogen oxygen recombination centers, DLTS, carrier lifetime, photovoltaic cells.**

I. Introduction

A key objective in silicon photovoltaics (PVs) is to increase the cell efficiency to levels approaching the Shockley Queisser limit (~30% at 1 sun). The starting point in this process is to achieve high carrier lifetimes in the silicon and to maintain this lifetime during cell manufacturing. The question which needs to be answered is what recombination process limits the carrier lifetime? Obviously the answer to the question depends on the silicon used and the cell processing it undergoes. In this paper we report part of a study we have undertaken on n-type Czochralski (Cz) material grown by conventional and continuous Cz techniques.

N-type silicon is attractive for solar cells because it usually has a higher "as grown" lifetime than p-type for comparable resistivities, is less susceptible to lifetime reduction due to metallic contamination and exhibits little light induced degradation compared to boron doped material. In this paper we show that in n-type silicon an important recombination centre can be formed resulting from the reaction of oxygen in Czochralski Si with hydrogen. As hydrogen is normally present in cell processing from, among other sources, the nitride layer used for passivation/antireflection this reaction can limit the ultimate carrier lifetime of the silicon.

II. Experimental Summary

We have studied Cz silicon with interstitial oxygen concentrations in the range 12 to 20 ppma (1 ppma = 5×10^{16} cm^{-3}) and for comparison float zone (FZ) silicon with $[O_i]$ < 0.2 ppma. All our samples are n-type phosphorous doped with resistivities in the range 1 to 8 Ω·cm. We have incorporated hydrogen by wet etching, by remote plasma at temperatures up to 250°C and from hydrogen rich silicon nitride deposited on the silicon. The recombination centers produced have been studied by Laplace and conventional DLTS and MCTS, carrier lifetime measurements and local vibrational mode optical absorption spectroscopy.

III. Experimental detail

The electronic grade (semi-grade) silicon we have studied was supplied by SunEdison Semiconductors Ltd in the form of wafers with one side polished and an oxygen content of 13 to 17.5 ppma. The continuous Cz (CCz) solar grade silicon was supplied by SunEdison Inc and also some legacy solar grade HiCz™ material from Confluence Solar was used. Both these materials had an oxygen content of 12-20 ppma and were etch polished. All the material was n-type with resistivities in the range 1-8 Ω·cm.

Strips of silicon were cut from the wafers. These strips were RCA cleaned, then hydrogen was introduced into the silicon by three techniques. Firstly, this was done by wet etching either in KOH or in a HF/HNO_3 solution. Both these etches have been shown previously to result in the formation of hydrogen ions which diffuse into the silicon. The most evident effect of this is the passivation of shallow acceptors and donors [1]. Secondly hydrogen has been introduced by exposure to a 50 W remote H plasma for 30 minutes while the samples were heated to temperatures between 25°C and 250°C. Lastly, some samples were studied which had silicon nitride deposited on the surface as a source of hydrogen [2]. After annealing the nitride was etched off and the material processed for measurement.

The samples were prepared for electrical measurements by the deposition of Schottky barrier diodes (SBDs) formed by thermal evaporation of Au through a shadow mask. An Ohmic contact was deposited on the back surface using thermal evaporation of Al. For MCTS measurements a hole was made

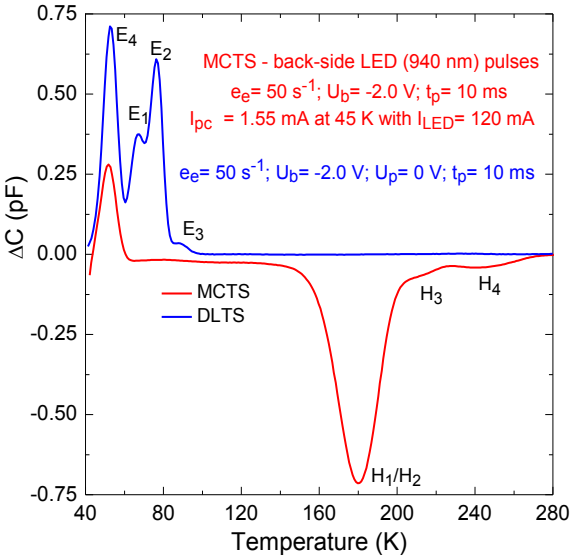

Fig. 1. DLTS (top) and MCTS (bottom) spectra of a Confluence CCz n-type 5 Ω·cm Si slice after HF/HNO_3 etching. Measurement conditions are shown in the figure.

in the back contact to provide optical access. The diodes were tested using C-V measurements giving the concentration of shallow uncompensated donors and the probing depth achievable.

DLTS [3], MCTS [4] and Laplace DLTS [5] measurements were carried out in order to characterise deep level electronic defects. Majority carrier capture cross sections were determined by varying the filling pulse width while minority carrier capture cross section measurements used back face illumination from a 850nm or 940nm LED. Carrier generation in this structure is almost exclusively outside the depletion region but carriers diffuse to the depletion edge where the depletion field repels the majority carriers but allows the minority carriers to drift through the depletion region. In n-type material this results in an almost pure hole flux enabling deep states to become hole occupied.

Carrier lifetime measurements were undertaken using SemiLab WT2000PVN equipment in the microwave photoconductive decay mode (μPCD) operating at ~10GHz with a 905 nm LASER with a fixed intensity of 1 sun. Surface passivation for the measurement was done by immersion of the slices in an iodine solution after an HF dip [6, 7].

IV. Results

Electronic grade Cz Si has a very low concentration of deep states (~10^{10} cm^{-3}). However in the Cz material during cooling, after growth, some of the oxygen forms electrically active states referred to as thermal donors [8]. In electronic grade material these are usually dissociated by a heat-treatment in the temperature range 650-750 ^{o}C prior to shipping … this is not done in the case of the solar grade CCz material which as a result contains thermal donors.

A. Defects Observed

Fig. 1 shows DLTS and MCTS spectra of CCz material which had hydrogen introduced by etching in a HF/HNO_3 solution. In the DLTS spectrum E_4 is the $E^{++/+}$ level of the thermal donors referred to above, E_1, E_2 and E_3 are related to the hydrogenation but they are not of importance in this work as they do not appear to be significant recombination centres. However, the minority carrier signal at 180 K could signify an important recombination center because of its position in the band gap and its high capture rate for minority carriers.

Fig. 2 shows a high resolution Laplace DLTS spectrum of the minority carrier signal shown in Fig. 1. It is evident that this signal represents the carrier emission from two states.

B. Dependence on Oxygen and the Oxygen Dimer

Fig. 3 shows the thermal emission characteristics of holes from three traps in hydrogenated Cz silicon. These traps are

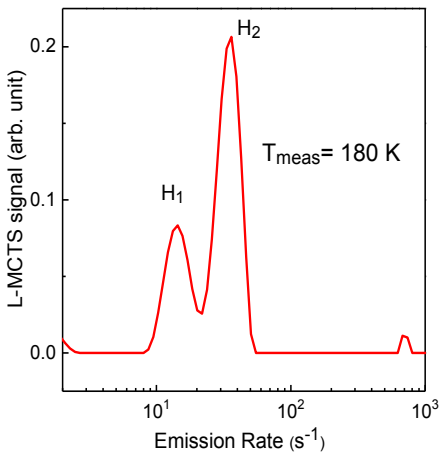

Fig. 2. Laplace MCTS spectrum of the hole emission shown in Fig. 1 using 940nm 10ms pulse backside illumination generating a photocurrent of 1.55mA at 45K, with a reverse bias of 2V.

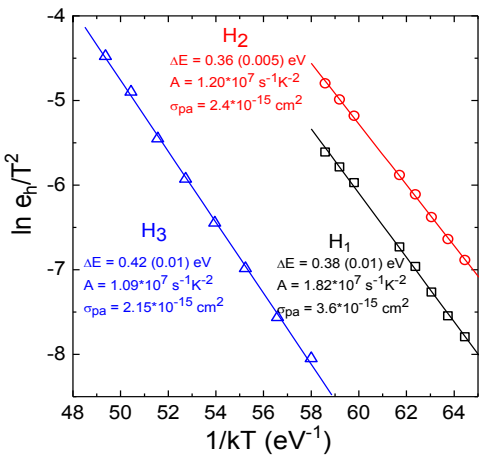

Fig. 3. Arrhenius plot of three of the hole traps observed in hydrogenated Cz samples. Parameters derived from the plots are shown in the diagram.

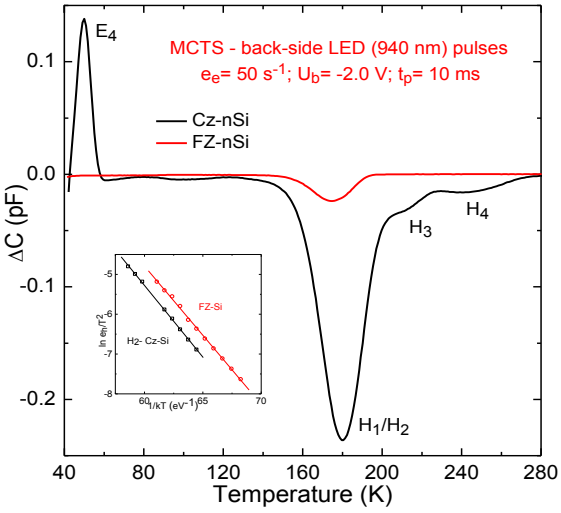

Fig. 4 Comparison of MCTS spectra in hydrogenated FZ and Cz silicon. The negative peak in the FZ spectrum is related to a different defect and is not H_1/H_2 as can be seen from the inset Arrhenius plot. The negative signal in the FZ material relates to a hydrogen-carbon center [9].

consistently observed in such material from all the sources we have used and whatever hydrogenation method has been applied. However we do not observe the states in FZ material as can be seen in Fig. 4. This provides very strong evidence that the H_1 to H_4 defects are oxygen related and as they are only present after hydrogenation it seems likely they are some form of oxygen-hydrogen complex.

If we now consider the concentration of these states, we find that the concentration increases rapidly with oxygen content of the Cz silicon. Fig. 5 shows the MCTS spectra for two slices with interstitial oxygen content measured to be 12.7

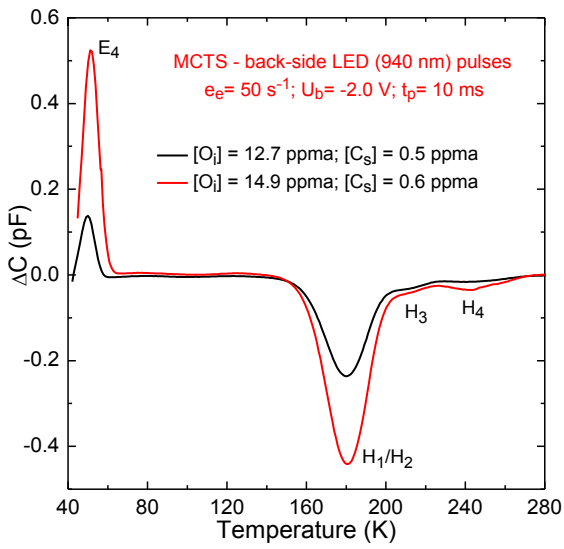

Fig. 5 Comparison of MCTS spectra derived from two electronic grade Cz Si slices with different oxygen content.

and 14.9 ppma. Taking data from a range of oxygen content it appears that the concentration of the H_1/H_2 traps is almost proportional to $[O_i]^2$, so indicating an involvement of two oxygen atoms into the defects.

A well-known defect in Cz silicon is the oxygen dimer. It can be identified from its distinctive optical absorption spectrum and exists in two configurations shown in Fig. 6 [10]. The absorption bands due to the oxygen dimer are weak and measurements have to be made at low temperatures. This is in contrast to the measurements of interstitial oxygen concentration reported in this paper which were carried out at 300 K by measuring the absorption coefficient in maximum of the band at 1107 cm^{-1} due to single interstitial oxygen atoms.

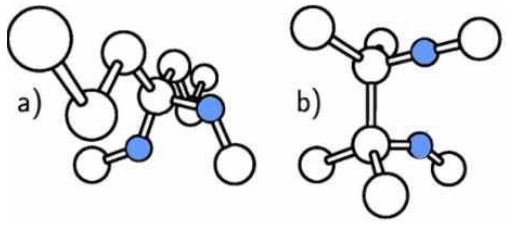

Fig. 6. Configurations of the oxygen dimer in silicon. Oxygen atoms are shown in blue. The different configurations give rise to different optical absorption spectra.

For the case where the two oxygen atoms are attached to a common silicon atom as depicted in Fig. 6(a), absorption lines at 1012 and 1060 cm^{-1} (measured at 10K) are observed. For the case where oxygen atoms are attached to two adjacent silicon atoms as shown in Fig 6(b), an absorption line at 1105 cm^{-1} is observed at 10K.

For ingots and slices with similar thermal history and similar C_s concentration we have shown previously [11] that the dimer concentration is almost proportional to $[O_i]^2$. However the dimer concentration can be reduced by annealing at 650 - 700°C and then increased again by annealing at 550°C. We have used these facts to relate the formation of the recombination centres in Cz-Si samples to the oxygen dimer.

Fig. 7 shows the effect of annealing slices of CCz material at 650°C, a temperature which decreases the dimer concentration, and at 550°C where the dimer concentration increases. Annealing at these temperatures for short time does not change the interstitial oxygen concentration significantly and any changes that do occur are in the opposite sense to the change in the dimer concentration. The initial 650°C anneal also annihilates the thermal donors, so the E_4 signal is not observed in the MCTS spectrum. It is evident that the concentration of the H_1/H_2 defects follows the change in concentration of the dimer during the annealing schedules rather than the interstitial oxygen concentration. It seems therefore that the centers are produced by a reaction between hydrogen and one of the oxygen dimer species rather than hydrogen and two independent interstitial oxygen atoms.

C. Relationship to Hydrogen

If we now consider the relationship to hydrogen in the slice, we find it difficult to be quantitative in deriving such a

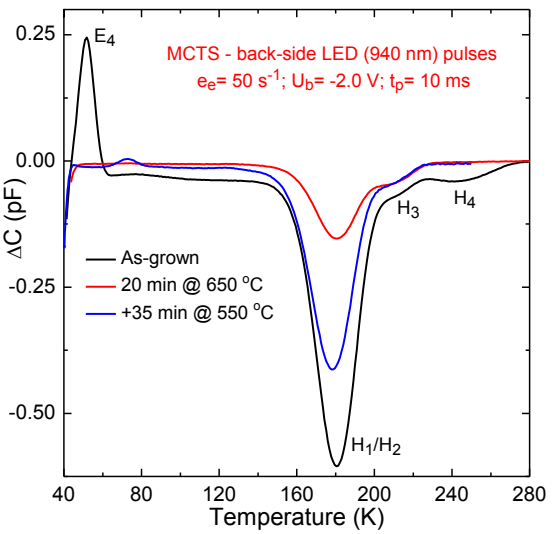

Fig. 7. DLTS spectra showing the effect of annealing CCz material prior to hydrogenation on the concentration of the hole traps after hydrogenation.

relationship because of the difficulty in determining the absolute hydrogen concentration. Using the wet etching described earlier, the concentrations are below SIMS detectivity even if deuterium were to be used as a hydrogen analogue.

However, we do know that hydrogen ions will diffuse with a near exponential profile and are trapped in the lattice by reactive species which limits the diffusivity.

In p-type material Coulombic attraction between H^+ at a bond center site and the ionised acceptor B^- results in carrier removal and so a profile of the carrier loss can be used to accurately profile the hydrogen concentration where [H] < [B]. In n-type P-doped Si this methodology is not as effective because the H atom becomes trapped at anti-bonding (AB) sites to Si atoms neighbouring the P donors, so forming a P-Si-H passivated center. Unlike the boron case the reaction is far from complete and depends on the concentration of other trapping centers in the silicon, most notably oxygen in this case. As a result, it is not possible to determine the absolute hydrogen concentration.

However, the shape of the hydrogen profile remains exponential and comparison of the defect profile with the expected hydrogen profile can provide sound evidence of hydrogen involvement in the formation of the defect. In some cases the exact shape of the profile has been used to estimate the number of hydrogen atoms in a defect [12].

Fig. 8 shows the measured depth profile of the H_2 defect. A similar profile has been measured for the H_1 centre. The shape of the profile is as expected for the penetration of hydrogen in this material. This provides solid evidence of the involvement of hydrogen and suggests that only one hydrogen atom is involved in the complex.

If we look at other methods of hydrogen incorporation we see states with identical electrical characteristics but for the same starting material different concentrations and different profiles. Fig. 9 shows the DLTS and MCTS spectra for the same material shown in Fig. 1 but with the hydrogen introduced from a H rich silicon nitride layer.

As the hydrogen has diffused in from the nitride at around 500°C the trapping effect of defects is negligible and so the effective diffusivity is probably sufficient for the hydrogen to permeate the entire thickness of the slice. On cooling, reactions with the oxygen occur but the hydrogen concentration near the surface, where the DLTS probes, is lower than for the etching case. However this is an important case because it is more representative of the situation in a real solar cell passivated with silicon nitride.

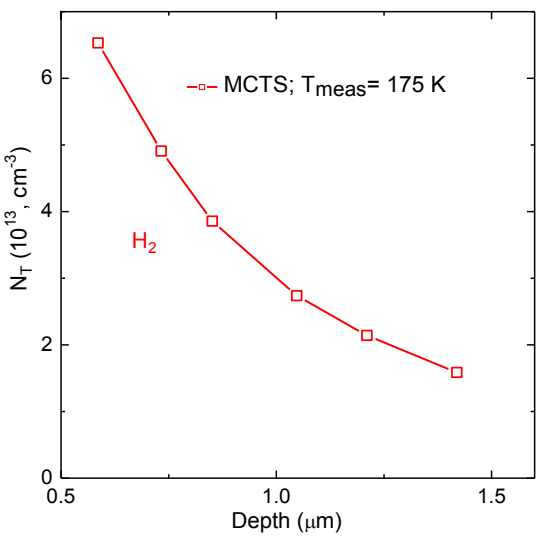

Fig. 8. Depth profile of the H_2 defect in Cz silicon where hydrogen has been introduced by etching in HF/HNO_3.

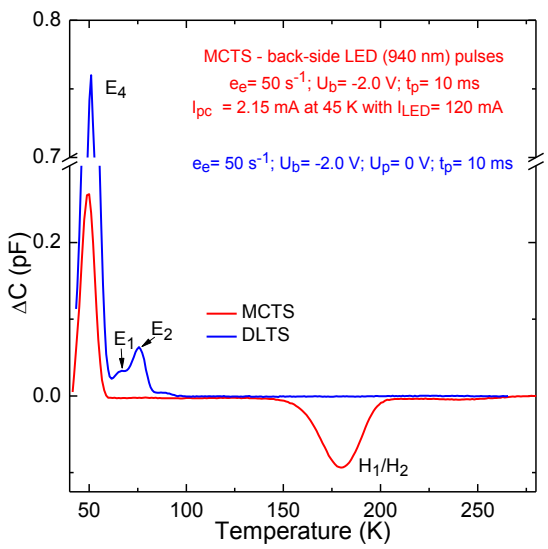

Fig. 9. DLTS and MCTS spectra of a Confluence CCz n-type 5 Ω·cm Si slice hydrogenated from a hydrogen rich silicon nitride film (removed before measurement). Measurement conditions are shown in the figure.

D. Thermal Stability

Although hydrogen ions are highly reactive in silicon the binding energy of hydrogen to defects is rather weak. The consequence is that most hydrogen related defects are easily dissociated. This is also the case for the H_1/H_2 defects, as shown in Fig. 10.

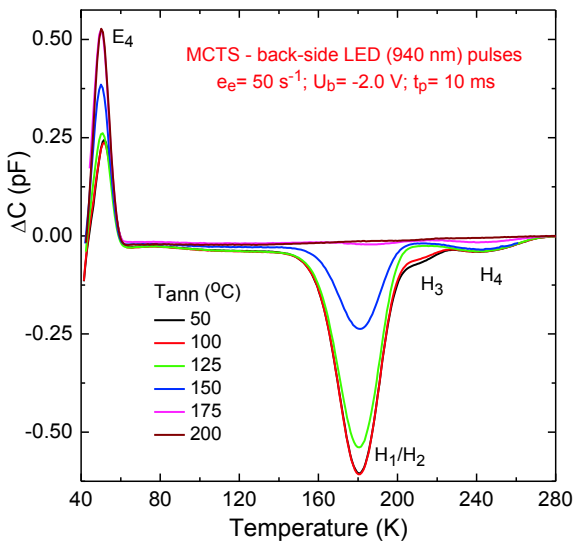

Fig. 10. Effect on the DLTS spectrum of annealing a Cz wafer hydrogenated by etching in HF/HNO_3 in the range 50 to 200°C.

It can be seen that all the hydrogen related hole traps are dissociated at 200°C in this etched sample. In this case the hydrogen which prior to annealing is in a thin surface layer but can diffuse away at 200°C into the bulk of the slice. However in the case of the hydrogen source being a nitride film the hydrogen is already well distributed throughout the slice and so after the elimination of the oxygen hydrogen recombination centers upon annealing it would be expected that the centers would re-form on cooling. The extent to which this happens is currently under investigation as it is of crucial importance in relation to the significance of these defects.

E. Atomistic and Electronic Structure Calculations

In order to unveil the microscopic details of the H_1/H_2 defects, we carried out first-principles density functional calculations within the generalized gradient approximation to the exchange-correlation energy [13]. The Kohn-Sham basis consisted on atomic-like Cartesian-Gaussian functions up to *l*=2 on Si and O atoms, and *sp*-functions on hydrogen. This translates into 28, 40 and 16 functions on Si, O and H atoms, respectively. The electron density and potential terms were described using plane-waves with kinetic energy of up to 200 Hartree. Defects were introduced in 216-Si atom supercells with cubic shape. Brillouin zones were sampled at 8 reducible (MP-2^3) **k**-points, and all atomic, electronic and magnetic degrees of freedom were fully relaxed until the total energy change was lower than 0.1 meV.

Several oxygen-dimer-hydrogen complexes were already scrutinized by us. Most of them are donors or do not possess a binding energy compatible with the thermal stability of H_1/H_2. A promising model is the one shown in Fig. 11, where H binds to the Si atom that is connected to both oxygen atoms of the dimer. Calculations indicate that this defect has an acceptor level around mid-gap, thus being a strong contender to be connected to H_1/H_2. The origin for such a deep state comes from the over-coordinated Si atom that is bound to H. This center can in principle bind to an additional H atom, and further work is necessary in order to make definite assignment.

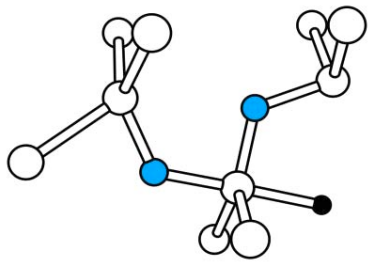

Fig. 11 Atomistic model of a O_2-H complex in silicon. Si, O and H atoms are shown in white, blue and black, respectively.

F. Effect on Minority Carrier Lifetime

We have measured the capture cross sections of these defects in order to asses their significance as recombination centers. For the case of the H_1/H_2 traps we find that the directly measured hole capture cross section $\sigma_p = 1\times10^{-15}$ cm^2 while the directly measured electron capture cross section $\sigma_n = 2.9\times10^{-17}$ cm^2. These figures, along with an activation energy of 0.36 eV for hole emission to the valence band, indicate that the defects are acceptors and rather powerful minority carrier recombination centers in n-type Si. The low level lifetime can be calculated from:

$$\tau = \left[\sigma_p V_{th} N_T\right]^{-1} \quad , \qquad (1)$$

where V_{th} is the hole thermal velocity and N_T the trap concentration. Taking $V_{th} = 1.6\times10^7$ cm s^{-1} and a value of $N_T = 4\times10^{13}$ cm^{-3} the low level minority carrier lifetime in the n-type material would be ~ 1.5µs. For the limit of the high level lifetime where p≈n the value is much higher, in this case ~ 40µs. This value of trap concentration N_T is the measured value near the surface of CCz samples where hydrogen has been introduced by etching as shown in Fig. 8. However, when the lifetime is measured using conventional instruments, the sampling depth is much greater depending on the specific instrument used. In general a weighted average is recorded. In the case of out Semilab WT200PVN using a 905 nm LASER in the µPCD mode at ~10GHz with 5 Ω·cm material the sampling depth is ~50µm determined by the LASER extinction depth and the minority carrier diffusion length. The precise calculation of the effect of recombination centers in a near surface layer as shown in Fig. 8 on effective lifetime as

determined by the WT2000PVN machine is not possible. However, an estimate can be made of the weighted average that a 1.5µm region with a mean lifetime of 1.5µs would show a measured lifetime of the slice of ~60µs.

We have used the fact that the 0.36 eV recombination center anneals out at 200°C to quantify the effect that it has on measured lifetime. We have measured the minority carrier lifetime using µPCD before and after the annihilation of the recombination centers in slices by annealing at 200°C.

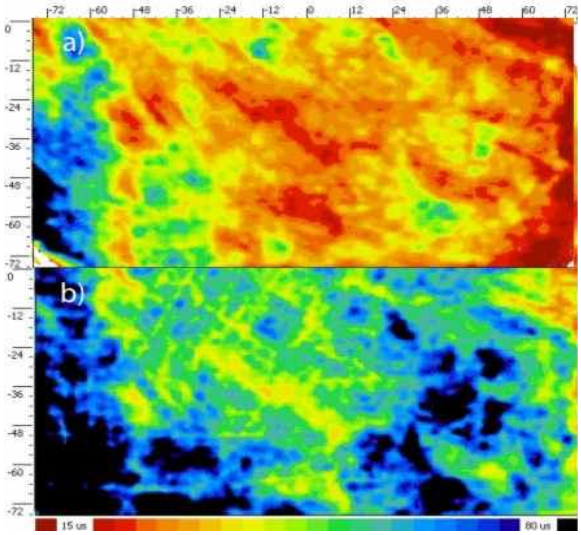

Fig. 12 Lifetime map of a Confluence CCz slice a) etched to inject hydrogen into the surface region and b) the same region after annealing at 200°C to dissociate the hydrogen-oxygen recombination center. The lifetime scale is 15µs (red) to 80µs (blue). The scale at the top and left are dimensions in mm.

Fig. 12 shows the low excitation level (~10^{15} cm^{-3}) lifetime map of a hydrogenated sample before and after annealing. The measured lifetime is compromised by cutting damage with the result that the average lifetime was much lower than the bulk ingot value. The average lifetime measured on the slice before anneal was 30µs and afterwards 57µs. Assuming that all the 0.36 eV recombination centers are lost as a result of the anneal the lifetime attributable to the 0.36 eV recombination path is 63µs. This is consistent with the calculated change expected from the measured concentrations and parameters of the recombination state. Both DLTS and the direct lifetime measurements indicate that the defect is an important recombination center.

V. Conclusion

Recombination centres are formed in n-type silicon by the interaction of hydrogen and oxygen dimers. In some circumstances our measurements indicate that the concentration of these recombination centres is sufficiently high to have an important effect on the minority carrier lifetime of the silicon and in consequence the efficiency of solar cells. The situation is most important in silicon with high oxygen content which has been heat treated at around 550°C. The properties of the defect are identical whether the hydrogen is introduced from wet etching, hydrogenated silicon nitride or from remote hydrogen plasma. The recombination centres have been seen in conventional Cz material and in continuous Cz but not in FZ material.

Acknowledgement

We would like to thank the UK Engineering and Physical Research Council for support under contract EP/M024911/1. JC thanks the FCT under contracts PTDC/CTM-ENE/1973/2012 and UID/CTM/50025/2013. We are grateful to Malachy McGowan and Ian Hawkins for their technical support. NCSU acknowledges NSF Phase II I/UCRC grant IIP-1338820.

References

[1] O. Feklisova, S. Knack, E.B. Yakimov, N. Yarykin, J. Weber, Physica B 308–310, 213 (2001).
[2] M. Sheoran, Dong Seop Kim, Ajeet Rohatgi, H. F. W. Dekkers, G. Beaucarne, M. Young, S. Asher, Photovoltaic Specialists Conference, 2008. PVSC '08. 33rd IEEE, San Diego, CA, USA, 2008, pp. 1-4. doi: 10.1109/PVSC.2008.4922638.
[3] D. V. Lang, J. Appl. Phys. 45, 3023 (1974).
[4] R. Brunwin, B. Hamilton, P. Jordan, and A. R. Peaker, Electron. Lett. 15, 349 (1979).
[5] L. Dobaczewski, A.R. Peaker and K. Bonde Nielsen, J.Appl. Phys. 96, 4689 (2004).
[6] B. Sopori, P. Rupnowski, J. Appel, V. Mehta, C. Li, and S. Johnston, Photovoltaic Specialists Conference, 2008. PVSC '08. 33rd IEEE Pages: 1 - 4, DOI: 10.1109/PVSC.2008.4922688.
[7] B. Sopori; S. Devayajanam, P. Basnyat, H. Moutinho, B. Nemeth; V. LaSalvia, S. Johnston; J. Binns; J. Appel, 2014 IEEE 40th Photovoltaic Specialist Conference (PVSC);Pages: 0649 - 0654, DOI: 10.1109/PVSC.2014.6925006.
[8] V. P. Markevich and L. I. Murin, Phys. Status Solidi A 111, K149 (1989).
[9] O. Andersen, A. R. Peaker, L. Dobaczewski, K. Bonde Nielsen, B. Hourahine, R. Jones, P. R. Briddon, and S. Öberg, Phys. Rev. B 66, 235205 (2002).
[10] L. I. Murin, T. Hallberg, V. P. Markevich, and J. L. Lindström, Phys. Rev. Lett. 80, 93 (1998).
[11] L. I. Murin, E. A. Tolkacheva, V. P. Markevich, A. R. Peaker, B. Hamilton, E. Monakhov, B. G. Svensson, J. L. Lindström, P. Santos, J. Coutinho, and A. Carvalho, Appl. Phys. Lett. 98, 182101 (2011).
[12] O. V. Feklisova and N. A. Yarykin, Semicond. Sci. Technol. 12, 742 (1997).
[13] P. R. Briddon and M. J. Rayson, physica status solidi (b) 248, 1309 (2011).

Publication No.2

Powerful recombination centers resulting from reactions of hydrogen with carbonoxygen defects in n-type Czochralski-grown silicon

Wiley Online Library
Early View publication on www.wileyonlinelibrary.com
(issue and page numbers not yet assigned;
citable using Digital Object Identifier – **DOI**)

Phys. Status Solidi RRL, 1700133 (2017) / **DOI** 10.1002/pssr.201700133

pss +++rapid research letters+++
www.pss-rapid.com

Powerful recombination centers resulting from reactions of hydrogen with carbon–oxygen defects in n-type Czochralski-grown silicon

M. Vaqueiro-Contreras*[,1], V. P. Markevich[1], M. P. Halsall[1], A. R. Peaker[1], P. Santos[2], J. Coutinho[2], S. Öberg[3], L. I. Murin[4], R. Falster[5], J. Binns[6], E. V. Monakhov[7], and B. G. Svensson[7]

[1] Photon Science Institute, University of Manchester, Manchester M13 9PL, UK
[2] Department of Physics and I3N, University of Aveiro, Campus Santiago, Aveiro 3810-193, Portugal
[3] Department of Engineering Sciences and Mathematics, Luleå University of Technology, SE-97187 Luleå, Sweden
[4] Materials Research Center of NAS of Belarus, Minsk 220072, Belarus
[5] SunEdison Semiconductor Ltd., viale Gherzi 31, 28100 Novara, Italy
[6] SunEdison Inc., 7832 N. Leadbetter Rd., Portland, Oregon 97203, USA
[7] Department of Physics, SMN, University of Oslo, Oslo N-0316, Norway

Received 28 April 2017, revised 15 June 2017, accepted 16 June 2017
Published online 27 June 2017

Keywords carbon–oxygen defects, Czochralski silicon, hydrogen, minority carrier transient spectroscopy, recombination centers

* Corresponding author: e-mail michelle.vaqueirocontreras@manchester.ac.uk

It has been acknowledged for over 50 years that treatments with hydrogen can improve silicon semiconductor devices. In recent years, these have been used to an advantage in silicon solar cells reducing the loss of photo-generated carriers at the silicon surface or at the silicon interface with dielectrics. However, we have found that in some types of silicon the in-diffusion of hydrogen can result in the formation of powerful recombination centers composed of carbon, oxygen, and hydrogen which reduce the carrier lifetime and ultimately the efficiency of solar cells made from such material.

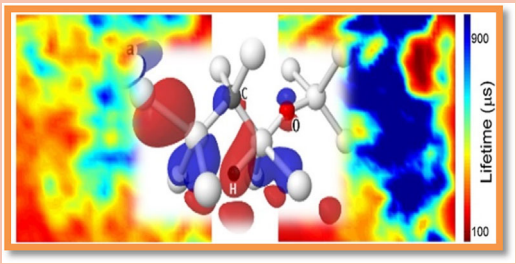

1 Introduction The target for silicon photovoltaics is to approach as closely as possible the Shockley–Queisser limit of efficiency of ~30% at 1 sun [1, 2]. Photovoltaic (PV) cell efficiencies >25% have been obtained in the lab by using high quality single crystal silicon but this contrasts with commercial devices which typically have module efficiencies <16%. In general these devices use cheaper multi-crystalline silicon. Obtaining materials with long minority carrier lifetime and its maintenance throughout the manufacturing processes is crucial for achieving high efficiencies and this is a major objective for future silicon solar technologies. The carrier lifetime is limited by recombination processes which depend on the material to be used and the cell processing that it undergoes. The reduction of surface recombination by the passivation of surface and interface states has long been a part of silicon PV manufacture. Among the most widely used materials for surface passivation are hydrogenated silicon nitride (SiN_x:H), aluminum oxide [3], and annealed Al/SiO_2 [4]. In these materials, hydrogen content has been found to play an important role for lifetime improvement [5, 6]. Moreover, a recent publication proposed that hydrogen passivation of recombination centers in bulk of Si materials can be enhanced by manipulating the charge states of the hydrogen atoms [7]. Although hydrogen passivation

mechanisms are not fully understood, they are accepted in silicon PV technology as beneficial for Si solar cells.

However, we have found that under some circumstances, contrary to the widely accepted views, hydrogenation can result in degradation of the carrier lifetime in silicon. In our study of n-type Si grown by Czochralski techniques, the appearance of two powerful recombination centers has been observed after the introduction of hydrogen into samples containing relatively high concentrations ($\geq 5 \times 10^{15}\,cm^{-3}$) of carbon impurity atoms. The same centers have been detected irrespective of the hydrogenation method. The most important observations were obtained by the application of the minority carrier transient spectroscopy (MCTS) technique [8], which allows us to measure positions of deep energy levels of the minority carrier traps in the silicon band gap and both the minority and majority carrier capture cross sections. Guided by *ab initio* calculations of possible defect structures and using a combination of MCTS, optical absorption and annealing a range of samples with different oxygen and carbon concentrations, we have obtained data about the composition of the centers and their thermal stability. The work reported here shows conclusively that the centers are related to carbon–oxygen–hydrogen complexes. So, as carbon is present as an impurity in some solar silicon materials including those grown by new methods under development commercially [9], our new findings suggest that this may be an important issue for future silicon PV technologies.

2 Experimental and modeling details In this work, we focus on n-type Czochralski (Cz) Si materials grown by conventional and the newer less expensive continuous Czochralski (C-Cz) techniques [10]. These types of materials are starting to be used in the solar industry for high efficiency products potentially replacing multicrystalline p-type material, at least in part because n-type Cz and C-Cz silicon when compared to p-type silicon has a higher "as grown" lifetime, lesser vulnerability to metallic contamination effects and little light induced degradation [11].

The materials that we have studied include a wide range of Cz and C-Cz silicon wafers with interstitial oxygen concentration in the range $12 < [O_i] < 20$ ppma (1 ppma $= 5 \times 10^{16}\,cm^{-3}$) and substitutional carbon concentration of $0.01 < [C_s] < 9$ ppma. A comparison has been made with float zone (FZ) silicon samples with $[O_i]$ and $[C_s] < 0.2$ ppma. The n-type Si samples that we used were phosphorous doped with resistivities between 1 and $8\,\Omega \cdot cm$. The characterization of the centers was done by means of conventional and high-resolution Laplace deep level transient spectroscopy (L-DLTS) [12], MCTS, and local vibrational mode optical absorption spectroscopy. Samples of each material were cut and RCA cleaned, then the hydrogen was introduced into the silicon by three different techniques: (i) wet etching with either KOH or HF/HNO_3 solutions; (ii) 50 W remote H plasma exposure for 30 min at temperatures between 25 and 250 °C; and (iii) in-diffusion of hydrogen from H-rich silicon nitride films (SiN_x:H). This latter technique simulates hydrogen introduction in a solar cell fabrication process. After cleaning, the samples were subjected to evaporation of Au through a shadow mask from the front side and Al evaporation without mask on the back side to produce Schottky barrier diodes (SBDs) and an Ohmic contact, respectively. An un-metalized region of the Ohmic contact was left on the back of the MCTS samples to allow optical excitation from a 940 nm light emitting diode (LED). In the case of the samples with SiN_x:H films, the films were etched off in diluted HF prior to metal deposition. Each diode was characterized firstly with current–voltage and capacitance–voltage measurements, and then DLTS, MCTS, and Laplace DLTS/MCTS measurements were carried out for detection and characterization of electrically active defects.

First-principles calculations of CO and COH complexes were carried out within density-functional theory using the projector-augmented wave method to account for the core electrons, and plane-waves limited by a 400 eV kinetic energy cut-off to describe the valence electrons [13, 14]. The generalized gradient approximation was used to describe the exchange and correlation energy, with the application of the Perdew, Burke, and Ernzerhof (PBE) functional [15]. Atomistic models of the CO and COH complexes were introduced in cubic supercells with 216 Si atoms and optimized lattice constant. Atomic coordinates of the resulting defective supercells were relaxed until the maximum force fell below 0.01 eV $Å^{-1}$. The electron density and Kohn–Sham orbitals were calculated self-consistently on a $2 \times 2 \times 2$ Monkhorst–Pack **k**-point grid [16], enforcing a convergence tolerance for the total energy of 1 μeV. The electrical activity of COH models was investigated using the marker method [17] with the OH defect as a marker [18]. To this end we also used the Heyd–Scuseria–Ernzerhof hybrid functional [19] (HSE06) which mixes a portion of exact exchange with the PBE exchange-correlation potential. The HSE06 functional has the advantage of leading to a theoretical band gap of about 1.2 eV, reducing errors related to the *narrow-gap syndrome* of (semi-) local exchange correlation approximations.

3 Observations and results In Ref. [20], we have shown the MCTS spectra for n-type Cz and C-Cz samples subjected to hydrogenation by the three methods described above. In all the spectra three peaks due to hole emission from defect levels to the valence band have been detected. A detailed analysis of the dominant peak, with its minimum at 180 K for the emission rate window of $50\,s^{-1}$, with the application of high resolution Laplace MCTS (L-MCTS) [12] has shown that this peak consists of two different emission signals, H_1 and H_2 [20]. Further, it has been shown that the concentration profiles of the H_1 and H_2 traps scale with the hydrogen concentration profiles, so confirming the involvement

of hydrogen atoms into the structure of the corresponding defects.

We have determined electronic characteristics of the dominant H_1 and H_2 hole traps from direct measurements of their hole emission rates and capture cross sections of holes and electrons using Laplace MCTS. From Arrhenius plots of T^2-corrected hole emission rates, the activation energies for hole emission from the defect levels to the valence band and pre-exponential factors have been found to be: 0.38 ± 0.01 eV and $1.8 \times 10^7\,s^{-1}\,K^{-2}$, and 0.36 ± 0.01 eV and $1.2 \times 10^7\,s^{-1}\,K^{-2}$ for the H_1 and H_2 traps, respectively. Direct measurements of the capture cross sections of minority carriers (σ_p) by the traps have been carried out by the application of back-side light pulses of different length from an LED. The minority carrier concentration needed for the calculation of σ_p has been determined from the measured value of the diode photo-current at a temperature of trap filling measurements. The values of σ_p for the H_1 and H_2 traps have been determined as 9.8×10^{-16} and $7.9 \times 10^{-16}\,cm^2$, respectively. No significant temperature dependence of the σ_p values has been detected. The values of majority carrier capture cross sections (σ_n) have been determined by the application of the so-called "clearance pulse" pulse of different lengths ("zero" bias voltage in this case) immediately after the application of a long optical filling pulse. The application of the clearance pulse resulted in capture of electrons by the traps filled by holes and corresponding reduction in the magnitude of the hole emission signals. The σ_n values for the H_1 and H_2 traps have been found to be 2.0×10^{-17} and $1.95 \times 10^{-17}\,cm^2$, respectively.

An analysis of the obtained σ_p and σ_n values indicate that both the H_1 and H_2 traps are of acceptor nature, and considering the positions of their levels in the gap it can be suggested that the traps are effective recombination centers for holes in n-type Si. Indeed, using the relationship, that at low injection level, the lifetime depends on the minority carrier capture cross section and trap concentration (N_T) as follows:

$$\tau = \left(\sigma_p v_{th} N_T\right)^{-1} \quad (1)$$

where v_{th} is the hole thermal velocity and taking $v_{th} = 1.7 \times 10^7\,cm \cdot s^{-1}$ and $N_T = 4 \times 10^{13}\,cm^{-3}$ (an average trap concentration probed by DLTS/MCTS in the sub-surface region of some of our studied samples) we obtain the lifetime value of about 1.5–1.9 μs. For the limit of the high injection level, i.e., when $p \approx n$, the lifetime value is higher, in this case ~40 μs. These calculations thus confirm the strong limiting impact of the centers on the minority carrier lifetime in the Cz n-type material.

Evidence for the involvement of oxygen impurity atoms in the structure of the H_1/H_2 centers has been presented by us in Ref. [20]. In Ref. [20], we have mentioned a quadratic dependence of concentration of the recombination centers on $[O_i]$ but after measuring many more samples since publishing that paper it appears that the dependence is less than quadratic. Further, it has been found that the concentration of the H_1/H_2 traps is negligible in some Cz-Si crystals with relatively high oxygen concentrations but with low carbon concentrations. Figure 1 show the MCTS spectra recorded on the hydrogenated n-type Si samples with similar values of the oxygen concentration ($\sim 7.5 \times 10^{17}\,cm^{-3}$) but different concentrations of carbon impurity atoms. An analysis of the data presented in Fig. 1 shows that the concentration of the H_1/H_2 traps is a nearly linear function of the carbon concentration. So, the obtained experimental data clearly indicates that the H_1/H_2 defects consist of centers incorporating oxygen and carbon impurity atoms to which a hydrogen atom is attached.

Substitutional carbon atoms are known to be effective traps for mobile interstitial oxygen atoms. From low-temperature infrared-absorption measurements of carbon and oxygen rich Cz silicon, the local vibrational modes of at least four CO_n complexes with different numbers of oxygen atoms have been identified [21–23]. Concentrations of the complexes can be varied by temperature and duration of heat-treatments in the temperature range 500–1100 °C [22, 23]. To determine which of the CO complexes can be precursors of the H_1/H_2 centers, we have heat-treated a few samples from a Cz-Si crystal with $[O_i] = 7.3 \times 10^{17}\,cm^{-3}$ and $[C_s] = 4.5 \times 10^{17}\,cm^{-3}$ in the temperature range 500–700 °C and carried out infrared absorption (IR) and MCTS measurements on them. Figure 2a shows the IR absorption spectra of the heat-treated samples in the wave-number range 1080–1120 cm^{-1} and Fig. 2b shows the MCTS spectra of the corresponding heat-treated and hydrogenated samples. It appears that there is a good correlation between the intensity of the IR absorption band

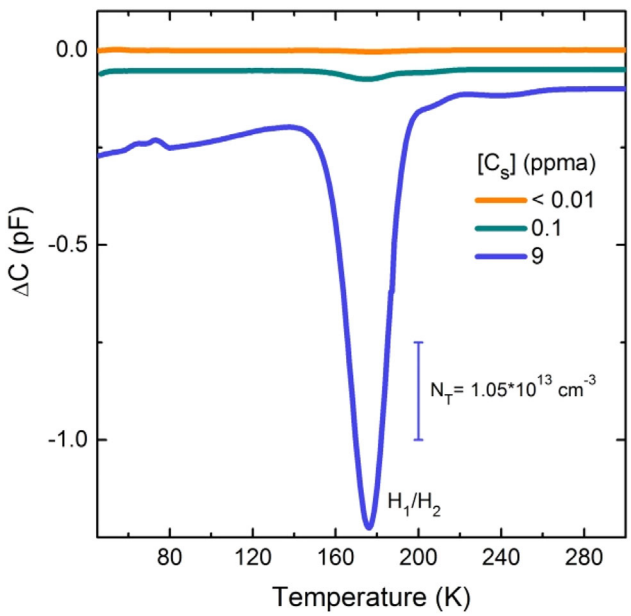

Figure 1 MCTS spectra for n-type Cz-Si samples with $[O_i] = 7.5 \times 10^{17}\,cm^{-3}$ and different $[C_s]$. Hydrogen was introduced by etching in $1HF/7HNO_3$ solution for 3 min.

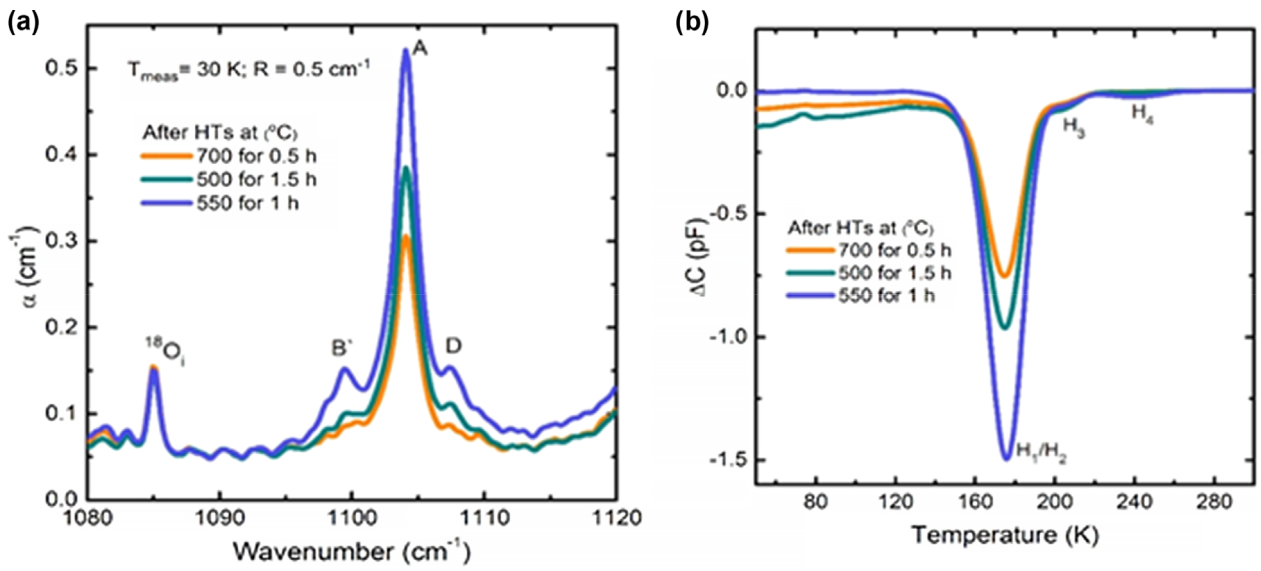

Figure 2 (a) Infrared-absorption spectra of a set of carbon and oxygen rich n-type Cz-Si samples after heat-treatments: at 700 °C for 30 min, at 500 °C for 1.5 h, and at 550 °C for 1 h. The absorption peaks, which are labelled as A, B', and D in the spectra are related to the CO_n complexes [22, 23]. (b) MCTS spectra recorded on neighboring samples to those used in the IR absorption measurements after same heat-treatments. All the samples we subjected to hydrogenation by etching in 1HF/7HNO_3 solution for 3 min prior to the measurements.

at 1104 cm^{-1} (A band), which has been related to a complex incorporating one oxygen and one carbon atom [21–23], and the magnitudes of the MCTS signal due to the H_1/H_2 traps.

From density functional calculations, the minimum energy configuration of the CO center consists of a substitutional carbon atom with an interstitial bond-centered oxygen atom separated from C_s by a silicon atom. The binding energy of the pair is 0.51 eV. This agrees with the results of previous calculations [24]. The calculated asymmetric stretching-mode frequency of the Si–O–Si unit in CO is 1074 cm^{-1}, which is about 20 cm^{-1} below the analogous mode frequency calculated for isolated O_i, and in good agreement with the infrared absorption data reported above. The CO pair is found to be an effective trap for hydrogen impurity atoms and the minimum energy configuration of the COH complex in the negative charge state (stable in n-type material) is shown in Fig. 3a. The binding energy of the H^- anion to the CO defect is found to be 0.74 eV, in line with the thermal stability of the H_1/H_2 traps. We predict that the COH complex shown in Fig. 3a introduces an acceptor level at about $E_v + 0.39$ eV into the band gap, which is very close to the experimentally determined values for the acceptor levels of the H_1/H_2 traps. Figure 3a also shows that the acceptor level of COH corresponds to a bonding state mostly localized on the Si–H bond and particularly on Si–Si bonds, therefore having a similar character to the topmost valence band states of Si. Combining this property with the fact that a negatively charged COH defect will attract holes, we may conclude that this complex has the right ingredients to be a rather effective minority carrier recombination center in n-type Si. As represented in Fig. 3b the mechanism involves capture of photo-generated holes, followed by capture of a majority carrier to recover equilibrium.

It has been found that like many other H-related defects in silicon the H_1/H_2 recombination centers anneal out at quite low temperatures, they have been shown to be eliminated after a 30-min anneal at 175 °C [20]. We have used this fact for studying an effect of the H_1/H_2 centers on minority carrier lifetime in silicon. Measurements of effective minority carrier lifetime in silicon wafers were carried out with the use of a Semilab WT-2000 PVN μ-PCD machine with the excitation of non-equilibrium carriers by pulses from a 904 nm semiconductor laser and microwave

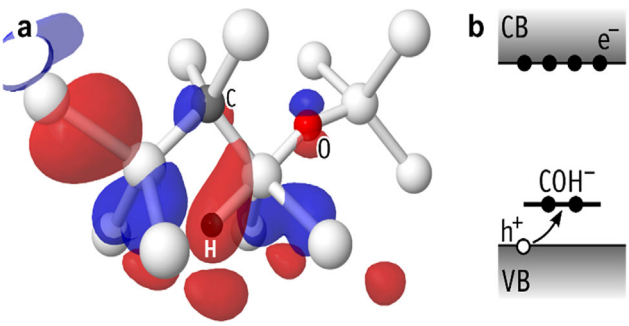

Figure 3 Structure of the COH complex. (a) Minimum energy configuration of the COH complex in the negative charged state. The isosurface depicts the highest occupied state for $\psi(\mathbf{k} = \Gamma, \mathbf{r}) = \pm 0.02$, with positive and negative phases shown in blue and red, respectively. (b) Band gap diagram showing the fully occupied acceptor state of COH depicted in (a), and how it interacts with minority carriers (h^+) in n-type material.

frequency of about 10 GHz. The wafers have been subjected to either wet chemical or H plasma treatments and their lifetime was then measured with iodine/ethanol surface passivation. The slices studied had a thickness of about 180 μm and resistivity 5 Ω · cm. The combination of microwave skin depth and LASER extinction depth results in the measured conductivity decay indicating a lifetime which is weighted to the region between the surface and a depth of ∼ 50 μm. This is much wider than the region in which we generate the H_1/H_2 recombination centers in our etching experiment (∼3 μm) [20] so this has to be considered when analyzing the effect of the recombination centers on the measured lifetime. The slices were then annealed at 200 °C for 10–20 min on a hot plate exposed to air so as to eliminate the COH defects and the lifetime measurements repeated. Figure 4 shows the comparison of two lifetime maps after KOH hydrogenation before (Fig. 4a) and after (Fig. 4b) a 200 °C anneal, the results show an increase of ∼45% in average lifetime. Overall the 200 °C anneal of the hydrogenated n-type Si:O + C samples resulted in an increase of the effective lifetime of 40–100% [20], so confirming the strong effect of the H_1/H_2 traps on the minority carrier lifetime despite the recombination due to H_1/H_2 being concentrated in a narrow surface region.

It should be mentioned, however, that the sample in which the annealing behavior of the H_1/H_2 traps was studied had hydrogen only present in a narrow sub-surface layer; during heat-treatments the hydrogen diffuses away to the surface and into the bulk. If hydrogen is retained in the slice (e.g., in samples with a SiN_x:H coating) then on cooling down after heat-treatments the recombination centers will reform and the minority carrier lifetime will remain degraded after thermal cycles. So, it is likely that the H_1/H_2 traps can survive after normal cell fabrication processes and hence reduce the efficiency of solar cells using n-type Si containing oxygen and carbon impurity atoms.

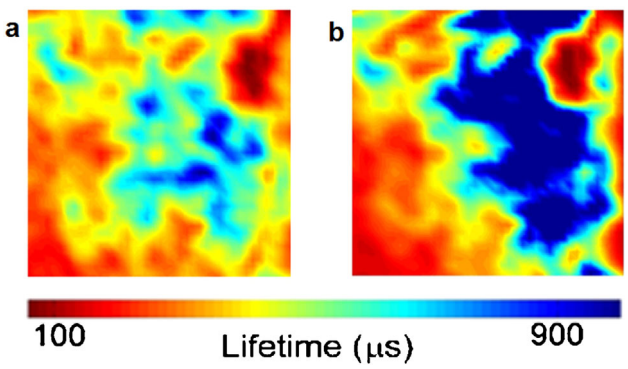

Figure 4 Maps of effective lifetime for an n-type C-Cz sample (4 cm × 4 cm) with iodine/ethanol surface passivation. (a) KOH etched sample to inject hydrogen into the sub-surface region. (b) Same sample after annealing at 200 °C to dissociate the hydrogen–oxygen recombination center. The averaged lifetime shows an increase from 381 to 549 μs after the annealing.

4 Conclusions It is shown in our work that very powerful recombination centers can be formed in n-type silicon by the interaction of hydrogen and carbon–oxygen defects. Our measurements indicate that under common manufacturing conditions the concentration of these recombination centers is sufficiently high to have an important effect on the minority carrier lifetime and, in consequence, on the efficiency of solar cells. The probability of this happening is large as carbon and oxygen are the main light element impurities in recent commercial Cz and C-Cz solar silicon [9], and hydrogen is readily introduced during solar cell processing. The properties of the defects are identical whether the hydrogen is introduced from wet etching, hydrogenated silicon nitride, or from remote hydrogen plasma. Hydrogen is thought to be a beneficial impurity in Si solar cells technology, however, as the solar industry moves to cheaper material manufacturing processes with higher carbon concentrations, care should be taken in order to prevent hydrogen interactions with carbon–oxygen defects and the formation of the detrimental COH complexes.

Acknowledgements The work was funded in the UK by EPSRC contract EP/M024911/1, and in Norway by the Research Centre for Solar Cell Technology (FME – Solar United). In Portugal, the work was funded by the FCT under projects PTDC/CTM-ENE/1973/2012 and UID/CTM/50025/2013, and funded by FEDER funds through the COMPETE 2020 Program. Computer resources were partially provided by the Swedish National Infrastructure for Computing (SNIC) at PDC. We would like to thank Alexander Hupfer at the University of Oslo for his assistance in the optical absorption measurements. Financial support was also given by CONACyT-Mexico.

References

[1] M. A. Green and S. P. Bremner, Nature Mater. **16**, 23 (2017).
[2] M. A. Green, Nature Energy **1**, 15015 (2016).
[3] G. Dingemans and W. M. M. Kessels, J. Vac. Sci. Technol. A **30**, 040802 (2012).
[4] A. G. Aberle, Prog. Photovolt. Res. Appl. **8**, 473 (2000).
[5] G. Dingemans, F. Einsele, W. Beyer, M. C. M. Van de Sanden, and W. M. M. Kessels, J. Appl. Phys. **111**, 093713 (2012).
[6] N. Nampalli, B. Hallam, C. Chan, M. Abbott, and S. Wenham, Appl. Phys. Lett. **106**, 173501 (2015).
[7] B. J. Hallam, P. G. Hamer, S. R. Wenham, M. D. Abbott, A. Sugianto, A. M. Wenham, C. E. Chan, G. Xu, J. Kraiem, J. Degoulange, and R. Einhaus, IEEE J. Photovolt. **4**, 88 (2014).
[8] R. Brunwin, B. Hamilton, P. Jordan, and A. R. Peaker, Electron. Lett. **15**, 349 (1979).
[9] K. Kakimoto, B. Gao, S. Nakano, H. Harada, and Y. Miyamura, Jpn. J. Appl. Phys. **56**, 020101 (2017).
[10] H. Xu, Energy Proc. **77**, 658 (2015).
[11] A. ur Rehman and S. H. Lee, Sci. World J. **2013**, 470347 (2013).

[12] L. Dobaczewski, A. R. Peaker, and K. B. Nielsen, J. Appl. Phys. **96**, 4689 (2004).
[13] G. Kresse and D. Joubert, Phys. Rev. B **59**, 1758 (1999).
[14] G. Kresse and J. Furthmüller, Phys. Rev. B **54**, 11169 (1996).
[15] J. P. Perdew, K. Burke, and M. Ernzerhof, Phys. Rev. Lett. **77**, 3865 (1996).
[16] H. J. Monkhorst and J. D. Pack, Phys. Rev. B **13**, 5188 (1976).
[17] A. Resende, R. Jones, S. Öberg, and P. R. Briddon, Phys. Rev. Lett. **82**, 2111 (1999).
[18] K. B. Nielsen, L. Dobaczewski, S. Søgård, and B. B. Nielsen, Phys. Rev. B **65**, 75205 (2002).
[19] A. V. Krukau, O. A. Vydrov, A. F. Izmaylov, and G. E. Scuseria, J. Chem. Phys. **125**, 224106 (2006).
[20] V. P. Markevich, M. V. Contreras, J. Mullins, M. Halsall, B. Hamilton, L. I. Murin, R. Falster, J. Binns, E. Good, J. Coutinho, J. Medford, C. L. Reynolds, and A. R. Peaker, Recombination centers resulting from reactions of hydrogen and oxygen in n-type Czochralski silicon, in: 2016 IEEE 43rd PV Spec. Conf., 2016, pp. 688–693.
[21] R. C. Newman and J. B. Willis, J. Phys. Chem. Solids **26**, 373 (1965).
[22] Y. Shirakawa, H. Yamada-Kaneta, and H. Mori, J. Appl. Phys. **77**, 41 (1995).
[23] Y. Shirakawa and H. Yamada-Kaneta, J. Appl. Phys. **80**, 4199 (1996).
[24] C. Kaneta, T. Sasaki, and H. Katayama-Yoshida, Phys. Rev. B **46**, 13179 (1992).

Publication No.3

Lifetime degradation of n-type Czochralski silicon after hydrogenation

Lifetime degradation of n-type Czochralski silicon after hydrogenation

M. Vaqueiro-Contreras, V. P. Markevich, J. Mullins, M. P. Halsall, L. I. Murin, R. Falster, J. Binns, J. Coutinho, and A. R. Peaker

Citation: Journal of Applied Physics **123**, 161415 (2018); doi: 10.1063/1.5011351
View online: https://doi.org/10.1063/1.5011351
View Table of Contents: http://aip.scitation.org/toc/jap/123/16
Published by the American Institute of Physics

JOURNAL OF APPLIED PHYSICS **123**, 161415 (2018)

Lifetime degradation of n-type Czochralski silicon after hydrogenation

M. Vaqueiro-Contreras,[1] V. P. Markevich,[1] J. Mullins,[1] M. P. Halsall,[1] L. I. Murin,[2] R. Falster,[3] J. Binns,[4] J. Coutinho,[5] and A. R. Peaker[1]
[1]*Photon Science Institute, University of Manchester, Manchester M13 9PL, United Kingdom*
[2]*Materials Research Center NAS, Minsk 220072, Belarus*
[3]*SunEdison Semiconductor, Ltd., viale Gherzi 31, 28100 Novara, Italy*
[4]*SunEdison Inc., 7832 N. Leadbetter Rd., Portland, Oregon 97203, USA, [Now owned by GCL Solar Materials, 7833 North Leadbetter Road, Portland, Oregon, 97203 USA]*
[5]*Department of Physics and I3N, University of Aveiro, Aveiro 3810-193, Portugal*

(Received 31 October 2017; accepted 21 February 2018; published online 14 March 2018)

Hydrogen plays an important role in the passivation of interface states in silicon-based metal-oxide semiconductor technologies and passivation of surface and interface states in solar silicon. We have shown recently [Vaqueiro-Contreras *et al.*, Phys. Status Solidi RRL **11**, 1700133 (2017)] that hydrogenation of n-type silicon slices containing relatively large concentrations of carbon and oxygen impurity atoms $\{[C_s] \geq 1 \times 10^{16}\,cm^{-3}$ and $[O_i] \geq 10^{17}\,cm^{-3}\}$ can produce a family of C-O-H defects, which act as powerful recombination centres reducing the minority carrier lifetime. In this work, evidence of the silicon's lifetime deterioration after hydrogen injection from SiN_x coating, which is widely used in solar cell manufacturing, has been obtained from microwave photoconductance decay measurements. We have characterised the hydrogenation induced deep level defects in n-type Czochralski-grown Si samples through a series of deep level transient spectroscopy (DLTS), minority carrier transient spectroscopy (MCTS), and high-resolution Laplace DLTS/MCTS measurements. It has been found that along with the hydrogen-related hole traps, H_1 and H_2, in the lower half of the gap reported by us previously, hydrogenation gives rise to two electron traps, E_1 and E_2, in the upper half of the gap. The activation energies for electron emission from the E_1 and E_2 trap levels have been determined as 0.12, and 0.14 eV, respectively. We argue that the E_1/H_1 and E_2/H_2 pairs of electron/hole traps are related to two energy levels of two complexes, each incorporating carbon, oxygen, and hydrogen atoms. Our results show that the detrimental effect of the C-O-H defects on the minority carrier lifetime in n-type Si:O + C materials can be very significant, and the carbon concentration in Czochralski-grown silicon is a key parameter in the formation of the recombination centers. https://doi.org/10.1063/1.5011351

I. INTRODUCTION

Hydrogen has been used for over 50 years in the semiconductor industry to passivate surface and interface states by satisfying dangling bonds. This was the important breakthrough in the 1970s,[1] which enabled metal-oxide-semiconductor (MOS) and complementary MOS (CMOS) signal processing devices to be made reproducibly and is still an important part in the processing of modern microelectronic devices ranging from semiconductor memory to processor chips.[2] Hydrogen passivation of interface states and recombination centers in multicrystalline and crystalline silicon materials has also been successfully used in solar cell processing[3–6] and has become a part of solar silicon research and technologies.[7,8] Such passivation results in fewer carriers being lost at the surface of the silicon solar cell, at the interface with the anti-reflection dielectric layers, and in the solar material bulk thereby contributing to increased cell efficiencies. Achieving higher efficiencies of solar cells has become the prime target for the solar cell industry as discussed in a recent review paper by Green.[9]

However, somewhat surprisingly we have found recently that hydrogen atoms can react with carbon-oxygen-related defects in silicon to produce powerful recombination centers, which reduce the minority carrier lifetime in n-type silicon containing O impurity atoms and higher than usual concentrations of C, thereby reducing the efficiency of any solar cells made from such material.[10,11] We have reported the observation of two very powerful recombination centers, H_1 and H_2, formed by carbon-oxygen and hydrogen (C-O-H) interactions in a range of n-type Czochralski (Cz) Si materials grown by conventional and continuous Czochralski (C-Cz) techniques.[11] These types of materials are gaining ground in the solar industry for high efficiency products because of a number of beneficial properties compared to p-type silicon. They have, particularly, a higher "as grown" lifetime, lesser sensitivity to metallic contaminations, and negligible light induced degradation.[12,13] However, the oxygen concentration is high ($\geq 5 \times 10^{17}\,cm^{-3}$) in Czochralski-grown silicon, and some Cz- and C-Cz-Si materials grown for solar applications contain rather high ($>2 \times 10^{16}\,cm^{-3}$) concentration of carbon atoms. As hydrogen is frequently encountered in the silicon solar materials either by deliberate introduction or as a result of wafer processing, the likelihood of the formation of the C-O-H complexes is quite significant in n-type Cz-Si and C-Cz-Si, thereby making the solar cells from these materials more susceptible to an efficiency decrease if the C-O-H reaction can

progress and the complex retained in the finished product. It has been found that like many other H-related defects in silicon, the H_1/H_2 recombination centers anneal out at quite low temperatures, and they have been shown to be eliminated after a 30-min heat-treatment at 175 °C.[10] However, as we have suggested in Refs. 10 and 11, when enough hydrogen is present in hydrogenated solar cells, the C-O-H complexes can reform upon cooling the cells after heat treatments at $T \geq 200$ °C and thereby reduce the cell efficiency.

In the present work, we show the results of a series of microwave photoconductance decay (μPCD) measurements, which validate the earlier suggestion and demonstrate lifetime deterioration in n-type Cz-Si samples after hydrogen injection from SiN_x coating, which is widely used in solar cell manufacturing, and after the introduction of hydrogen by other methods. Further, it is shown that along with the hydrogen-related H_1 and H_2 hole traps in the lower half of the gap, hydrogenation of n-type Cz-Si samples give rise to two electron traps (E_1 and E_2) in the upper half of the gap. These electron traps have been characterized and their origin is discussed.

II. EXPERIMENTAL DETAILS

We have carried out measurements of minority carrier lifetime and characterization of deep level defects on samples from a wide range of n-type phosphorus doped Cz- and C-Cz-Si wafers with resistivity between 1 and 8 Ω cm. The concentration of interstitial oxygen atoms, $[O_i]$, was in the range from 12 to 20 ppma (1 ppma $= 5 \times 10^{16}$ cm^{-3}), while the concentration of substitutional carbon atoms, $[C_s]$, varied from 0.01 to 9 ppma in the samples studied. Also a few float zone (FZ) grown silicon samples with $[O_i] < 0.2$ ppma have been studied for a comparison. The samples were cut and RCA cleaned, and hydrogen was then introduced into the silicon by three different techniques: (1) wet etching with either KOH or HF/HNO_3 solution, (2) 50 W remote H plasma exposure for 30 min at temperatures between 25 and 250 °C, and (3) in-diffusion of hydrogen from H-rich silicon nitride (SiN_x:H) films. SiN_x:H films were deposited by the Plasma-Enhanced Chemical Vapour Deposition (PECVD) technique, in a PlasmaPro 100 PECVD system, using Oxford Instruments. The deposition parameters were: 20:20 sccm SiH_4:NH_3 gas flow, 300 mTorr chamber pressure, 400 °C table temperature, 13.56 MHz plasma generated frequency, and 50 W of power. These parameters produced a 90 nm SiN_x:H film after 2 min of plasma exposure, which was then etched off in an Oxford Instruments System 100 180 RIE system before measurements of minority carrier lifetime. For etching the SiN_x:H films, the samples were exposed for 50 s to a 6 W RF plasma plus a 600 W inductively coupled plasma (ICP) of O_2:CHF_3:CF_4 (2:10:23 sccm) gas, at 13.56 MHz. The annealing of the samples, aimed at the dissociation of the hydrogen-related recombination active defects, has been carried at 200 °C in an oven in air ambient.

The microwave photoconductivity decay (μPCD) lifetime mapping was carried out with the use of a Semilab WT-2000 PVN machine, which has 905 nm LASER excitation and a microwave source operating at ~10 GHz. The lifetime maps thus represent an averaged lifetime in the sample at a depth of a few tens of microns from the surface. For suppression of surface recombination, the maps were recorded with both surfaces of the samples covered with iodine/ethanol solution.[14]

For deep level transient spectroscopy (DLTS) and minority carrier transient spectroscopy (MCTS) measurements,[15] the samples were cleaned and subjected to evaporation of Au through a shadow mask from the front side and to Al evaporation without mask on the back side, to produce Schottky barrier diodes and an Ohmic contact, respectively. An un-metalized region of the Ohmic contact was left on the back of the MCTS samples to allow an optical excitation from a 940 nm light emitting diode (LED). Each diode was characterized first with the current-voltage and capacitance-voltage measurements, and subsequently DLTS, MCTS, and high resolution Laplace DLTS/MCTS[16] measurements were carried out for the detection and characterization of electrically active defects.

III. EXPERIMENTAL RESULTS AND DISCUSSION

A. Effect of hydrogenation treatments on minority carrier lifetime in n-type Cz-Si

We have carried out a series of μPCD measurements to observe the reduction of the minority carrier lifetime induced by hydrogen introduction with different methods into an n-Si sample with $[O_i] = 7.5 \times 10^{17}$ cm^{-3}, $[C_s] = 4.5 \times 10^{17}$ cm^{-3}, and 2 mm thickness. Figure 1 shows a set of minority carrier lifetime maps recorded on the Si:O + C sample, which was subjected to the following subsequent hydrogenation treatments: (a) wet etching in $1HF + 7HNO_3$ solution for 3 min at room temperature (RT), (b) 50 W remote H plasma exposure for 30 min at RT, (c) wet etching in 20% KOH solution for 10 min at 60 °C. Figure 1 also shows a lifetime map recorded on the other side of the same sample after in-diffusion of hydrogen from H-rich silicon nitride (SiN_x:H) films (the deposition temperature was 400 °C). All the maps were recorded immediately after each hydrogenation treatment and then after annealing at 200 °C for 20 min to destroy the C-O-H complexes.

An inspection of the lifetime maps in Fig. 1 shows that each hydrogenation step resulted in the lifetime degradation of the material and its partial recovery after the heat treatments at 200 °C. Further, some decrease in the averaged lifetime (τ_{av}) occurred in the course of the subsequent hydrogenation-annealing steps from the first cycle with HF/HNO_3 etching ($\tau_{av} = 273$ μs) to the last one with KOH etching ($\tau_{av} = 111$ μs). Such a reduction can be associated with the accumulated introduction of hydrogen into the sample after each hydrogenation step, thereby making the thermally induced recovery of lifetime more difficult after each of the subsequent hydrogenation-annealing cycles. The depth of the hydrogen penetration into the sample upon the SiN_x:H film deposition procedure is greater than in any other hydrogenation treatments used in this study because of the higher processing temperature, so it is likely that the recombination active C-O-H complexes have been re-formed in the SiN-processed sample during cooling down after the 200 °C annealing. The re-formed C-O-H complexes are responsible for the low τ_{av} value, 117 μs, after the recovery annealing treatment. The results of lifetime mapping presented in Fig. 1 validate the idea suggested in Refs. 10 and 11 regarding the recovery of the C-O-H

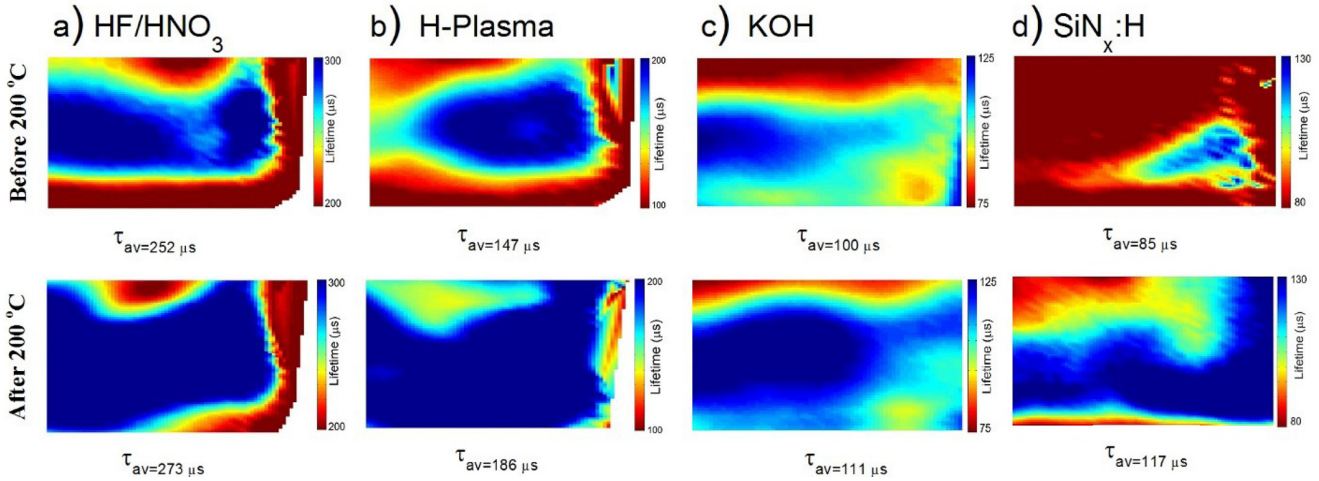

FIG. 1. Lifetime maps of an n-Si sample with $[O_i] = 7.5 \times 10^{17}\,cm^{-3}$, $[C_s] = 4.5 \times 10^{17}\,cm^{-3}$, and 2 mm thickness recorded with the use of Semilab WT-2000 PVN machine and iodine/ethanol surface passivation after hydrogenation with four different methods and subsequent heat-treatments at 200 °C for 20 min to destroy the C-O-H recombination centers.

complexes upon cooling down the n-type Si:O + C samples after their heat-treatments at temperatures higher than 200 °C when enough hydrogen is present in the samples. It is very likely that the C-O-H complexes can survive in n-type Cz-Si-based solar cells throughout the manufacture processing, which incorporate a SiN_x:H film deposition step, thereby resulting in a reduction of efficiency of the finished solar cells.

B. Electronic properties of the hydrogenation induced electron traps in n-type Cz-Si and their possible origin

In our previous paper,[10] the DLTS and MCTS spectra for one of the hydrogenated n-type Si:C + O samples have been shown. In the DLTS spectra, four peaks due to electron traps labelled as E_1 to E_4 have been detected, and in the MCTS spectra, four negative peaks due to hole traps labelled as H_1 to H_4 have occurred. These peaks can be seen in Figs. 2, 4, and 5 in the present paper. In Ref. 11, we have characterized and identified the dominant hole traps, H_1 and H_2, in hydrogenated n-type Cz-Si samples. From a series of Laplace MCTS measurements, the positions of energy levels of the H_1 and H_2 traps have been determined as $E_v + 0.38$ eV and $E_v + 0.36$ eV, respectively, and the ratios of the capture cross sections of minority (holes) and majority (electrons) carriers as 50 and 40, respectively.[11] The measured parameters indicate that both the H_1 and H_2 traps are related to the acceptor levels of two defects, which are powerful recombination centers for holes in n-type Si crystals and are responsible for the lifetime degradation in the hydrogenated n-type Cz-Si crystals. We have demonstrated the involvement of carbon, oxygen, and hydrogen atoms in the formation of centers responsible for the H_1 and H_2 traps, and with the use of low temperature infrared absorption measurements, it has been found that a complex consisting of a substitutional carbon and an interstitial oxygen atom (C-O) is a pre-cursor of these defects.[11] The possible structures of the C-O-H complex with electronic properties close to those for the H_1 and H_2 traps have been found from the first principles calculations.[11,17]

Here, we present results of a study of the electronic properties and thermal stability of the E_1, E_2, and E_4 electron traps and some results on the relation of these traps to the most abundant oxygen, carbon, and hydrogen impurities. It should be noted, however, that the E_1 – E_4 traps do not appear to be the significant recombination centers for holes in n-type Si crystals because of the closeness of their energy levels to the conduction band edge.

Figure 2 shows the development of the DLTS and MCTS spectra upon 30-min isochronal annealing of a hydrogenated n-type Cz-Si sample in the temperature range from 50 °C to 200 °C. It can be seen that the annealing behaviour of the E_1 and E_2 electron traps is similar to that of the H_1/H_2 hole traps. Both pairs of traps disappear upon heat-treatments in the temperature range of 150–175 °C. In contrast, the magnitude of the peak related to the E_4 trap has increased after the 150 °C and 175 °C annealing steps. The E_4 trap has been assigned in our previous work (Ref. 10) to the second donor level of the oxygen-related thermal double donors (TDDs).[18] Even though hydrogen can passivate TDDs, the binding energy of H atoms to the TDDs centers is not high, and the electrical activity of TDDs is restored after heat-treatments in the temperature range of 150–175 °C.[19] We have roughly estimated the activation energy for the E_4 trap recovery from the isochronal annealing data in Fig. 2 and obtained the value of 1.65 ± 0.05 eV, which is close to that found in Ref. 19 for the elimination of the TDD-H complexes. So, our results on the annealing behavior of the E_4 trap validate the assignment of this trap to TDDs and are consistent with the previous DLTS results on TDDs and their passivation with hydrogen.[18,19]

The similarity in the elimination behaviour of the E_1/H_1 and E_2/H_2 trap pairs (Fig. 2) suggests that these pairs can be related to two energy levels of two defects. Later on, we present some results, which confirm this suggestion. Figure 3 shows the concentration profiles of the H_2 and E_2 traps in a Cz-Si sample, which was subjected to etching in $1HF + 7HNO_3$ solution for 3 min at room temperature. The profiles have been obtained with the use of Laplace DLTS/MCTS techniques; however, the

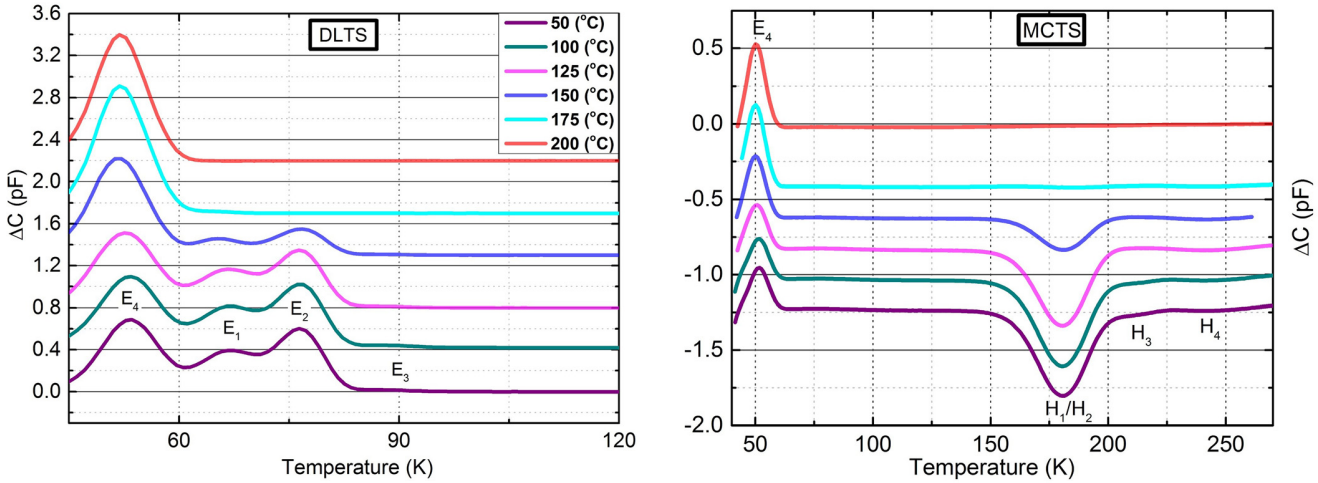

FIG. 2. DLTS and MCTS spectra of a hydrogenated n-type Cz-Si sample, which was subjected to 30-min isochronal annealing in the temperature range of 50 °C to 200 °C. The spectra are shifted on the vertical axis for clarity. Hydrogen was introduced into the sample by etching in $1HF + 7HNO_3$ solution for 3 min at room temperature.

measurement conditions for the E_2 and H_2 traps were different. The concentration profile for the E_2 trap has been obtained using L-DLTS by changing both bias and pulse voltages (U_b and U_p, respectively) and a fixed difference between U_b and U_p. So, the concentration values for the E_2 trap have been determined in nearly equidistant relatively narrow probing areas.[20,21] In MCTS measurements, only the reverse bias can be changed, and the probing area for minority carrier traps extends from the junction ($W_1 = 0$) to the depletion depth under reverse bias ($W_2 = W_b$). So, the concentration values for the H_2 trap in Fig. 3 are the mean concentration values for the relatively wide probing areas (e.g. the deepest point for the H_2 trap concentration in Fig. 3 corresponds to the mean concentration in a region between 0 and 2.85 μm). Taking into account the earlier and other possible sources of errors in the determination of minority carrier trap concentration using MCTS measurements,[15,22] it appears that the profiles presented in Fig. 3 are almost certainly related to the same defect. The profiles are characteristics of the defects induced by hydrogen in-diffusion during wet chemical etching of n-type Si samples.[10,23–25]

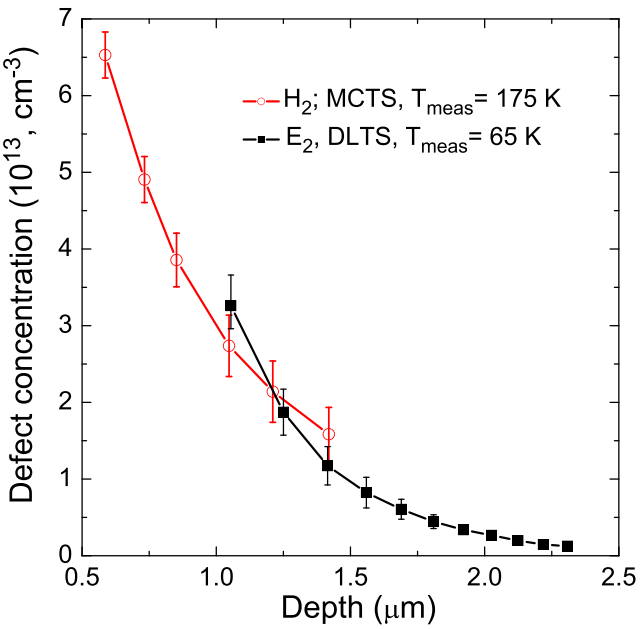

FIG. 3. Concentration profiles of the H_2 hole traps and E_2 electron trap in a Cz-Si sample. Hydrogen was introduced into the sample by etching in $1HF + 7HNO_3$ solution for 3 min at room temperature. The profiles were measured with the use of L-DLTS and L-MCTS techniques for the E_2 and H_2 traps, respectively. Further details of the measurements and analysis are given in the text.

The E_1 and E_2 electron traps have been observed in the DLTS spectra of hydrogenated Cz-Si samples but not in the spectra of hydrogenated FZ-Si samples. This observation indicates an involvement of oxygen impurity atoms into the corresponding defect structures. We have further investigated the possible links of the E_1 and E_2 electron traps to carbon and oxygen impurities. In Fig. 4, the DLTS and MCTS spectra are compared for four hydrogenated as-grown n-type Cz samples with different C_s and nearly equal O_i concentrations. In order to take into account the differences in resistivity of the samples studied, we have plotted the value of $2 \times N_d \times \Delta C/C_b$ on the vertical axis of Fig. 4, where ΔC is the magnitude of a capacitance change related to carrier emission from traps, N_d is the concentration of doping atoms, and C_b is the bias capacitance. Figure 4 show similar changes in concentrations of the E_1 and E_2 electron traps and H_1/H_2 hole traps with changes in the carbon concentration in the samples. It should be noted here that the dependence of the concentration of the C-O complex on $[C_s]$ and $[O_i]$ values is not straightforward, as the [C-O] value depends on thermal prehistory of Si samples.[11,26–28] It is possible to change the [C-O] value significantly by heat-treatments of the Si:O + C samples in the temperature range of 500–800 °C.[27,28] The DLTS and MCTS spectra presented in Fig. 5 show similar changes in the concentration of the E_1/E_2 electron traps and H_1/H_2 hole traps in samples from a carbon and oxygen rich Si material, which were subjected to heat-treatments in the temperature range of 500–750 °C with subsequent hydrogenation.

A comparison of the introduction and annealing behaviours of the E_1 and E_2 electron traps and H_1 and H_2 hole traps (Figs. 2–5) strongly indicates that the E_1/H_1 and E_2/H_2 pairs

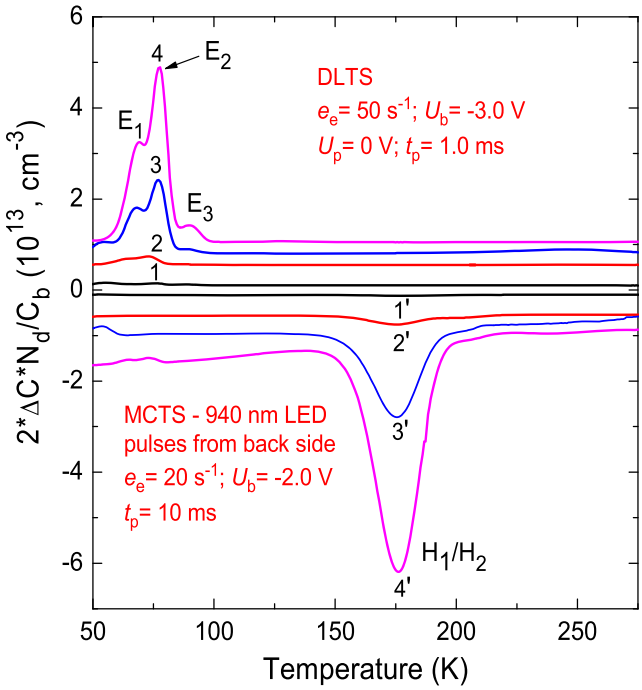

FIG. 4. DLTS (1 to 4) and MCTS (1′ to 4′) spectra for a set of four hydrogenated n-type Cz-Si samples with $[O_i] \sim 7.5 \times 10^{17}\,cm^{-3}$ and different $[C_s]$: 1, 1′ – 0.01 ppma; 2, 2′ – 0.1 ppma; 3, 3′ – 1.2 ppma; and 4, 4′ – 9 ppma. The measurements parameters are given in the graph. The spectra are shifted on the vertical axis for clarity. Hydrogen was introduced into the sample by etching in $1HF + 7HNO_3$ solution for 3 min at room temperature.

can be associated with two energy levels of two complexes each incorporating one oxygen, one carbon, and one hydrogen atom. We have argued in our previous study (Ref. 11) that the H_1 and H_2 hole traps are related to the first acceptor levels of two C-O-H complexes. So, if the E_1/H_1 and E_2/H_2 pairs are related to two energy levels of two C-O-H defects, it is reasonable to associate the E_1 and E_2 traps with the second acceptor levels of the defects.

We have carried out Laplace DLTS measurements of electron emission rates (e_n) and capture cross sections (σ_n) for the E_1 and E_2 traps to determine their electronic characteristics. From the Arrhenius plots of T^2-corrected emission rates, we have derived the activation energies for the electron emission from the defect levels to the conduction band and pre-exponential factors as follows: 0.12 ± 0.005 eV and $3.3 \times 10^7\,s^{-1}K^{-2}$; 0.14 ± 0.005 eV and $2.1 \times 10^7\,s^{-1}K^{-2}$ for the E_1, and E_2 traps, respectively. From direct measurements of the majority carrier capture cross sections, we found the following σ_n values for the E_1 and E_2 traps 5.7×10^{-16} cm^2 and 7.35×10^{-16} cm^2, respectively. No significant temperature dependences of σ_n have been detected for both traps.

The E_1 and E_2 electron traps have been observed and characterized in previous works by Yoneta *et al.*[24] and by Gwozdz *et al.*[25] The results presented in Refs. 24 and 25 are, in general, consistent with our results on the E_1 and E_2 electron traps. There are, however, some discrepancies related to the identification of the charge state of the E_1 and E_2 traps. Yoneta *et al.*[24] have said that "the results on depth profiles of these traps and carriers suggested the donor character of the traps, but they hardly exhibited the Poole-Frenkel effect." On the other hand, Gwozdz *et al.* on the basis of their analysis of dependencies of electron emission rates from the E_1 and E_2 traps (labelled as E65 and E75 traps in Ref. 25) on the electric field strength have related these traps to single acceptor levels.[25] It should be noted that the values of the directly measured electron capture cross sections for the E_1 and E_2 traps given in Ref. 25 ($\sigma_n = 2 \times 10^{-18}$ cm^2 for both the traps) indicate the electron capture by a negatively charged defect (and so the second acceptor level) rather than a neutral one.

To obtain some further data to resolve the question regarding the charge state of the E_1 and E_2 traps, we have studied the dependencies of the electron emission rates from these traps on the electric field strength with the use of Laplace double DLTS technique.[16] The obtained dependencies are shown in Fig. 6. It appears that the dependencies can be described well by a $e_n \propto \exp(E^2)$ law, thereby indicating the phonon-assisted tunnelling as the mechanism for the electric field enhancement of electron emission.[29,30] The phonon-assisted tunnelling has been shown to be the mechanism of the electric field enhancement of carrier emission for a number of defect levels related to the double to single charge state transitions in Si and Ge.[31–33] So, the results obtained support our assignment of the E_1 and E_2 electron traps to the second acceptor levels of two C-O-H complexes.

The first principles calculations in Refs. 11 and 17 have revealed several possible structures of the C-O-H defect with the first acceptor in the lower part of the gap. The possible existence of a second acceptor level has not been calculated for these structures. So, further experimental and ab-initio

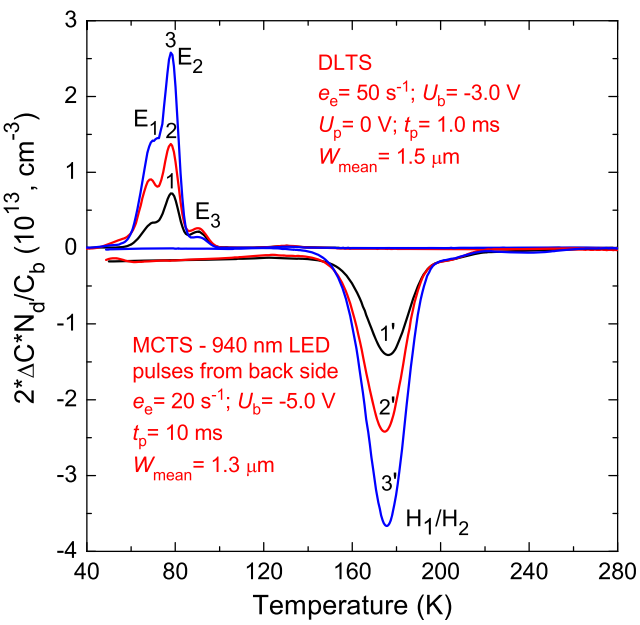

FIG. 5. DLTS (1 to 3) and MCTS (1′ to 3′) spectra for a set of three hydrogenated samples from n-type Cz-Si material with $[O_i] \approx 7.5 \times 10^{17}\,cm^{-3}$ and $[C_s] \approx 4.5 \times 10^{17}\,cm^{-3}$. Before hydrogenation, the samples were subjected to the following heat-treatments: 1, 1′ – 0.5 h at 750 °C; 2, 2′ – 1.5 h at 500 °C; and 3, 3′ – 1 h at 550 °C. The measurements parameters are given in the graph. The spectra are shifted on the vertical axis for clarity. Hydrogen was introduced into the sample by etching in $1HF + 7HNO_3$ solution for 3 min at room temperature.

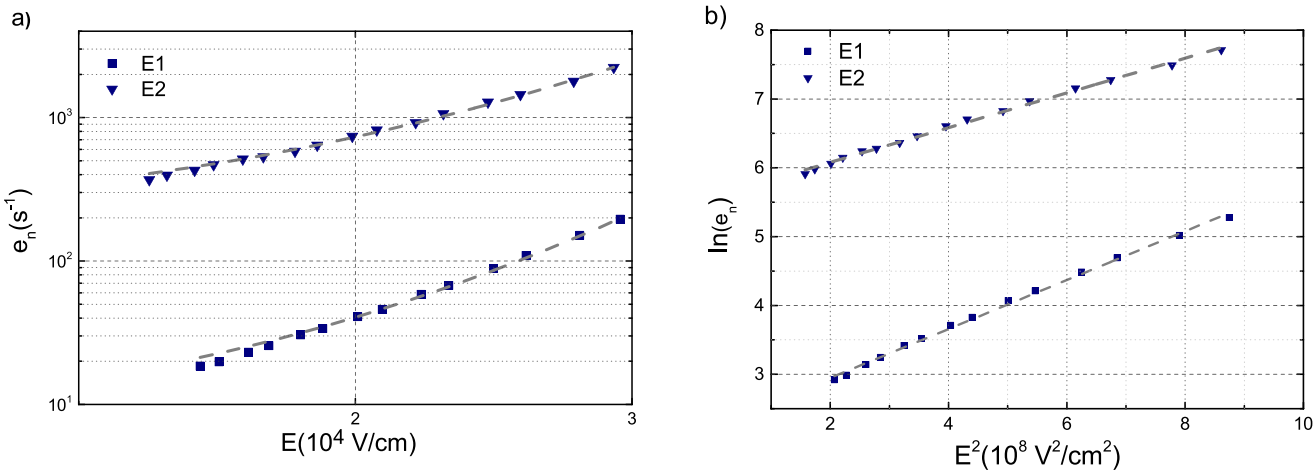

FIG. 6. Dependencies of the rate of electron emission, e_n, on (a) electric field, and (b) ln(e_n) on squared electric field for the E_1 and E_2 electron traps. The e_n values have been measured at 70 K for the E_1 trap and at 80 K for the E_2 trap with the use of Laplace double DLTS technique. The dashed lines in (a) represent the data fitted to $e(E) = e(0)\exp(E^2/E^2_{ch})$ (Refs. 29 and 30) and linear fits in (b).

modelling studies are needed to identify configurations and explain the electronic structures of the two C-O-H complexes responsible for the E_1/H_1 and E_2/H_2 electron/hole traps responsible for the lifetime degradation in hydrogenated n-type Si crystals containing a relatively large carbon concentration.

IV. CONCLUSIONS

A number of minority and majority carrier traps are observed in phosphorous doped silicon containing oxygen and carbon impurity atoms after the introduction of hydrogen. Some of the traps act as powerful recombination centres, which severely decrease minority carrier lifetime in the Si:O + C materials. We demonstrate such an effect by μPCD mapping of the effective lifetime in a carbon and oxygen rich Cz-Si sample, which was subjected to hydrogenation by four different techniques. The dominant recombination active defects are identified as two complexes each incorporating carbon, oxygen, and hydrogen atoms. Our results indicate that even though the defects are disassociated by heat-treatments at relatively low temperatures (~200 °C), they are likely to reform upon cooling the samples down when enough hydrogen is retained in the silicon. Particularly, it is shown that such a scenario can be realized in the case of Cz-Si-based solar cells covered with SiN_x:H dielectric films, which are widely used in solar cell industry for anti-reflection and surface passivation purposes. The rise in C_s concentrations in recent commercial Cz and C-Cz solar silicon increases the probability of the formation of the C-O-H complexes and the associated decrease in efficiency of the solar cell produced from such materials. So, care should be taken for controlling the carbon concentration in solar grade silicon as it is one of the key parameters for the formation of the detrimental C-O-H traps.

ACKNOWLEDGMENTS

Special thanks are due to Dr. Ernie Hill and Maddison Coke for their support and advice during PECVD and plasma etch in the UK National Graphene Institute. The work was supported by the UK Engineering and Physical Sciences Research Council (EPSRC) under the SuperSilicon PV Contract (EP/M024911/1). Financial support was also given by CONACyT-Mexico.

[1]A. B. Fowler, U.S. patent 3,849,204 (1974).
[2]A. R. Peaker, V. P. Markevich, and L. Dobaczewski, in *Defects in Microelectronic Materials and Devices*, edited by D. M. Fleetwood, S. T. Pantelides, and R. D. Schrimpf (CRC Press, Boca Raton, 2009), Chap. 2, pp. 27–56.
[3]C. Dubé, J. I. Hanoka, and D. B. Sandstrom, Appl. Phys. Lett. **44**, 425 (1984).
[4]B. Sopori, J. Electron. Mater. **31**, 972 (2002).
[5]G. Hahn and A. Schönecker, J. Phys.: Condens. Matter **16**, R1615 (2004).
[6]L. J. Geerlings, Y. Komatsu, I. Röver, K. Wambach, I. Yamaga, and T. Saitoh, J. Appl. Phys. **102**, 093702 (2007).
[7]B. J. Hallam, P. G. Hamer, S. R. Wenham, M. D. Abbott, A. Sugiantov *et al.*, IEEE J. Photovoltaics **4**, 88 (2014).
[8]N. Nampalli, B. Hallam, C. Chan, M. Abbott, and S. Wenham, Appl. Phys. Lett. **106**, 173501 (2015).
[9]M. A. Green, Nat. Energy **1**, 10015 (2016).
[10]V. P. Markevich, M. V. Contreras, J. Mullins, M. Halsall, B. Hamilton *et al.*, in *Proceedings of the 43rd IEEE Photovoltaic Specialists Conference* (2016), pp. 688–693.
[11]M. Vaqueiro-Contreras, V. P. Markevich, M. P. Halsall, A. R. Peaker, P. Santos *et al.*, Phys. Status Solidi RRL **11**, 1700133 (2017).
[12]H. Xu, Energy Proc. **77**, 658 (2015).
[13]A. ur Rehman and S. H. Lee, Sci. World J. **2013**, 470347 (2013).
[14]N. Batra, S. Kumar, M. Sharma, S. K. Shrivastava, P. Sharma, and P. K. Singh, Sol. Energy Mater. Sol. Cells **100**, 43 (2012).
[15]R. Brunwin, B. Hamilton, P. Jordan, and A. R. Peaker, Electron. Lett. **15**, 349 (1979).
[16]L. Dobaczewski, A. R. Peaker, and K. B. Nielsen, J. Appl. Phys. **96**, 4689 (2004).
[17]P. Santos, J. Coutinho, S. Oberg, M. Vaqueiro-Contreras, V. P. Markevich *et al.*, Phys Status Solidi A **214**, 1700309 (2017).
[18]L. C. Kimerling and J. L. Benton, Appl. Phys. Lett. **39**, 410 (1981).
[19]D. I. Bohne and J. Weber, Phys. Rev. B **47**, 4037 (1993).
[20]P. I. Rocket and A. R. Peaker, Appl. Phys. Lett. **40**, 957 (1982).
[21]D. Stievenard and D. Vuillaume, J. Appl. Phys. **60**, 973 (1986).
[22]J. A. Davidson and J. H. Evans, J. Appl. Phys. **81**, 251 (1997).
[23]Y. Tokuda, I. Katoh, H. Ohshima, and T. Hattori, Semicond. Sci. Technol. **9**, 1733 (1994).
[24]M. Yoneta, Y. Kamiura, and F. Hashimoto, J. Appl. Phys. **70**, 1295 (1991).
[25]K. Gwozdz, R. Stübner, V. Kolkovsky, and J. Weber, Appl. Phys. Lett. **111**, 32102 (2017).
[26]R. C. Newman and J. B. Willis, J. Phys. Chem. Solids **26**, 373 (1965).
[27]Y. Shirakawa, H. Yamada-Kaneta, and H. Mori, J. Appl. Phys. **77**, 41 (1995).

[28]Y. Shirakawa and H. Yamada-Kaneta, J. Appl. Phys. **80**, 4199 (1996).
[29]S. D. Ganichev, W. Prettl, and I. N. Yassievich, Phys. Solid State **39**, 1703 (1997).
[30]S. D. Ganichev, E. Ziemann, W. Prettl, I. N. Yassievich, A. A. Istratov *et al.*, Phys. Rev. B. **61**, 10361 (2000).
[31]N. Zangenberg, J.-J. Goubet, and A. Nylandsted Larsen, Nucl. Instrum. Methods Phys. Res., Sect. B **186**, 71 (2002).
[32]V. P. Markevich, A. R. Peaker, V. V. Litvinov, L. I. Murin, and N. V. Abrosimov, Physica B **376–377**, 200 (2006).
[33]V. P. Markevich, A. R. Peaker, B. Hamilton, S. B. Lastovskii, and L. I. Murin, J. Appl. Phys. **115**, 012104 (2014).

Publication No.4

Theory of a carbon-oxygen-hydrogen recombination center in n-type Si

Wiley Online Library
Early View publication on www.wileyonlinelibrary.com
(issue and page numbers not yet assigned;
citable using Digital Object Identifier – **DOI**)

Phys. Status Solidi A, 1700309 (2017) / **DOI** 10.1002/pssa.201700309

physica status solidi a
www.pss-a.com
applications and materials science

Theory of a carbon-oxygen-hydrogen recombination center in n-type Si

Paulo Santos[1], José Coutinho[*,1], Sven Öberg[2], Michelle Vaqueiro-Contreras[3], Vladimir P. Markevich[3], Matthew P. Halsall[3], and Anthony R. Peaker[3]

[1] Department of Physics and I3N, University of Aveiro, Campus Santiago, 3810-193 Aveiro Portugal
[2] Department of Engineering Sciences and Mathematics, Luleå University of Technology, SE-97187 Luleå, Sweden
[3] Photon Science Institute, University of Manchester, M13 9PL, UK

Received 17 December 2016, revised 18 May 2017, accepted 18 May 2017
Published online 22 June 2017

Keywords carbon, charge carrier recombination, defects, hydrogen, oxygen, silicon

* Corresponding author: e-mail jose.coutinho@ua.pt, Phone: +351 234 247 051, Fax: +351 234 378 197

We have recently found that in-diffusion of hydrogen into n-type Si crystals containing oxygen and carbon impurities can result in the formation of powerful recombination centers (M. Vaqueiro-Contreras et al., to appear in PSS RRL). Here, we describe a combination of first-principles calculations and electrical measurements to investigate the composition, structure, electrical activity and recombination mechanism of a carbon-oxygen-hydrogen complex (COH) in Si. We found a defect comprising a carbon-oxygen complex connected to an H atom whose location depends on the charge state of the complex, and showing a calculated acceptor level at $E_v + 0.3$ eV, a few meV away from the observations.

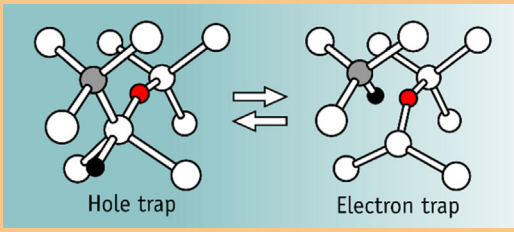

Bistable carbon–oxygen–hydrogen complex in silicon. Carbon, oxygen, hydrogen, and silicon atoms are shown in gray, red, black, and white, respectively.

1 Introduction Hydrogen, oxygen and carbon species are common contaminants in several kinds of silicon materials. Their origin is broad-based, ranging from the graphite components in the Czochralski (Cz) furnace (carbon), to the intrinsic composition of the SiO_2 crucible (oxygen), or simply, they may be unavoidable (such as hydrogen) [1–3]. Their presence is not always unintentional though. For instance, during solar cell fabrication, specific impurities are deliberately introduced, one prominent example being the deposition of a front-facing silicon nitride anti-reflection layer, which introduces large quantities of fast-diffusing atomic hydrogen into the Si [4]. This process brings important benefits, such as the reduction of surface recombination, although the underlying mechanism and possible side-effects of H injection are far from clear.

Isolated carbon and oxygen impurities in Si are electrically inert and have been subjected to extensive experimental and theoretical studies. In as-grown Cz-Si, they occur in large concentrations (usually in magnitudes of ppm atoms), normally occupying substitutional (C_s) and bond-centered interstitial (O_i) sites of the Si lattice, respectively. More than four decades ago, Newman, Willis and Bean assigned an infrared absorption band at 1104 cm^{-1} to a vibrational mode localized on a substitutional-carbon-interstitial-oxygen (CO) complex in Si [5, 6]. Combined annealing and isotope frequency shift data led the authors to the interpretation that the band resulted from the capture of a diffusing O_i impurity, which becomes mobile above ~450 °C, by a substitutional carbon atom. These results were later supported and translated into an atomistic model by Kaneta and co-workers [7], where the O atom was not directly connected to C. Instead, C and O atoms were separated by an intermediate Si atom forming a C_s-Si-O_i unit, avoiding the formation of a C–O bond, in favor of

stronger Si-O and C-Si bonds. The electronic activity of this center was not addressed at the time, but considering the coordination of the C, O, and Si-ligand atoms, the complex is expected to be electrically inactive.

Atomic hydrogen is an amphoteric impurity with negative-U ordered donor and acceptor occupancy levels at $E_c - 0.18$ eV and $\sim E_c - 0.5$ eV [8–11], respectively. It is a bistable impurity – in the positive charge state it is most stable on the site of highest electron density, that is at the bond-center site (H_{BC}^{+}), while in the negative charge state it avoids high electron density regions due to Coulomb repulsion, preferring to be located at the tetrahedral interstitial site (H_T^{-}) [3]. The neutral defect is more stable at the BC site, meaning that the donor level involves essentially a direct transition between bond-centered H_{BC}^{0} and $H_{BC}^{+} + e^{-}$ states, hereafter referred to as a $H_{BC}(0/+)$ transition, where the final state includes a free electron in the conduction band. On the other hand, the acceptor is the energy difference between H_T^{-} and $H_{BC}^{0} + e^{-}$, therefore involving a considerable lattice relaxation energy. This indirect transition is referred to as $H_{T/BC}(-/0)$.

Atomic H is known to interact effectively with both carbon and oxygen impurities in Si. For the case of carbon, theory and (Laplace) deep-level transient spectroscopy (DLTS) studies agree that the most stable form of a CH complex is the one in which the H sits between the C atom and its Si first neighbor [12]. Unlike isolated bond-centered H, it was reported that the C-H-Si defect (labeled CH_{II}) shows a positive-U ordering of its donor and acceptor states at $E_v + 0.33$ eV and $E_c - 0.16$ eV, respectively [12]. An additional donor level at $E_c - 0.22$ eV (labeled CH_I) was connected to a metastable precursor of CH_{II}, and was suggested to consist on a Si-H-Si unit neighboring the C_s atom [12]. In a recent report by Stübner and co-workers [13], from the analysis of DLTS, field-induced change of emission rates, annealing and depth-profile data, it was confirmed that the $E_c - 0.16$ eV level (CH_{II} in Ref. [12], but now referred to as CH_A) is an acceptor. However, they could not find any sign of CH_I. Instead, a shallower donor transition at $E_c - 0.14$ eV (labeled CH_B) was assigned to a CH_n complex involving $n > 1$ hydrogen atoms [13].

With regards to the interaction of atomic H with O_i, we know from DLTS that the electrical levels of OH are close to those of isolated H. Accordingly, donor and acceptor occupancy transitions at $E_c - 0.17$ eV and $E_c - 0.68$ eV were assigned to OH in Si [10, 11]. Although first-principles modeling predict that hydrogen enhances oxygen diffusivity and that it does not bind directly to O [14–16], calculations of the electronic structure and electronic levels of OH in Si have not been reported so far.

We have recently reported the formation of powerful recombination centers in n-type silicon as a result of the reaction between hydrogen, carbon and oxygen species [17]. Accordingly, hole traps H_1 and H_2 at 0.38 and 0.36 eV above E_v, respectively, were detected in Cz-Si subject to wet etching, remote plasma exposure and silicon nitride deposition, and they were assigned to COH complexes. We also demonstrated that the concentration of these COH defects is high enough to have a substantial impact on the minority carrier lifetime of Si-based solar cells.

Below we report on our latest results on the search for the atomistic and electronic details of the COH-related recombination center in Si by combining first-principles calculations with DLTS and LVM infrared absorption measurements. The next section starts with a description of the methods employed, which is followed by a summary of the key observations related to the complex. We then report on the interaction of atomic H with C and O. These results are particularly instructive. They provide us with the fundamental physical-chemical guidelines behind the model that explains the formation and properties of COH. Among the calculated observables we report binding energies, vibrational mode frequencies and electronic transitions.

2 Methods

2.1 Experimental details For this work we selected a range of Cz and continuous Cz (CCz) n-type silicon slices with oxygen concentrations in the range $12 < [O_i] < 20$ ppma (1 ppma $= 5 \times 10^{16}$ cm^{-3}) and substitutional carbon concentration of $0.01 < [C_s] < 9$ ppma. In addition, as a control sample we included silicon grown by the float zone (FZ) method which had $[O_i]$ and $[C_s] < 0.2$ ppma. All the material was phosphorus doped with resistivities in the range 1–8 Ω-cm. The samples were hydrogenated in three different ways. Hydrogen was introduced into the samples, firstly, by wet etching with HF/HNO_3 solutions, secondly, by immersion in a 50 W remote H plasma for 30 min at temperatures between 25 and 250 °C, and, finally, in a way intended to simulate hydrogenation in a typical solar cell manufacturing process by in-diffusion of hydrogen from a H-rich silicon nitride film.

Schottky diodes and Ohmic contacts were fabricated on the samples prior to capacitance-voltage and DLTS measurements. Minority carrier transient spectroscopy (MCTS) [18] using a 940 nm light emitting diode for optical excitation from the back of the slice was used to determine the electronic properties of hole traps including directly measured capture cross sections used to calculate the contribution of carrier recombination at the traps to the minority carrier lifetime.

Local mode optical absorption measurements were undertaken at 30 K in the wavenumber range 500–1500 cm^{-1} in order to observe the vibrational modes of CO_n complexes in the samples.

Minority carrier lifetime measurements were made using a Semilab WT-2000 PVN μ-PCD machine and iodine/ethanol surface passivation of the wafers.

2.2 Theoretical details First-principles density functional calculations were carried out using the VASP package [19], which uses the projector-augment wave (PAW) method [20] to deal with core-electrons and planewaves with a maximum kinetic energy $E_{cut} = 370$ eV for the valence. Exchange-correlation interactions were

dealt within the generalized gradient approximation [21], and the electron density (potential) was assumed to be converged when the energy change between two consecutive self-consistent steps was less than 1 μeV.

Substitutional C, interstitial O, and interstitial H impurities were inserted into pristine 216-Si-atom supercells with cubic shape, optimized lattice constant $a = 5.4687$ Å, and respective Brillouin zones sampled over a $2 \times 2 \times 2$ grid of special **k**-points. All defect structures were optimized using a quasi-Newton algorithm, until the forces acting on the atoms were converged within 0.01 eV Å^{-1}.

Electronic transitions were evaluated using the marker method [22]. Experimental levels from isolated interstitial H and from the vacancy-oxygen-hydrogen complex (VOH), were used as markers. When compared to bulk markers, these choices increase the accuracy of the calculated levels (often by about 0.1 eV) of complexes that incorporate bond-centered/tetrahedral H or a Si broken bond, respectively. The levels considered were $H_{BC}(0/+) = E_c - 0.175$ eV, $H_{T/BC}(-/0) = E_c - 0.5$ eV, $VOH(0/+) = E_v + 0.27$ eV, and $VOH(-/0) = E_c - 0.32$ eV [8–11, 23].

LVM frequencies were obtained through diagonalization of a dynamical matrix composed of Hessian submatrices with respect to the displacement of impurity atoms plus their Si ligands. Hessian matrix elements were obtained numerically with explicit atomic displacements of 0.015 Å along all symmetry-independent directions.

3 Experimental results In MCTS and DLTS spectra of the hydrogenated oxygen and carbon rich Si samples, four electron and four hole emission peaks were detected. In the DLTS spectrum shown in Fig. 1, the peak labeled as E_4 is associated with the so-called thermal double donors originating from oxygen complexes [24], whereas the peaks E_1–E_3 are related to hydrogen complexes [25, 26].

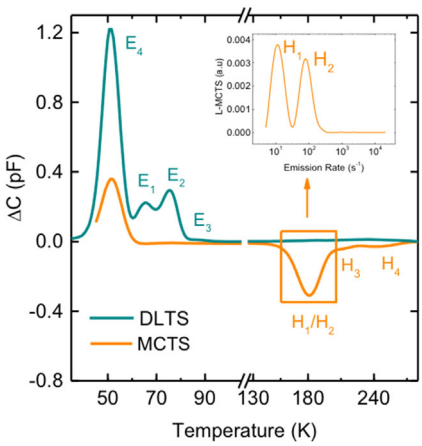

Figure 1 DLTS and MCTS spectra recorded on a sample from an n-type Cz-Si wafer, which was etched in 1HF/7HNO$_3$ solution for 2.5 min. We used $e_e = 50\,s^{-1}$, $U_b = -2$ V, and $t_p = 10$ ms in all measurements and 940 nm LED pulses for the MCTS. The insert shows the separation of the H_1 and H_2 emission signals in the Laplace MCTS spectrum recorded at 190 K.

The E_1–E_4 traps are not significant in terms of lifetime degradation and will not be further considered in this work. The MCTS spectrum and the L-MCTS spectrum, presented as an inset in the same figure, show hole emission related signals H_1 to H_4. We have found that the dominant H_1/H_2 signals are dependent of carbon, oxygen and hydrogen content.

Firstly, we have compared the DLTS and MCTS spectra of a FZ sample with almost negligible [O_i] and [C_s] with the spectra for Cz and CCz samples after hydrogenation. In the FZ hydrogenated samples the H_1 and H_2 signals were not detected [27], while for the Cz and CCz samples the signals showed a proportional increase with O_i and C_s content in the crystals. Secondly, the concentration depth profiles of the H_1 and H_2 traps are found to be similar to that for the phosphorus-hydrogen complex formed in the hydrogenated samples. This provides an evidence of the involvement of a single hydrogen atom into the defects, which give rise to the H_1 and H_2 traps. Finally, a good correlation has been found between the intensity of the LVM band with its maximum at 1104 cm^{-1} observed in the infrared absorption spectra of carbon and oxygen rich samples subjected to different heat-treatments in the temperature range 550–700 °C and magnitudes of the MCTS signals due to the H_1/H_2 traps in similarly heat-treated neighboring samples, which were hydrogenated and prepared for MCTS measurements [17]. The band at 1104 cm^{-1} is related to an LVM of the CO complex [5, 6]. The results mentioned above give solid evidence of the carbon-oxygen-hydrogen composition of the complexes responsible for the H_1/H_2 traps.

With L-MCTS we have carried out direct measurements of electron and hole capture cross-sections and hole emission rates of the H_1 and H_2 traps. The details of the measurement technique can be found in Ref. [27]. Capture cross-section measurements of minority and majority carriers resulted respectively in values of 9.8×10^{-16} and 2.0×10^{-17} cm^2 for H_1, and of 7.9×10^{-16} and 1.95×10^{-17} cm^2 for H_2. The defect levels obtained from the Arrhenius plots of T^2-corrected hole emission rates correspond to 0.38 ± 0.01 eV and 0.36 ± 0.01 eV from the valence band for the H_1 and H_2 centers, respectively. These characteristics indicate that the defects have an acceptor-like behavior and likely to be powerful recombination centers in n-type material. Furthermore, it has been found that the H_1/H_2 traps anneal out in the temperature range from 150 to 200 °C and their elimination resulted in significant improvement of lifetime in silicon wafers (see Refs. [17] and [27]).

4 Theoretical results

4.1 Carbon–hydrogen interactions Figure 2(a) shows a substitutional carbon atom in Si with several Si ligands. It also shows some sites (black dots) among many at which we placed a hydrogen atom to investigate the relative stability of CH complexes. In agreement with Andersen et al. [12], we found that for all charge states investigated (−, 0, and +), H prefers to connect directly to the carbon atom, close to site BC1. Other low-energy structures are

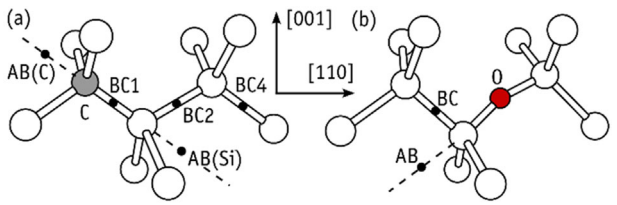

Figure 2 Low-energy sites (black dots), for hydrogen next to (a) substitutional carbon and (b) interstitial oxygen impurities. These diagrams are only schematic, representing approximate structures of defects obtained after atomic relaxation. C, O, and Si are represented in gray, red, and white, respectively.

BC2 and AB(C). In the neutral charge state, their energies are 0.51 and 0.64 eV above the BC1 ground state.

The formation of a short C–H bond is an important stabilization factor for CH_{BC1}, in spite of the fact that it also leaves an unsaturated radical on the nearest Si atom. This dangling bond creates a semi-occupied one-electron state deep in the gap, making VOH an excellent marker to calculate its electronic levels. Comparing ionization energies and electron affinities of CH_{BC1} with the same quantities from VOH we obtain donor and acceptor levels for CH_{BC1} at $E_v + 0.28$ eV and $E_c - 0.17$ eV, respectively, at most $\sim$0.05 eV away from the transitions observed at $E_v + 0.33$ eV and $E_c - 0.16$ eV (labeled CH_{II}) [12, 13].

Also in line with Ref. [12], we found that in the positive and negative charge states the BC2 and AB(C) structures are metastable by only 0.30 and 0.23 eV, respectively. The former configuration comprises a Si-H^+_{BC}-Si unit next to C_s, and therefore it is expected to show donor activity in close resemblance to that of isolated H in Si. Here, isolated H_{BC} should be a good marker. Accordingly, we obtain a $CH_{BC2}(0/+)$ transition at $E_c - 0.24$ eV, about 0.02 eV deeper than the measured additional CH-related donor reported in Ref. [12] and labeled CH_I. It is relevant to note that the calculated $H_{BC2}(0/+)$ location is deeper than $CH_{BC1}(-/0)$ and also deeper than isolated $H_{BC}(0/+)$. This is in excellent agreement with the relative locations of the CH_I, CH_{II} and $E3'$ DLTS signals [9, 11, 12]. We also found that $CH_{BC4}(0/+)$ (where H sits at the fourth neighboring BC-site to the C atom) has a donor level at 0.22 eV below E_c, that is closer but still deeper than $H_{BC}(0/+)$ and also still below $H_{BC1}(-/0)$.

Following the suggestion of Ref. [13], that a CH_n complex (with $n > 1$) could be responsible for a donor level at $E_c - 0.14$ eV (labeled CH_B), we actually investigated that possibility for $n = 2$. We found that CH_2 can adopt two nearly degenerate configurations (within 30 meV) similar to that of H_2^* in Si, forming C-$H_{BC1} \cdots$ Si-$H_{AB(Si)}$ and $H_{AB(C)}$-C $\cdots$ H_{BC1}-Si trigonal structures. The configuration with both H atoms bound to the C atom is metastable by 0.6–1 eV (depending on the charge state). We also found that the two lowest-energy structures are electrically inert, and therefore, should the $E_c - 0.14$ eV level belong to a CH_n complex, our results indicate that $n > 2$, most likely with one H atom located on a Si–Si bond.

4.2 Oxygen–hydrogen interactions Among the oxygen-hydrogen complexes investigated, those obtained after placing H next to interstitial O, as depicted in Fig. 2(b), had the lowest energy. While OH_{BC} is the ground state in the positive charge state, OH_{AB} was the most stable configuration in the negative charge state. The neutral defect is more stable with H at the BC-site (with OH^0_{AB} being metastable by 0.23 eV only). We note that the H atom in OH_{BC} adopts a puckered configuration, making a Si-H-Si angle of 136° after structural relaxation. This means that some of the compressive strain, which is present in isolated Si-H^+_{BC}-Si and Si-O-Si defects along their 111 bond directions, is released in OH^+_{BC} and that corresponds to a calculated binding energy of 0.30 eV. The binding energy of atomic H^- to interstitial O (with OH^-_{AB} as a reaction product) is estimated as 0.47 eV after considering independent supercells with H^-_T and O_i defects. Here, the negatively charged hydride ion establishes an ionic bond with the oxidized (positively charged) silicon atom that is connected to oxygen. The above figures match the experimentally determined binding energies of 0.29 and $\sim$0.5 eV for defects which give rise to the $E3''$ and AT'' signals [10, 11], assigned to oxygen perturbed (0/+) and (−/0) transitions of bond-centered and tetrahedral hydrogen, respectively.

Further confirmation of the above model comes from the calculated electrical levels. In this case, isolated atomic H is expected to do a good job as marker. Accordingly, we place $OH_{BC}(0/+)$ and $OH_{T/BC}(-/0)$ transitions at $E_c - 0.16$ eV and $E_c - 0.69$ eV, respectively, in excellent agreement with the measured $E3''$ and AT'' signals with levels at $E_c - 0.17$ eV and $E_c - 0.68$ eV, respectively.

4.3 Carbon–oxygen–hydrogen complex In line with Ref. [7], we found that in the ground state of the CO complex, the O atom is located at the BC2-site with respect to carbon (see Fig. 2(a)). CO_{BC1} and CO_{BC4} configurations were metastable by 1.23 and 0.15 eV, respectively. The binding energy of CO_{BC2} (against formation of uncorrelated substitutional carbon and interstitial oxygen impurities) was found to be 0.51 eV. Inspection of the band structure revealed a clean band gap and no electrical levels were found.

The CO complex gives rise to three C-related LVM absorption bands at 589, 640, and 690 cm^{-1}, respectively 18 cm^{-1} below and 33 and 83 cm^{-1} above the unperturbed C_s-related triplet mode at 607 cm^{-1}. It also produces an O-related band at 1104 cm^{-1}, 32 cm^{-1} below the prominent 1136 cm^{-1} band from interstitial O [5, 6]. LVM frequency calculations for the CO_{BC2} model give C-modes at 557, 608, and 663 cm^{-1} plus one O-mode at 1074 cm^{-1}. The C-modes are 18 cm^{-1} below and 34, and 88 cm^{-1} above the calculated 575 cm^{-1} mode of isolated carbon. Analogously, we find the calculated O-mode frequency at 1074 cm^{-1}, 20 cm^{-1} below that of isolated O (calculated at 1094 cm^{-1}). These figures improve previous modeling results [7], account very well for the observations, and provide undisputable evidence for the correctness of the atomistic model.

For the interaction of H with CO, we found several low-energy configurations, which differ on the defect charge state. For a negatively charged COH (which should be stable under equilibrium in n-type material) we found that the structure shown in Fig. 3(a) and labeled COH_{AB}, is distinctly stable. Analogously to OH^{-}_{AB}, the H^{-} anion is attached to the electron-depleted Si atom, which in this case is further oxidized due to the bond with an electronegative C atom.

For the neutral defect, we found the COH_{BC1} configuration shown in Fig. 3(b) to be the ground state. COH^{0}_{AB} is now metastable by 0.18 eV. The BC1 structure is made of a CH_{BC1} defect perturbed by a nearby interstitial O atom, so it is expected to show rather similar electronic properties to CH_{BC1}. Another low energy configuration was COH^{0}_{BC2} (0.05 eV above the ground state), which is depicted in Fig. 3(c).

Finally, for positively charged COH, the ground state configuration is now COH_{BC2} (Fig. 3(c)), which resembles an OH^{+}_{BC} complex stabilized by a nearby tensile C_s defect. Another stable structure is COH^{+}_{BC1} (0.08 eV above the BC2 ground state).

Now we proceed to the calculation of the electrical levels of COH. On this report, we will focus on the acceptor activity only. Accordingly, the relevant acceptor transitions are $COH_{AB}(-/0)$, $COH_{AB/BC1}(-/0)$ and $COH_{AB/BC2}(-/0)$. While the last two involve electronic states similar to that of the $H_{T/BC}(-/0)$ marker, the $COH_{AB}(-/0)$ direct transition finds no resemblance with either $H_{T/BC}(-/0)$ or $VOH(-/0)$. Conversely, the $OH_{AB}(-/0)$ transition (observed at $E_c - 0.79$ eV [11]) should closely describe the $COH_{AB}(-/0)$ level. Hence, we obtain indirect $COH_{AB/BC1}(-/0)$ and $COH_{AB/BC2}(-/0)$ levels at $E_c - 0.81$ eV and $E_c - 0.76$ eV, respectively, that is, $E_v + 0.31$ eV and $E_v + 0.36$ eV if we consider 1.12 eV for the band gap of Si. We also find a direct $COH_{AB}(-/0)$ at $E_c - 0.80$ eV.

Although all three calculated levels agree very well with the location of the H_1/H_2 hole traps, we note that we have two rather different mechanisms that could explain the recombination activity. These are (i) a direct $COH_{AB}(-/0)$ transition, or (ii) a mechanism involving indirect $COH_{AB/BC1}(-/0)$ and $COH_{AB/BC2}(-/0)$ levels which imply a structural change in the neutral charge state. A deeper understanding of the above processes will involve the calculation of the potential energy surface between the AB, BC1, and BC2 configurations. We leave this for a future report to be published elsewhere.

The structural distinction between the H_1 and H_2 traps is also an open question. Until now, we have considered the interactions between single C, O, and H species. It is possible that one of these traps involves two O or H atoms, and we intend to look at this problem in the near future.

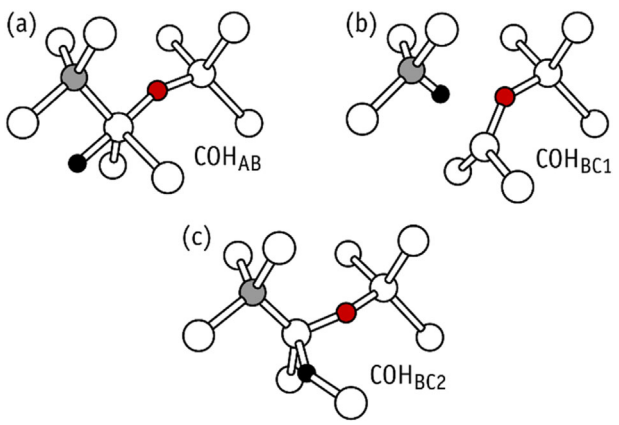

Figure 3 Ground state structures for COH in the negative (a), neutral (b), and positive (c) charge states. Si, C, O, and H atoms are shown in white.

Table 1 Calculated (calc) and experimental (exp) electronic levels of the defects investigated in this work. All values are given in eV.

electronic level	calc	exp
$E_c - CH_{BC1}(-/0)$	0.17	0.16 [12]
$CH_{BC1}(0/+) - E_v$	0.28	0.33 [12]
$E_c - CH_{BC2}(0/+)$	0.24	0.22 [12]
$E_c - OH_{AB/BC}(-/0)$	0.69	0.68 [11]
$E_c - OH_{BC}(0/+)$	0.16	0.17 [10]
$E_c - COH_{AB}(-/0)$	0.80	
$E_c - COH_{AB/BC1}(-/0)$	0.81	
$E_c - COH_{AB/BC2}(-/0)$	0.76	

5 Conclusions We presented a joint theoretical and experimental study of the interaction of H with carbon- and oxygen-related defects in silicon. For convenience, we summarize all calculated levels and experimental assignments in Table 1.

We started by reporting on the interaction of H with a C_s impurity, where based on the total energies and calculated levels, we confirm the support from first-principles theory to the assignment of CH_{II} and CH_I DLTS signals in Ref. 12 to carbon-hydrogen defects with the H atom on the first- and second-neighboring BC sites with respect to a C_s impurity, respectively. We did not find any CH defect with two or less H atoms, which could give rise to a donor transition above $H_{BC}(0/+)$. This suggests that the CH_B level at $E_c - 0.14$ eV reported in Ref. [13] could be related to a CH_n complex involving $n > 2$ hydrogen atoms.

The calculations support the interpretation of earlier experimental work [11], according to which H can bind to interstitial oxygen to from either OH^{+} or OH^{-} with negative-U ordering of the donor and acceptor levels. We found that for the positive charge state H is nearly bond-centered forming a Si-H^{+}_{BC}-Si-O_i-Si zig-zag chain (like the O-dimer in Si), while the negative defect adopts an anti-bonding configuration that results in a nearly trigonal H^{-}_{AB}-Si-O-Si linear defect. The calculated binding energies and electrical levels are in excellent agreement with the observations.

We finally investigated the CO complex and its interaction with H. We confirm that C and O atoms in CO are bound to a common Si atom – no direct C–O bond is established. The calculated local vibrational mode frequencies for this complex account very well for all four bands observed by infra-red absorption measurements.

The COH complex is predicted to adopt different configurations in all three charge states that were investigated (−, 0, and +). In the negative charge state, and particularly in n-type material, the complex takes the form of an OH_{AB}^{-} defect perturbed by a nearby C_s impurity, being therefore referred to as COH_{AB}^{-}. We suggest that this structure, shown in Fig. 3(a), corresponds to the observed hole-trapping center reported in Section 3. The neutral charge state was found to have several virtually degenerate configurations with the H atom either connected to the C atom, or at a nearby BC site (see Fig. 3(b) and (c)). Several calculated electrical levels are close to the observed H_1/H_2 traps, although further work is needed in order to understand eventual defect transformations upon carrier trapping/emission events.

Acknowledgements This work was supported by the FCT under projects PTDC/CTM-ENE/1973/2012 and UID/CTM/50025/2013, funded by FEDER funds through the COMPETE 2020 Program. Computer resources were partially provided by the Swedish National Infrastructure for Computing (SNIC) at PDC. In the UK this work was funded by EPSRC contract EP/M024911/1.

References

[1] R. Jones (Ed.), Early stages of oxygen precipitation in silicon, in: NATO Advance Science Institutes, Series 3: High Technology, Vol. 17 (Kluwer Academic, Dordrecht, 1996), https://doi.org/10.1007/978-94-009-0355-5

[2] R. C. Newman and R. Jones, Curr. Opin. Solid State Mater. Sci. **2**, 40–47 (1997). https://doi.org/10.1016/S1359-0286(97)80103-9

[3] S. K. Estreicher, M. Stavola, and J. Weber, Hydrogen in Si and Ge, in Silicon, Germanium, and Their Alloys: Growth, Defects, Impurities, and Nanocrystals, edited by G. Kissinger and S. Pizzini (CRC, Boca Raton, 2015), pp. 217–254.

[4] F. Duerinckx and J. Szlufcik, Sol. Energy Mater. Sol. Cells **72**, 231 (2002). https://doi.org/10.1016/S0927-0248(01)00170-2

[5] R. C. Newman and J. B. Willis, J. Phys. Chem. Solids **26**, 373–379 (1965). https://doi.org/10.1016/0022-3697(65)90166-6

[6] A. R. Bean and R. C. Newman, J. Phys. Chem. Solids **33**, 255–268 (1972). https://doi.org/10.1016/0022-3697(72)90004-2

[7] C. Kaneta, T. Sasaki, and H. Katayama-Yoshida, Phys. Rev. B **46**, 13179 (1992). https://doi.org/10.1103/PhysRevB.46.13179

[8] B. Holm, K. Bonde Nielsen, and B. Bech Nielsen, Phys. Rev. Lett. **66**, 2360 (1991). https://doi.org/10.1103/PhysRevLett.66.2360

[9] N. M. Johnson, C. Herring, and C. G. Van de Walle, Phys. Rev. Lett. **74**, 1889 (1995). https://doi.org/10.1103/PhysRevLett.74.1889

[10] K. Bonde Nielsen, B. Bech Nielsen, J. Hansen, E. Andersen, and J. U. Andersen, Phys. Rev. B **60**, 1716 (1999). https://doi.org/10.1103/PhysRevB.60.1716

[11] K. Bonde Nielsen, L. Dobaczewski, S. Søgård, and B. Bech Nielsen, Phys. Rev. B **65**, 075205 (2002). https://doi.org/10.1103/PhysRevB.65.075205

[12] O. Andersen, A. R. Peaker, L. Dobaczewski, K. Bonde Nielsen, B. Hourahine, R. Jones, P. R. Briddon, and S. Öberg, Phys. Rev. B **66**, 235205 (2002). https://doi.org/10.1103/PhysRevB.66.235205

[13] R. Stübner, V. Kolkovsky, and J. Weber, J. Appl. Phys. **118**, 055704 (2016). https://doi.org/10.1063/1.4928146

[14] S. K. Estreicher, Phys. Rev. B **41**, 9886 (1990). https://doi.org/10.1103/PhysRevB.41.9886

[15] R. Jones, S. Öberg, and A. Umerski, Mater. Sci. Forum **83-87**, 551 (1992). https://doi.org/10.4028/www.scientific.net/MSF. 83-87. 551

[16] S. K. Estreicher, Early stages of oxygen precipitation in silicon, in: NATO Advance Science Institutes, Series 3: High Technology, Vol. 17, edited by R. Jones (Kluwer Academic, Dordrecht, 1996), pp. 179–195. https://doi.org/10.1007/978-94-009-0355-5

[17] M. Vaqueiro-Contreras, V. P. Markevich, M. Halsall, A. R. Peaker, P. Santos, J. Coutinho, S. Öberg, L. Murin, R. Falster, J. Binns, E. Monakhov, and B. G. Svensson, to appear in Phys. Status Solidi RRL.

[18] R. Brunwin, B. Hamilton, P. Jordan, and A. R. Peaker, Electron. Lett. **15**, 349 (1979). https://doi.org/10.1049/el:19790248

[19] G. Kresse and J. Furthmüller, Comput. Mater. Sci. **6**, 15 (1996). https://doi.org/10.1016/0927-0256(96)00008-0

[20] P. E. Blöchl, Phys. Rev. B **50**, 17953 (1994). https://doi.org/10.1103/PhysRevB.50.17953

[21] J. P. Perdew, K. Burke, and M. Ernzerhof, Phys. Rev. Lett. **77**, 3865 (1996). https://doi.org/10.1103/PhysRevLett.77.3865

[22] A. Resende, R. Jones, S. Öberg, and P. R. Briddon, Phys. Rev. Lett. **82**, 2111 (1999). https://doi.org/10.1103/PhysRevLett.82.2111

[23] J. Coutinho, O. Andersen, L. Dobaczewski, K. Bonde Nielsen, A. R. Peaker, R. Jones, S. Öberg, and P. R. Briddon, Phys. Rev. B **68**, 184106 (2003). https://doi.org/10.1103/PhysRevB.68.184106

[24] L. Kimerling and J. Benton, Appl. Phys. Lett. **39**, 410 (1981). https://doi.org/10.1063/1.92755

[25] M. Yoneta, Y. Kamiura, and F. Hashimoto, J. Appl. Phys. **70**, 1295 (1991). https://doi.org/10.1063/1.349586

[26] Y. Tokuda, I. Katoh, H. Ohshima, and T. Hattori, Semi. Sci. Tech. **9**, 1733 (1994). https://doi.org/10.1088/0268-1242/9/9/026

[27] V. P. Markevich, M. Vaqueiro Contreras, J. Mullins, M. Halsall, B. Hamilton, L. I. Murin, R. Falster, J. Binns, E. Good, J. Coutinho, J. Medford, C. L. Reynolds Jr., and A. R. Peaker, 2016 IEEE 43rd Photovoltaic Specialists Conference (PVSC), (Portland, 2016), pp. 0688–0693. https://doi.org/10.1109/PVSC. 2016.7749689

3.3 Oxygen-related Bistable Thermal Double Donors

Publication No.5

Electron emission and capture by oxygen-related bistable thermal double donors in silicon studied with junction capacitance techniques

Electron emission and capture by oxygen-related bistable thermal double donors in silicon studied with junction capacitance techniques

V.P. Markevich[1], M. Vaqueiro-Contreras[1], S.B. Lastovskii[2], L.I. Murin[2], M.P. Halsall[1], and A.R. Peaker[1]

[1] *Photon Science Institute and School of Electrical and Electronic Engineering, the University of Manchester, Manchester M13 9PL, United Kingdom*

[2] *Scientific-Practical Materials Research Center of the National Academy of Sciences of Belarus, Minsk 220072, Belarus*

It has been recently suggested that oxygen-related bistable thermal double donors (BTDDs) are responsible for the reduction of minority carrier lifetime and conversion efficiency of novel amorphous-crystalline Si hetero-junction solar cells with their base formed from n-type Czochralski-grown (Cz) silicon *(M. Tomassini et al., J. Appl. Phys.* ***119****, 084508 (2016))*. To test this hypothesis we have studied processes associated with carrier emission and capture by BTDDs in p^+-n and Schottky barrier diodes on n-type Cz-Si materials with the use of junction capacitance techniques. By means of deep level transient spectroscopy we have detected electron emission signals from deep donor state of the BTDD-0 and BTDD-1 centers. The values of activation energy for electron emission (E_{em}) have been determined as 1.01 ± 0.01 and 0.91 ± 0.01 eV for the BTDD-0 and BTDD-1 centers, respectively. Such high E_{em} values are very unusual for defects in Si. We have carried out measurements of electron capture kinetics and associated shallow donor – deep donor transformations for the BTDD-0 and BTDD-1 defects at different temperatures in the diodes with different doping levels. Energy barriers for the capture-transformation processes have been determined. It is argued that BTDDs are responsible for carrier trapping in n-type Cz-Si crystals but are not effective recombination centers.

I. INTRODUCTION

It has been known since the 1950's that heat-treatments of oxygen-rich Si crystals in the temperature range 350-500 ^{o}C result in the formation of a family of defects with shallow donor levels.[1,2] It has been further found that the defects are helium-like centers with the donor levels

$E(0/+)$ and $E(+/+2)$ located in the energy ranges from 0.05 to 0.07 eV below the conduction band edge [E_c-(0.05-0.07) eV] and E_c-(0.12-0.16) eV, respectively.[3-6] Strong evidence has been presented that the formation of the centers is associated with clustering of interstitial oxygen atoms upon heat-treatments.[7-9] Therefore, the defects are usually referred to as oxygen-related thermal double donors (TDDs).[8] The TDD defect family consists of up to 17 species (from-TDD-0 to TDD-16) differing by the number of oxygen atoms incorporated.[8,10,11] It is thought that oxygen atoms in TDDs are arranged in linear chains lying in <110> planes. Structural models of TDD species with some differences in details of positions and bonding of O and Si atoms and different explanations of the origin of their electrical activity have been proposed in *ab initio* modelling studies.[12-14]

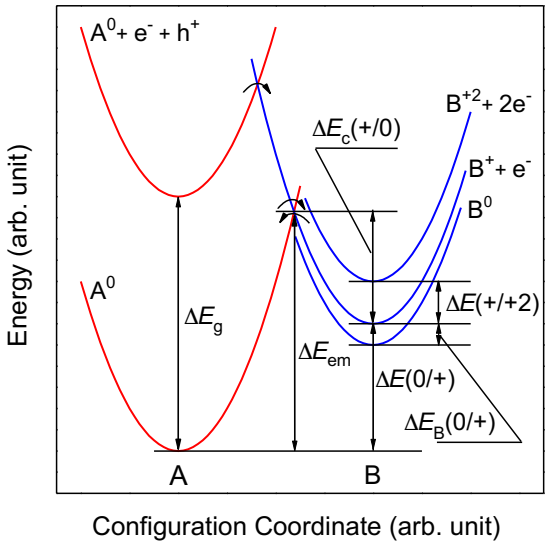

FIG. 1. Configuration coordinate diagram for the bistable thermal double donors in silicon.

It has been found that three first species of the TDD family (TDD-0 to TDD-2) are bistable defects with negative-U properties.[15-20] The bistable TDDs (BTDDs) can exist in two configurations with very different electronic properties: in one of the configurations, called A, the binding energy of an electron is rather high, i.e. the defect is a deep donor; while in another configuration, called B, it is a helium-like center with two shallow donor levels.[15-20] Emission or capture of electrons or holes by the BTDDs in one of the configurations can trigger a transition of the defects to other configurations. Electronic properties of the BTDDs have been studied by a number of different experimental techniques and are relatively well understood.[15-22] Figure 1 shows a configuration coordinate diagram for the BTDDs defects which we have constructed from

published data and Table I presents energy parameters for all three species of the BTDD family, which were determined in previous works.

Table I. Energy parameters (in eV) of bistable thermal double donors in silicon. The values given in brackets have been determined in the present work.

Defect	ΔE_{em}	$\Delta E_c(+/0)$	$\Delta E(0/+)$	$\Delta E_B(0/+)$	$\Delta E(+/+2)$	$E(0/+2) = 0.5[\Delta E(0/+) + \Delta E(+/+2)]$	$U = \Delta E(0/+) - \Delta E(+/+2)$
BTDD-0	(1.01)	0.28[a] (0.29)	~0.75[a] (0.72)	0.073[b]	0.164[b]	~0.45[a] (0.44)	~ -0.59[a] (-0.56)
BTDD-1	0.91[a] (0.91)	0.43-0.45[a] (0.44)	0.48[a] (0.47)	0.069[b]	0.156[b]	0.32[a,c] (0.315)	-0.32[a] (-0.315)
BTDD-2	0.90[a]	0.59-0.60[a]	0.29[a]	0.067[b]	0.150[b]	0.22[a,c]	-0.14[a]

[a] Refs. 18, 19 and 20
[b] Ref. 11
[c] Refs. 16 and 17

The origin of the bistability and possible atomic configurations of the small oxygen clusters, which are associated with BTDDs, have been discussed in *ab initio* modelling studies.[12-14] It should be noted, however, that practically all experimental information about the electronic properties of BTTDs have been obtained from observations of the defects in the shallow donor configuration. No signals from the deep donor configuration of BTDDs have been detected by spectroscopic techniques, such as electron spin resonance, deep level transient spectroscopy (DLTS), or infrared absorption spectroscopy. An exception is a weak infrared absorption line assigned to a local vibrational mode of the BTDD-1 and BTDD-2 centers in the deep donor state.[23]

The recent growing use of n-type Czochralski (Cz) silicon materials for photovoltaic (PV) applications (Refs. 24 and 25) has resulted in renewed interest in oxygen-related TDDs.[26-30] These defects have been suggested to be responsible for the reduction of the lifetime of minority carriers and therefore conversion efficiency of Cz-Si based solar cells.[26-30] Furthermore, it has been speculated in a recent study (Ref. 29) that BTTDs in the deep donor state are the effective recombination centers and their presence can cause the reduction in conversion efficiency of novel amorphous-crystalline Si hetero-junction solar cells with the base from n-type Czochralski-grown silicon. On the other hand, it is known that the BTDDs are responsible for persistent photoconductivity in n-type Si crystals and can be considered as carrier trapping centers.[15,18-20,27]

Existence of such trapping centers can result in some errors in measurements of minority carrier lifetime by photoconductance decay and quasi-steady-state photoconductance techniques.[27,31] It is possible to take into account effects of the trapping centres on the minority carrier lifetime measurements but this requires information about the electronic characteristics of the centers. So a deeper understanding of electronic and recombination properties of BTDDs is required.

II. EXPERIMENTAL DETAILS

We have used p^+-n-n^+ and Schottky barrier diodes on n-type Czochralski-grown Si materials to study the BTDD defects. P^+-n-n^+ diodes were formed by implantation and subsequent thermal activation of 60 keV boron ions (front side) and 60 keV phosphorus ions (back side) in the phosphorus-doped ($\rho \approx 5$ Ω·cm) commercial electronic grade Cz-Si wafers. The area of the p^+-n-n^+ diodes was 6 mm^2 and the leakage current at 10 V reverse bias was about 10^{-6} A. Concentration of interstitial oxygen (O_i) in these diodes was estimated as $(9 \pm 1)\times10^{17}$ cm^{-3} from the rates of capture of interstitial carbon atoms by the O_i atoms upon annealing of the diodes irradiated with alpha particles at 260 K.[32,33] Schottky barrier diodes (1 mm in diameter) were prepared by thermal evaporation of gold through a shadow mask on samples from a few n-type Cz-Si crystals with initial resistivity from 0.7 to 5 Ω·cm. The oxygen concentration in the crystals was in the range from 7×10^{17} cm^{-3} to 1×10^{18} cm^{-3} and the carbon concentration was below 2×10^{16} cm^{-3}, as determined by infrared absorption at room temperature. Some of the samples have been treated in the temperature range from 350 to 450 ^{o}C to generate TDDs. The heat-treatments resulted in increases in shallow donor concentration and, therefore, capacitance of the diodes, however it did not result in significant changes of their leakage current and ideality factor.

Current-voltage (*I-V)* and capacitance-voltage (*C-V*) measurements have been carried out in order to evaluate the quality of the diodes and to determine the uncompensated shallow donor concentration and width of the probed depletion regions. Deep level transient spectroscopy (DLTS) and high-resolution Laplace DLTS (L-DLTS) techniques have been used for the detection of electron emission from deep defect states.[34] Measurements of changes in total capacitance of the diodes resulted from filling in the depletion regions with electrons have been used to monitor transformations of the BTDD defects from the shallow donor state to the deep donor state.

III. EXPERIMENTAL RESULTS AND DISCUSSION

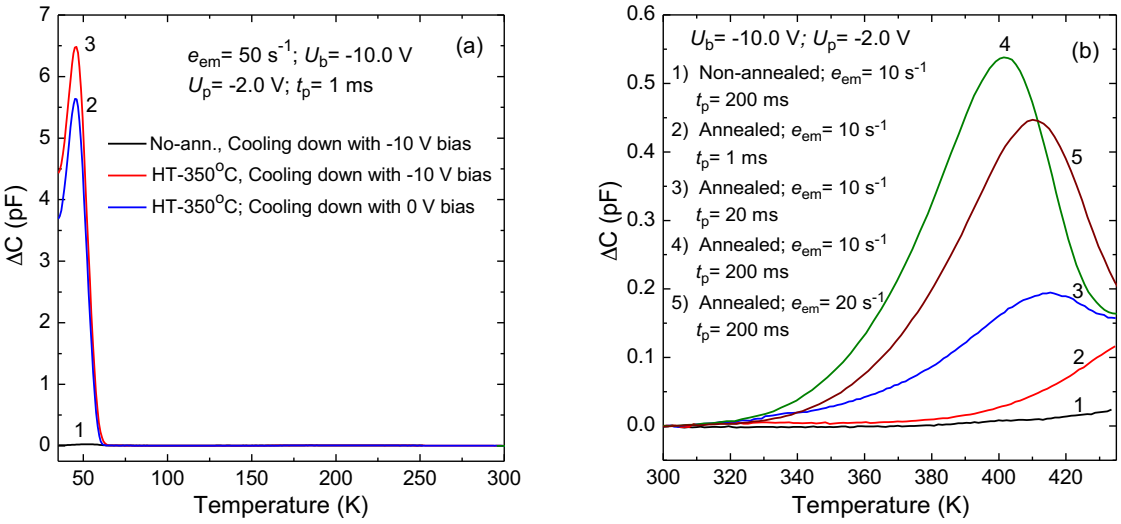

FIG. 2. Conventional DLTS spectra recorded on p^+-n-n^+ diodes from 5 Ω·cm n-type Cz-Si material. The spectra with label 1 were recorded on an as-processed diode and the spectra with labels 2 to 5 correspond to an identical diode which was subjected to a heat-treatment at 350 °C for 10 hours. Measuring conditions are given in the figures.

Figure 2 shows conventional DLTS spectra in the temperature ranges 35-300 K and 300-435 K for p^+-n-n^+ diodes fabricated on phosphorus-doped 5 Ω·cm Czochralski-grown silicon. The spectra were recorded for an as-processed diode and a diode subjected to a heat-treatment at 350 °C for 10 hours. The heat-treatment resulted in an increase in uncompensated shallow donor concentration from $(1.05 \pm 0.1) \times 10^{15}$ cm^{-3} to $(1.65 \pm 0.1) \times 10^{15}$ cm^{-3}. It should be noted that all the spectra were recorded upon temperature scanning from low to high values. A small peak with its maximum at about 52 K (for an emission rate (e_{em}) window of 50 s^{-1}) occurs in the spectrum of the as-processed diode. The magnitude of this peak has increased significantly and its maximum has been shifted to about 46 K after the heat-treatment. It has been found that magnitude of the low-temperature peak depends on the cooling down conditions before DLTS measurements. In the spectrum recorded after cooling down with the applied reverse bias the magnitude of the peak is significantly higher than in the spectrum recorded after cooling down without bias [Fig. 2(a)]. A comparison of the DLTS spectra in Fig. 2(a) with those reported in the literature for heat-treated n-type Cz-Si samples (Refs. 21, 35, and 36) indicates that the low-temperature peak can be associated with electron emission from the second donor level of oxygen-related TDDs. Changes

in magnitude of the peak resulted from different cooling down conditions show that a part of the TDDs are the bistable TDDs species.[21] Upon cooling down with the applied bias BTDDs can be frozen in the metastable shallow donor configuration and contribute to the electron emission signal at 46 K in the DLTS spectra, while after cooling down without bias some of BTDDs are in the minimum-energy deep donor configuration, electron emission from which does not occur at low temperatures.[21] Qualitatively similar DLTS spectra have been recorded on other p^+-n and Schottky barrier diodes subjected to heat-treatments in the temperature range 350-450 ^oC.

In the DLTS spectra recorded in the temperature range 300-435 K for the heat-treated Si diode, a previously unreported broad peak with its maximum at about 402 K (for e_{em} = 10 $s^{-1}$and filling pulse length (t_p) of 200 ms) occurs [Fig. 2(b)]. The magnitude and position of this peak depend significantly on the t_p value. Clear detection of the peak requires rather long filling pulses in the range of hundreds of milliseconds. Also, the magnitude of the peak decreases with the increase in emission rate window, so indicating a smaller electron population of the corresponding trap with increasing temperature. This peak has not been observed in the spectra of as-processed diodes without the 350 ^oC heat-treatment, therefore its appearance is caused by defects which form upon annealing.

The application of the high-resolution Laplace DLTS technique allows us to resolve two electron emission signals contributing to the broad peak in the conventional DLTS spectra. The L-DLTS spectrum recorded at 435 K is shown in Fig. 3(a). The peaks in the L-DLTS spectrum are sharp, so indicating that electron emission signals are related to well-defined point defects.[34] Figure 3(b) shows Arrhenius plots of the T^2-corrected emission rates for both traps. The values of activation energy for electron emission (E_{em}) have been determined as 0.91±0.01 eV and 1.01±0.01 eV. Such high E_{em} values are very unusual for defects in silicon detected by DLTS. The obtained E_{em} values are close to those reported for electron emission from deep donor state of the BTDD species determined from photoconductance decay measurements on heat-treated n-type Cz-Si crystals.[15,18-20] Thus it is reasonable to suggest that the observed emission signals are related to BTDDs. It should be noted here that the concentration of BTDDs, which are the main subject in this work, in all the samples studied has not exceeded 5% of the uncompensated shallow donor concentration, so the application of conventional methods of analysis of DLTS and L-DLTS signals due to these defects is justified. Further, it should be mentioned that E_{em} values determined from carrier emission measurements in charge space regions for defects with strong lattice

relaxations can differ significantly from E_{em} values determined from monitoring charge state transitions under charge neutrality conditions.[37]

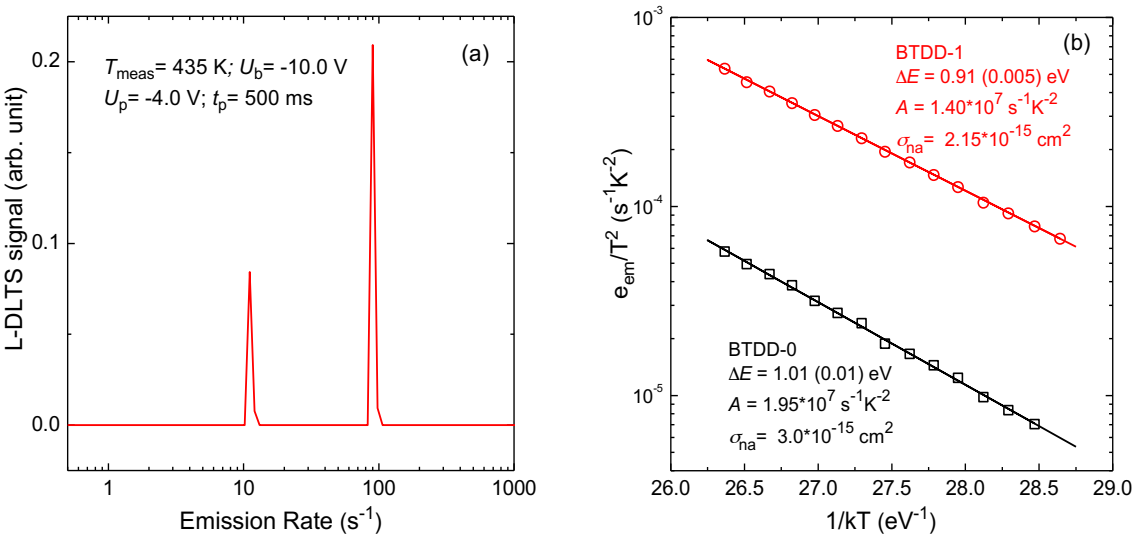

FIG. 3. (a) Laplace DLTS spectrum recorded at 435 K on a p^+-n-n^+ diode from 5 Ω·cm n-type Cz-Si material, which was subjected to a heat-treatment at 350 °C for 10 hours. Measurements conditions are given in the figure. (b) Arrhenius plots of T^2-corrected electron emission rates measured with the use of Laplace DLTS technique for two electron traps, emission signals of which are shown in Fig. 3(a).

For further characterization of the traps responsible for the high-temperature electron emission signals we have carried out: a) measurements of electron population of the traps (which is proportional to the DLTS ΔC signal) upon changes in filling pulse length, i.e. the so-called direct capture cross section measurements and b) measurements of transitions of the traps from ionized shallow donor state to the filled deep donor state by monitoring changes in capacitance, C, of the reverse-biased diodes in the temperature range 230-320 K after application of long filling pulses. To observe the capacitance changes according to measurements b), the diodes were usually cooled down under applied reverse bias (RB) from a temperature above 400 K to a measurement temperature (T_m) and then subjected to the application of multiple long filling pulses with the pulse voltage close to 0 V, which was interrupted after certain periods of time for bias capacitance measurements. The RB cooling down step used to keep BTDDs in the shallow donor configuration can be replaced for p^+-n junctions by the application of a forward bias pulse at T_m = 230-320 K.

The forward bias pulse results in injection of minority carriers (holes) into the probed region and deep-shallow transformation of BTDDs according to the following transition (Fig. 1): $A^0 + h^+ + e^- \rightarrow B^+ + e^-$.

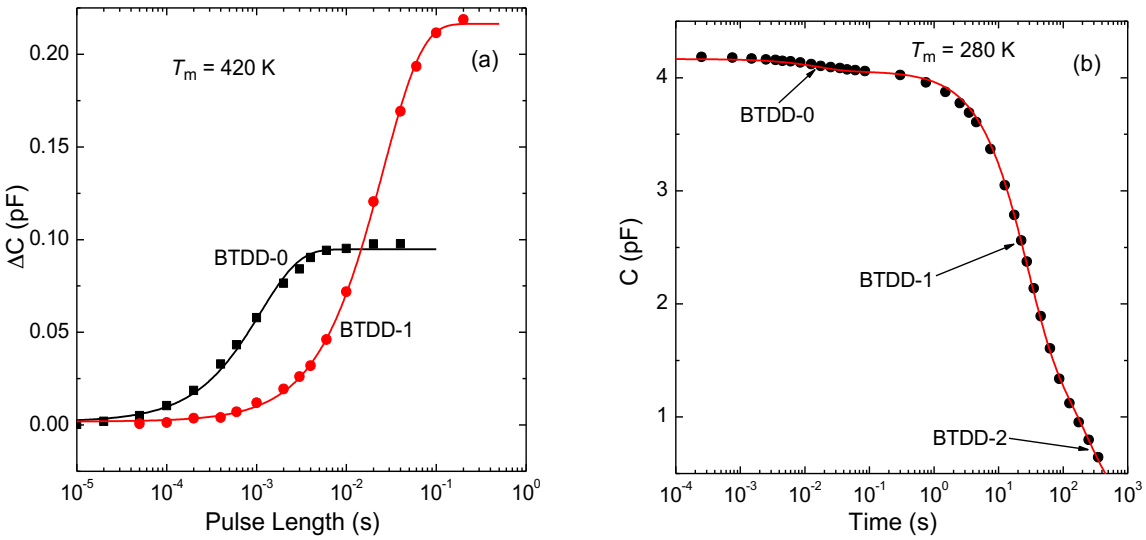

FIG. 4. (a) Changes in magnitudes of the L-DLTS signals due to the BTDD-0 and BTDD-1 centers upon changes in the filling pulse length. L-DLTS measurements were carried at 420 K with the following measurement conditions: U_b = -11 V, U_p = -4 V. The solid lines are calculated for mono-exponential growth process with least-square fitting values of ΔC_{max} and characteristic growth rates. (b) Changes in compensated diode capacitance ($C_d - C_b$) at U_b = -11 V and T_m = 280 K. The changes were induced by the application of multiple filling pulses with U_p = -4 V. Further details of the measurement are described in the text. The solid line is calculated for a three-exponent decay process with least-square fitting values of ΔC_n (n from 1 to 3) and characteristic decay rates. For the improvement of signal-to-noise ratio in these measurements we have used a backing off capacitor of C_b = 200 pF to compensate the capacitance of the diode studied (C_d).
All the measurements were carried out on a p^+-n-n^+ diode from 5 Ω·cm n-type Cz-Si material, which was annealed at 350 °C for 10 hours.

Changes in the ΔC and C values according to the above a) and b) processes at 420 K and 280 K, respectively, are shown in Fig. 4. The solid lines in Figs. 4(a) and 4(b) are calculated for mono-exponential growth and multi-exponential decay processes with least-square fitting of exponent parameters. The fitting parameters were ΔC values and characteristic occupancy times/rates. It should be mentioned here that an analysis of the data shown in Figs. 4a) and 4b) indicates that the ΔC values for BTDD-1 differ significantly at 420 K and 280 K (ΔC_{420K} = 0.215 pF and ΔC_{280K} = 2.4 pF, respectively). This difference can be explained by partial (about 10 %) filling of the BTDD-

1 center with electrons in the high temperature (350-430 K) range, in which the Fermi level is below the $E(0/+2) = E_c - 0.315$ eV occupancy level of the defect.[16] Usually DLTS and L-DLTS signals in diodes with the base from n-type semiconductors are recorded when Fermi level in bulk of the material is located higher than an energy level of a defect, so the defect level can be fully occupied with electrons upon filling pulse conditions. However, in the case of BTDDs the activation energies of electron emission from a deep donor state are very high, so, with the equipment, which we have used, the electron emission from the BTDD-1 defect can be observed only in the range of rather high temperatures, where in the samples studied $E_F \leq E(0/+2)$.

In Figure 5 the temperature dependencies of the occupancy rates for both traps are plotted together with the electron emission rates. The values have been derived from an analysis of capacitance measurements described above on diodes from 5 Ohm·cm n-type Cz-Si, which were subjected to 10-hours heat-treatments at 350 ^{o}C and 425 ^{o}C.

Occupancy kinetics for defects with negative-U properties and different structural models have been considered in Refs. 18, 19 and 37. There are some characteristic features in temperature dependencies of occupancy and emission rates for defects with $U < 0$, which indicate on details of their electronic structure. From an analysis of such characteristic features in the temperature dependencies of emission and occupancy rates presented in Fig. 5, and taking into account positions of the Fermi level at the measurement temperatures, some preliminary information about electronic and structural properties of the traps can be obtained. First, it is found that the capture rate for both traps is proportional to the squared concentration of free electrons when Fermi level is in the range E_c-0.26 eV < E_F < E_c-0.18 eV. This finding clearly indicates negative-U properties of the traps studied.[18,19,37] Further, the occupancy rates are nearly the same as the emission rates for the BTDD-1 traps when Fermi level is lower than E_c-0.36 eV. The rates do not depend on the free carrier concentration in this E_F range. This observation indicates that most likely there are no singly positively charged state for BTDD-1 in configuration A.[37] Both findings are consistent with structure and electronic properties of BTDDs and indicate that these defects give rise to the electron emission signals, which are observed in the conventional and Laplace DLTS spectra in the temperature range 320-435 K [Figs. 2(b) and 3(a)].

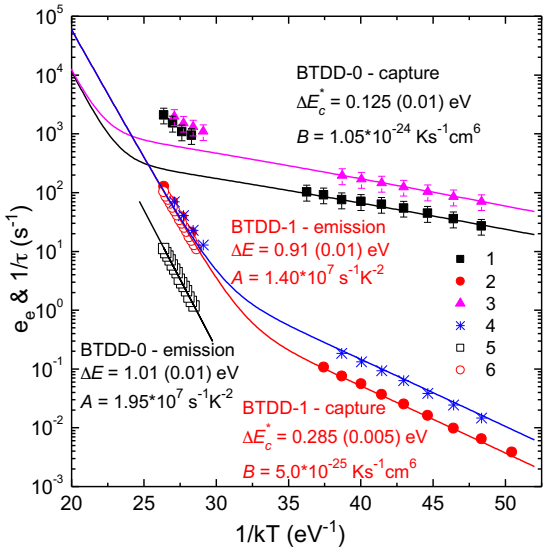

FIG. 5. Arrhenius plots of electron occupancy (filled symbols) and emission (empty symbols) rates for the BTDD-0 (symbols 1, 3, and 5) and BTDD-1 (symbols 2, 4, and 6) traps, whose emission signals are shown in Figs. 2(b) and 3(a). The values have been derived from an analysis of capacitance measurements described above on diodes from 5 Ω·cm n-type Cz-Si, which were subjected to 10-hours heat-treatments at 350 °C (symbols 1, 2, 5, and 6) and 425 °C (symbols 3 and 4). Solid lines were calculated with the use of Eqs. (1) and (2) and with A and B coefficients and energy values as fitting parameters. Fitting parameters are given in the graph. Concentrations of uncompensated shallow donors determined from *C-V* measurements were (1.65±0.1) × 10^{15} cm^{-3} and (2.75±0.1) × 10^{15} cm^{-3} in the diodes subjected to heat-treatments at 350 °C and 425 °C, respectively.

Temperature dependencies of occupancy rates for defects with such electronic properties can be described by the following equations:[18,19,37]

$$\tau^{-1} = e_{em} = A \cdot T^2 \cdot exp[-\Delta E_{em}(0/+)/kT] = \\ = A \cdot T^2 exp\left\{-\frac{[\Delta E(0/+) + \Delta E_c(+/0)]}{kT}\right\}, \quad (1)$$

when $E_F < E(0/+2)$ and

$$\tau^{-1} = B \cdot T^{-1} \cdot n^2 \cdot exp\left[-\frac{\Delta E_c^*}{kT}\right] = B \cdot T^{-1} \cdot n^2 \cdot exp\left\{-\frac{[\Delta E_c(+/0) - \Delta E(+/+2)]}{kT}\right\}, \quad (2)$$

when $E(0/+2) < E_F < E(+/+2)$. In these equations, E_{em} is the activation energy for electron emission from the neutral deep donor state, $\Delta E(0/+)$ and $\Delta E(+/+2)$ are the energy differences between the states with corresponding charges, $\Delta E_c(+/0)$ is the energy barrier for transition from the positively

charged shallow donor state to the neutral deep donor state, and *n* is concentration of free electrons. The solid curves in Fig. 5 were calculated with the use of Eqs. (1) and (2) and with A and B coefficients and energy values as fitting parameters. The fitting parameters obtained are presented in Fig. 5 and the calculated energy values are given in Table I. The capture rate values for BTDD-0 traps in the high temperature (400 K – 440 K) region deviate from the values obtained by extrapolation of low temperature capture data and electron emission data (solid lines calculated according to Eqs. 1 and 2). It was concluded in Refs. 18-20 that in these temperature region the $B^+ \rightarrow A^0$ transformation of BTDD-0 is related to a hole emission from the B^+ state to the valence band. Because of limitations of our experimental set-up in relation to measurement temperature and filling pulse length and the relatively small concentration [$(1.0\text{-}1.5)\times10^{12}$ cm^{-3}] of the BTDD-0 traps we could not determine precise values of activation energy and power in electron concentration dependence for the hole emission process from the data obtained.

A comparison of the obtained data with those reported in studies of photo-conductance decays related to recharging of BTDDs allows us to assign the emission signal with $E_{em} = 1.01 \pm 0.01$ eV to BTTD-0 or the so-called α traps, and the emission signal with $E_{em} = 0.91 \pm 0.01$ eV to BTTD-0 or the so-called β traps.[15,18-20] Further, the values of energy barriers for transitions from the shallow donor state to deep donor state of the BTDD-0 and BTDD-1 defects, which have been derived from the analysis of the results presented in Fig. 5 and are given in Table I, are close to those obtained in Refs. 15 and 18-20 for the corresponding traps from photoconductance decay measurements on heat-treated n-type Cz-Si crystals.

IV. CONCLUSION

It is reasonable to conclude from the analysis of the given data, that electron emission signals from the deep donor state of the BTDD-0 and BTDD-1 defects have been detected for the first time by means of the DLTS technique in the present work. By monitoring changes in magnitudes of the detected emission signals at different bias and temperature conditions in the diodes with different doping levels we have managed to obtain detailed information on electronic properties of the BTDD-0 and BTDD-1 centers. With the knowledge of electronic structure of the BTDD

species it is possible to predict their effects on minority carrier lifetime in silicon crystals. The recombination of light- or forward-bias-injection-induced charge carriers through BTDDs in n-type Si consists of the following processes (Fig. 1): i) capture of a hole by a BTDD defect in deep donor configuration and its relatively fast transformation into the shallow donor state ($A^0 + h^+ + e^- \rightarrow B^+ + e^-$);[18,19] ii) capture of an electron by the defect in B configuration and its transformation to the initial deep donor A configuration ($B^+ + e^- \rightarrow A^0$). Results shown in Figs. 4 and 5 indicate that the rate of process ii) is not high in the temperature range of operation of solar cells around 300 K, ~10^2 s^{-1} for BTTD-0 and ~10^{-1} s^{-1} for BTDD-1. According to the results presented in Refs. 18 and 19, the rate of process ii) is even slower for the BTDD-2 defect. The $B^+ + e^- \rightarrow A^0$ process is slow because of the existence of relatively high energy barrier, $\Delta E_c(+/0)$, for this transformation (Table 1). So, the whole cycle of the A → B → A transformations of a BTDD defect, which can be considered as a recombination event, is relatively long, in the range of hundreds of milliseconds even for the fastest cycle through the BTDD-0 center. So, it appears that the BTDD defects can be considered as minority carrier trapping centers in n-type Cz-Si crystals but not as effective recombination centers. So, the recent suggestion by Tomassini et al. (Ref. 29) that BTDDs in the deep donor state are responsible for the reduction of minority carrier lifetime and conversion efficiency of novel amorphous-crystalline Si hetero-junction solar cells with the base from n-type Czochralski-grown (Cz) silicon is not valid.

It is likely that in n-type Cz-Si crystals with a high concentration of TDDs and decreased resistivity, the Fermi level is shifted to the conduction band and because of this a significant part of the helium-like TDD species, which have the E(+/+2) level at about E_c-0.15 eV, are in the singly ionized state. These singly ionized centers can effectively capture holes and become doubly positively charged. The TDD centers in the +2 state are extremely effective traps for electrons, so rate of electron capture and the back transition to the singly ionized state is very high. Therefore in n-type Si crystals with a high concentration of TDDs these defects could serve as recombination centers in the shallow donor configuration.

Acknowledgements

This work has been supported by the EPSRC-UK under the Supergen Contract No. EP/M024911/1. Financial support was also given by CONACyT-Mexico.

References

[1] S. S. Fuller, J. A. Ditzenberger, N. B. Hannay, and E. Buehler, Phys. Rev. **96**, 833 (1954).

[2] W. Kaiser, Phys. Rev. **105**, 1751 (1957).

[3] D. Wruck and P. Gaworzewski, Phys. Status Solidi A **82**, 557 (1979).

[4] R. Oeder and P. Wagner, in *Defects in Semiconductors II*, ed. by S. Mahajan and J. W. Corbett, Mater. Res. Soc. Symp. Proc. **14**, 171 (1982).

[5] B. Pajot, H. Compain, J. Lerouille, and B. Clerjaud, Physica B **117-118**, 110 (1983).

[6] M. Suezawa and K. Sumino, Matter. Lett. **2**, 85 (1983).

[7] W. Kaiser, H. L. Frisch, and H. Reiss, Phys. Rev. **112**, 1546 (1958).

[8] R. C. Newman, J. Phys. Condens. Matter **12**, R335 (2000).

[9] L. I. Murin, J. L. Lindström, V. P. Markevich, T. Hallberg, V.V. Litvinov, J. Coutinho, R. Jones, P. R. Briddon, and S. Öberg, Physica B **308-310**, 290 (2001).

[10] W. Götz, G. Pensl, and W. Zulehner, Phys. Rev. B **46**, 4312 (1992).

[11] L. I. Murin, V. P. Markevich, J. L. Lindström, and M. Kleverman, Physica B **340-342**, 1046 (2003).

[12] J. Coutinho, R. Jones, L. I. Murin, V. P. Markevich, J. L. Lindström, S. Öberg, and P. R. Briddon, Phys. Rev. Lett. **87**, 235501 (2001).

[13] M. Pesola, Y. J. Lee, J. von Boehm, M. Kaukonen, and R. M. Nieminen, Phys. Rev. Lett. **84**, 5343 (2000).

[14] Y. J. Lee, J. von Boehm, M. Pesola, and R. M. Nieminen, Phys. Rev. B **65**, 085205 (2002).

[15] V. D. Tkachev, L. F. Makarenko, V. P. Markevich, and L. I. Murin, Sov. Phys. Semicond. **18**, 324 (1984).

[16] L. F. Makarenko, V. P. Markevich, and L. I. Murin, Sov. Phys. Semicond. **19**, 1192 (1985).

[17] Ya. I. Latushko, L. F. Makarenko, V. P. Markevich, and L. I. Murin, Phys. Status Solidi A **93**, K181 (1986).

[18] L. F. Makarenko and L. I. Murin, Phys. Status Solidi B **145**, 241 (1988).

[19] L. I. Murin, L. F. Makarenko, and V. P. Markevich, in *Defects in Crystals*, ed. by E. Mizera, (World Scientific, Singapore, 1988), p. 262.

[20] L. F. Makarenko, Phys. Status Solidi A **106**, K153 (1988).

[21] A. Chantre, Appl. Phys. Lett. **50**, 1500 (1987).

[22] P. Wagner and J. Hage, Appl. Phys. A **49**, 123 (1989).

[23] T. Hallberg and J. L. Lindström, Appl. Phys. Lett. **68**, 3458 (1996).

[24] H. Xu, Energy Proc. **77**, 658 (2015).

[25] A. ur Rehman and S. H. Lee, Sci World J. **2013**, 470347 (2013).

[26] Yu Hu, H. Schøn, E. J. Øvrelid, Ø. Nielsen, and L. Arnberg, AIP Advances **2**, 032169 (2012).

[27] Yu Hu, H. Schøn, E. J. Øvrelid, Ø. Nielsen, and L. Arnberg, J. Appl. Phys. **111**, 053101 (2012).

[28] F. Jay, J. Veirman, N. Najid, D. Muñoz, S. Dubois, and A. Jouini, Energy Procedia **55**, 533 (2014).

[29] M. Tomassini, J. Veirman, R. Varache, E. Letty, S. Dubois, and Ø. Nielsen, J. Appl. Phys. **119**, 084508 (2016).

[30] J. Li, X. Yu, S. Yuan, L. Yang, Z. Liu, and D. Yang, Sol. Energy Mater. Sol. Cells **179**, 17 (2018).

[31] D. Macdonald, R. A. Sinton, and A. Cuevas, J. Appl. Phys. **89**, 2772 (2001).

[32] V. P. Markevich and L. I. Murin, Fiz. Tech. Poluprovodn. (S.-Peterburg) **22**, 769 (188) [Sov. Phys. Semicond. **22**, 574 (1988)].

[33] L. F. Makarenko, M. Moll, F. P. Korshunov, and S. B. Lastovski, J. Appl. Phys. **101**, 113537 (2007).

[34] L. Dobaczewski, A. R. Peaker, and K. Bonde Nielsen, J. Appl. Phys. **96**, 4689 (2004).

[35] L. C. Kimerling and J. L. Benton, Appl. Phys. Lett. **39**, 410 (1981).

[36] W. W. Keller, J. Appl. Phys. **55**, 3471 (1984).

[37] V. P. Markevich, L. I. Murin, T. Sekiguchi, and M. Suezawa, Mater. Sci. Forum **258-263**, 217 (1997).

CHAPTER 4

LIFETIME LIMITING DEFECTS IN BORON-DOPED SILICON

4.1 The BO-Complex-Precursor Responsible for Light Induced Degradation

Draft No.1

Direct Observation of the Boron-Oxygen Complex Precursor Responsible for Light Induced Degradation in Silicon Photovoltaic Cells

Direct Observation of the Boron-Oxygen Complex Precursor Responsible for Light Induced Degradation in Silicon Photovoltaic Cells

M. Vaqueiro-Contreras[1]*, V. P. Markevich[1]*, M. P. Halsall[1]*, J. Coutinho[2] and A. R. Peaker[1]

[1] Photon Science Institute, University of Manchester, M13 9PL, UK
[2] Department of Physics and I3N, University of Aveiro, Campus Santiago, 3810-193, Portugal

Degradation of the conversion efficiency of solar cells made from boron-doped Czochralski-grown (Cz) silicon during the first hours of operation under light (Light Induced Degradation – LID) has been a major problem for the photovoltaic industry for several decades. Solid arguments have been presented that the degradation is related to a defect containing boron and oxygen atoms, the oxygen being present in large concentrations in Cz Si. Even though many studies on the physical and chemical properties of this complex have been reported in literature, most of them are based on the indirect characterisation of its effects through minority carrier lifetime measurements, leading to some contradictory theories and wide-spread debates on the topic. Despite many previous attempts, no signals related to the LID defect have been detected by means of any spectroscopic characterization methods such as Deep Level Transient Spectroscopy (DLTS). In this paper, the observation of a previously unreported peak in the DLTS spectra of every B-doped Cz sample measured by us is presented. The peak has been found to be associated with the formation of a recombination centre which we believe to be a boron-oxygen related complex. The disappearance of the peak has been directly correlated with lifetime degradation in the Si crystals upon carrier injection and its reappearance upon thermal treatments with the material's lifetime recovery, thus suggesting the corresponding defect is the BO-LID complex precursor. From the analysis of the capture and emission kinetics of holes by the defect its configuration-coordinate diagram has been constructed. It is argued that capture and emission of charge carriers by the defect result in changes in the atomic configurations of the complex. Electronic properties of the defect are very different in different atomic configurations. Depending on the position of the Fermi level (E_F), the defect can be either a deep donor or be in two configurations with shallow acceptor levels. It is suggested the light induced degradation of minority carrier lifetime in solar cells containing boron and oxygen atoms is associated with Auger type recombination of charge carriers through a BO complex with a shallow acceptor level.

I. INTRODUCTION

The use of boron doped silicon is essential to the silicon photovoltaics (PV) market which is currently >90% of new installations, in 2017 >30% of these installations were monocrystalline silicon cells, overwhelmingly grown by the Czochralski (Cz) technique. However, for over four decades it has been known that cells fabricated in this way are subject to minority carrier lifetime degradation, and hence efficiency loss, due to a process occurring in boron-doped Czochralski

silicon under illumination [1]. This process has become known in the PV community as Light-Induced Degradation (LID). To the present time there have been over 1000 articles in the literature on LID, the effect which loses mankind many GW's of generating capacity over the world. The LID term however was later found to be inaccurate for the process since it was not the injected photons causing the degradation, but rather the minority carriers presence in the material, as forward biasing of the PN junctions was found to cause the same process to occur [2]. Thus it has also been referred to as the Carrier-Induced Degradation (CID). Nevertheless, since LID is now a widely known term in literature we adopt it for this work.

LID has been observed to reduce the cell relative efficiencies by up to 10% and up to 2% absolute efficiencies [1], [3], and consequently has been under investigation for a long time [2]–[6]. Si solar cell manufacturers are aware of the problem LID poses to the stability of their devices and some LID mitigation measures have already been studied and implemented in commercial panels. For instance, the LG Mono X Plus series has adapted the so called LiLY (LID-improvement for Lifetime Yield) Technology, which relies on hydrogen injection to their p-type Cz materials for LID reduction, as hydrogen has been reported to play an important role in the LID-defect deactivation [7]–[10]. Distinctively, however, other approaches to LID mitigation have been taken by the same manufacturers on their LG NeON 2 series and by the X-Series from SunPower Corp., whereby their solar panel manufacturing process has been switched from having a p-type mono-crystalline (mc) Si base to an n-type base in order to avoid LID.

Despite all the available literature on the topic, however, the mechanisms behind the LID in Cz silicon is still debated [11]–[13], as no evidence from direct measurements of the chemical nor physical properties of the LID-responsible defect other than lifetime spectroscopy has been reported so far [4]. However, strong evidence has been published that suggests that the LID-responsible metastable defect(s) has its origin in the presence of boron and oxygen atoms [1], [14], [15] therefore it is usually regarded as the "BO-defect". This is in spite of disagreement about the nature of the BO-defect in the available literature which will be discussed in Section III B. In the present work we argue on the basis of our latest observations and *ab-initio* calculations, the likelihood of the LID effect being caused by a single species of BO-defect, which has various configurations, and thus henceforth we will be referring to a single LID-responsible defect in this work.

In this paper we discuss the key aspects related to LID available in literature and report recent observations of what appears to be a trap signal arising from the BO-defect precursor by means of DLTS. The signal has been characterised by the application of junction-based techniques and is found to act as an effective deep trapping center with an activation energy for hole emission (E_{eD}) of 0.97 eV. The trap appearance has been observed to behave in the reverse way to what is expected from the LID-responsible defect i.e. its concentration decreases as the degradation increases and the annihilation-appearance process can be cycled indefinitely by the subsequent LID and 200 °C annealing recovery treatments. Therefore, the defect giving rise to the trap (H_{390}) is proposed to be a precursor for the degradation induced recombination center similar to what has been defined as the "state A" of the BO-related complex in the BO-degradation model presented in Ref. [8] by Hallam *et al*. Furthermore, evidence of the transformation from the deep donor state to what appears to be two shallow acceptor states after carrier injection by either above-bandgap illumination or forward biasing (FB) is shown. Discussion of the possible structure of the LID-responsible complex is then presented by relating the obtained electrical

characteristics with *ab-initio* calculations, and the possible recombination mechanism giving rise to the degradation is proposed.

II. EXPERIMENTAL DETAILS

For this work a set of Cz grown and boron-doped Si wafers of 3 and 10 Ω·cm with $[O_i]$ of (7-9)×10^{17} cm^{-3} were used. Some of these were used to fabricate either n^+p diodes of 2 mm × 2 mm and 3mm × 2mm, respectively, or processed to form 1 mm of diameter Schottky barrier diodes (SBDs). The n^+p diodes were processed with the use of phosphorous diffusion in the front, and Al evaporation on both sides for electrode formation. The SBDs were formed by sputtering Ti through a shadow mask with circle openings on the front, and their Ohmic contacts created through Al thermal evaporation on the back surface. For Minority-Carrier Transient Spectroscopy (MCTS) measurements an un-metalized area on the back surface of the SBDs was left open, or a similar sized area etched from the back surface of the n^+p diodes, this was to allow back face optical excitation from a 940 nm light emitting diode. Similarly, for the above-bandgap illumination procedure used for degradation when forward bias was not applied, a small metalized area on the n^+p diodes' top surface was protected by photoresist for contacting and the rest etched away to permit light penetration. Illumination was done by a halogen lamp of 500 W with the equivalent of ~1 sun intensity and ~65 °C sample temperature. Capacitance-voltage and current-voltage characteristic curves have been measured on each sample to test their quality and to acquire their uncompensated dopant concentration and profile.

The samples were characterised by means of DLTS[16], MCTS[17], Laplace-DLTS (LDLTS)[18], Admittance Spectroscopy (AS) [19] and Reverse Recovery (RR) [20] measurements. The DLTS, MCTS and LDTLS techniques have been applied as outlined in previous publications and recent reviews [21]–[23]. For the AS technique the measurements for the detection of majority carrier traps were carried out in a vacuum chamber cooled by a closed-cycled helium cryocooler (the same cryostat used for DLTS/MCTS measurements) by monitoring the change in conductance and capacitance when the n^+p diodes were subjected to a frequency sweep from 100 Hz to 30 MHz at various fixed temperatures in the range 20 - 50K. In the case of the RR method used for effective carrier bulk lifetime (τ_{eff}) measurements, the n^+p diodes were subjected to an abrupt change in applied bias, then by and monitoring the forward (I_f) and reverse (I_r) current behaviour through a series resistance at various reverse voltage values τ_{eff} was determined. Noting that the condition $I_r \ll I_f$ was always maintained to avoid the effect of the emitter recombination in the measurements [24].

III. FORMATION AND ELECTRONIC PROPERTIES OF THE BO-DEFECT PRECURSOR

By means of DLTS measurements in the temperature range from 300 K to 430 K performed in all our n^+p diodes made for this work from B-doped Cz-grown material, a signal arising from a deep state (H_{390}) has for the first time been detected. This peak disappears upon minority carrier injection by either illumination or forward biasing for relatively long (hours) periods of time, and reappears upon heat-treatments at T > 130 °C. Figure 1 (a) shows the spectra taken from one of

the samples (S1) which was firstly annealed at 350 °C for 20 h on a hot plate, then subjected to forward biasing for 1200 min at 320 K, inside the temperature controlled DLTS kit, and subsequently annealed in the dark at 430 K for 300 min. It can be seen that the signal originally appearing in the sample disappears after carrier injection and can be then restored after a short period of annealing treatment. Such cycles of annihilation-recovery can be repeated indefinitely following the behavioural characteristics of the LID process discussed in Section III A (i). Furthermore, measured spectra of a sister sample (S2) from the same wafer, which was annealed at 350 °C for 10 h and subsequently illuminated for 5, 20 and 70 accumulated hours, are shown in an inset in Figure 1 (a). The inset clearly shows a decrease in magnitude of the H_{390} trap in relationship to the photo-generated carrier injection time. In addition, we have found that there is an increase in defect concentration (N_T) after annealing treatments in the temperature range 350 – 425 °C, in which oxygen dimers are known to be mobile. These observations suggest that oxygen dimers are involved in the defect formation, this agrees well with the BO_2 model of the defect precursor proposed by Schmidt et al. in Ref. [25]. The peak maxima of the signal occurs at about 390 K in the spectra, when a filling pulse length (t_p) of 200 ms and a rate window (e_h) of 10 s^{-1} is used. From a T^2-corrected Arrhenius plot the hole emission activation energy E_{eD} = 0.97 ± 0.01 eV has been determined. Emission signals with so high activation energy is rather difficult to observe in silicon by means of DLTS technique since its observation requires the application of unusual measurement conditions as the ones described in Figure 1 (a). We believe this to be the reason why other workers have not reported it previously.

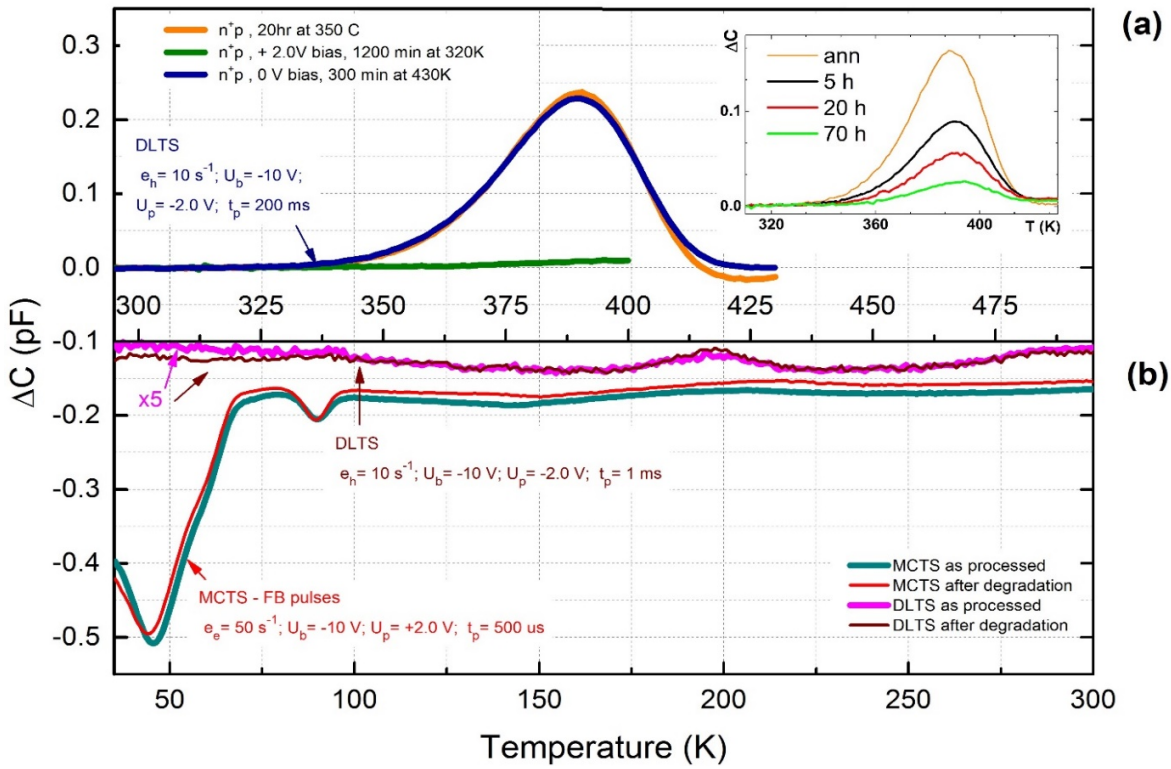

Fig. 1 Conventional DLTS and forward-bias pulsed MCTS spectra recorded from n^+p diodes made from 3 Ω·cm B-doped Cz material. (a) High temperature range DLTS scan of a sample (S1) after 20 h anneal at 350, then after 1200 min carrier injection and subsequent 300 min HT at 430 K. Inset shows the DLTS peak evolution before and after accumulated illuminated time from a sister sample (S2). (b) Low temperature range DLTS and MCTS spectra from S1. Measurement conditions are given in the figure.

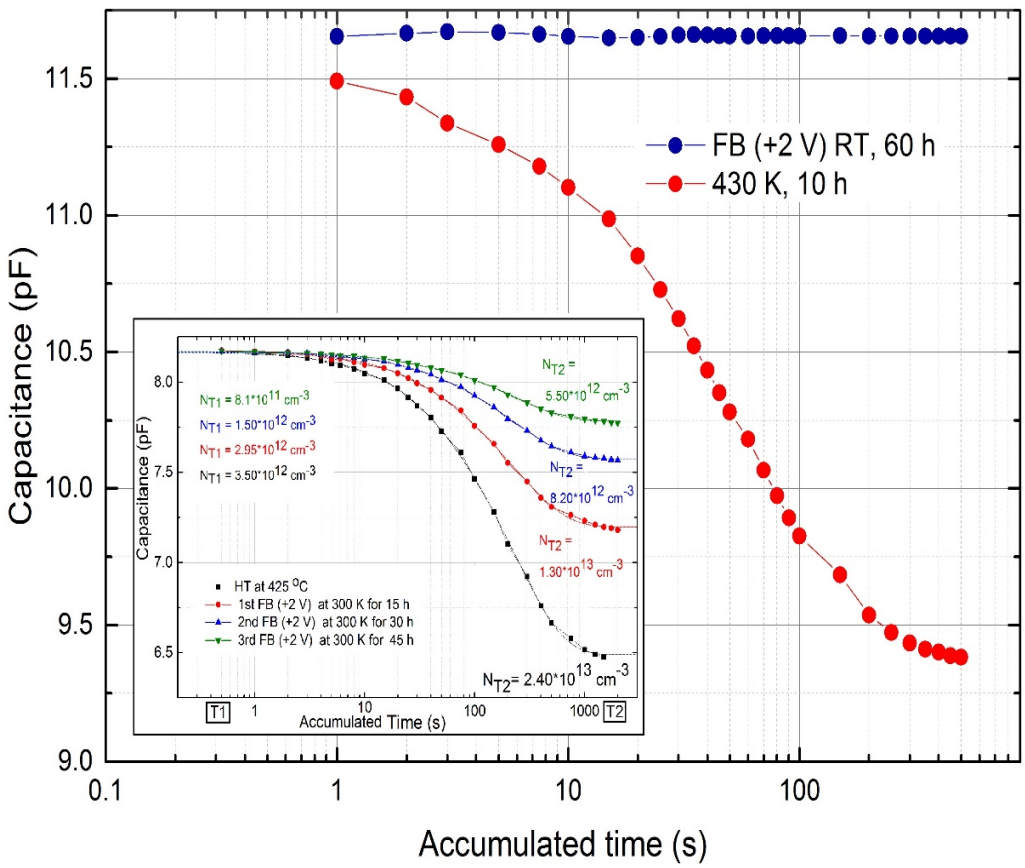

Fig. 2 Trap occupancy dependent capacitance changes due to BO-defect-related transformations. (S1) (Red dots) Changes in capacitance induced by multiple filling pulses due to transformations of shallow acceptor traps to deep donor traps in a n^+p (10 Ω·cm) diode which was annealed at 430 K for 10 h. (Blue dots) capacitance monitoring with respect of accumulated filling pulse length of the same sample after FB injection for 60 h. A similar FB injection method was used for degradation as for those samples whose DLTS spectra are shown in Figure 1. (S2) (Inset) *C(fill$_{acc}$-time)* dependency progression after 15, 30 and 45 h of accumulated carrier injection time. Measurement conditions: U_b= -10 V, U_p = - 2 V and T_{meas} = 270 K.

The relationship between the H_{390} deep level formation and the transformation characteristics of the BO-defect can be taken as an indication that the H_{390} trap arises from a BO-defect configuration which acts as a precursor of the recombination active BO-defect. Furthermore as is shown in Figure 1 (b), the conventional DLTS and MCTS spectra of the studied samples do not show any detectable changes in other observed emission signals after carrier injection and heat treatments. These results thus support the fact that there are no other sources of electrically-active defects in the sample, and brings into question the claimed introduction upon illumination of BO-defect-related deep levels acting as recombination centres as reported by various authors (see e.g [5], [12], [26]). We have therefore characterised the H_{390} trap by a series of junction techniques measurements, firstly to study its capture kinetics and secondly to obtain stronger evidence of its relationship to the BO-related recombination defect.

One of these techniques involved the measurements of the capacitance changes upon application of multiple subsequent filling pulses to the n^+p diodes kept under reverse bias at a temperature of 270 K. From these measurements the transformation of the H_{390} trap from a shallow acceptor

state to the deep donor state has been observed. Figure 2 shows the capacitance changes occurring in one of the samples which was subjected to a 430 K heat-treatment in dark for 10 h and subsequently cooled down under reverse bias to 270 K and then measured after various periods of accumulated filling pulses. The exponential decay of the capacitance displayed towards increasingly-accumulated filling pulse length indicates either a decrease in concentration of uncompensated shallow acceptors or an increase in concentration of compensating deep donor defects upon filling pulse exposure. This phenomenon can also be explained by the transformation of shallow acceptor traps in the material into deep donor centers filled with holes and so reducing the diodes' capacitance. Moreover, the magnitude of this transformation can be observed, in the same figure, to decrease upon prolonged carrier injection, leading to a capacitance saturation level after 60 hr of injection.

The inset in Figure 3 shows the progression of the capacitance changes after 15, 30 and 45 h of accumulated FB-injection time measured from a qualitatively similar sample as in the main figure. Values of the trap concentrations in the measured samples are given in the figure. These are in the range of 10^{12}-10^{13} cm^{-3}. Note that similar values have determined in every measured sample after the heat-treatments at temperatures in the range between 350 and 425 °C. Data from the degraded sample shown in Figure 2 thus demonstrate no capacitance changes upon exposure to the filling pulses, and also an increased capacitance value with respect to that of the non-degraded material, resulting from the BO-defect being in its deep donor configuration. However, it is important to point out that this transformation effect is only observed when the sample is cooled down to the measurement temperature under reverse bias, or when a short forward bias pulse at a temperature of 270 K is used, hence demonstrating changes in BO-defect configurations in dependence of the Fermi level position.

Analysis of the results presented in Figure 2 can therefore be interpreted as a clear indication of the formation of shallow acceptor traps after degradation in p-type Cz-Si material, a case that has been largely overlooked despite some earlier observations of shallow level formation in degraded samples reported by Glunz *et al.* in Ref. [3]. Moreover, the observation of multiple minority carrier traps in p-type silicon even before carrier injection degradation has been reported as early as in 1955 by Hornbeck and Haynes in Ref. [27]. There, by means of photoconductivity measurements three well defined steps in the decay curves were attributed to the combination of multiple deep and shallow traps. Some of the deep traps, they suggested, acted as recombination centres in a rather fast process , while subsequent trapping from other deep and shallow traps manifested themselves as steps with slower rates in the photo-conductance decay curves. Furthermore, from their observations it was concluded that the concentration of the dominant trap was linearly proportional to the boron concentration, similar to what has been observed to occur in LID affected samples [28], [29]. Furthermore, later in 2002 Schmidt et al. [30] also reported the observation of the effect of hole trapping in O_i rich B-doped Cz samples which they speculated could be related to the BO-defect, however the idea of an identical physical origin was discarded due to the large differences between the trapping center concentration and the light-induced recombination center concentration. All these results however point to the existence of trapping centers with concentrations in the order of 10^{12} to 10^{13} cm^{-3} which, in most

cases, should be observable by DLTS measurements, but nevertheless has not been reported until now.

Temperature dependencies of the occupancy (τ^{-1}) and emission (e_h) rates for the H_{390} trap in two n^+p samples with 3 and 10 Ω · cm resistivity, respectively, are shown in Figure 3. The peculiar behaviour of the capture kinetics shown in Figure 2 and 3(a) indicates the amphoteric properties of the defect. On the one hand, Figure 2 shows that according to the changes in capacitance the majority-carrier flooding by bias pulses induce the transformation of an acceptor-like trap to a deep donor trap as described in the previous section. On the other hand, the $\tau^{-1}(1/T)$ dependences shown in Figure 3(a) demonstrate changes in occupancy rates at low- and high- temperature regimes, i.e there is an apparent difference in slope values in the curves, this is a property commonly observed for defects with negative electron correlation energy (U<0 centers) [31], however it does not account for the observed $\tau^{-1} > e_h$ characteristic also present in the plot. Furthermore, comparison of capture kinetics of Si crystals with different doping concentrations, N_{A3}= 4 × 10^{15} and N_{A10}= 1.2 × 10^{15}, for the 3 and 10 Ω · cm materials, respectively, at the high-temperature end of the graph demonstrate an unusual relationship $\tau^{-1}\sim 1/n$ which cannot be predicted by common statistic models. It has been shown earlier that these features of $\tau^{-1}(1/T)$ dependencies can be perfectly described by the introduction of a metastable neutral charge state [32] as shown in the constructed configuration-coordinate diagram in Figure 3(b).

Temperature dependencies of occupancy rates for defects with such electronic properties can hence be described by the following equations [31], [32]:

$$\tau^{-1} = e_{em} = A \cdot T^{1.5} \cdot p^{-1} \cdot exp[-E_{em}(+/0)/kT] =$$
$$= A \cdot T^{1.5} \cdot p^{-1} \cdot exp\left\{-\frac{[E_{eD}(+/0) + \Delta E_1 - \Delta E_{cX}(0/+)]}{kT}\right\}, \qquad (1)$$

when $E_F < E(-/+)$ and

$$\tau^{-1} = B \cdot T^{-1.5} \cdot p \cdot exp\left[-\frac{\Delta E_c^*}{kT}\right] = B \cdot T^{-1.5} \cdot p \cdot exp\left\{-\frac{[\,\Delta E_2 - \Delta E(0/-)]}{kT}\right\}, \qquad (2)$$

when $E(-/+) < E_F < E(0/-)$ and with $E(-/+) = ½[E(+/0) + E(0/-)]$. In these equations, E_{eD} is the activation energy for transition from the positively charged deep donor state (D^+) to the minimum energy neutral state (H^0), $\Delta E(+/0)$ and $\Delta E(0/-)$ are the energy differences between the states with corresponding charges, $\Delta E_{cX}(0/+)$ is the energy barrier for transition from the neutral X state to the positively charged deep donor state, ΔE_1 and ΔE_2 are energy barriers for transition between the neutral X and H states, and p is concentration of free electrons. The solid curves in Figure 3 were calculated with the use of Eqs. (1) and (2) and with A and B coefficients and energy values as fitting parameters. The obtained fitting parameters and the calculated energy values given in Table I.

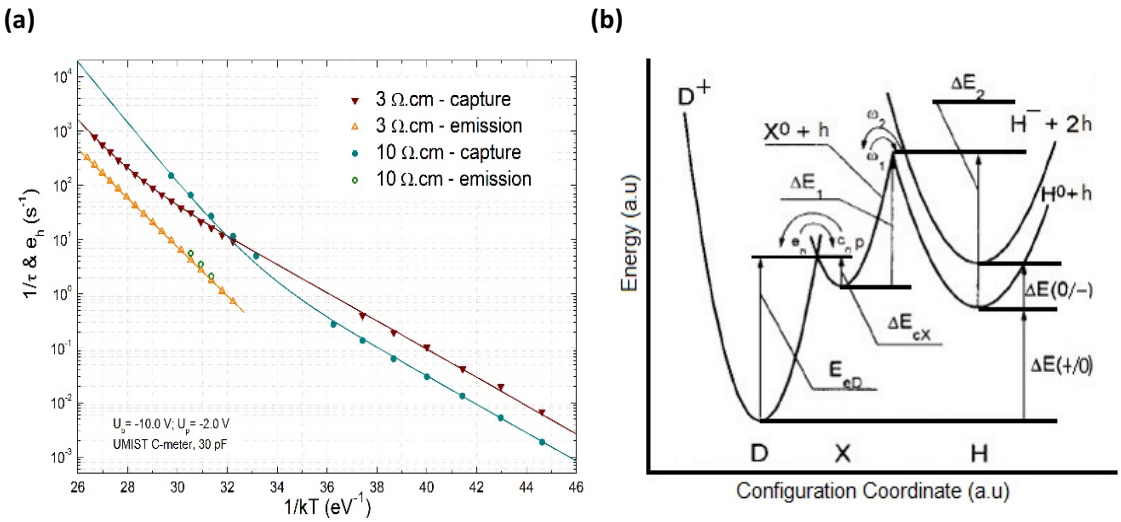

Fig.3 (a) Arrhenius plots of electron occupancy and emission rates for the H390 trap from two (3 and 10 Ω · cm) integral n^+p diodes which were annealed at 425 °C for 600 min. Measurement conditions are given in the figure. Solid lines were calculated with the use of Eqs. (1) and (2) with the parameters given in Table I. **(b)** Configuration coordinate diagram for the metastable BO-defect in silicon.

Table I. Fitting parameters and determined energy values of the metastable BO-defect in p-type silicon.

Parameters	ΔE_{em}	$E_{eD}(+/0)$	ΔE_2	$E(0/-)$	$E(0/+) = \Delta E_{em} - \Delta E_2$
$A_3 = 1.2x10^{13}s^{-1}k^{-2}$ $B_3 = 6.8x10^{13}Ks^{-1}cm^6$ $p_3 = 3.95x10^{15}$ $A_{10} = 4.9x10^{13}s^{-1}k^{-2}$ $B_{10} = 7.0x10^{13}Ks^{-1}cm^6$ $p_{10} = 1.22x10^{15}$	1.24 eV	0.968 (±0.0015) eV	0.67 eV	~0.04 eV	0.57 eV

A. NEW DEFECT MODEL FOR THE BO-RELATED DEFECT IN P-TYPE CZ SILICON

i. Defect transformations observed by effective lifetime measurements

Even though there are many uncertainties with respect the physical mechanisms leading to the LID in Cz Si some well identified characteristics on the behaviour of the LID process have been studied (see e.g [5], [8]), behaviours that have been summarised in the form of a four state model [8] as shown in Figure 5. These characteristics include the substantial reduction of minority carrier lifetimes in B-doped Cz materials upon carrier injection [1], which is believed to be related to transformations of the BO-defect from its inactive state D to its recombination active state B through the firstly appearing state A. This lifetime decay has been observed to occur in two subsequent phases with distinguishable time constants [33], [34], recently linked to the transformations A→B (fast) and D→A→B (slow) [12], [35], together with the observation of the full recovery of the material's initial lifetime after 200 °C heat-treatments under dark conditions. Such heat-treatment process in dark is now known as the "annihilation" process [1], [15], and whose length of application to the material has been shown to influence the lifetime decay time constants attributed to the transformation rates $R_{A\rightarrow B}$ and $R_{D\rightarrow A\rightarrow B}$ [12]. Nevertheless, the annihilation process results in a just temporary lifetime restoration, since subsequent carrier injection is observed to lead to the reduction of minority carrier lifetime repeatedly and indefinitely. To date there is only one reported process ("regeneration") which leads to a more stable state of the BO-defect (i.e. the transformation to the "passivated" state C), which was introduced by Herguth *et al.* [36], [37] in 2006, and involves the exposure of the degraded material to above-bandgap illumination or carrier injection at temperatures between 70 and 230°C [37], [38]. This process, however, has been further studied and developed leading to a more recent, and rather unexpected, findings which show that high intensity and higher temperature treatments (250-300 °C) result in a degradation rate increase [28]. Interestingly, the accelerated degradation has been shown to be of critical importance when trying to mitigate, or at least stabilise, the effects of the BO-defect, since the regeneration process appears only to be effective when the defect is on its B state [39]. Thus, by accelerating the degradation process an subsequently perform illuminated-annealing, some more industrially feasible processes can be implemented [9].

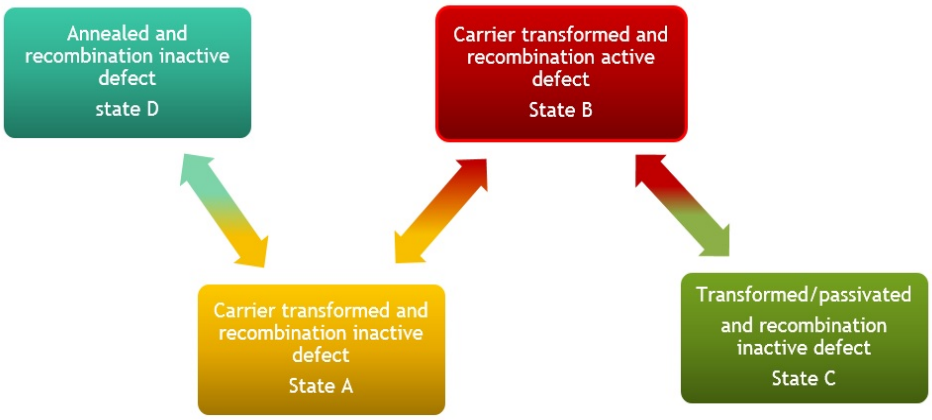

Fig. 5 BO-defect transformation schematic

So, in accordance to these well documented transition behaviours in boron-doped Cz material attributed to the BO-defect, we have studied the observed DLTS peak shown in Fig. 1 to determine its relationship to the defect. The first evidence of such a relationship was presented in Fig. 1, where a clear correlation of the appearance and disappearance of the H_{390} trap to the annealed and degraded state of the BO-related complex is observed. In addition, we have carried

out measurements of the effective lifetime (τ_{eff}) by means of the RR method, and found a remarkable correlation between the formation and disappearance rates of the DLTS peak and the BO-defect annihilation and creation rates, respectively. From direct measurements of τ_{eff} from a set of n^+p diodes made from Cz p-Si and annealed at 350 °C for 10 h, and measurements of the changes in concentration of the H_{390} trap in the same samples we have obtained the data presented in Figure 5. The changes in the trap concentration were monitored by measurements of changes in magnitude (ΔC) of the H_{390} peak in conventional DLTS spectra. Changes in τ_{eff} and ΔC were monitored after several hours of accumulated time of carrier injection for degradation, and subsequent accumulated annealing time at 430 K. Figure 6 (a) shows the normalised effective defect concentration (N^*_T) decay as calculated by $1/\tau_{eff}(t) - 1/\tau_{eff_{max}}$ and the ΔC decrease resulting from the carrier injection at 320 K. Figure 6 (b) on the other hand shows the exponential increase in ΔC related to the increase in the H_{390} trap concentration upon subsequent 430 K annealing together with the exponentially decreasing N^*_T. Exponential fitting of the data resulted in time constant values of 25 ± 0.5 min for both, N^*_T and ΔC, measurements of the degradation kinetics, and 19 ± 0.5 min for the recovery, which demonstrate the almost perfect agreement between the changes in magnitude of the DLTS signal and the lifetime degradation in the sample. We have observed an increase in degradation rate when higher levels of excess carrier injection and temperatures are used, this in line with the observations reported by Hamer *et al.* [28] of LID affected samples. Furthermore, it is worth noting that full recovery of the initial DLTS signal and effective lifetime was found attainable by either maintaining the sample in dark

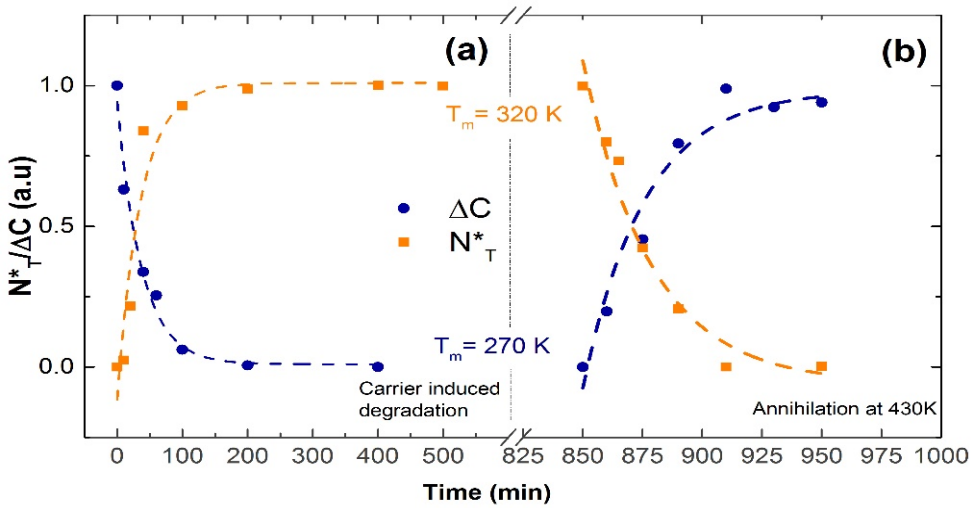

Fig. 6 Normalised effective defect concentration (N^*_T) and ΔC changes as a function of accumulated time under: (a) Forward biasing (+ 2.0 V) at 340 K, and (b) 430 K annealing in dark. Measurement temperatures are given in the figure. All measurements were recorded from an n^+p diode made from 3 Ω·cm B-doped Cz material.

conditions under reverse or zero bias. It is thus reasonable to argue after those observations that no minority carriers are required for the back transformation from the recombination-active state B to the recombination-inactive states D/A. With respect to the "passivated" state C however, we have tried the illuminated-annealing process at a temperature of 200 °C and direct halogen lamp

exposure, and also 430 K dark annealing under applied FB (+2 V) for periods up to 120 h and 60 h, respectively, yet no "passivated" state was achieved. Such behaviour could be explained by the almost non-existent levels of atomistic hydrogen in the samples, nevertheless, further investigations (e.g. longer

injection periods) are required for a definite answer to these observations.

ii. Evidence of shallow acceptor level introduction upon carrier injection

In order to investigate the proposed shallow acceptor formation in our samples, we have carried out capacitance and conductance measurements from various n^+p diodes before and after prolonged FB injection by means of AS. Figure 7 shows the measured data of one of the samples of resistivity 10 Ω·cm at various fixed temperatures in the range from 20K to 50 K, which was annealed for 10 h at 410 K and then FB injected (+2 V) for 60 h. Each temperature scan was measured 5 times and averaged to increase the signal-to-noise ratio, and temperatures below 30 K were able to be kept at the set temperature with an error ≤ 1 mK in the apparatus used.

From the measured data we were able to distinguish a small but very clear shift of the angular frequency maxima (ω_{max}) towards higher frequencies on the degraded sample on both, G/ω (Figure 7(a)) and $\omega C/\omega$ (Figure 7(b)) , spectra. It should be mentioned that there was an unexpected tail observed at the low frequency end of the conductance spectra (see Fig. 7(a)) which never led to a peak formation, therefore we attribute this tail to a measurement artefact. Measurements of the $\omega C/\omega$ spectra shown in Figure 7(b) also display an increase in capacitance of the samples after degradation as observed by the accumulated-filling-pulse technique shown in Figure 2. Temperature dependencies of the ln (ω_{max}) from the $\omega C/\omega(\omega)$ spectra were fitted to a line and resulted in activation energies of the annealed (E_{ann}) and degraded (E_{deg}) states equal to 44.6 ± 0.001 and 43.6 ± 0.001 meV, respectively. Moreover, from simple arithmetic subtraction of the annealed from the degraded spectra we have observed the appearance of two peaks, H_1 and H_2. The subtraction is shown in Figure 8, which includes a magnified image of the spectra in the range 20-26 K, as an inset, where H_2 can be observed. The activation energy of the dominant peak was determined from an Arrhenius plot and resulted in a value of $E_{H1} = 42.5 \pm 0.001$ meV.

Unfortunately, the activation energy of the second peak could not be determined due to its disappearance at > 26 K temperatures in the fast frequency range. All these activation energies appear to be very close to the acceptor level introduced by substitutional boron atoms as was expected to be the case for the introduced shallow acceptor from the BO-defect and shown in Table I. However even though these results suggest that a shallow level formation occurs in the material after degradation, the resolution of the AS technique did not allow a full characterisation of the defect. Therefore, further studies, perhaps with alternative techniques, are required.

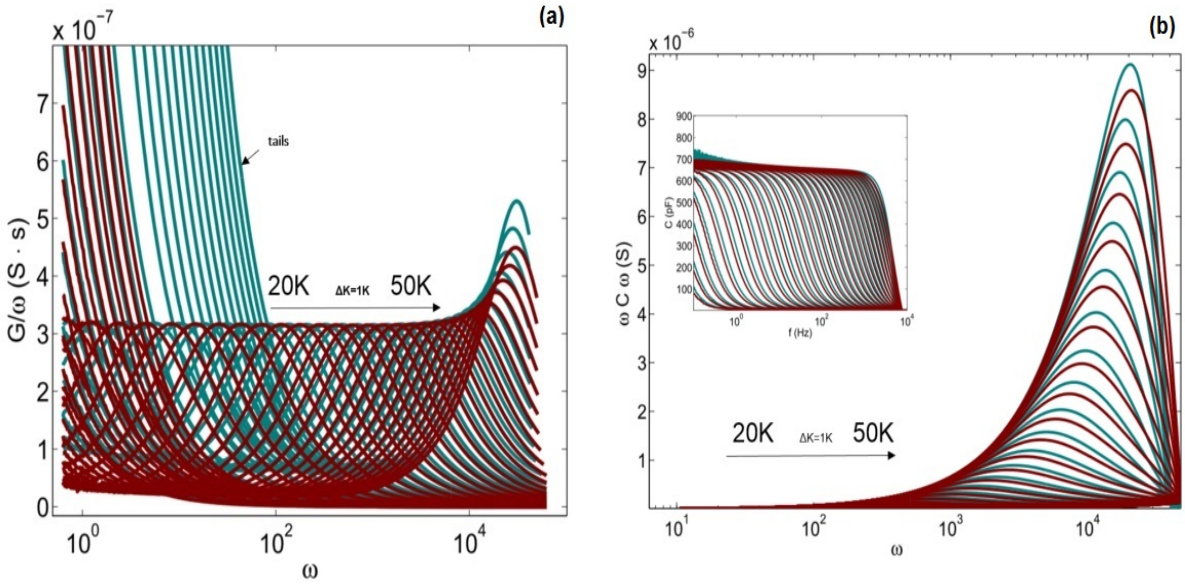

Fig. 7 Admittance spectroscopy data measured in the range 20 – 50 K from an n^+p diode made from 10 Ω·cm B-doped Cz material which was annealed in dark at 410K for 10 h (red line) and degraded by FB injection for 60 h (blue line). (a) Conductance spectra. (b) Capacitance spectra. Measurement conditions: V_{osc} = 0.05 V, Freq. range: 100 Hz – 10 MHz.

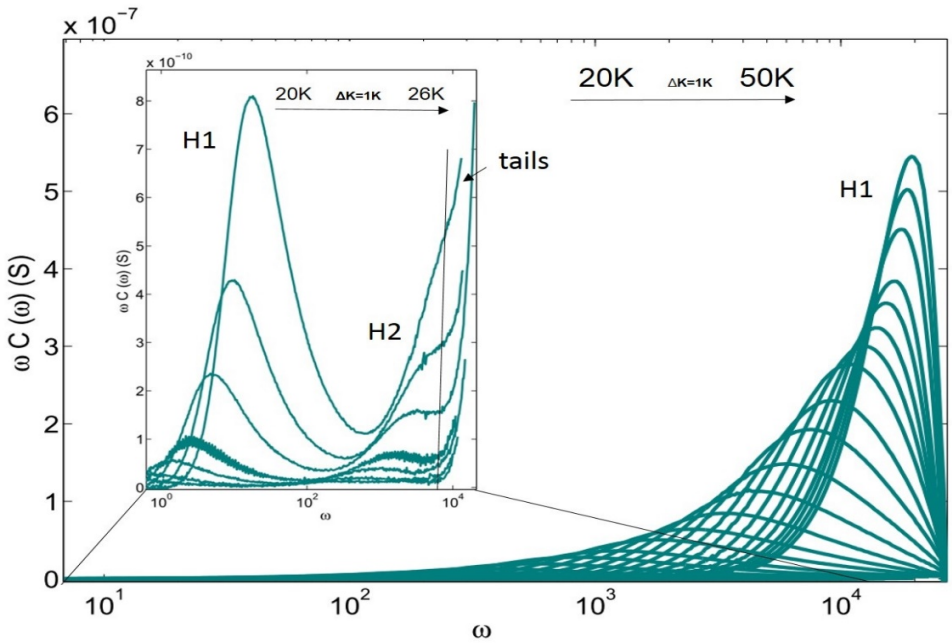

Fig. 8 Admittance spectroscopy data obtained by the difference between the data shown in blue on Figure 7 (b) (annealed state) minus the data in red on the same figure (degraded state). The apparent formation of two distinct peaks is shown in the inset magnification of the data in the range 20 - 26 K.

iii. Proposed atomic structure of the BO_2 defect

The experimental results obtained by us and available literature results strongly indicate that the LID effect is associated with a defect incorporating one boron and two oxygen atoms. With the use of first-principles density functional calculations minimum-energy atomic configurations of the BO_2 defect in different charge states have been found and configuration-coordinate diagram of the center has been constructed. Figure 8 show the results of the calculations. The results are consistent with the experimental findings. It is found that the minimum-energy configuration of the BO_2 defect in the singly positively charge state consists of the oxygen dimer in the so called squared configuration in a <110> crystal plane with a boron attached to a silicon atom which is connected to both oxygen atom. For the BO_2 defect in neutral and singly negatively charges states there are two minimum energy configurations with oxygen atoms in two staggered forms and with approximately the same location of the boron atom. The ground-state structure of the defect in p-type Si is "sq^+". In this configuration the defect can emit hole or capture an injection induced electron and transform to the "$sq^0 + h^+$" state. This state, however, is metastable and a fast transition to the "$st'^0 + h^+$" state occurs.

The ionization energy of hole in the "st'^0" state is very small, so the defect does not stay long in this state and go to the "$st'^- + 2h^+$" state by emitting a hole. So, these are transitions between the "sq^+" and "$st'^- + 2h^+$" states which are responsible for the experimentally observed H_{390} hole emission signal and the capacitance transients presented in Fig. 2. The release of energy upon transition from the "$st'^- + 2h^+$" state to the "sq^+" state can promote a transition of the BO_2 defect from the "$sq^0 + h^+$" state to the "$st^0 + h^+$" and then to the "$st^- + 2h^+$" state, which is likely to be the recombination active LID state. The back transition from the "$st^- + 2h^+$" state to the "sq^+" state occurs through a relatively high energy barrier between the "$st^0 + h^+$" and "$sq^0 + h^+$" states,

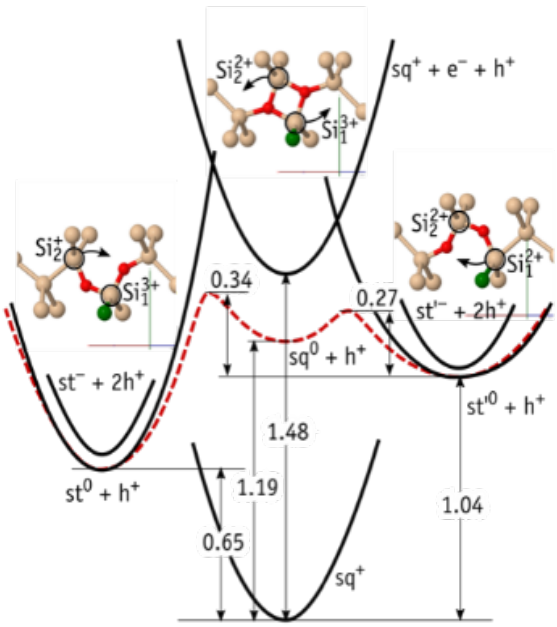

Fig. 9 Structure of the metastable LID-responsible defect in p-type silicon in its minimum energy configurations together with their configuration-coordinate diagram. Oxygen and boron are coloured in red and green, respectively. The configurational coordinate diagram curves are schematic and only the minima and saddle point energies were calculated by first-principles. e^- and h^+ represent free electrons

so it can occur only at a relatively high temperature, in the range of T for experimentally observed "LID annihilation" process. Regarding the recombination activity of the BO_2 defect in the "st^-" configuration it can be suggested that this activity is related to the Auger type recombination through the shallow acceptor state [40,41].

IV. CONCLUSIONS

By means of various junction capacitance techniques we have studied several n^+p and Schottky barrier diodes made from B-doped Cz silicon which we have observed suffers from light induced degradation. In the DLTS spectra of every measured sample we have detected a peak with its maximum at about 390 K. The magnitude of the peak has been observed to increase upon long heat-treatments in the temperature range 350 – 425 °C. Observation of this peak requires the utilisation of rather unusual measurement conditions and therefore it has not been previously reported. We have found a direct correlation between the appearance of this peak and the LID process reported extensively in literature yet never-before observed by direct spectroscopic characterization techniques. Since the peak's magnitude has been found to decrease after carrier injection and to re-appear after heat-treatments > 130 °C, we attribute the signal to arise from the BO-defect in its recombination-inactive (i.e precursor) state. Furthermore, from the monitored changes in capacitance at various multiple-filling-pulse lengths in every measured n^+p diode after 350 – 425 °C heat-treatments strong evidence of deep donor to shallow acceptor transformations was obtained.

Furthermore, from Arrhenius plots distinct occupancy rates at low- and high- temperature regimes were apparent. These features, in addition to an unusual $\tau^{-1} \sim 1/n$ dependency at the high-temperature regime, was only possible to describe by the introduction of a metastable neutral charge state. Hence, from the close analysis of temperature dependencies of hole emission and capture rates for, what we argue is, the BO-related center its electronic structure and energy barriers have been determined and a configuration-coordinate diagram of the defect has been constructed. In addition, from first principles density functional calculations an atomistic structure of the defect is presented. It is argued that the LID-responsible defect is formed by an interstitial B-atom and an oxygen dimer which in its latent state introduce a deep donor level in the gap which acts as an effective trapping center. This defect is metastable and thus after small FB injection at < 270 K temperatures or when the crystal is cooled down from > 390 K temperatures under reverse bias transforms to produce a shallow acceptor level, which also acts a trapping center in the material. An additional transformation occurs, however, when the crystal is subjected to prolonged-time FB injection or illumination. This later transformation results in the introduction of another shallow acceptor level of activation energy close to that of the B-atom, which is recombination-active and produces the material lifetime degradation. To our knowledge, the single other publication reporting observations of shallow trap formation after carrier injection in p-type Cz-Si has been that from Glunz *et al.* [3] in 2001. However there, the authors attributed this trap to the BO-related defect on its passive state and to be responsible for only weak recombination activity. In this work, we attribute the shallow acceptor level

introduced after carrier injection to be the source of the substantial lifetime decrease in the material as described by the trap-assisted Auger recombination process.

ACKNOWLEDGMENTS

This work has been supported by the EPSRC-UK under the Supergen Contract No. EP/M024911/1. Financial support was also received from CONACyT-Mexico (Consejo Nacional de Ciencia y Tecnologia- Mexico).

REFERENCES

[1] H. Fischer and W. Pschunder, "Proceedings of the Tenth IEEE Photovoltaic Specialists Conference." IEEE New York, 1973.

[2] K. Bothe and J. Schmidt, "Electronically activated boron-oxygen-related recombination centers in crystalline silicon," *J. Appl. Phys.*, vol. 99, no. 1, 2006.

[3] S. W. Glunz, S. Rein, J. Y. Lee, and W. Warta, "Minority carrier lifetime degradation in boron-doped Czochralski silicon," *J. Appl. Phys.*, vol. 90, no. 5, pp. 2397–2404, 2001.

[4] S. Rein, "The metastable defect in boron-doped Czochralski silicon , Chapter 5," Lifetime Spectroscopy: A Method of Defect Characterization in Silicon for Photovoltaic Applications, Springer Berlin Heidelberg, 2006.

[5] T. Niewelt, J. Sch, W. Warta, S. W. Glunz, and M. C. Schubert, "Degradation of Crystalline Silicon Due to Boron – Oxygen Defects," *IEEE J. Photovoltaics*, no. 1, pp. 1–16, 2016.

[6] J. Lindroos and H. Savin, "Review of light-induced degradation in crystalline silicon solar cells," *Sol. Energy Mater. Sol. Cells*, vol. 147, pp. 115–126, 2016.

[7] S. Wilking, A. Herguth, and G. Hahn, "Influence of hydrogen on the regeneration of boron-oxygen related defects in crystalline silicon," *J. Appl. Phys.*, vol. 113, no. 19, 2013.

[8] B. Hallam, A. Herguth, P. Hamer, N. Nampalli, S. Wilking, M. Abbott, S. Wenham, and G. Hahn, "Eliminating Light-Induced Degradation in Commercial p-Type Czochralski Silicon Solar Cells," *Appl. Sci.*, vol. 8, no. 1, p. 10, 2017.

[9] B. J. Hallam, C. E. Chan, R. Chen, S. Wang, J. Ji, L. Mai, M. D. Abbott, D. N. R. Payne, M. Kim, D. Chen, C. Chong, and S. R. Wenham, "Rapid mitigation of carrier-induced degradation in commercial silicon solar cells," *Jpn. J. Appl. Phys.*, vol. 56, 2017.

[10] D. C. Walter and J. Schmidt, "Impact of hydrogen on the permanent deactivation of the boron-oxygen-related recombination center in crystalline silicon," *Sol. Energy Mater. Sol. Cells*, vol. 158, pp. 91–97, 2016.

[11] D. C. Walter, R. Falster, V. V. Voronkov, and J. Schmidt, "On the equilibrium concentration of boron-oxygen defects in crystalline silicon," *Sol. Energy Mater. Sol. Cells*, vol. 173, no. March, pp. 33–36, 2017.

[12] B. Hallam, M. Kim, M. Abbott, N. Nampalli, T. Nærland, B. Stefani, and S. Wenham,

"Recent insights into boron-oxygen related degradation: Evidence of a single defect," *Sol. Energy Mater. Sol. Cells*, vol. 173, no. April, pp. 25–32, 2017.

[13] A. Inglese, A. Focareta, F. Schindler, J. Schön, J. Lindroos, M. C. Schubert, and H. Savin, "Light-induced Degradation in Multicrystalline Silicon: The Role of Copper," *Energy Procedia*, vol. 92, pp. 808–814, 2016.

[14] J. Schmidt, A. G. Aberle, and R. Hezel, "Investigation of carrier lifetime instabilities in Cz-grown silicon," *Conf. Rec. Twenty Sixth IEEE Photovolt. Spec. Conf. - 1997*, pp. 13–18, 1997.

[15] S. W. Glunz, S. Rein, W. Warta, J. Knobloch, and W. Wettling, "Degradation of carrier lifetime in Cz silicon solar cells," *Sol. Energy Mater. Sol. Cells*, vol. 65, no. 1, pp. 219–229, 2001.

[16] D. V Lang and D. V Lang, "Deep-level transient spectroscopy: A new method to characterize traps in semiconductors," *J. Appl. Phys.*, vol. 45, no. January, p. 3023, 1974.

[17] R. Brunwin, B. Hamilton, P. Jordan, and A. R. Peaker, "Detection of minority-carrier traps using transient spectroscopy," *Electron. Lett.*, vol. 15, no. 12, pp. 349–350, 1979.

[18] L. Dobaczewski, A. R. Peaker, and K. B. Nielsen, "Laplace-transform deep-level spectroscopy: The technique and its applications to the study of point defects in semiconductors," *J. Appl. Phys.*, vol. 96, no. 9, pp. 4689–4728, 2004.

[19] J. L. Pautrat, B. Katircioglu, N. Magnea, D. Bensahel, J. C. Pfister, and L. Revoil, "Admittance spectroscopy: A powerful characterization technique for semiconductor crystals—Application to ZnTe," *Solid. State. Electron.*, vol. 23, no. 11, pp. 1159–1169, 1980.

[20] R. Kingston, "Switching time in junction diodes and junction transistors," *Proc. IRE*, vol. 28, pp. 829–834, 1954.

[21] M. Vaqueiro-Contreras, V. P. Markevich, M. P. Halsall, A. R. Peaker, P. Santos, J. Coutinho, S. Öberg, L. I. Murin, R. Falster, J. Binns, E. V. Monakhov, and B. G. Svensson, "Powerful recombination centers resulting from reactions of hydrogen with carbon–oxygen defects in n-type Czochralski-grown silicon," *Phys. Status Solidi - Rapid Res. Lett.*, vol. 11, no. 8, 2017.

[22] A. R. Peaker, V. P. Markevich, and J. Coutinho, "Junction spectroscopy techniques and deep-level defects in semiconductors," *J. Appl. Phys.*, vol. 123, no. 16, 2018.

[23] M. V. Contreras, V. P. Markevich, J. Mullins, M. P. Halsall, L. I. Murin, R. Falster, and J. Binns, "Lifetime degradation of n-type Czochralski silicon after hydrogenation," pp. 7–8, 2016.

[24] H. J. Kuno, "Analysis and Characterization of P-N Junction Diode Switching," *IEEE Trans. Electron Devices*, vol. 11, no. 1, pp. 8–14, 1964.

[25] J. Schmidt and K. Bothe, "Structure and transformation of the metastable boron- and oxygen-related defect center in crystalline silicon," *Phys. Rev. B - Condens. Matter Mater. Phys.*, vol. 69, no. 2, pp. 1–8, 2004.

[26] T. Niewelt, J. Schon, J. Broisch, W. Warta, and M. Schubert, "Electrical characterization of the slow boron oxygen defect component in Czochralski silicon," *Phys. Status Solidi - Rapid Res. Lett.*, vol. 9, no. 12, pp. 692–696, 2015.

[27] J. A. Hornbeck and J. R. Haynes, “Trapping of Minority Carriers in Silicon. I. P-type Silicon,” *Phys. Rev.*, vol. 97, no. 2, pp. 311–321, 1955.

[28] P. Hamer, B. Hallam, M. Abbott, and S. Wenham, “Accelerated formation of the boron-oxygen complex in p-type Czochralski silicon,” *Phys. Status Solidi - Rapid Res. Lett.*, vol. 9, no. 5, pp. 297–300, 2015.

[29] D. Macdonald, P. N. K. Deenapanray, A. Cuevas, S. Diez, and S. W. Glunz, “The Role of Silicon Interstitials in the Formation of Boron-Oxygen Defects in Crystalline Silicon,” *Solid State Phenom.*, vol. 108–109, pp. 497–502, 2005.

[30] J. Schmidt, K. Bothe, and R. Hezel, “Oxygen-related minority-carrier trapping centers in p-type Czochralski silicon,” *Appl. Phys. Lett.*, vol. 80, no. 23, pp. 4395–4397, 2002.

[31] L. F. Makarenko and L. I. Murin, “Trapping of Minority Carriers in Thermal U Donors in n-Si,” *Phys. Stat. Sol. b*, vol. 145, p. 241, 1988.

[32] V. P. Markevich, L. I. Murin, T. Sekiguchi, and M. Suezawa, “Emission and Capture Kinetics for a Hydrogen-Related Negative-U Center in Silicon: Evidence for Metastable Neutral Charge State,” *Mater. Sci. Forum*, vol. 258–263, no. March 2016, pp. 217–222, 1997.

[33] H. Hashigami, Y. Itakura, and T. Saitoh, “Effect of illumination conditions on Czochralski-grown silicon solar cell degradation,” *J. Appl. Phys.*, vol. 93, no. 7, pp. 4240–4245, 2003.

[34] K. Bothe and J. Schmidt, “Fast-forming boron-oxygen-related recombination center in crystalline silicon,” *Appl. Phys. Lett.*, vol. 87, no. 26, pp. 1–3, 2005.

[35] M. Kim, D. Chen, M. Abbott, N. Nampalli, S. Wenham, B. Stefani, and B. Hallam, “Impact of interstitial iron on the study of meta-stable B-O defects in Czochralski silicon: Further evidence of a single defect,” *J. Appl. Phys.*, vol. 123, no. 16, 2018.

[36] A. Herguth, G. Schubert, M. Kaes, and G. Hahn, “A new approach to prevent the negative impact of the metastable defect in boron doped CZ silicon solar cells,” *Conf. Rec. 2006 IEEE 4th World Conf. Photovolt. Energy Conversion, WCPEC-4*, vol. 1, pp. 940–943, 2007.

[37] G. Herguth, A., Schubert, G., Kaes, M., & Hahn, “Avoiding boron-oxygen related degradation in highly boron doped Cz silicon. In 21st European Photovoltaic Solar Energy Conference: 21th EC PVSEC,” 2006.

[38] A. Herguth and G. Hahn, “Kinetics of the boron-oxygen related defect in theory and experiment,” *J. Appl. Phys.*, vol. 108, no. 11, 2010.

[39] P. Hamer, B. Hallam, M. Abbott, C. Chan, N. Nampalli, and S. Wenham, “Investigations on accelerated processes for the boron-oxygen defect in p-type Czochralski silicon,” *Sol. Energy Mater. Sol. Cells*, vol. 145, pp. 440–446, 2016.

[40] W. Schmid, Auger lifetimes of bound excitons to neutral donors and acceptors in Si, Phys. Status Solidi B 84, (1977) 529-540.

[41] G. C. Osbourn, S. A. Lyon, K. R. Elliott, D. L. Smith, and T. C. McGill, Auger and radiative recombination of acceptor bound excitons in semiconductors, Sol. St. Electronics 21, (1978) 1339-1342.

CHAPTER 5

NEW MATERIALS FOR SURFACE PASSIVATION: GRAPHENE OXIDE

Graphite oxide monolayer, also known as graphene oxide (GO), is a carbon based material whose properties have been investigated since its discovery and first fabrication which can be traced back to over a hundred years ago [174]. Moreover, GO attention has boosted after the successful isolation and characterization of monolayer graphite (graphene) in 2004 by professors Andre Geim and Kostya Novoselov [175] due to its outstanding properties. This is because it has been demonstrated that GO chemical/thermal reduction (oxygen-group removal) is a feasible approach to graphene mass production even more so because it can be easily dispersed in water. Nevertheless, GO itself is known for a variety of remarkable characteristics. In this chapter we will begin presenting a review on GO's general structure and properties giving emphasis on those related to optics and electronics. The review will be followed by the latest results on the surface passivation ability of GO and the responsible mechanism for the passivation in the form of a published article (Publication No. 6). It is demonstrated that the intrinsic properties of GO serve as a potential cheap alternative for silicon surface passivation capable of achieving surface recombination velocities as low as 14.4 cm^{-1}. Furthermore, by means of a series of experimental techniques such as FTIR, Kelvin probe force microscopy (KPFM) and microwave photo-conductance decay (μPCD) it is argued that the primary source of the passivation is related to the GO's negative charge. This charge thus allows the formation of a negative field potential that penetrates the silicon surface repelling negative charges and reducing recombination (i.e surface field passivation).

In general thin film dielectrics are a very active research area [4, 87, 176, 177], this is because besides the required low surface recombination velocities for high efficiency cells it is also needed to achieve lower manufacturing costs. Even though extremely

low recombination velocities have already been achieved through the application of various techniques, the later requirement has not been met, because most of the applied materials require high temperature treatments for dielectric growth and/or activation, and/or involve expensive and slow deposition procedures i.e plasma-enhanced chemical vapour deposition (PECVD) or atomic layer deposition (ALD) [4, 47, 87, 176, 177]. This is why it is technologically relevant to continue to explore new passivation materials which may allows us to meet the current industrial demands.

5.1 Graphene oxide optical and electrical properties

As previously stated, GO consists of a single layer of graphite which is covered with oxygen groups on its basal plane and edges. Even though there is still a debate on the actual structure of GO the most popular models are: the Hofmann and Holst model (1939) [178], the Ruess model (1947) [179], the Scholz and Boehm model (1969) [180], the Lerf-Klinowski model (1997) [181, 182, 183], the Nakajima model (1988) [184, 185] and the Szabó model (2006) [186]. Figure 5.1. depicts the proposed structures of each model. As can be seen from the figure, GO has a similar structure to graphite with single layers of carbon atoms distributed in a honeycomb lattice. However an important distinction is that the addition of oxygen groups give rise to a larger d-spacing of ~ 0.83 nm compared to graphite's ~ 0.34 nm d-spacing [187].

Graphene oxide is generally regarded as an insulating material. With typical resistance sheet values of $\sim 10^{10}\Omega$ sq^{-1} or higher due to large quantity of sp^3 hybridized carbons bonded with the oxygen functional groups [188]. However, sheet resistance and thus the conductivity of GO are highly dependant on annealing time and temperature. In fact, a dramatic change in GO's resistance from $\sim 10^{11}$ to $\sim 10^5\Omega$ sq^{-1} after annealing at 200 °C in nitrogen (or vacuum) is reported in [188]. This is because increased temperature disassociates the oxygen functional groups, which lead to the widely used thermal reduction of GO for graphene production. Nevertheless, such behaviour of GO under changing thermal conditions has an exponential nature and reaches its saturation value at certain time and temperature [188].

Also dependent on the functional groups, GO exhibit a fixed negative charge on the surface due to the presence of negatively charged oxygen layers laying above and below the carbon grid [183]. In addition, it has been reported that an increased pH level results in an increased concentration of carboxylic acid (-COOH) and hydroxyl

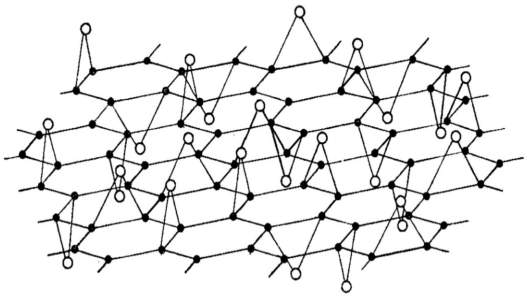

(a) Hofmann [178].

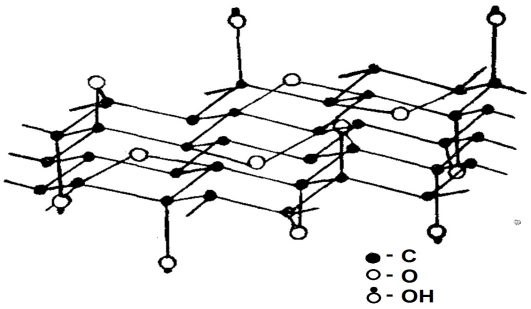

(b) Ruess [179].

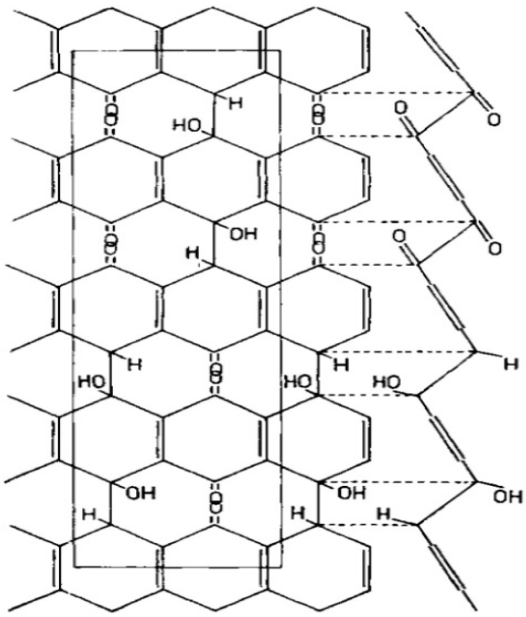

(c) Scholz - Boehm [180].

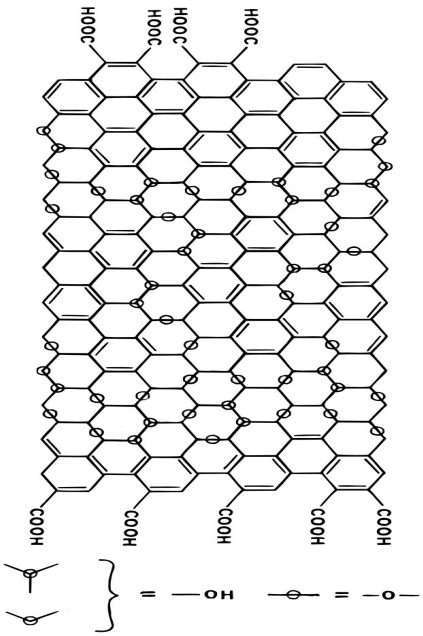

(d) Lerf - Klinowski [183].

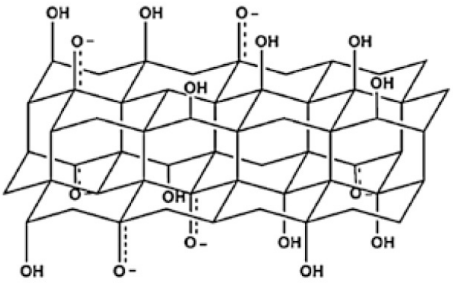

(e) Nakajima - Matsuo [174]

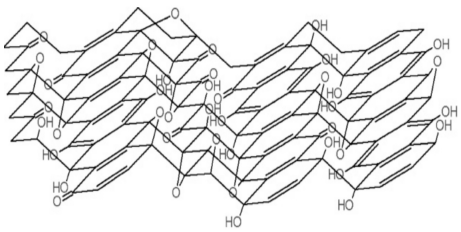

(f) Szabó [186].

Figure 5.1: Graphene oxide model sketches.

(-OH) ionised groups [189]. This implies that an enhanced negative surface charge can be obtained by a more alkaline GO dispersion.

Several applications of GO on Si have already been reported. A common practice is to use the simple spin coating technique for deposition and posterior drying on a hot plate. Even though most of the water can be evaporated by this procedure in reality there is always a portion of water molecules between the GO layers, even after thermal reduction [190, 191]. This moisture can affect the optical properties of GO to some extent. Nevertheless, a refractive index ≥ 1.7 and up to ≈ 1.99 has been reported [192, 193].

Other optical property of GO is its transmittance. GO monolayer displays high transmittance in the visible spectrum [194]. Zhu *et al.* [195] show that GO suspensions of 0.5 mg/ml have an optical transmittance of 96 % at $\lambda = 550$ nm. In addition, GO's optical transmittance is highly tuneable by changes in oxidation degree and thickness of the deposited material. Becerril *et al.* [8] published the study of the effect of thickness of GO on its transmittance, demonstrating a direct relationship as depicted in Figure 5.1 (a). Moreover, Mattevi *et al.* [9] show that there is a decrease in transmittance with increased chemical reduction time, while the temperature did not show major changes in transmittance after 24 hours reduction time, due to the reached saturation (see fig. 5.1 (b) (full dots)). In contrast the dramatic change on transmittance of non-reduced GO is clearly observed in Figure 5.1 (b) (empty dots) with increased temperature. In the inverse case of transmittance, the absorbance spectra of GO in the UV-visible range has shown a red shift with increased chemical reduction time as depicted in 5.1 (c).

Graphene oxide displays a range of adjustable characteristics that makes it an appealing material for diverse optical applications. Therefore it is investigated here for potential applications as a surface and/or emitter passivation layer, anti-reflection coating and replacement for aluminium backsurface field for silicon based solar cells. In the next section, results specifically on the application of GO as surface passivation material and the mechanisms that allow it are presented in the form of a published article.

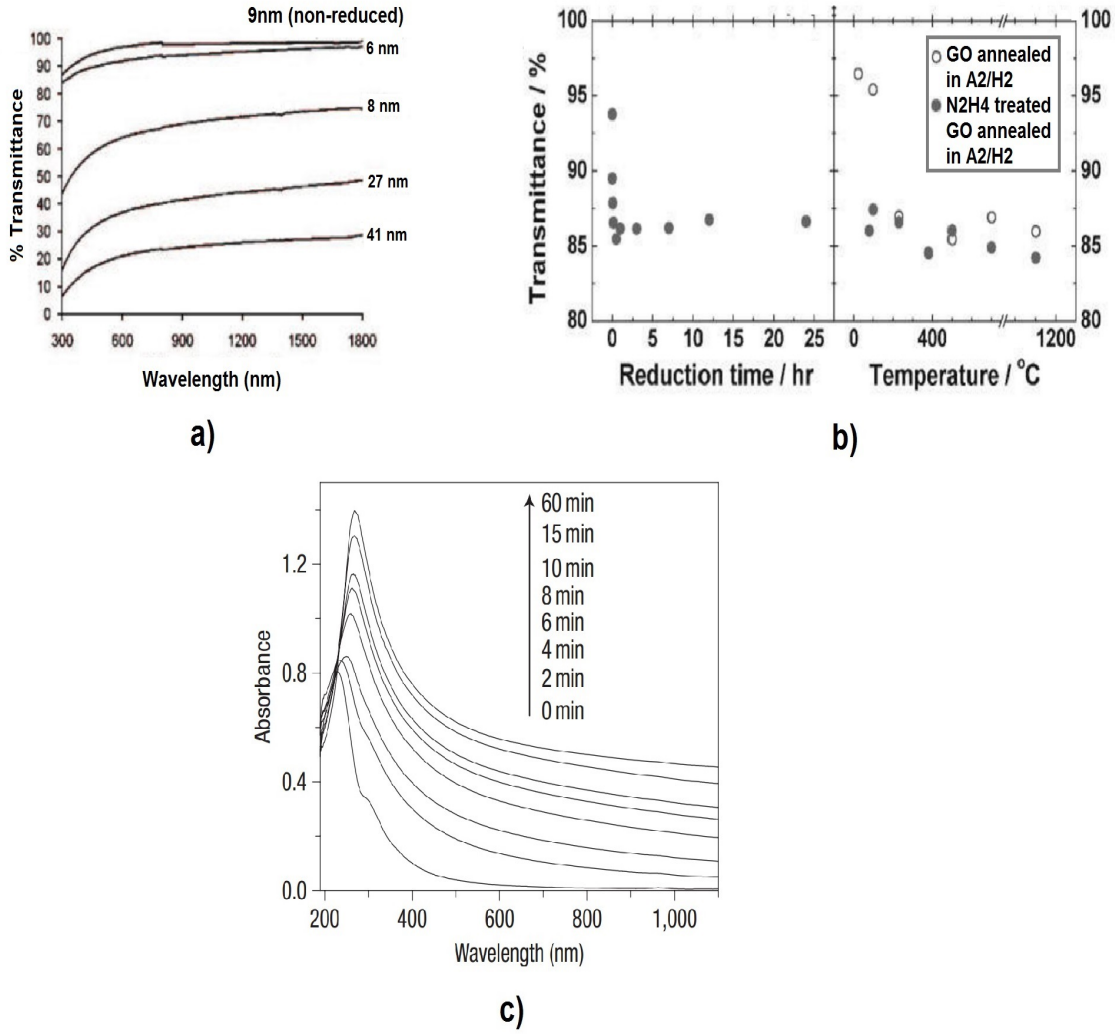

Figure 5.2: a) GO optical transmittance as a function of wavelength and GO film thickness adapted from [8]. b) Three layer GO film optical transmittance as a function of reduction time and temperature adapted from [9]. c) UV-vis absorption spectra of GO as a function of reduction reaction time (chemical reduction N_2H_4) adapted from [10].

5.2 Graphene oxide films for field effect passivation

Publication No.6

Graphene oxide films for field effect surface passivation of silicon for solar cells

Solar Energy Materials and Solar Cells 187 (2018) 189–193

Contents lists available at ScienceDirect

Solar Energy Materials and Solar Cells

journal homepage: www.elsevier.com/locate/solmat

Graphene oxide films for field effect surface passivation of silicon for solar cells

M. Vaqueiro-Contreras[a,*], C. Bartlam[b], R.S. Bonilla[c], V.P. Markevich[a], M.P. Halsall[a], A. Vijayaraghavan[b], A.R. Peaker[a]

[a] School of Electrical and Electronic Engineering, University of Manchester, Manchester M13 9PL, UK
[b] School of Materials, University of Manchester, Manchester M13 9PL, UK
[c] Department of Materials, University of Oxford, Oxford OX1 3PH, UK

ARTICLE INFO

Keywords:
Surface passivation
Graphene oxide
Solar cells
Dielectric charge

ABSTRACT

In recent years it has been shown that graphene oxide (GO) can be used to passivate silicon surfaces resulting in increased photocurrents in metal-insulator-semiconductor (MIS) tunneling diodes, and in improved efficiencies in Schottky-barrier solar cells with either metal or graphene barriers, however, the source of this passivation is still unclear. The suggested mechanisms responsible for the enhanced device performance include the dangling bond saturation at the surface by the diverse functional groups decorating the GO sheets which reduce the recombination sites, or field effect passivation produced by intrinsic negative surface charge of GO. In this work through a series of measurements of minority carrier lifetime with the microwave photo-conductance decay (μPCD) technique, infrared absorption spectra, and surface potential with Kelvin probe force microscopy (KPFM) we show that there is no evidence of significant chemical passivation coming from the GO films but rather negative field effect passivation. We also discuss the stability of GO's passivation and the flexibility of this material for its application as temporary passivation layer for bulk lifetime measurements, or as a potential cheap alternative to current passivation materials used in solar cell fabrication.

1. Introduction

It is well known that one of the most effective approaches to improve the efficiency of silicon-based solar cells, whilst maintaining low cost, is to increase the lifetime of photo-generated carriers by reducing recombination at the surface and in the bulk of low cost materials [1]. Therefore the study of new materials which may suppress surface recombination in such materials is important both because they may promote a minority carrier lifetime improvement in commercial solar cells but also, in the laboratory, they may allow more accurate measurements of silicon's bulk lifetime. For these reasons such new materials remain a topic of widespread interest [2–4].

Generally, for surface passivation materials we need to consider three material property aspects: the characteristics of the material to be passivated (doping type and resistivity); the physical properties of the passivating materials (optical, chemical and electrical), to determine the type of passivation that the material will provide including bond saturation, the field effect control of carriers, refractive index, and stability; and processing requirements like surface cleaning and synthesis methods. With this in mind, in this work we have studied the passivation capabilities of graphene oxide which we know fulfils some key requirements for surface passivation including: high transmittance [5], fixed surface negative charge [6,7] and high refractive index [8,9]. This is all combined with the fact that GO is water dispersible making its deposition and removal extremely simple. Most common GO deposition techniques include: dip coating, spin coating, and spray coating, techniques which can be easily incorporated to a production line. In addition, it has been recently shown that for a GO derivative dispersion with an optimal dilution, it is possible to obtain uniform coverage even on textured silicon surfaces for solar cells [10].

While passivation effects in structures incorporating GO interlayers, such as MOS and graphene/GO/Si devices, have already been reported in literature [11–16], these do not include the study of graphene oxide as a passivation material for solar cells in a scalable to manufacture system. Furthermore, to our knowledge there is no definitive answer as to what is causing the passivation on the surface from the available literature. Thus in this work we aim to answer such a question by providing strong evidence of the influence of the negative surface charge of GO in the passivation of silicon. Additionally, we demonstrate the passivation effect of GO in different silicon materials and the inclusion of GO's passivation capabilities compared to that of the industry standard material, silicon nitride (SiN_x) used for solar cell passivation

* Corresponding author.

https://doi.org/10.1016/j.solmat.2018.08.002
Received 20 February 2018; Received in revised form 29 June 2018; Accepted 2 August 2018

[17] and the widespread temporary passivation attained from Iodine-Ethanol (I-E) solution immersion for bulk lifetime measurements [3].

2. Materials and methods

In this work a range of float zone (FZ) and Czochralski (Cz) grown, boron-doped silicon wafers with ‹100› crystal orientation, double (DSP) and single (SSP) side polished, with resistivities between 1 and 1000 Ω·cm, and thicknesses from 200 to 625 µm have been used to study the passivation effect of GO. Most of the measurements were carried out in cut samples of $2 \times 2\,cm^2$ which were subjected to the standard cleaning "RCA 1" procedure as described in Ref. [18]. However, the usually applied subsequent HF dip of the samples was not performed since it was found that such step resulted in a diminished passivation of the silicon surface due to the lack of hydrophilicity on the surface provided by either the native oxide or the oxide left by the H_2O_2. It must be noted as well that the samples were cleaned and left in the desiccator for at least 3 days before the GO deposition, and their lifetime measured before and after the deposition to avoid the inclusion of the RCA 1 passivation effect into consideration, it was determined that this process takes place within that period before stabilisation.

GO was prepared by a modified Hummers method [19] whereby natural flake graphite (30 mesh, 96%C) was oxidised and exfoliated. Sulphuric acid (H_2SO_4, 98%), hydrogen peroxide (H_2O_2, 30%), ammonium hydroxide (NH_4OH, 35%) (Sigma Aldrich); sodium nitrate and potassium permanganate ($KMnO_4$, Alfa Aesar) were all used as supplied and without any further purification. The oxidised graphite was repeatedly washed and exfoliated using a 3% wt. H_2SO_4/ 0.5% wt. H_2O_2 mixture and then washed further with deionised water until a pH of 7 was reached for the supernatant to ensure the removal of the H_2SO_4. The GO pellet had a pH of 3.6. To adjust the pH of GO, 100 µl of ammonium hydroxide was added to under stir to give a pH of 9.9 ± 0.01 measured with a Mettler Toledo F20 pH meter.

For the silicon nitride deposition we used the Plasma-Enhanced Chemical Vapour Deposition (PECVD) technique for 2 min, to achieve a film thickness of 90 nm ± 3 nm according to spectroscopic ellipsometry. This was done on a PlasmaPro 100 PECVD system from Oxford Instruments with: 20:20 sccm SiH4: NH3 gas flow, 300 mTorr chamber pressure, 400 °C table temperature, 13.56 MHz plasma generated frequency and 50 W of power as deposition parameters.

Kelvin Probe force microscopy on the PeakForce tapping frequency-modulated mode (FM-KPFM) using SCM-PIT-V2 tips was used to map the surface potential of single GO flakes on a Bruker Dimension FastScan. Samples for this measurements were prepared by spin coating 0.5 mg/ml of GO for 60 s at a speed of 1000 rpm and left to dry on a desiccator overnight. Infrared absorption spectroscopy on 200 nm ± 20 nm thick GO coated silicon samples was carried out with a Hyperion 3000 FT-IR microscope with a resolution of $4\,cm^{-1}$ in transmission mode.

A Semilab WT-2000 PVN was used for minority carrier lifetime mapping by the microwave photoconductivity decay (µPCD) technique, with a 905 nm LASER excitation and a microwave source operating at ~10 GHz. Hence the presented effective lifetime maps show the averaged lifetime down to a few tens of microns into the sample. The level of passivation achieved by GO layers was tested in several samples by the measurement of their effective lifetime (τ_{eff}) by µPCD mapping, with the assumption that both sides of each sample were equally passivated. Next, what is considered the upper limit of the surface recombination velocity (S_{UL}) was calculated by assuming the bulks lifetime (τ_{bulk}) to be infinite, thus giving $S_{UL} = W/2(\tau_{eff})$, with W representing the sample thickness.

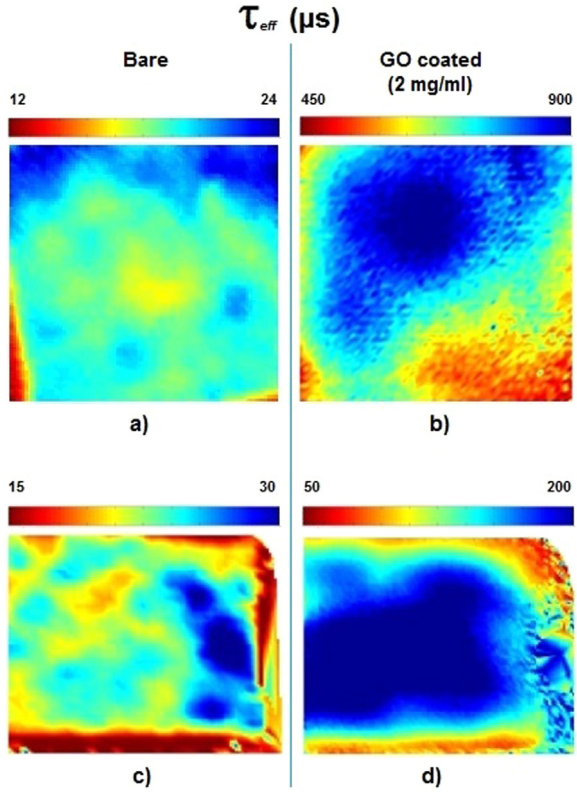

Fig. 1. Effective lifetime maps of a DSP FZ p-type (> 1000 Ω·cm) silicon sample (a) bare and (b) GO coated, and a SSP Cz p-type (2.8 Ω·cm) silicon sample (c) bare and GO coated.

3. Results and discussion

3.1. GO effect on minority carrier lifetime

We have carried out transient photoconductance mapping to compare the level of surface passivation achieved by GO in various sets of samples, here we present the comparison of GO's passivation on an electronic grade FZ material to that of a solar grade Cz material. Fig. 1 show the lifetime maps of the FZ and the Cz boron doped samples before (**a**, **c**), and after (**b**, **d**) GO passivation, respectively. For the FZ sample it can be observed that the τ_{eff} approaches 1 ms in some areas. Nevertheless, considering the maximum effective lifetime in the sample to be τ_{max} = 900 µs and W = 500 µm we obtain a $S_{UL} \approx 27\,cm\,s^{-1}$, whereas from the τ_{max} = 820 µs and W = 200 µm of the Cz sample the calculation results in a $S_{UL} \approx 30\,cm\,s^{-1}$. These values are comparable to the surface recombination velocities of some existent surface passivation materials [3,4]. Moreover, we have compared the surface passivation of GO to that of PECVD deposited SiN_x and I-E solution immersion. The passivation was carried out on samples cut from a solar grade SSP Cz p-type wafer (25 ± 7.5 Ω·cm), the lifetime comparison is presented in Fig. 2. The calculated upper limit surface recombination velocities from each sample are: $363\,cm\,s^{-1}$, $322\,cm\,s^{-1}$ and $202\,cm\,s^{-1}$ for GO (Fig. 2a), I-E (Fig. 2b) and SiN_x (Fig. 2c), respectively. These results indicate that in some silicon materials it is possible to attain very similar levels of surface passivation with GO coatings to those obtained by the widely used SiN_x and I-E techniques.

With respect to the surface passivation stability we have found that the GO passivation effect can last for several days, however there appears to be some unpredictable behaviour in GO's passivation after storage. We have observed there is an increase in averaged lifetime after a few days of air ambient storage of the samples, which we suggest to be attributed to the interlayer water molecule release which

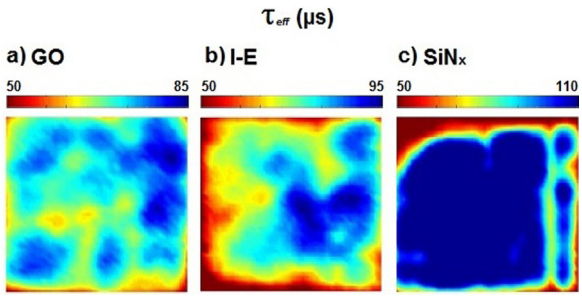

Fig. 2. Effective lifetime maps of samples cut from a B-doped Cz wafer of thickness 625 ± 25 μm, passivated with (a) 4 mg/ml GO, (b) I-E solution, and (c) PECVD SiN_x.

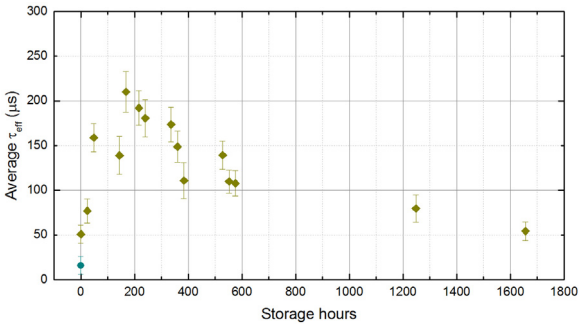

Fig. 3. Averaged effective lifetime values of samples cut from a B-doped Cz wafer of thickness 200 ± 5 μm. Initial non-passivated value is identified with the circular marker, whereas the diamond marker represents the passivated averaged values with 2 mg/ml GO after air ambient storage.

decreases the spacing between GO sheets and increases the negative charge on the surface. Thus, after reaching an average τ_{eff} maxima, the lifetime begins to decrease slowly as shown in Fig. 3, where effective lifetime degradation is shown for a B-doped (2.8 Ω·cm), SSP, Cz grown silicon sample coated with 2 mg/ml GO after air storage during 70 days. It must be noted that Fig. 3 shows the averaged effective lifetimes of $3 \times 3\,cm^2$ samples with some deviations due to GO aggregation sites, thus making it difficult to appreciate the amount of stability obtained within the first two weeks of deposition. The data point with a circular marker in Fig. 3 represents the averaged lifetime of the bare sample which in comparison to the data taken after 1600 h shows that even after the 70 day lifetime degradation there is still some passivation present from the GO coating. We believe that it may be possible to improve the stability with the application of an encapsulation or capping method. This approach would avoid the gradual reduction of dried GO at ambient conditions in the presence of humidity and high pH which is likely to be the cause of the passivation degradation.

3.2. Passivation mechanism

We have demonstrated the capability of GO to passivate silicon surfaces by τ_{eff} mapping of silicon samples. This is in line with the observations of higher efficiencies from some authors in literature [11–16], however the mechanism responsible of the passivation is still under debate. On the one hand Yang et al. [14] has suggested the passivation to be due to surface dangling bond saturation provided by the hydroxyl and carbonyl groups which decorate the graphene-like sheet of GO, whereas Hsu et al. [12] and Jiao et al. [13] attribute the passivation to the negative surface charge of GO. Henceforth we provide some evidence to support the latter as the source of the passivation.

It has been largely acknowledged in the literature that the abundant oxygen containing functional groups of GO such as: hydroxyls (C-OH), carboxyls (COOH), and epoxides (C-O-C) are the source of a strong negative surface charge in the GO sheets [7,20,21]. Even though there still exist some dispute on the distribution of these functional groups and their impact on GO's properties, the negative charge attributed to them has been accepted by the 2D material community. GO's negative charge has been observed to be significantly dependent on the pH of GO's colloidal dispersion, and has been measured mostly by the zeta potential technique [16,22–24] and more recently by Kelvin-probe microscopy [25]. In this work we have thus studied the impact of pH on the surface passivation ability of GO in a range of samples, primarily observing the effect of low (3.6 ± 0.01) and high (10 ± 0.01) pH GO solutions in the passivation, this because there were no observable trends from intermediate values as could be expected from the small zeta potential increase in mid values reported in various references [16,22–24].

Firstly, to observe the effect of pH on the surface potential of the GO single flakes (see Fig. 4**a** and **b** for topography illustration) we used the PeakForce-KPFM technique on both materials. Images of the measurements are shown in Fig. 4**c** and **d** for the low and high pH dispersions, respectively. A cross-section profile of the measured surface potential is also shown in Fig. 4 for both pH's. From these measurements the contact potential difference (V_{CPD}) between the tip and the sample presents a threefold increase in negative potential going from $V_{CPD} = 24 \pm 7$ mV for the low pH GO flake to $V_{CPD} = 62 \pm 4$ mV for the high pH GO flake. These results indicate that there is indeed an increase

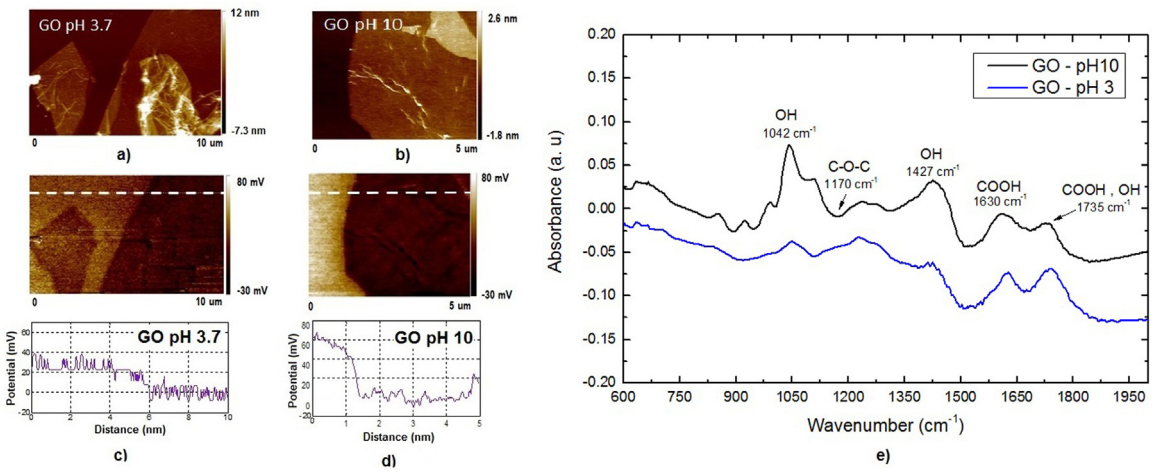

Fig. 4. AFM images of sheets from a low (a) and high (b) pH GO dispersion. PeakForce-KPFM maps from the same GO sheets with low (c) and high (d) pH. (e) Transmission IR absorption spectra from silicon samples coated with low and high pH 3 mg/ml GO.

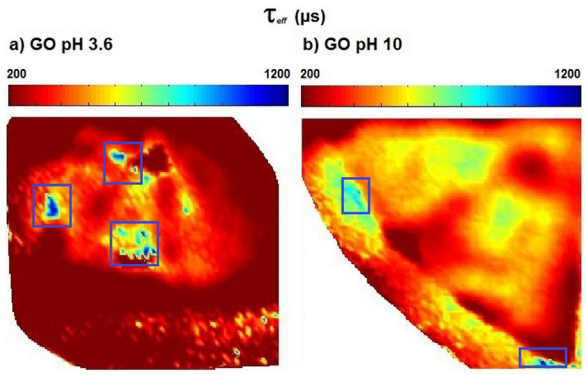

Fig. 5. Effective lifetime maps of samples cut from a B-doped FZ wafer of thickness 300 ± 5 µm, passivated with 2 mg/ml GO with (a) pH 3.6 (as prepared) and (b) pH 10. The blue boxes highlight the highest lifetime areas.

in negative charges on each GO flake from the basic solution. Moreover an increase in potential with number of GO layers was observed, confirming the results reported by Salomao et al. in [26]. We have carried out FTIR measurements on silicon samples coated with thick layers of the same low and high pH GO dispersions to correlate with functional group content, results are shown in Fig. 4**e**. The IR spectra at distinct points of the sample show a rather significant increase in the vibrational frequencies 1042 cm^{-1} and 1427 cm^{-1} typically assigned to hydroxyl groups, some increase in the range 1600 − 1750 cm^{-1}, frequencies commonly assigned to carboxyl and hydroxyl groups and a slight decrease in the band 1170 cm^{-1} assigned to the epoxides [27]. This evidence adds to the argument of having the oxygen-containing groups as the source of negative charge in GO. We then performed photoconductance decay measurements to compare the passivation level attained with each material. In Fig. 5**a** and **b** we show the compared τ_{eff} maps of samples taken from a high resitivity p-type FZ wafer passivated with 2 mg/ml GO solutions with low and high pH, respectively. In these samples the averaged τ_{eff} increased from 236 µs in the low pH sample to 389 µs in the high pH sample, suggesting that the added negative charge from the hydroxyl groups improves the passivation. In terms of S_{UL} however, we calculated a value of 17.4 cm s^{-1} for the low pH sample and 19.5 cm s^{-1} for the high pH sample, considering the τ_{max} measured of 1430 µs and 1282 µs respectively for each sample, these high lifetime areas have been highlighted in Fig. 5. On these areas, an increase of a few tens of nm in GO thickness was measured, indicating that these effect may be the result of a higher aggregation of GO sheets in the low pH solution [22,24] which in turn increases the net negative charge in the area and consequently the field effect passivation. This is in agreement with the negative field effect passivation obtained with GO coating. It must be also noted that, as mentioned in the methods section, the passivation of GO was significantly decreased by the oxide removal from the samples. This fact suggests that there is no dangling bond saturation involved in the passivation mechanism of GO, since a SiO_2 thin interlayer (less than 10 nm) has been found to be required for an improved passivation. Such observations contradict the possibility of physical bonding between GO's functional groups and silicon atoms at the surface as suggested by Yang et al. in [14].

4. Conclusions

In this work we have reported the effectiveness of graphene oxide as a surface passivation coating for silicon solar cells. Surface recombination velocities as low as 14.4 cm s^{-1} have been obtained. Studies on the passivation mechanism attained by GO and its stability are discussed. We found the passivation to be likely explained by the negative fixed charge coming from the oxygen-containing groups, hydroxyl groups in particular, surrounding the GO's flakes and discard previous suggestions of predominant chemical passivation. The simplicity of GO's deposition and removal without surface damage make this process a good alternative for temporary surface passivation for bulk lifetime measurements. Furthermore, with the use of an appropriate encapsulation method or capping layer deposition, results in here presented demonstrate that GO can be a potential cheap and low risk alternative to currently used surface passivation materials for silicon-based solar cells.

Acknowledgments

We would like to thank Engineering and Physical Sciences Research Council, (EPSRC), United Kingdom for funding under contract under the SuperSilicon PV contract (EP/M024911/1). Financial support was also given by Consejo Nacional de Ciencia y Tecnologia, Mexico CONACyT-Mexico. R.S. Bonilla is the recipient of an EPSRC (UK) Postdoctoral Research Fellowship, EP/M022196/1.

References

[1] M.A. Green, S.P. Bremner, Energy conversion approaches and materials for high efficiency photovoltaics, Nat. Mater. 16 (2017) 23–34.
[2] R.S. Bonilla, C. Reichel, M. Hermle, P.R. Wilshaw, Extremely low surface recombination in 1 $Ω$ cm n-type monocrystalline silicon, Phys. Status Solidi - Rapid Res. Lett. 11 (2017) 1600307.
[3] N.E. Grant, J.D. Murphy, Temporary surface passivation for characterisation of bulk defects in silicon: a review, Phys. Status Solidi - Rapid Res. Lett. 11 (2017).
[4] R.S. Bonilla, B. Hoex, P. Hamer, P.R. Wilshaw, Dielectric surface passivation for silicon solar cells: a review, Phys. Status Solidi 214 (2017) 1700293.
[5] H.A. Becerril, J. Mao, Z. Liu, R.M. Stoltenberg, Z. Bao, Y. Chen, Evaluation of solution-processed reduced graphene oxide films as transparent conductors, ACS Nano. 2 (2008) 463–470.
[6] A. Lerf, H. He, M. Forster, J. Klinowski, Structure of graphite oxide revisited, J. Phys. Chem. B. 102 (1998) 4477–4482.
[7] D. Chen, H. Feng, J. Li, Graphene oxide: preparation, functionalization, and electrochemical applications, Chem. Rev. 112 (2012) 6027–6053.
[8] I. Jung, M. Vaupel, M. Pelton, R. Piner, D.A. Dikin, S. Stankovich, J. An, R.S. Ruoff, Characterization of thermally reduced graphene oxide by imaging ellipsometry, J. Phys. Chem. C. 112 (2008) 8499–8506.
[9] L.-C. Chen, C.-T. Yu, Y.-C. Peng, J.-J. Hung, H.-M. Chang, S.-D. Tzeng, C.-M. Wang, C.-C. Lin, C.-H. Lin, Antireflection with graphene oxide, Opt. Mater. Express 6 (2016) 8.
[10] A. Nandi, S. Majumdar, S.K. Datta, H. Saha, S.M. Hossain, Optical and electrical effects of thin reduced graphene oxide layers on textured wafer-based c-Si solar cells for enhanced performance, J. Mater. Chem. C 5 (2016) 1920–1934.
[11] C.H. Lin, W.T. Yeh, M.H. Chen, Metal-insulator-semiconductor photodetectors with different coverage ratios of graphene oxide, IEEE J. Sel. Top. Quantum Electron. 20 (2014).
[12] W.-T. Hsu, Z.-S. Tsai, L.-C. Chen, G.-Y. Chen, C.-C. Lin, M.-H. Chen, J.-M. Song, C.-H. Lin, Passivation ability of graphene oxide demonstrated by two-different-metal solar cells, Nanoscale Res. Lett. 9 (2014) 1–5.
[13] K. Jiao, X. Wang, Y. Wang, Y. Chen, Graphene oxide as an effective interfacial layer for enhanced graphene/silicon solar cell performance, J. Mater. Chem. C 2 (2014) 7715.
[14] L. Yang, X. Yu, M. Xu, H. Chen, D. Yang, Interface engineering for efficient and stable chemical-doping-free graphene-on-silicon solar cells by introducing a graphene oxide interlayer, J. Mater. Chem. A 2 (2014) 16877–16883, https://doi.org/10.1039/C4TA02216E.
[15] L. Lancellotti, L. Sansone, E. Bobeico, E. Lago, M. Della Noce, P. Delli Veneri, A. Borriello, M. Casalino, G. Coppola, M, I.M. Giordano, Graphene oxide as an interfacial layer in silicon based schottky barrier solar cells, IET Conf. Publ. 2015 (2015) 1–4.
[16] V. Georgakilas, J.N. Tiwari, K.C. Kemp, J.A. Perman, A.B. Bourlinos, K.S. Kim, R. Zboril, Noncovalent Funct. Graph. Graph. Oxide Energy Mater., Biosensing, Catal., Biomed. Appl. (2016).
[17] A. Aberle, Overview on SiN surface passivation of crystalline silicon solar cells, Sol. Energy Mater. Sol. Cells 65 (2001) 239–248.
[18] W. Kern, J.E. Soc, The evolution of silicon wafer cleaning technology, J. Electrochem. Soc. 137 (1990) 1887–1892.
[19] J.P. Rourke, P.A. Pandey, J.J. Moore, M. Bates, I.A. Kinloch, R.J. Young, N.R. Wilson, The real graphene oxide revealed: stripping the oxidative debris from the graphene-like sheets, Angew. Chem. - Int. Ed. 50 (2011) 3173–3177.
[20] M. Li, C. Liu, Y. Xie, H. Cao, H. Zhao, Y. Zhang, The evolution of surface charge on graphene oxide during the reduction and its application in electroanalysis, Carbon N. Y 66 (2014) 302–311.
[21] M.M. Gudarzi, Colloidal stability of graphene oxide: aggregation in Two Dimensions, Langmuir 32 (2016) 5058–5068.
[22] C.J. Shih, S. Lin, R. Sharma, M.S. Strano, D. Blankschtein, Understanding the pH-dependent behavior of graphene oxide aqueous solutions: a comparative experimental and molecular dynamics simulation study, Langmuir 28 (2012) 235–241.

[23] D. Li, M.B. Mueller, S. Gilje, R.B. Kaner, G.G. Wallace, Processable aqueous dispersions of graphene nanosheets, Nat. Nanotechnol. 3 (2008) 101–105.
[24] S. a. Hasan, J.L. Rigueur, R.R. Harl, A.J. Krejci, I. Gonzalo-Juan, B.R. Rogers, J.H. Dickerson, SI-Transferable graphene oxide films with tunable microstructures, ACS Nano. 4 (2010) 7367–7372.
[25] M. Jaafar, Step like surface potential on few layered graphene oxide Step like surface potential on few layered graphene oxide, Appl Phys Lett. 101, 2012, 263109.
[26] F.C. Salomão, E.M. Lanzoni, C.A. Costa, C. Deneke, E.B. Barros, Determination of high-frequency dielectric constant and surface potential of graphene oxide and influence of humidity by kelvin probe force microscopy, Langmuir 31 (2015) 11339–11343.
[27] M. Acik, G. Lee, C. Mattevi, A. Pirkle, R.M. Wallace, M. Chhowalla, K. Cho, Y. Chabal, The role of oxygen during thermal reduction of graphene oxide studied by infrared absorption spectroscopy, J. Phys. Chem. C. 115 (2011) 19761–19781.

CHAPTER 6

CONCLUSIONS AND FURTHER WORK

In this chapter, a summary of the contributions and conclusive remarks conferred in each previous chapter together with their relevance to the PV community is presented. What is more, highlights on the required further work from the corresponding chapter's topic is bestowed.

In chapter 3 we have presented results on studies realised on phosphorous doped Czochralski and Continuous-Czochralski crystals. Our studies firstly describe the interactions between C,O and H in several samples in Section 3.2. Secondly in Section 3.3, oxygen-rich Si-samples after thermal-donor formation have been characterized. Both sections have been aimed to investigate the effects of the aforementioned impurities in the minority carrier lifetime of the material.

So, in *Section 3.2* we have shown that in every measured Cz/Cz-Si sample containing high levels of carbon and oxygen impurities, a couple of minority carrier lifetime limiting recombination centers are formed in the presence of atomic hydrogen (i.e the COH-complexes). Detailed studies, which are presented in the form of four published papers, hence describe the mechanisms of these COH-complex formation, and the proposed atomistic structure of the observed dominant center together with the full description of its electrical activity. In the following, the highlights of the findings given on these publications are the recognised.

- --→ By means of DLTS, LDLTS, MCTS, FTIR and μPCD, a range of *n*-type Cz material with various O, C and H contents have been studied.

- --→ The DLTS, LDLTS and MCTS spectra from the C, O and H contaminated samples (Si:O+C) show the formation of six centers. Four of which have been identified to arise from C, O and H interactions, two of them corresponding to electron traps and two more to hole traps.

- --→ Careful electrical characterization of the hole traps, which includes their position in the gap and their capture cross-section ratios, have disclosed their high recombination activity. Identification of their presence in the material as a lifetime limiting factor for high efficiency cells fabrication has thus been suggested.

- --→ Detailed characterization of the electron traps demonstrated that these are not very effective recombination canters, however, they appear to be closely related to the same complexes giving rise to the COH hole traps. What is more, our results indicate that these traps correspond to the second acceptor levels of the COH complexes, and studies of their field-dependent emission behaviour are found to be well described by phonon-assisted tunnelling.

- --→ Evidence of the minority carrier lifetime reduction due to the COH-complexes presence has been provided by μPCD mapping of the contaminated material.

- --→ Even though dissociation of the complexes has been achieved by the application of short-term low temperature ($\approx 200\,^{\circ}$C) heat-treatments, their re-formation has been shown to occur upon cooling when high-enough H levels were available in the material.

- --→ Degradation of the Si:O+C samples was also observed after hydrogenation from SiN_x coatings, demonstrating the relevance of the COH-complex studies for high-efficiency PV-cell manufacture.

- --→ From first-principles calculations, an atomistic model from the bistable COH-complex giving rise to the dominant peak observed by DLTS was constructed and presented. Excellent agreement between the experimentally-obtained characteristic energy values of the complex and the resulting theoretical calculations is shown.

- --→ It is argued that although H presence in Si crystals is often considered to be beneficial for the devices, care should be taken when deliberately introducing it into C-rich materials to avoid degradation.

From the careful analysis of our results it was concluded that the COH-complexes can be very harmful for the efficiency of the solar cells made from Si:O+C material. However, some relevant work has been left pending to further support our hypothesis. For instance, the fabrication and testing of complete cells made from a range of Si:O+C material with various C, O and H concentrations has been left as pending work.

In *Section 3.3* on the other hand, we have studied a set of commercially available P-doped Cz samples with high oxygen concentrations. This material has been lately reported to suffer from lifetime degradation and attributed to the presence of bistable-thermal double donors (BTDDs). Therefore, we have carried out careful studies by means of DLTS on several samples to investigate the proposed theory. Our findings, which were presented in the form a paper which is currently under editorial revision, can be summarised as follows:

- --→ By means of DLTS and LDLTS measurements in the range 300 to 430 K, the formation of two peaks related to the BTDD-0 and BTDD-1 defects on their deep donor state have been for the first time been detected.
- --→ Even though thermal double donors in silicon have largely been documented in literature, the peculiarity of electron-emission activation energies of the observed BTDDs have prevented, we believe, its prior observation.
- --→ Careful studies of the capture and emission kinetics of the defects, together with previously reported BTDDs transformation characteristics, suggest that even though these complex are very effective minority carrier trapping centers, they do not have a significant effect on the minority carrier lifetime of the material.

Due to the increased interest from industrial manufacturers to switch their base material from *p*-type to *n*-type material for commercial cell production in recent years, thermal-donors in Si have regained attention in literature. Although a plethora of available investigations on the topic already exists, it may be necessary for forthcoming technological advances to gain a better understanding on the effect of TDD species when they are present in the crystal in large quantities.

In chapter 4 we have shown the results of our extensive investigations on B-doped Cz material which has been found to be prone to light-induced degradation. This degradation has been a topic of tremendous interest for the PV community for decades due to the huge detrimental effect it poses on the cell efficiencies. Hence, more than a 1000 papers have been published throughout the past four decades demonstrating advances on the underlying physical mechanisms responsible for the degradation. Nevertheless, little experimentally-supported evidence has been published yet, that provide a definite answer to all the suggested hypothesis and posed questions in relation to the responsible defect and/or recombination mechanisms for the observed degradation. From our

recent experimental findings however, we have been able to construct a new model for the responsible BO-defect supported by strong evidence provided by several junction capacitance techniques. Accordingly, in Section 4.1 we have presented our latest results in the topic in the form or a paper draft which is to be completed in the following weeks for journal submission. The highlights of the sections' contributions reads as follows:

- --→ For the first time the direct observation of what we think is a precursor of the BO-defect responsible for LID in B-doped Cz Si is shown by means of DLTS.
- --→ A direct correlation between the DLTS signal disappearance and the degradation of the minority carrier lifetime in the material has been found and presented.
- --→ A configuration-coordinate diagram has been constructed after capture and emission kinetics of holes analysis.
- --→ From first-principles calculations a proposed BO-defect structure on three different configurations has been shown.
- --→ By means of capacitance junction techniques we have identified the formation of two shallow levels and a deep donor after capture and emission of carriers from the defect. Hence it is argued that the BO-complex can change its atomistic configuration upon charge carrier capture and emission.
- --→ It is suggested that the LID mechanism of recombination occurs through a shallow acceptor level introduced by the one of the BO-complex configurations, and could be described by a trap-assisted Auger recombination process.

Analysis of our recent results point us to the belief that the long-standing LID problem in *p*-type Cz Si has not been able to be resolved due to the likelihood of the recombination mechanism to be related to the introduction of very shallow levels in the gap which are in close proximity to the B-atom acceptor level. Such shallow levels tend not to be strong recombination centers from the perspective of Shockley-Read-Hall statistics. Nevertheless, one possibility for these traps to act as true minority carrier sinks, is for them to be associated to an Auger type of recombination process. Even though our presented results give strong evidence of the appearance of such shallow levels after degradation, further work is currently been carried out towards their direct spectroscopic observation for characterization. Consequently, it is of our current interest to carefully study the implications of the existence of these uncommon

shallow traps in Si, and thus be able to develop a full theory on their recombination mechanisms.

In chapter 5 studies on graphene oxide as a new surface passivation material for silicon is bestowed. It has been shown within the chapter that some of GO's chemical and physical intrinsic properties makes it a very good candidate for its application on Si-surfaces as passivation layer. However, in the literature just a few of these properties have been studied for the efficiency improvement of Si solar cells. Accordingly, in Section 5.2 we have presented in the form of a published paper the evidence obtained from several characterization methods of GO's ability to reduce the surface recombination velocities in various Si crystals. The key findings of the such publication are summarised as follows:

- --→ GO has been found to serve as an effective surface passivation material for Si.
- --→ The passivation mechanism offered by GO is found to be mostly related to its surface negative charge and thus associated to a field-effect passivation.
- --→ Opposite to some previous literature claims, we have found no significant evidence of chemical passivation.
- --→ Demonstrated stability of the GO passivation makes it a good candidate for temporary passivation layer.
- --→ It is suggested that the application of some capping-layer techniques are required for a feasible GO-passivation utilisation in solar cell fabrication.

From the analysis of our presented results together with some preliminary data obtained from corona-discharge and X-ray photoelectron spectroscopy studies it is our belief that besides the use of GO as passivation material, some other possible GO applications need to be explored. For instance, we suggest that GO can potentially be used in Si-based cells as emitter passivation layer, anti-reflection coating and replacement for aluminium backsurface field. Nevertheless, further work to thoroughly evaluate these industrial applications is still required.

REFERENCES

[1] "Renewable capacity statistics 2018." http://www.irena.org, 2018. [Online; accessed March 2018].

[2] "Photovoltaics report." http://www.ise.fraunhofer.de, 2018. [Online; released June 2018; accessed March 2018].

[3] S. Kasap and P. Capper, *Springer handbook of electronic and photonic materials*. Springer Science & Business Media, 2006.

[4] R. S. Bonilla, B. Hoex, P. Hamer, and P. R. Wilshaw, "Dielectric surface passivation for silicon solar cells: A review," *physica status solidi (a)*, vol. 214, no. 7, p. 1700293, 2017.

[5] J. Bollmann and A. Venter, "Admittance spectroscopy or deep level transient spectroscopy: A contrasting juxtaposition," *Physica B: Condensed Matter*, vol. 535, pp. 237–241, 2018.

[6] P. Blood and J. Orton, "The electrical characterization of semiconductors: Majority carriers and electron states academic," *New York*, vol. 13, 1992.

[7] "Semilab wt200pvn quasi-steady-state microwave detected photoconductance decay technology." https://www.semilab.hu/category/products/carrier-lifetime-u-pcd-qss-upcd, 2009. [Online; accessed July 2018].

[8] H. A. Becerril, J. Mao, Z. Liu, R. M. Stoltenberg, Z. Bao, and Y. Chen, "Evaluation of solution-processed reduced graphene oxide films as transparent conductors," *ACS nano*, vol. 2, no. 3, pp. 463–470, 2008.

[9] C. Mattevi, G. Eda, S. Agnoli, S. Miller, K. A. Mkhoyan, O. Celik, D. Mastrogiovanni, G. Granozzi, E. Garfunkel, and M. Chhowalla, "Evolution of electrical, chemical, and structural properties of transparent and conducting chemically derived graphene thin films," *Advanced Functional Materials*, vol. 19, no. 16, pp. 2577–2583, 2009.

[10] D. Li, M. B. Mueller, S. Gilje, R. B. Kaner, and G. G. Wallace, "Processable aqueous dispersions of graphene nanosheets," *Nature nanotechnology*, vol. 3, no. 2, pp. 101–105, 2008.

[11] "Renewable power generation costs in 2017." http://www.irena.org, 2018. [Online; accessed July 2018].

[12] "X-series solar panels." https://us.sunpower.com/solar-panels-technology/x-series-solar-panels/, 2018. [Online; accessed July 2018].

[13] M. Kivambe, B. Aissa, and N. Tabet, "Emerging technologies in crystal growth of photovoltaic silicon: Progress and challenges," *Energy Procedia*, vol. 130, pp. 7–13, 2017.

[14] C. Lan, A. Lan, C. Yang, H. Hsu, M. Yang, A. Yu, B. Hsu, W. Hsu, and A. Yang, "The emergence of high-performance multi-crystalline silicon in photovoltaics," *Journal of Crystal Growth*, vol. 468, pp. 17–23, 2017.

[15] C. Khattak and K. Ravi, *Silicon processing for photovoltaics II*. Materials processing, theory and practices, North-Holland, 1987.

[16] C. Lan, C. Yang, A. Lan, M. Yang, A. Yu, H. Hsu, B. Hsu, and C. Hsu, "Engineering silicon crystals for photovoltaics," *CrystEngComm*, vol. 18, no. 9, pp. 1474–1485, 2016.

[17] N. Stoddard, B. Wu, I. Witting, M. C. Wagener, Y. Park, G. A. Rozgonyi, and R. Clark, "Casting single crystal silicon: Novel defect profiles from bp solar's mono2 tm wafers," in *Solid State Phenomena*, vol. 131, pp. 1–8, Trans Tech Publ, 2008.

[18] Y. Yang, A. Yu, B. Hsu, W. Hsu, A. Yang, and C. Lan, "Development of high-performance multicrystalline silicon for photovoltaic industry," *Progress in Photovoltaics: Research and Applications*, vol. 23, no. 3, pp. 340–351, 2015.

[19] C. Lan, "Growth of multicrystalline silicon: The high-performance casting method," *Handbook of Photovoltaic Silicon*, pp. 1–17, 2017.

[20] G. Teal and J. Little, "Growth of germanium single crystals," *Phys*, no. 647, 1950.

[21] "International technology roadmap for photovoltaic results 2017." http://www.itrpv.net, 2018. [Online; accessed July 2018].

[22] S. Meyer, S. Wahl, A. Molchanov, K. Neckermann, C. Möller, K. Lauer, and C. Hagendorf, "Influence of the feedstock purity on the solar cell efficiency," *Solar Energy Materials and Solar Cells*, vol. 130, pp. 668–672, 2014.

[23] L. Raabe, O. Pätzold, I. Kupka, J. Ehrig, S. Würzner, and M. Stelter, "The effect of graphite components and crucible coating on the behaviour of carbon and oxygen in multicrystalline silicon," *Journal of Crystal Growth*, vol. 318, no. 1, pp. 234–238, 2011.

[24] G. Fiegl, "Recent advances and future directions in cz-silicon crystal growth technology," *Solid state technology*, vol. 26, no. 8, pp. 121–131, 1983.

[25] R. Willardson, E. Weber, A. Beer, and F. Shimura, *Oxygen in Silicon*. Semiconductors and Semimetals, Elsevier Science, 1994.

[26] C. H.Theuere, "Device for the treatment of hiccups," 1962.

[27] T. Ciszek and T. Wang, "Silicon defect and impurity studies using float-zone crystal growth as a tool," *Journal of Crystal Growth*, vol. 237, pp. 1685–1691, 2002.

[28] N. E. Grant, V. P. Markevich, J. Mullins, A. R. Peaker, F. Rougieux, and D. Macdonald, "Thermal activation and deactivation of grown-in defects limiting the lifetime of float-zone silicon," *physica status solidi (RRL)–Rapid Research Letters*, vol. 10, no. 6, pp. 443–447, 2016.

[29] N. Grant, F. Rougieux, D. Macdonald, J. Bullock, and Y. Wan, "Grown-in defects limiting the bulk lifetime of p-type float-zone silicon wafers," *Journal of Applied Physics*, vol. 117, no. 5, p. 055711, 2015.

[30] T. Niewelt, M. Selinger, N. Grant, W. Kwapil, J. Murphy, and M. Schubert, "Light-induced activation and deactivation of bulk defects in boron-doped float-zone silicon," *Journal of Applied Physics*, vol. 121, no. 18, p. 185702, 2017.

[31] D. Sperber, A. Heilemann, A. Herguth, and G. Hahn, "Temperature and light-induced changes in bulk and passivation quality of boron-doped float-zone silicon coated with sinx: H," *IEEE Journal of Photovoltaics*, vol. 7, no. 2, pp. 463–470, 2017.

[32] S. Rein, *Lifetime Spectroscopy: A Method of Defect Characterization in Silicon for Photovoltaic Applications*. Springer Berlin Heidelberg, 2006.

[33] A. Hangleiter and R. Hacker, "Enhancement of band-to-band auger recombination by electron-hole correlations," *Phys. Rev. Lett.*, vol. 65, 1990.

[34] W. Shockley and W. T. Read, "Statistics of the recombinations of holes and electrons," *Phys. Rev.*, vol. 87, pp. 835–842, September 1952.

[35] R. N. Hall, "Electron-hole recombination in germanium," *Phys. Rev.*, vol. 87, pp. 387–387, July 1952.

[36] W. D. Eades and R. M. Swanson, "Calculation of surface generation and recombination velocities at the si-sio2 interface," *Journal of applied Physics*, vol. 58, no. 11, pp. 4267–4276, 1985.

[37] G. Dingemans and W. Kessels, "Status and prospects of al2o3-based surface passivation schemes for silicon solar cells," *Journal of Vacuum Science & Technology A*, vol. 30, no. 4, p. 040802, 2012.

[38] J. Schmidt, R. Peibst, and R. Brendel, "Surface passivation of crystalline silicon solar cells: Present and future," *Solar Energy Materials and Solar Cells*, vol. 187, pp. 39 – 54, 2018.

[39] A. G. Aberle, S. Glunz, and W. Warta, "Field effect passivation of high efficiency silicon solar cells," *Solar Energy Materials and Solar Cells*, vol. 29, no. 2, pp. 175 – 182, 1993.

[40] G. Dingemans, R. Seguin, P. Engelhart, M. Van de Sanden, and W. Kessels, "Silicon surface passivation by ultrathin al2o3 films synthesized by thermal and plasma atomic layer deposition," *physica status solidi (RRL)-Rapid Research Letters*, vol. 4, no. 1-2, pp. 10–12, 2010.

[41] E. H. Nicollian, J. R. Brews, and E. H. Nicollian, *MOS (metal oxide semiconductor) physics and technology*, vol. 1987. Wiley New York et al., 1982.

[42] B. Sopori, X. Deng, J. Benner, A. Rohatgi, P. Sana, S. Estreicher, Y. Park, and M. Roberson, "Hydrogen in silicon: A discussion of diffusion and passivation mechanisms," *Solar Energy Materials and Solar Cells*, vol. 41, pp. 159–169, 1996.

[43] S. Glunz, D. Biro, S. Rein, and W. Warta, "Field-effect passivation of the sio 2 si interface," *Journal of Applied Physics*, vol. 86, no. 1, pp. 683–691, 1999.

[44] M. Schofthaler, R. Brendel, G. Langguth, and J. Werner, "High-quality surface passivation by corona-charged oxides for semiconductor surface characterization," in *Photovoltaic Energy Conversion, 1994., Conference Record of the Twenty Fourth. IEEE Photovoltaic Specialists Conference-1994, 1994 IEEE First World Conference on*, vol. 2, pp. 1509–1512, IEEE, 1994.

[45] J. Schmidt and A. G. Aberle, "Easy-to-use surface passivation technique for bulk carrier lifetime measurements on silicon wafers," *Progress in Photovoltaics: Research and Applications*, vol. 6, no. 4, pp. 259–263, 1998.

[46] J. Benick, K. Zimmermann, J. Spiegelman, M. Hermle, and S. Glunz, "Rear side passivation of perc-type solar cells by wet oxides grown from purified steam," *Progress in Photovoltaics: Research and Applications*, vol. 19, no. 3, pp. 361–365, 2011.

[47] R. S. Bonilla, C. Reichel, M. Hermle, and P. R. Wilshaw, "Extremely low surface recombination in 1 ω cm n-type monocrystalline silicon," *physica status solidi (RRL)–Rapid Research Letters*, vol. 11, no. 1, p. 1600307, 2016.

[48] R. S. Bonilla, C. Reichel, M. Hermle, and P. R. Wilshaw, "On the location and stability of charge in sio2/sinx dielectric double layers used for silicon surface passivation," *Journal of Applied Physics*, vol. 115, no. 14, p. 144105, 2014.

[49] P. Hamer, G. Bourret-Sicotte, G. Martins, A. Wenham, R. S. Bonilla, and P. Wilshaw, "A novel source of atomic hydrogen for passivation of defects in silicon," *physica status solidi (RRL)–Rapid Research Letters*, vol. 11, no. 5, p. 1600448, 2017.

[50] G. Bourret-Sicotte, P. Hamer, R. S. Bonilla, K. Collett, A. Ciesla, J. Colwell, and P. R. Wilshaw, "Shielded hydrogen passivation- a potential in-line passivation process," *physica status solidi (a)*, vol. 214, no. 7, p. 1700383, 2017.

[51] M. J. Kerr and A. Cuevas, "Very low bulk and surface recombination in oxidized silicon wafers," *Semiconductor Science and Technology*, vol. 17, no. 1, p. 35, 2002.

[52] G. Dingemans, C. Van Helvoirt, M. Van de Sanden, and W. Kessels, "Plasma-assisted atomic layer deposition of low temperature sio2," *ECS Transactions*, vol. 35, no. 4, pp. 191–204, 2011.

[53] Y. Wan, K. R. McIntosh, A. F. Thomson, and A. Cuevas, "Low surface recombination velocity by low-absorption silicon nitride on c-si," *IEEE Journal of Photovoltaics*, vol. 3, no. 1, pp. 554–559, 2013.

[54] R. S. Bonilla, F. Woodcock, and P. R. Wilshaw, "Very low surface recombination velocity in n-type c-si using extrinsic field effect passivation," *Journal of Applied Physics*, vol. 116, no. 5, p. 054102, 2014.

[55] S. Y. Herasimenka, C. J. Tracy, V. Sharma, N. Vulic, W. J. Dauksher, and S. G. Bowden, "Surface passivation of n-type c-si wafers by a-si/sio2/sinx stack with ¡ 1 cm/s effective surface recombination velocity," *Applied Physics Letters*, vol. 103, no. 18, p. 183903, 2013.

[56] S. De Wolf, C. Ballif, and M. Kondo, "Kinetics of a-si: H bulk defect and a-si: H/c-si interface-state reduction," *Physical Review B*, vol. 85, no. 11, p. 113302, 2012.

[57] A. Descoeudres, Z. C. Holman, L. Barraud, S. Morel, S. De Wolf, and C. Ballif, "21% efficient silicon heterojunction solar cells on n-and p-type wafers compared," *IEEE Journal of Photovoltaics*, vol. 3, no. 1, pp. 83–89, 2013.

[58] R. Hezel and K. Jaeger, "Low temperature surface passivation of silicon for solar cells," *Journal of The Electrochemical Society*, vol. 136, no. 2, pp. 518–523, 1989.

[59] G. Agostinelli, P. Vitanov, Z. Alexieva, A. Harizanova, H. Dekkers, S. De Wolf, and G. Beaucarne *in Proceedings of the 19th European Photovoltaic Solar Energy Conference*, 2004.

[60] G. Agostinelli, A. Delabie, P. Vitanov, Z. Alexieva, H. Dekkers, S. De Wolf, and G. Beaucarne, "Very low surface recombination velocities on p-type silicon wafers passivated with a dielectric with fixed negative charge," *Solar Energy Materials and Solar Cells*, vol. 90, no. 18-19, pp. 3438–3443, 2006.

[61] B. Hoex, S. Heil, E. Langereis, M. Van de Sanden, and W. Kessels, "Ultralow surface recombination of c-si substrates passivated by plasma-assisted atomic layer deposited al 2 o 3," *Applied Physics Letters*, vol. 89, no. 4, p. 042112, 2006.

[62] B. Hoex, J. Gielis, M. Van de Sanden, and W. Kessels, "On the c-si surface passivation mechanism by the negative-charge-dielectric al 2 o 3," *Journal of Applied Physics*, vol. 104, no. 11, p. 113703, 2008.

[63] J. Schmidt, A. Merkle, R. Brendel, B. Hoex, M. v. de Sanden, and W. Kessels, "Surface passivation of high-efficiency silicon solar cells by atomic-layer-deposited al2o3," *Progress in photovoltaics: research and applications*, vol. 16, no. 6, pp. 461–466, 2008.

[64] A. Richter, S. W. Glunz, F. Werner, J. Schmidt, and A. Cuevas, "Improved quantitative description of auger recombination in crystalline silicon," *Physical Review B*, vol. 86, no. 16, p. 165202, 2012.

[65] G. Dingemans, M. van de Sanden, and W. Kessels, "Plasma-enhanced chemical vapor deposition of aluminum oxide using ultrashort precursor injection pulses," *Plasma Processes and Polymers*, vol. 9, no. 8, pp. 761–771, 2012.

[66] L. Kimerling, "Defect characterization by junction spectroscopy," *MRS Online Proceedings Library Archive*, vol. 2, 1980.

[67] A. Peaker, V. Markevich, and J. Coutinho, "Tutorial: Junction spectroscopy techniques and deep-level defects in semiconductors," *Journal of Applied Physics*, vol. 123, no. 16, p. 161559, 2018.

[68] D. K. Schroder, *Semiconductor material and device characterization*. John Wiley & Sons, 2006.

[69] A. R. Peaker and V. P. Markevich, "Electrical and optical defect evaluation techniques for electronic and solar grade silicon," in *Defects and Impurities in Silicon Materials*, pp. 129–180, Springer, 2015.

[70] C. Sah, L. Forbes, L. Rosier, and A. Tasch, "Thermal and optical emission and capture rates and cross sections of electrons and holes at imperfection centers in semiconductors from photo and dark junction current and capacitance experiments," *Solid-State Electronics*, vol. 13, no. 6, pp. 759 – 788, 1970.

[71] D. V. Lang, "Deep level transient spectroscopy: A new method to characterize traps in semiconductors," *Journal of Applied Physics*, vol. 45, no. 7, pp. 3023–3032, 1974.

[72] A. Peaker, V. Markevich, I. Hawkins, B. Hamilton, K. Bonde-Nielsen, and K. Gościński, "Laplace deep level transient spectroscopy: Embodiment and evolution," *Physica B: Condensed Matter*, vol. 407, no. 15, pp. 3026–3030, 2012.

[73] L. Dobaczewski, P. Kaczor, I. D. Hawkins, and A. R. Peaker, "Laplace transform deeplevel transient spectroscopic studies of defects in semiconductors," *Journal of Applied Physics*, vol. 76, no. 1, pp. 194–198, 1994.

[74] C. Groetsch, "The theory of tikhonov regularization for fredholm equations," *Boston Pitman Publication*, 1984.

[75] S. W. Provencher, "Contin: a general purpose constrained regularization program for inverting noisy linear algebraic and integral equations," *Computer Physics Communications*, vol. 27, no. 3, pp. 229–242, 1982.

[76] J. P. Brunwin R., Hamilton B. and P. A.R., "Detection of minority-carrier traps using transient spectroscopy," *Electronics Letters*, vol. 15, no. 12, pp. 349 – 350, 1979.

[77] B. Hamilton, A. R. Peaker, and D. R. Wight, "Deep-state-controlled minority carrier lifetime in n-type gallium phosphide," *Journal of Applied Physics*, vol. 50, no. 10, pp. 6373–6385, 1979.

[78] C. Sah, L. Forbes, L. Rosier, and A. Tasch Jr, "Thermal and optical emission and capture rates and cross sections of electrons and holes at imperfection centers in semiconductors from photo and dark junction current and capacitance experiments," *Solid-State Electronics*, vol. 13, no. 6, pp. 759–788, 1970.

[79] D. Åberg, M. Linnarsson, B. Svensson, T. Hallberg, and J. Lindström, "Ultra-shallow thermal donor formation in silicon by annealing in ambient oxygen," *Journal of applied physics*, vol. 85, no. 12, pp. 8054–8059, 1999.

[80] E. Pell, "Recombination rate in germanium by observation of pulsed reverse characteristic," *Physical Review*, vol. 90, no. 2, p. 278, 1953.

[81] R. H. Kingston, "Switching time in junction diodes and junction transistors," *Proceedings of the IRE*, vol. 42, no. 5, pp. 829–834, 1954.

[82] B. Lax and S. F. Neustadter, "Transient response of a p-n junction," *Journal of Applied Physics*, vol. 25, no. 9, pp. 1148–1154, 1954.

[83] R. Dean and C. Nuese, "A refined step-recovery technique for measuring minority carrier lifetimes and related parameters in asymmetric pn junction diodes," *IEEE Transactions on Electron Devices*, vol. 18, no. 3, pp. 151–158, 1971.

[84] D. L. Mauch, F. J. Zutavern, J. J. Delhotal, M. P. King, J. C. Neely, I. C. Kizilyalli, and R. J. Kaplar, "Ultrafast reverse recovery time measurement for wide-bandgap diodes," *IEEE Trans. Power Electron.*, vol. 32, no. 12, pp. 9333–9341, 2017.

[85] H. Kuno, "Analysis and characterization of pn junction diode switching," *IEEE Transactions on Electron Devices*, vol. 11, no. 1, pp. 8–14, 1964.

[86] D. T. Stevenson and R. J. Keyes, "Measurement of carrier lifetimes in germanium and silicon," *Journal of Applied Physics*, vol. 26, no. 2, pp. 190–195, 1955.

[87] N. E. Grant and J. D. Murphy, "Temporary surface passivation for characterisation of bulk defects in silicon: a review," *physica status solidi (RRL)–Rapid Research Letters*, vol. 11, no. 11, p. 1700243, 2017.

[88] M. Kunst and G. Beck, "The study of charge carrier kinetics in semiconductors by microwave conductivity measurements," *Journal of Applied Physics*, vol. 60, no. 10, pp. 3558–3566, 1986.

[89] N. Schüler, S. Anger, K. Dornich, J. Niklas, and K. Bothe, "Limitations in the accuracy of photoconductance-based lifetime measurements," *Solar Energy Materials and Solar Cells*, vol. 98, pp. 245–252, 2012.

[90] M. A. Green and S. P. Bremner, "Energy conversion approaches and materials for high-efficiency photovoltaics," *Nature materials*, vol. 16, no. 1, p. 23, 2017.

[91] F. Kersten, P. Engelhart, H.-C. Ploigt, A. Stekolnikov, T. Lindner, F. Stenzel, M. Bartzsch, A. Szpeth, K. Petter, J. Heitmann, *et al.*, "A new mc-si degradation effect called letid," in *Photovoltaic Specialist Conference (PVSC), 2015 IEEE 42nd*, pp. 1–5, IEEE, 2015.

[92] B. Singha and C. Solanki, "N-type solar cells: advantages, issues, and current scenarios," *Materials Research Express*, vol. 4, no. 7, 2017.

[93] A. Cuevas, S. Riepe, M. Kerr, D. Macdonald, G. Coletti, and F. Ferrazza, "N-type multicrystalline silicon: a stable, high lifetime material," in *Photovoltaic Energy Conversion, 2003. Proceedings of 3rd World Conference on*, vol. 2, pp. 1312–1315, IEEE, 2003.

[94] R. Newman, "Oxygen diffusion and precipitation in czochralski silicon," *Journal of Physics: Condensed Matter*, vol. 12, no. 25, p. R335, 2000.

[95] M. Tomassini, J. Veirman, R. Varache, E. Letty, S. Dubois, Y. Hu, and Ø. Nielsen, "Recombination activity associated with thermal donor generation in monocrystalline silicon and effect on the conversion efficiency of heterojunction solar cells," *Journal of Applied Physics*, vol. 119, no. 8, p. 084508, 2016.

[96] J. Li, X. Yu, S. Yuan, L. Yang, Z. Liu, and D. Yang, "Effects of oxygen related thermal donors on the performance of silicon heterojunction solar cells," *Solar Energy Materials and Solar Cells*, vol. 179, pp. 17–21, 2018.

[97] R. Willardson, E. Weber, A. Beer, and F. Shimura, *Oxygen in Silicon*. Semiconductors and Semimetals, Elsevier Science, 1994.

[98] C. Fuller, J. Ditzenberger, N. Hannay, and E. Buehler, "Resistivity changes in silicon single crystals induced by heat treatment," *Acta Metallurgica*, vol. 3, no. 1, pp. 97–99, 1955.

[99] B. Pajot, E. Artacho, C. Ammerlaan, and J.-M. Spaeth, "Interstitial o isotope effects in silicon," *Journal of Physics: Condensed Matter*, vol. 7, no. 35, p. 7077, 1995.

[100] A. Goetzberger and W. Shockley, "Metal precipitates in silicon p-n junctions," *Journal of Applied Physics*, vol. 31, no. 10, pp. 1821–1824, 1960.

[101] K. Graff, *Metal impurities in silicon-device fabrication*, vol. 24. Springer Science & Business Media, 2013.

[102] W. Kaiser, "Electrical and optical properties of heat-treated silicon," *Physical Review*, vol. 105, no. 6, p. 1751, 1957.

[103] W. Kaiser and P. Keck, "Oxygen content of silicon single crystals," *Journal of Applied Physics*, vol. 28, no. 8, pp. 882–887, 1957.

[104] E. Sgourou, D. Timerkaeva, C. Londos, D. Aliprantis, A. Chroneos, D. Caliste, and P. Pochet, "Impact of isovalent doping on the trapping of vacancy and interstitial related defects in si," *Journal of Applied Physics*, vol. 113, no. 11, p. 113506, 2013.

[105] P. Wagner and J. Hage, "Thermal double donors in silicon," *Applied Physics A*, vol. 49, no. 2, pp. 123–138, 1989.

[106] V. Tkachev, L. Makarenko, V. Markevich, and L. Murin, "Modifiable thermal donors in silicon," *Sov. Phys. Semicond*, vol. 18, pp. 324–328, 1984.

[107] Y. Latushko, L. Makarenko, V. Markevich, and L. Murin, "Electrical and optical characterization of thermal donors in silicon," *physica status solidi (a)*, vol. 93, no. 2, pp. K181–K184, 1986.

[108] L. Makarenko and L. Murin, "Trapping of minority carriers in thermal u–donors in n-si," *physica status solidi (b)*, vol. 145, no. 1, pp. 241–253, 1988.

[109] L. Murin, V. Markevich, J. Lindström, and M. Kleverman, "Spectroscopic observation of the tdd0 in silicon," *Physica B: Condensed Matter*, vol. 340, pp. 1046–1050, 2003.

[110] L. Murin and V. Markevich, "Effect of carbon on thermal double donor formation in silicon," in *Materials Science Forum*, vol. 196, pp. 1315–1320, 1995.

[111] M. I. Helander, "Thermal donors in czochralski silicon wafers investigated by spectral imaging," Master's thesis, Norwegian University of Life Sciences, Ås, 2018.

[112] W. Kaiser, H. Frisch, and H. Reiss, "Mechanism of the formation of donor states in heat-treated silicon," *Physical Review*, vol. 112, no. 5, p. 1546, 1958.

[113] W. Götz, G. Pensl, and W. Zulehner, "Observation of five additional thermal donor species td12 to td16 and of regrowth of thermal donors at initial stages of the new oxygen donor formation in czochralski-grown silicon," *Physical Review B*, vol. 46, no. 7, p. 4312, 1992.

[114] D. Åberg, B. Svensson, T. Hallberg, and J. Lindström, "Kinetic study of oxygen dimer and thermal donor formation in silicon," *Physical Review B*, vol. 58, no. 19, p. 12944, 1998.

[115] D. Karg, G. Pensl, M. Schulz, C. Hässler, and W. Koch, "Oxygen-related defect centers in solar-grade, multicrystalline silicon. a reservoir of lifetime killers," *physica status solidi (b)*, vol. 222, no. 1, pp. 379–387, 2000.

[116] K. Bothe and J. Schmidt, "Electronically activated boron-oxygen-related recombination centers in crystalline silicon," *Journal of Applied Physics*, vol. 99, no. 1, p. 013701, 2006.

[117] J. Lindroos and H. Savin, "Review of light-induced degradation in crystalline silicon solar cells," *Solar Energy Materials and Solar Cells*, vol. 147, pp. 115 – 126, 2016.

[118] K. Glinchuk, N. Litovchenko, and Z. Salntik, "Structure and formation kinetics of oxygen-induced recombination centres in heat-treated silicon," *physica status solidi (a)*, vol. 71, no. 1, pp. 83–87, 1982.

[119] K. Yang, H. Kappert, and G. Schwuttke, "Minority carrier lifetime in annealed silicon crystals containing oxygen," *physica status solidi (a)*, vol. 50, no. 1, pp. 221–235, 1978.

[120] A. Borghesi, B. Pivac, A. Sassella, and A. Stella, "Oxygen precipitation in silicon," *Journal of Applied Physics*, vol. 77, no. 9, pp. 4169–4244, 1995.

[121] J.-M. Hwang and D. Schroder, "Recombination properties of oxygen-precipitated silicon," *Journal of applied physics*, vol. 59, no. 7, pp. 2476–2487, 1986.

[122] J. Murphy, K. Bothe, V. Voronkov, and R. Falster, "On the mechanism of recombination at oxide precipitates in silicon," *Applied Physics Letters*, vol. 102, no. 4, p. 042105, 2013.

[123] A. Hallén, N. Keskitalo, F. Masszi, and V. Nágl, "Lifetime in proton irradiated silicon," *Journal of Applied Physics*, vol. 79, no. 8, pp. 3906–3914, 1996.

[124] C. Londos, E. Sgourou, D. Hall, and A. Chroneos, "Vacancy-oxygen defects in silicon: the impact of isovalent doping," *Journal of Materials Science: Materials in Electronics*, vol. 25, no. 6, pp. 2395–2410, 2014.

[125] S. Brotherton and P. Bradley, "Defect production and lifetime control in electron and γ-irradiated silicon," *Journal of Applied Physics*, vol. 53, no. 8, pp. 5720–5732, 1982.

[126] V. Markevich, A. Peaker, B. Hamilton, S. Lastovskii, and L. Murin, "Donor levels of the divacancy-oxygen defect in silicon," *Journal of Applied Physics*, vol. 115, no. 1, p. 012004, 2014.

[127] H. Möller, L. Long, M. Werner, and D. Yang, "Oxygen and carbon precipitation in multicrystalline solar silicon," *physica status solidi (a)*, vol. 171, no. 1, pp. 175–189, 1999.

[128] R. Bock, P. P. Altermatt, J. Schmidt, and R. Brendel, "Formation of aluminum-oxygen complexes in highly aluminum-doped silicon," *Semiconductor Science and Technology*, vol. 25, no. 10, p. 105007, 2010.

[129] T. Shi, W.-J. Yin, Y. Wu, M. Al-Jassim, and Y. Yan, "The structure and properties of (aluminum, oxygen) defect complexes in silicon," *Journal of Applied Physics*, vol. 114, no. 6, p. 063520, 2013.

[130] C. Londos, "Deep-level transient spectroscopy studies of the interstitial carbon defect in silicon," *Physical Review B*, vol. 35, no. 12, p. 6295, 1987.

[131] D. D. Berhanuddin, M. A. Lourenço, R. M. Gwilliam, and K. P. Homewood, "Co-implantation of carbon and protons: An integrated silicon device technology compatible method to generate the lasing g-center," *Advanced Functional Materials*, vol. 22, no. 13, pp. 2709–2712, 2012.

[132] A. Mattoni, F. Bernardini, and L. Colombo, "Self-interstitial trapping by carbon complexes in crystalline silicon," *Physical Review B*, vol. 66, no. 19, p. 195214, 2002.

[133] H. Wong, N. Cheung, P. Chu, J. Liu, and J. Mayer, "Proximity gettering with mega-electron-volt carbon and oxygen implantations," *Applied physics letters*, vol. 52, no. 12, pp. 1023–1025, 1988.

[134] S. Zhang, M. Juel, E. J. Øvrelid, and G. Tranell, "Investigating the effect of carbon on oxygen behavior in n-type czochralski silicon for pv application," *journal of Crystal Growth*, vol. 411, pp. 63–70, 2015.

[135] N. Inoue, "Carbon concentration measurement in silicon down to 1014 cm-3: second generation ir, sims, cpaa and standardization," *physica status solidi (c)*, vol. 13, no. 10-12, pp. 842–847, 2016.

[136] H. Kiuchi, M. Tajima, F. Higuchi, A. Ogura, N. Iida, S. Tachibana, I. Masada, and E. Nishijima, "Determination of low carbon concentration in czochralski-grown si crystals for solar cells by luminescence activation using electron irradiation," *Japanese Journal of Applied Physics*, vol. 56, no. 7, p. 070305, 2017.

[137] S. Nakagawa and K. Kashima, "Quantitative analysis of carbon impurity concentration in silicon epitaxial layers by luminescence activation using carbon ion implantation and electron irradiation," *physica status solidi (c)*, vol. 11, no. 11-12, pp. 1597–1600, 2014.

[138] D. Backlund and S. Estreicher, "Theoretical study of the cioi and isicioi defects in si," *Physica B: Condensed Matter*, vol. 401, pp. 163–166, 2007.

[139] Y. Nagai, S. Nakagawa, H. Tsubota, and H. Matsumura, "Crystal growth and evaluation of ultra-long carrier lifetime czochralski silicon," *Japanese Journal of Applied Physics*, vol. 57, no. 8S3, p. 08RB14, 2018.

[140] H. Wang, A. Chroneos, C. Londos, E. Sgourou, and U. Schwingenschlögl, "Carbon related defects in irradiated silicon revisited," *Scientific reports*, vol. 4, p. 4909, 2014.

[141] O. Andersen, A. Peaker, L. Dobaczewski, K. B. Nielsen, B. Hourahine, R. Jones, P. Briddon, and S. Öberg, "Electrical activity of carbon-hydrogen centers in si," *Physical Review B*, vol. 66, no. 23, p. 235205, 2002.

[142] A. Ali, T. Gouveas, M.-A. Hasan, S. H. Zaidi, and M. Asghar, "Influence of deep level defects on the performance of crystalline silicon solar cells: Experimental

and simulation study," *Solar Energy Materials and Solar Cells*, vol. 95, no. 10, pp. 2805 – 2810, 2011.

[143] E. Sirtl, J. Goorissen, and E. S. E. Division, *Aggregation Phenomena of Point Defects in Silicon: Proceedings of the Satellite Symposium to ESSDERC '82, Munich*. Electrochemical Society: Proceedings, Electrochemical Society, 1983.

[144] F. Shimura, "Carbon enhancement effect on oxygen precipitation in czochralski silicon," *Journal of applied physics*, vol. 59, no. 9, pp. 3251–3254, 1986.

[145] K. Kinoshita, T. Kojima, H. Kobayashi, Y. Ohshita, and A. Ogura, "Evaluation of oxygen precipitation behavior in n-type czochralski-si for photovoltaic by infrared tomography: Effects of carbon concentration and annealing process conditions," *Japanese Journal of Applied Physics*, vol. 57, no. 8S3, p. 08RB01, 2018.

[146] J. Schmidt and K. Bothe, "Structure and transformation of the metastable boron- and oxygen-related defect center in crystalline silicon," *Physical review B*, vol. 69, no. 2, p. 024107, 2004.

[147] M. Xie, X. Yu, Y. Wu, and D. Yang, "Impact of carbon codoping on generation and dissociation of boron–oxygen defects in czochralski silicon," *Journal of Electronic Materials*, vol. 47, no. 9, pp. 5092–5098, 2018.

[148] J. Chevallier and M. Aucouturier, "Hydrogen in crystalline semiconductors," *Annual Review of Materials Science*, vol. 18, no. 1, pp. 219–256, 1988.

[149] J. Hauser, "Effect of hydrogen on amorphous silicon," *Solid State Communications*, vol. 19, no. 11, pp. 1049–1051, 1976.

[150] C. Seager and D. Ginley, "Passivation of grain boundaries in polycrystalline silicon," *Applied Physics Letters*, vol. 34, no. 5, pp. 337–340, 1979.

[151] C. Seager, R. Anderson, and J. Panitz, "The diffusion of hydrogen in silicon and mechanisms for unintentional hydrogenation during ion beam processing," *Journal of Materials Research*, vol. 2, no. 1, pp. 96–106, 1987.

[152] C. Seager and R. Anderson, "Real-time observations of hydrogen drift and diffusion in silicon," *Applied physics letters*, vol. 53, no. 13, pp. 1181–1183, 1988.

[153] B. Sopori, Y. Zhang, and N. Ravindra, "Silicon device processing in h-ambients: H-diffusion mechanisms and influence on electronic properties," *Journal of Electronic Materials*, vol. 30, no. 12, pp. 1616–1627, 2001.

[154] B. Sopori, "Silicon solar-cell processing for minimizing the influence of impurities and defects," *Journal of Electronic Materials*, vol. 31, no. 10, pp. 972–980, 2002.

[155] B. Hallam, D. Chen, M. Kim, B. Stefani, B. Hoex, M. Abbott, and S. Wenham, "The role of hydrogenation and gettering in enhancing the efficiency of next-generation si solar cells: An industrial perspective," *physica status solidi (a)*, vol. 214, no. 7, p. 1700305, 2017.

[156] S. Lee, M. Bhopal, D. Lee, and S. Lee, "Review of advanced hydrogen passivation for high efficient crystalline silicon solar cells," *Materials Science in Semiconductor Processing*, vol. 79, pp. 66–73, 2018.

[157] W. Soppe, H. Rieffe, and A. Weeber, "Bulk and surface passivation of silicon solar cells accomplished by silicon nitride deposited on industrial scale by microwave pecvd," *Progress in photovoltaics: Research and applications*, vol. 13, no. 7, pp. 551–569, 2005.

[158] A. G. Aberle, "Overview on sin surface passivation of crystalline silicon solar cells," *Solar energy materials and solar cells*, vol. 65, no. 1-4, pp. 239–248, 2001.

[159] R. Singh, S. Fonash, and A. Rohatgi, "Interaction of low-energy implanted atomic h with slow and fast diffusing metallic impurities in si," *Applied physics letters*, vol. 49, no. 13, pp. 800–802, 1986.

[160] R. Jones, B. Coomer, J. P. Goss, B. Hourahine, and A. Resende, "The interaction of hydrogen with deep level defects in silicon," in *Solid State Phenomena*, vol. 71, pp. 173–248, Trans Tech Publ, 2000.

[161] A. Chantre, S. Pearton, L. Kimerling, K. Cummings, and W. Dautremont-Smith, "Interaction of hydrogen and thermal donor defects in silicon," *Applied physics letters*, vol. 50, no. 9, pp. 513–515, 1987.

[162] N. Johnson, D. Biegelsen, and M. Moyer, "Deuterium passivation of grain-boundary dangling bonds in silicon thin films," *Applied Physics Letters*, vol. 40, no. 10, pp. 882–884, 1982.

[163] B. J. Hallam, C. E. Chan, R. Chen, S. Wang, J. Ji, L. Mai, M. D. Abbott, D. N. Payne, M. Kim, D. Chen, *et al.*, "Rapid mitigation of carrier-induced degradation in commercial silicon solar cells," *Japanese Journal of Applied Physics*, vol. 56, no. 8S2, p. 08MB13, 2017.

[164] S. Pearton, "Hydrogen in crystalline silicon," *MRS Online Proceedings Library Archive*, vol. 59, 1985.

[165] P. Hamer, B. Hallam, S. Wenham, and M. Abbott, "Manipulation of hydrogen charge states for passivation of p-type wafers in photovoltaics," *IEEE J. Photovolt*, vol. 4, no. 5, pp. 1252–1260, 2014.

[166] B. J. Hallam, P. G. Hamer, S. R. Wenham, M. D. Abbott, A. Sugianto, A. M. Wenham, C. E. Chan, G. Xu, J. Kraiem, J. Degoulange, *et al.*, "Advanced bulk defect passivation for silicon solar cells," *IEEE Journal of Photovoltaics*, vol. 4, no. 1, pp. 88–95, 2014.

[167] N. p Johnson, F. Ponce, R. Street, and R. Nemanich, "Defects in single-crystal silicon induced by hydrogenation," *Physical Review B*, vol. 35, no. 8, p. 4166, 1987.

[168] J. Corbett, P. Deák, C. Ortiz-Rodriguez, and L. Snyder, "Embrittlement of materials: Si (h) as a model system," *Journal of Nuclear Materials*, vol. 169, pp. 179–184, 1989.

[169] S. K. Estreicher, "Interstitial o in si and its interactions with h," *Physical Review B*, vol. 41, no. 14, p. 9886, 1990.

[170] S. K. Estreicher, "Hydrogen-related defects in crystalline semiconductors: a theorist's perspective," *Materials Science and Engineering: R: Reports*, vol. 14, no. 7, pp. 319 – 412, 1995.

[171] M. Roberson and S. Estreicher, "Vacancy and vacancy-hydrogen complexes in silicon," *Physical Review B*, vol. 49, no. 24, p. 17040, 1994.

[172] W. Jost, J. Weber, and H. Lemke, "Hydrogen-cobalt complexes in p-type silicon," *Semiconductor science and technology*, vol. 11, no. 4, p. 525, 1996.

[173] D. Chen, P. G. Hamer, M. Kim, T. H. Fung, G. Bourret-Sicotte, S. Liu, C. E. Chan, A. Ciesla, R. Chen, M. D. Abbott, B. J. Hallam, and S. R. Wenham, "Hydrogen induced degradation: A possible mechanism for light- and elevated temperature- induced degradation in n-type silicon," *Solar Energy Materials and Solar Cells*, vol. 185, pp. 174 – 182, 2018.

[174] J. Zhao, L. Liu, and F. Li, *Graphene oxide physics and applications*. Springer Briefs in Physics, Berlin: Springer, 2015.

[175] A. K. Geim and K. S. Novoselov, "The rise of graphene," *Nature materials*, vol. 6, no. 3, pp. 183–191, 2007.

[176] J. Cui, Y. Wan, Y. Cui, Y. Chen, P. Verlinden, and A. Cuevas, "Highly effective electronic passivation of silicon surfaces by atomic layer deposited hafnium oxide," *Applied Physics Letters*, vol. 110, no. 2, p. 021602, 2017.

[177] Y. Wan, J. Bullock, M. Hettick, Z. Xu, D. Yan, J. Peng, A. Javey, and A. Cuevas, "Zirconium oxide surface passivation of crystalline silicon," *Applied Physics Letters*, vol. 112, no. 20, p. 201604, 2018.

[178] U. Hofmann and R. Holst, "Über die säurenatur und die methylierung von graphitoxyd," *Berichte der deutschen chemischen Gesellschaft (A and B Series)*, vol. 72, no. 4, pp. 754–771, 1939.

[179] G. Ruess, "Über das graphitoxyhydroxyd (graphitoxyd)," *Monatshefte für Chemie und verwandte Teile anderer Wissenschaften*, vol. 76, no. 3-5, pp. 381–417, 1947.

[180] W. Scholz and H. Boehm, "Untersuchungen am graphitoxid. vi. betrachtungen zur struktur des graphitoxids," *Zeitschrift für anorganische und allgemeine Chemie*, vol. 369, no. 3-6, pp. 327–340, 1969.

[181] H. He, T. Riedl, A. Lerf, and J. Klinowski, "Solid-state nmr studies of the structure of graphite oxide," *The Journal of physical chemistry*, vol. 100, no. 51, pp. 19954–19958, 1996.

[182] A. Lerf, H. He, T. Riedl, M. Forster, and J. Klinowski, "13 c and 1 h mas nmr studies of graphite oxide and its chemically modified derivatives," *Solid State Ionics*, vol. 101, pp. 857–862, 1997.

[183] A. Lerf, H. He, M. Forster, and J. Klinowski, "Structure of graphite oxide revisited," *The Journal of Physical Chemistry B*, vol. 102, no. 23, pp. 4477–4482, 1998.

[184] T. Nakajima, A. Mabuchi, and R. Hagiwara, "A new structure model of graphite oxide," *Carbon*, vol. 26, no. 3, pp. 357–361, 1988.

[185] T. Nakajima and Y. Matsuo, "Formation process and structure of graphite oxide," *Carbon*, vol. 32, no. 3, pp. 469–475, 1994.

[186] T. Szabó, O. Berkesi, P. Forgó, K. Josepovits, Y. Sanakis, D. Petridis, and I. Dékány, "Evolution of surface functional groups in a series of progressively oxidized graphite oxides," *Chemistry of materials*, vol. 18, no. 11, pp. 2740–2749, 2006.

[187] D. A. Dikin, S. Stankovich, E. J. Zimney, R. D. Piner, G. H. Dommett, G. Evmenenko, S. T. Nguyen, and R. S. Ruoff, "Preparation and characterization of graphene oxide paper," *Nature*, vol. 448, no. 7152, pp. 457–460, 2007.

[188] G. Eda, G. Fanchini, and M. Chhowalla, "Large-area ultrathin films of reduced graphene oxide as a transparent and flexible electronic material," *Nature nanotechnology*, vol. 3, no. 5, pp. 270–274, 2008.

[189] M. Li, C. Liu, Y. Xie, H. Cao, H. Zhao, and Y. Zhang, "The evolution of surface charge on graphene oxide during the reduction and its application in electroanalysis," *Carbon*, vol. 66, pp. 302–311, 2013.

[190] N. V. Medhekar, A. Ramasubramaniam, R. S. Ruoff, and V. B. Shenoy, "Hydrogen bond networks in graphene oxide composite paper: structure and mechanical properties," *Acs Nano*, vol. 4, no. 4, pp. 2300–2306, 2010.

[191] A. Buchsteiner, A. Lerf, and J. Pieper, "Water dynamics in graphite oxide investigated with neutron scattering," *The Journal of Physical Chemistry B*, vol. 110, no. 45, pp. 22328–22338, 2006.

[192] I. Jung, M. Vaupel, M. Pelton, R. Piner, D. A. Dikin, S. Stankovich, J. An, and R. S. Ruoff, "Characterization of thermally reduced graphene oxide by imaging ellipsometry," *The Journal of Physical Chemistry C*, vol. 112, no. 23, pp. 8499–8506, 2008.

[193] L. Chen, C. Yu, Y. Peng, J. Hung, H. Chang, S. Tzeng, C. Wang, C. Lin, and C. Lin, "Antireflection with graphene oxide," *Optical Materials Express*, vol. 6, no. 1, pp. 8–18, 2015.

[194] K. P. Loh, Q. Bao, G. Eda, and M. Chhowalla, "Graphene oxide as a chemically tunable platform for optical applications," *Nature chemistry*, vol. 2, no. 12, pp. 1015–1024, 2010.

[195] Y. Zhu, W. Cai, R. D. Piner, A. Velamakanni, and R. S. Ruoff, "Transparent self-assembled films of reduced graphene oxide platelets," *Applied Physics Letters*, vol. 95, no. 10, p. 103104, 2009.